MgB_2 SUPERCONDUCTOR WIRES: FABRICATION AND PROPERTIES

by
ERSİN YÜCEL

THESIS SUBMITTED TO
THE GRADUATE SCHOOL OF NATURAL AND APPLIED SCIENCES
OF
THE ABANT İZZET BAYSAL UNIVERSITY
IN PARTIAL FULFILLMENT OF THE REQUIREMENT FOR THE DEGREE OF
DOCTOR OF PHILOSOPHY
IN
THE DEPARTMENT OF PHYSICS

APRIL 2010

Aproval of the Graduate School of Natural and applied Science

Prof. Dr. Nihat ÇELEBİ
Director

I certify that this thesis satisfies all the requirements as a thesis for the degree of Doctor of Philosophy.

Prof. Dr. Kıvılcım KILIÇ
Head of Physics Department

This is to certify that we have read this thesis and that in our opinion it is fully adequate, in scope and quality as a thesis for the degree of Doctor of Philosophy.

Prof. Dr. Ahmet VARİLCİ
Co-Supervisor

Prof. Dr. İbrahim BELENLİ
Supervisor

Examining Committee Members

1. Prof. Dr. İbrahim BELENLİ .....
2. Prof. Dr. Ali GENCER .....
3. Prof. Dr. Resul ERYİĞİT .....
4. Assoc. Prof. Dr. Cabir TERZİOĞLU .....
5. Assist. Prof. Dr. Erdal BEKİROĞLU .....

ABSTRACT

MgB_2 SUPERCONDUCTOR WIRES: FABRICATION AND PROPERTIES

Yücel, Ersin
Ph.D., Department of Physics
Supervisor: Prof. Dr. İbrahim Belenli
Co-Supervisor: Prof. Dr. Ahmet Varilci

April 2010, 244 pages

In this thesis, we have fabricated monofilament (MgB_2/Fe, MgB_2/Ag and MgB_2/SS) and multifilament (6 and 7 filament MgB_2/Fe/Cu, 7 and 23 filament MgB_2/Ag/Fe and 6 filament MgB_2/SS/Cu) superconducting MgB_2 wires and tapes by using powder-in-tube (PIT) method and continuous tube forming and filling (CTFF) method following the ex situ and mixture of ex situ and in situ reaction routes. We have investigated the effect of annealing temperatures and times on the formation of MgB_2 phase, transition temperature (T_c), lattice parameters (*a* and *c*), full width at half maximum (FWHM), crystallinity, resistivity (ρ), residual resistivity ratio (RRR), active cross-sectional area fraction (A_F), temperature dependence of irreversibility

field $H_{irr}(T)$, temperature dependence of upper critical field $H_{c2}(T)$, activation energy U(B,T) and critical current densities (J_c) of MgB_2/Fe monofilament tapes fabricated using ex-situ powder-in-tube (PIT) method without any intermediate annealing. To obtain the optimum annealing temperature, MgB_2/Fe monofilament tapes were annealed at 650°C, 750°C, 850°C, 950°C and 1050°C for 60 minutes. Then, to obtain the optimum annealing time, the samples were annealed at 950°C for 15, 30, 60, 120, 180 and 240 minutes. From these investigations, we found that the optimum annealing temperature and time are 950°C and 60 minutes, respectively. The MgB_2/Fe monofilament tapes were characterized using X-ray diffraction (XRD), scanning electron microscope (SEM), energy dispersive X-ray spectrometer (EDS), optical microscope, critical transition temperature (T_c), critical current density (J_c), magnetoresistivity and magnetization measurements. The transport and microstructure investigations show that T_c, J_c and microstructure properties are remarkably enhanced with increasing annealing temperature. The highest value of critical current density is obtained after annealing at 950°C for 60 minutes. The J_c and T_c^{offset} values of the MgB_2/Fe monofilament tape annealed at 950°C for 60 minutes were found to be 260.43 A/cm^2 at 20 K and 38.1 K, respectively. Also, we have investigated the superconducting properties of monofilament and multifilament MgB_2 superconducting samples employing XRD, SEM, EDS, optical microscope, critical transition temperature, and critical current density, magnetoresistivity and magnetization measurements. The results of the transport, magnetic and microstructure investigations of the monofilament and multifilament MgB_2 wires and tapes were given and discussed in the thesis. Moreover, we have investigated the effect of extreme rolling on the superconducting properties of commercial MgB_2

tapes. The results of the electrical resistivity and critical current density measurements of the commercial MgB_2 tapes were given and discussed in the thesis.

Keywords: Superconductivity, MgB_2, Monofilament wires and tapes, Multifilament wires and tapes, PIT method, CTFF method, ex-situ, in-situ, Critical transition temperature, Critical current density.

ÖZET

MgB_2 SÜPERİLETKEN TELLER: ÜRETİM VE ÖZELLİKLER

Yücel, Ersin
Doktora, Fizik Bölümü
Tez Danışmanı: Prof. Dr. İbrahim Belenli
Ortak Tez Danışmanı: Prof. Dr. Ahmet Varilci

Nisan 2010, 244 sayfa

Bu tezde, tek damarlı (MgB_2/Fe, MgB_2/Ag ve MgB_2/SS) ve çok damarlı (6 ve 7 damarlı MgB_2/Fe/Cu, 7 ve 23 damarlı MgB_2/Ag/Fe ve 6 damarlı MgB_2/SS/Cu) süperiletken MgB_2 telleri ve şeritleri, powder-in-tube (PIT) yöntemini ve continuous tube forming and filling (CTFF) yöntemini, ex-situ ve ex-situ ile in-situ reaksiyon yollarının karışımını kullanarak ürettik. Herhangi bir ara tavlama işlemi yapılmaksızın ex-situ PIT yöntemi kullanılarak üretilmiş olan tek damarlı MgB_2/Fe şeritlerin tavlama sıcaklıklarının ve sürelerinin MgB_2 faz oluşumu, geçiş sıcaklığı (T_c), örgü parametreleri (*a* and *c*), FWHM, kristalleşme, özdirenç, residual özdirenç

oranı (RRR), aktif kesit alanı kesri (A_F), sıcaklığa bağlı tersinmez alan $H_{irr}(T)$, sıcaklığa bağlı üst kritik alan $H_{c2}(T)$, aktivasyon enerjisi U(B,T) ve kritik akım yoğunlukları (J_c) üzerindeki etkisini inceledik. En uygun tavlama sıcaklığını elde etmek için, tek damarlı MgB_2/Fe şeritler 650^{o}C, 750^{o}C, 850^{o}C, 950^{o}C ve 1050^{o}C de 60 dakika tavlandı. Sonra, en uygun tavlama süresini elde etmek için, numuneler 950^{o}C de 15, 30, 60, 120, 180 ve 240 dakika tavlandı. Bu incelemelerden, en uygun tavlama sıcaklığını ve süresini sırasıyla 950^{o}C ve 60 dakika olarak bulduk. Tek damarlı MgB_2/Fe şeritler, X-ışını kırınımı (XRD), taramalı elektron mikroskobu (SEM), enerji dağıtıcı X-ışını spektrometresi (EDS), optik mikroskop, kritik geçiş sıcaklığı (T_c), kritik akım yoğunluğu (J_c), manyetik özdirenç ve mıknatıslanma ölçümleri kullanılarak karakterize edildi. Transport ve mikro yapı incelemeleri, artan tavlama sıcaklığının, T_c, J_c ve mikro yapı özelliklerini olağanüstü olarak artırdığını gösterdi. En yüksek kritik akım yoğunluğu değeri, 950^{o}C de 60 dakika tavlama sonrasında elde edildi. 950^{o}C de 60 dakika tavlanmış tek damarlı MgB_2/Fe şeridin J_c ve T_c^{offset} değerleri sırasıyla 260.43 A/cm^2 (20 K' de) ve 38.1 K olarak bulundu. Birde, tek damarlı ve çok damarlı MgB_2 süperiletken numunelerin süperiletkenlik özelliklerini, XRD, SEM, EDS, optik mikroskop, kritik geçiş sıcaklığı, kritik akım yoğunluğu, manyetik özdirenç ve mıknatıslanma ölçümleri kullanılarak inceledik. Tek damarlı ve çok damarlı MgB_2 tellerin ve şeritlerin transport, manyetik ve mikro yapı incelemelerinin sonuçları tezde verildi ve tartışıldı. Bundan başka, aşırı haddelemenin ticari MgB_2 şeritlerin süperiletkenlik özellikleri üzerine etkisini inceledik. Ticari MgB_2 şeritlerin elektriksel özdirenç ve kritik akım yoğunluğu ölçümlerinin sonuçları tezde verildi ve tartışıldı.

Anahtar Kelimeler: Süperiletkenlik, MgB_2, Tek damarlı teller ve şeritler, Çok damarlı teller ve şeritler, PIT yöntemi, CTFF yöntemi, ex-situ, in-situ, Kritik geçiş sıcaklığı, Kritik akım yoğunluğu.

To My Parents

ACKNOWLEDGMENTS

It is a great pleasure to thank many people who have contributed to the completion of this thesis through their knowledge, guidance, support and friendship. First of all, I would like to thank my supervisor, Prof. Dr. Ibrahim Belenli for his continuous support, guidance, advice, patience, encouragement and supervision during the preparation, revision of scientific content and style of this thesis.

I would like to thank my instructor, Assoc. Prof. Dr. Cabir Terzioglu for his valuable suggestions and assistances in the revision of scientific content and style of this thesis.

I would like to thank for their useful discussions, suggestions and valuable contributions to Prof. Dr. Ali Gencer, Prof. Dr. Ahmet Varilci and Assist. Prof. Dr. Erdal Bekiroglu. I also, thank to Prof. Dr. Ekrem Yanmaz for magnetic measurements at Karadeniz Technical University and R. A. Dr. Mustafa Akdogan and R. A. Dr. Murat Erdem for valuable assistances.

Finally, I would like to thank, my mother, father and brother for their continuous supports and motivations.

This work is financially supported by the National Boron Research Institute (BOREN) (Project no: 2006-22-Ç21-15) and partly by the Scientific and Technological Research Council of Turkey (TUBITAK) (Project no: 108M201), and partly by the Turkish State Planning Organization (DPT) (Project no: 2004K120200).

TABLE OF CONTENTS

Page

LIST OF TABLES

TABLES **Page**

LIST OF FIGURES

FIGURES **Page**

CHAPTER 1

INTRODUCTION

Superconductivity was discovered in 1911 by Dutch physicist Heike Onnes while investigating electrical properties of metals at very low temperatures. Onnes observed that the electrical resistance of mercury abruptly dropped to zero when the sample cooled below 4.2 K. This phenomenon was defined as superconductivity by Onnes [1, 3]. Heike Onnes won Nobel Prize in Physics for his superconductivity research in 1913. He also showed that other metals such as tin and lead exhibit superconductivity at below 3.8 K and 7.2 K respectively [2]. A lot of researches were done about superconductivity by Physicists until today. Many materials including Niobium, Iron, C_{60} and MgB_2 lose their electrical resistance at low temperatures [8, 23, 38]. Superconductors are used in various areas such as generators, loss-free electrical transmission cables, motors, energy storages and levitation trains etc [7].

Superconducting materials have a characteristic transition temperature which is called the critical temperature (T_c) from normal conductivity to superconductivity. A superconducting material loses all of its electrical resistance under the critical temperature (T_c) [23]. The highest T_c value is still held by the Hg-based superconductor (153 K) that was found in 1993 [8]. Wires which are made of superconducting materials can be used to carry huge currents without any resistive loss of electrical energy [9, 37]. However, there was a threshold value for the current density above which the superconducting materials would return to the normal state,

even though they may be below their transition temperature. This threshold value is called critical current density (J_c) [41]. Because superconducting materials can carry large currents without loss of energy, they are suitable for making strong electromagnets. When a magnetic field is applied to a superconducting material which is cooled below its T_c, this magnetic field is called external magnetic field. If the magnetic field higher than a critical value, the superconducting material will return to the normal resistive state. This magnetic field value is called the critical magnetic field (H_c) and it is temperature dependent [40].

In 1933, Walther Meissner and Robert Ochsenfeld discovered an important magnetic property of superconducting materials. They observed that a superconductor expels the magnetic field from its interior. This is called 'the Meissner effect' that this effect can be used to define the superconducting state [45]. Due to the Meissner effect, if an external magnetic field exists, an electric current is produced near the surface of sample. This electrical current (surface current) creates a magnetic field that exactly cancels the external magnetic field. This surface current flows in a very thin layer of thickness λ, which is called the London penetration depth [42].

In 1950, theoretical explanation for superconductors based on general symmetry properties was developed by V. Ginzburg and L. Landau [10].

Superconductor materials divided into two groups which is called Type I and Type II superconductors according to their behaviors in magnetic fields by A.A. Abrikosov in 1958 [11]. In Type I superconductors, the strength of the applied magnetic field required to completely destroy the perfect diamagnetic state in the interior of superconductor is called the critical magnetic field (H_c). In Type II superconductors, there are two critical fields, the lower critical magnetic field (H_{c1})

and the upper critical magnetic field (H_{c2}). If the external magnetic field is lower than H_{c1}, the magnetic field is completely repelled and the material behaves like a type-I superconductor. When the magnetic field is increased above H_{c1} the magnetic flux partially penetrates into the superconducting material as vortices. While the magnetic field is increased above H_{c2} the magnetic flux fully penetrates the whole material and it returns to the normal state [40].

In 1962, Brain D. Josephson who was a 22 years old British student at Cambridge University showed that if there is a very thin electrically insulating layer between two pieces of superconducting materials a tunneling electric current will flow [12]. This phenomenon which is widely used in applications of superconductors is called the Josephson effect.

A lot of superconducting elements and inter-metallic compounds are called LTS 'Low Temperature Superconductor' because their critical temperature values are lower than copper oxide superconductors. $Nb_{0.6}Ti_{0.4}$ alloy which has a T_c of 9.8 K and Nb_3Sn inter-metallic compound which has a T_c of 18.1 K are example of low T_c superconductors. Nb_3Sn superconducting materials are economically manufactured in a ductile form and they are capable of sustaining high critical current densities [8, 38].

In 1986, new class of materials which are called HTS 'High Temperature Superconductors' discovered by K. A. Müller and J. G. Bednorz. They made LaBaCuO ceramic superconductor which has a transition temperature of 35 K [22]. HTS have higher critical temperatures than LTS and they can be made superconducting by immersion in liquid nitrogen which has a boiling temperature of 77 K [23].

In 1987, bismuth-based and yttrium-based superconductors are synthesized. These materials are generally known as BSCCO which include bismuth, strontium, calcium, copper and oxygen and YBCO which include yttrium, barium, copper and oxygen respectively. $Bi_2Sr_2Ca_2Cu_3O_x$ (Bi-2223) HTS ceramic superconductor has T_c value of 110 K [8]. YBCO superconductor which is formulated as $YBa_2Cu_3O_7$ (Y123) has a transition temperature of 93 K [13].

In 1988, Tl-Ca-Ba-Cu-O (TBCCO) superconducting material synthesized with a T_c value of 120 K [8,41]. Five years later the mercury based oxide superconductor $HgBa_2Ca_2Cu_3O_8$ with a T_c of 133 K was discovered in 1993 [15].

In 2001, Professor J. Akimitsu discovered superconductivity at 39 K in MgB_2 and announced at the Symposium on Transition Metal Oxides in Sendai, Japan [16]. The discovery of MgB_2 superconductor has generated a great interest world wide in both fundamental research and practical applications. MgB_2 has the highest T_c value among the inter-metallic superconductors and it does not have weak link problem at grain boundaries. MgB_2 superconducting wires and tapes can be made of low cost elements of Mg and B. In addition, MgB_2 has a low anisotropy, the large coherence length, strong grain connectivity and high J_c value. MgB_2 is good candidate for the practical applications with these properties. Also MgB_2 can be fabricated in different types which are single crystals, tapes, bulk samples, wires and thin films [38].

In this thesis, we have fabricated monofilament and multifilament superconducting MgB_2 wires and tapes by using powder-in-tube (PIT) method and continuous tube forming and filling (CTFF) method following the ex situ and mixture of ex situ and in situ reaction routes. We have investigated the superconducting properties of monofilament and multifilament MgB_2 superconducting samples employing X-ray diffraction (XRD), scanning electron

microscope (SEM), scanning electron microscope (SEM) in a combination with an energy dispersive X-ray spectrometer (EDS), optical microscope, critical transition temperature, critical current density, magnetoresistivity measurements, magnetization measurements. Moreover, we have investigated the effect of extreme rolling on the superconducting properties of commercial MgB_2 tapes.

CHAPTER 2

THE PROPERTIES OF SUPERCONDUCTIVITY

2.1. Introduction

Energy requirement has been quickly increasing with the population growth and developments of industrialization in modern society. Scientists not only investigate new energy sources but also they work for efficient use of existing energies. One of the most common energy types is electrical energy in worldwide. At this point, the most important topic is transporting of electrical current with possible lowest losses. Scientists have attempted to understand the theoretical background of this phenomenon, and also have carried out a lot of experiments to understand the properties of the new superconducting materials. New improvements revealed that MgB_2 is a promising candidate to reform the existing superconductor industry.

2.2. The Discovery of MgB_2

Scientists have been trying to find new superconductors with high critical temperatures from the discovery of superconductivity till today. Several materials have been studied to increase the T_c value. At present, the highest T_c value is steel held by the Hg-based superconductor (153 K) that was found in 1993 [8]. The

historical development of superconducting critical temperature since 1911 is schematically shown in Figure 2.1.

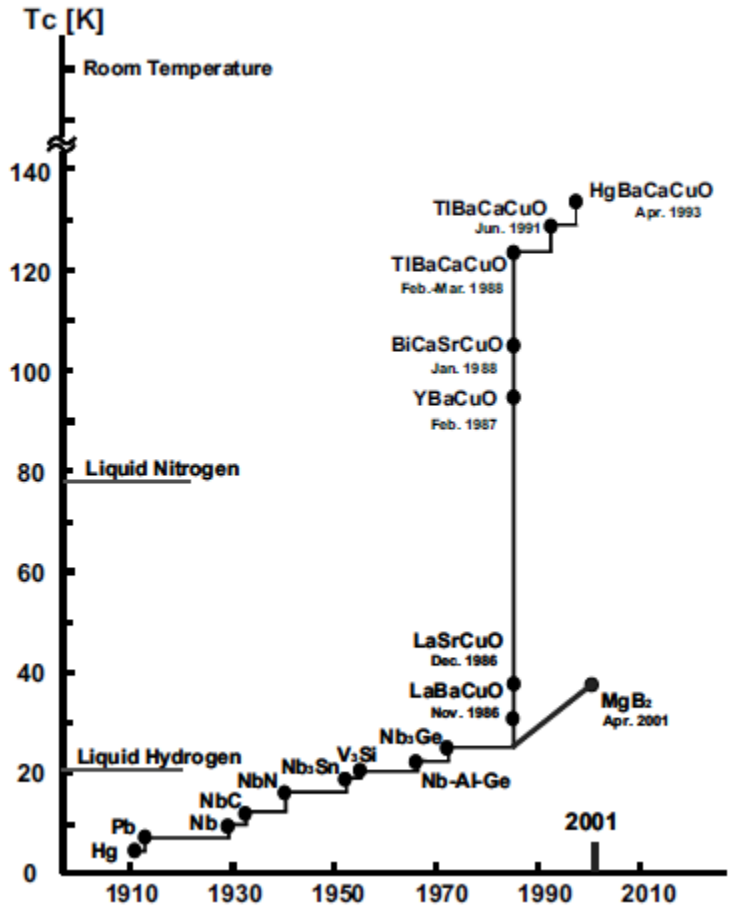

Figure 2.1 The historical development of critical temperatures in the superconducting materials [6].

In 2001, magnesium diboride (MgB_2) which has been known for approximately 50 years discovered by Professor J. Akimitsu and announced at the Symposium on Transition Metal Oxides in Sendai, Japan [16]. MgB_2 superconductor has the highest transition temperature (39 K) in intermetallic compounds. The discovery of MgB_2 superconductor has created a great interest at all over the world. Many groups in worldwide attempted to work on the theoretical studies and practical applications of MgB_2 superconductors. After discovering of MgB_2, intermetallic

compounds which have higher T_c value have been investigated by scientist. However, so far higher T_c has not been found in intermetallic materials. Also, magnesium and boron are both cheap and abundant. In addition, MgB_2 can cool to a practical temperature by inexpensively. With its interesting properties and potential application, MgB_2 is an important superconducting material and MgB_2 is a future promising candidate to reform existing superconductor industry.

Figure 2.2 shows the temperature dependence of the resistivity of MgB_2 under zero magnetic field.

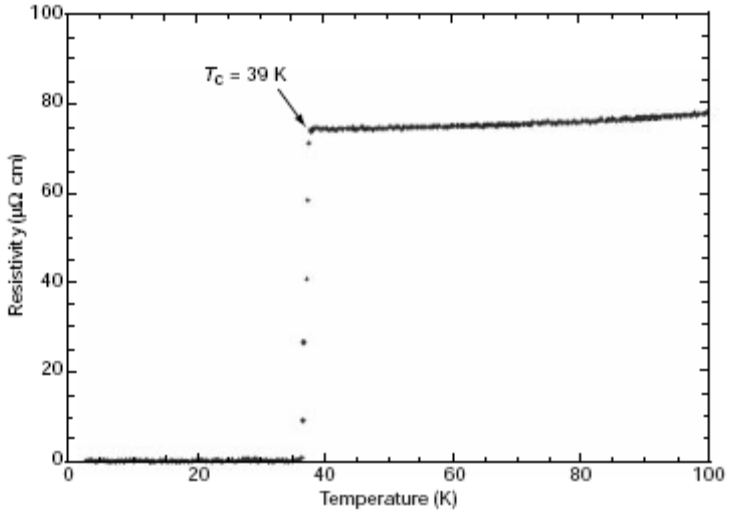

Figure 2.2 Temperature dependence of the resistivity of MgB_2 under zero magnetic field [16].

2.3. Critical Temperature (T_c)

A superconducting material loses its electrical resistivity below a certain temperature. This temperature is called the critical temperature (T_c). Superconducting materials have a characteristic critical temperature.

2.4. Critical Current (I_c)

A superconducting material can carry the maximum current before losing its superconductivity. There is a threshold value for the current density even though the material may be below its transition temperature. This threshold value is called as the critical current (I_c).

2.5. Critical Magnetic Field (H_c)

If an electrical current pass in a wire creates a magnetic field around the wire. When the current in the wire increases, the strength of the magnetic field increases. Superconductors can carry large currents without loss of energy therefore, they can constitute strong magnetic field. If a superconducting material is placed in a sufficiently strong magnetic field, the superconducting material will go from superconductivity to normal state. The minimum magnetic field required to destroy the superconductivity is called the critical magnetic field and denoted by H_c. This value depends on the shape and adaptation of the sample at a given temperature. Critical magnetic field can be defined as

$$H_c(T) = H_c(0)\left[1 - \left(\frac{T}{T_c}\right)^2\right] \tag{2.1}$$

Where $H_c(0)$ denotes the critical field at zero temperature and T_c is the transition temperature of the superconductor. Type I superconductors exclude a magnetic field until superconductivity is destroyed suddenly then the magnetic field penetrates in

the material completely. Type II superconductors differ from Type I superconductors because they determine two critical fields called H_{c1} and H_{c2}. Type II superconductor excludes the magnetic field completely until H_{c1}. Above H_{c1} the magnetic field is partially excludes, but the specimen remains electrically superconducting. At a much higher magnetic field (H_{c2}) the flux penetrates completely and superconductivity vanishes [45].

2.6. Meissner Effect

Meissner effect is an important magnetic property of superconducting materials. If a superconductor specimen is cooled below T_c under external magnetic field, it expels the magnetic field from its interior. This effect is called the Meissner Effect and it can be used to make high speed magnetically levitated trains. Meissner effect is shown in Figure 2.3.

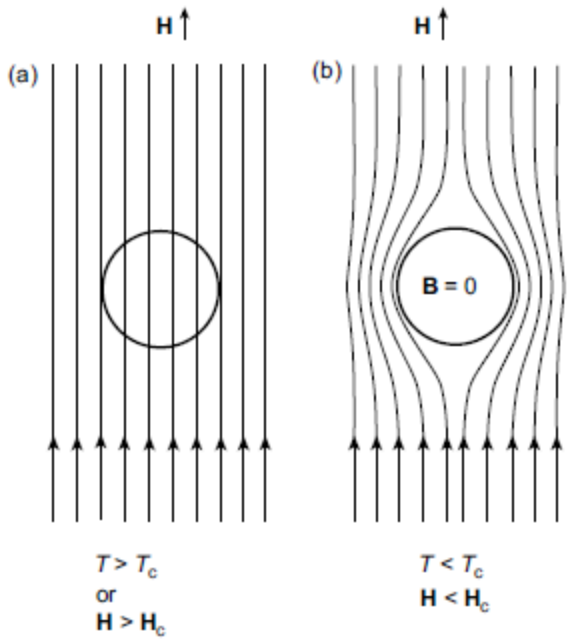

Figure 2.3 The Meissner effect. The magnetic lines of force (flux lines) in and around a metal, which goes superconducting: (a) In the normal state above the critical temperature Tc or when the applied magnetic field is greater than the critical field Hc. (b) When the sample is cooled below Tc, the metal becomes superconducting and the magnetic field is completely expelled from the superconductor; hence the flux density B inside is zero [4].

2.7. Penetration Depth (λ)

When a superconducting sample is in an applied magnetic field, the screening currents which circulate to cancel the flux inside must flow within a surface layer. So, the flux density does not fall abruptly to zero at the boundary of the metal but dies away within the region where the screening currents are flowing. For this reason the depth within which the currents flow is called the penetration depth [40]. It is given the symbol λ as shown in Figure 2.4.

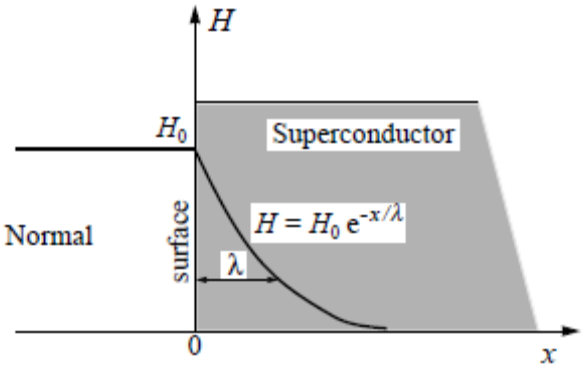

Figure 2.4 Penetration of the magnetic field into a superconducting sample. λ is the penetration depth [25].

2.8. Coherence Length (ξ)

When a superconducting material is cooled below the transition temperature additional order establishes between conduction electrons. There are two types conduction electrons, the first types behaves as superelectrons and they can pass through the material without resistance, the second types behaves as normal electrons and they can be scatters. The superelectrons form pairs of electrons which is called Cooper pairs. The size of a Cooper pair in a superconductor is known as the coherence length and denoted by ξ.

2.9. Type I Superconductors

The Type I group of superconductors is mainly comprised of metals and metalloids which have some conductivity at room temperature. They have to be cooled to very low temperatures for electron flow without resistance in accordance with BCS theory. As seen in Figure 2.5 Type I superconductors exhibit a very sharp transition to a superconducting state and also perfect diamagnetism.

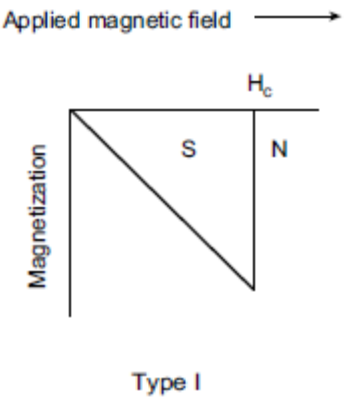

Figure 2.5 Transition to a superconducting state for Type I superconductors. As the applied magnetic field is increased, it is completely rejected from the interior of the superconductor. Note that to correspond to this diamagnetic behavior, the magnetization is plotted in the negative direction on the vertical scale. Above the critical field H_c the specimen is a normal conductor and the magnetization is too small to be seen on the scale shown. N refers to the normal state and S to the superconducting state [27].

There is no difference in the mechanism of superconductivity in Type I and Type II superconductors. Both types have similar thermal properties at the superconductor-normal transition in zero magnetic fields. But the magnetic field behaviors are completely different. A Type I superconductor excludes a magnetic field until superconductivity is destroyed suddenly then the magnetic field penetrates in the material completely [45]. Another important difference in Type I and Type II superconductors is in the mean free path of the conduction electrons in the normal state. If the coherence length (ξ) is longer than the penetration depth (λ) the superconductor will be Type I as shown in Figure 2.6.

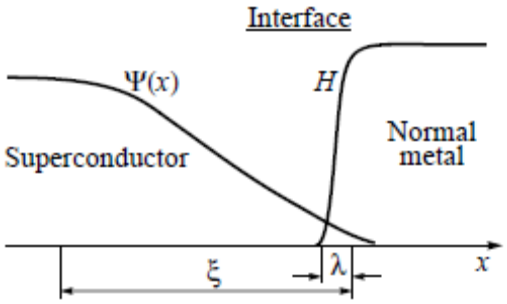

Figure 2.6 Spatial variations of the order parameter ψ and the magnetic field H in the vicinity of a superconductor-normal metal interface for k <<1 [29].

Critical fields for type I superconductors depend on the temperature. The dependence $H_c(T)$ is schematically shown in Fig. 2.7.

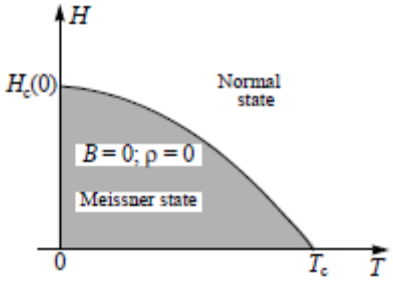

Figure 2.7 $H_c(T)$ dependence for a type-I superconductor, shown schematically [29].

2.10. Type II Superconductors

The Type II group of superconductors is mainly comprised of metallic compound, alloys and metal oxide ceramics which are recently discovered. Type II superconductors have higher T_c values than Type I superconductors by a mechanism that is still not completely understood. General opinion about the mechanism is that it relates to the planar layering within the crystalline structure [43]. Type II superconductors also known as the hard superconductors that they have stronger structure as mechanically than Type I superconductors. Also Type II superconductors

differ from Type I superconductors because they determine two critical fields called H_{c1} and H_{c2}. As seen in Figure 2.8 Type II superconductor excludes the magnetic field completely until H_{c1}. Above H_{c1} the magnetic field is partially excludes, but the specimen remains electrically superconducting. At a much higher magnetic field (H_{c2}) the flux penetrates completely and superconductivity vanishes [45].

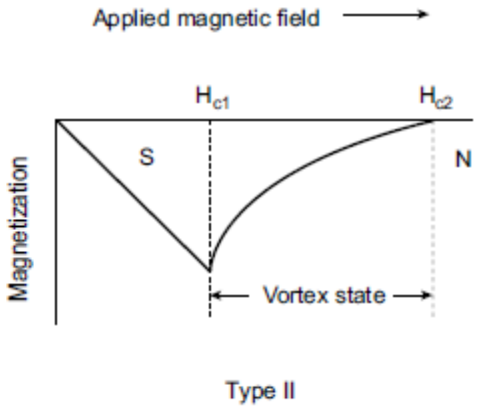

Figure 2.8 Transition to a superconducting state for Type II superconductors The flux starts to penetrate the specimen at a field H_{c1} and penetration is completed at H_{c2}. The material is in a vortex state between H_{c1} and H_{c2} and it can carry supercurrent up to H_{c2}. Above H_{c2} the material is a normal (N) conductor [27].

Another difference in Type I and Type II superconductors is in the main free path of the conduction electrons in the normal state. If the main free path is short, the coherence length (ξ) is short and the penetration depth (λ) is great. This is the situation when $\kappa = \frac{\lambda}{\xi} \rangle 1$, and the superconductor will be Type II as shown in Figure 2.9.

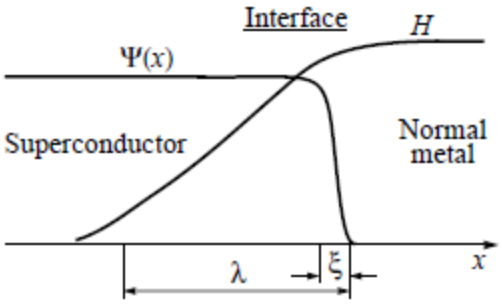

Figure 2.9 Spatial variations of the order parameter ψ and the magnetic field H in the vicinity of a superconductor-normal metal interface for k >>1 [29].

Critical fields for type II superconductors depend on the temperature. The dependence $H_c(T)$ is schematically shown in Fig. 2.10.

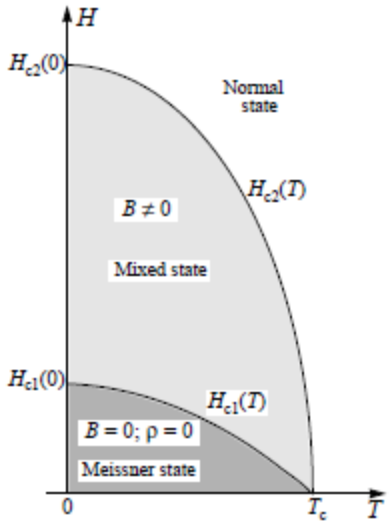

Figure 2.10 $H_{c1}(T)$ and $H_{c2}(T)$ dependences for a type-II superconductor, shown schematically [29].

2.11. London Theory

The Meissner effect could not be explained by any conventional model of electricity in solids. Electrical conduction in normal state of a metal is described by Ohm's law

$$J = \sigma E \tag{2.2}$$

We need to modify this drastically to describe conduction and the Meissner effect in the superconducting state. In 1935, a hypothesis was put forward by the brothers H. and F. London. In this model, there is a phenomenological description of the basic facts of superconductivity by proposing a scheme based on a two fluid type concept with super fluid and normal fluid densities n_s and n_n associated with velocities v_s and v_n. The average free electron densities n,

$$n = n_s + n_n \tag{2.3}$$

The two current densities satisfy

$$\frac{\partial J_s}{\partial t} = \frac{n_s e^2}{m} E \qquad (J_s = -en_s v_s) \tag{2.4}$$

$$J_n = \sigma_n E \qquad (J_n = -en_n v_n) \tag{2.5}$$

The first equation is nothing but the Newton equation for particles of charge -e and density n_s. The other London equation is

$$\nabla \Lambda J_s = -\frac{n_s e^2}{mc} B \tag{2.6}$$

From this equation the Meissner effect follows. We know from Maxwell's equations that,

$$\nabla \Lambda B = \frac{4\pi}{c} J_s \tag{2.7}$$

where we have neglected displacement currents and the normal fluid current. By taking the curl of this expression and using

$$\nabla \Lambda \nabla \Lambda B = -\nabla^2 B \tag{2.8}$$

in conjunction with Eq. (2.6) we get

$$\nabla^2 B = \frac{4\pi n_s e^2}{mc^2} B = \frac{1}{{\lambda_L}^2} B \tag{2.9}$$

Where λ_L is the penetration depth defined by

$$\lambda_L(T) = \left(\frac{mc^2}{4\pi n_s e^2} \right)^{1/2} \tag{2.10}$$

According to the Meissner effect, the internal magnetic field are excluded (B=0). The variable solution has the general form

$$B_{(x)} = B_0 \exp(-x/\lambda_L) \tag{2.11}$$

Which are known as the London equations and λ_L is also called the London penetration depth [45, 69].

2.12. Ginzburg-Landau Theory

The Ginzburg-Landau theory is an alternative to the London theory. In 1950, Ginzburg and Landau formulated their theory of superconductivity with using quantum mechanics. They assumed that the behavior of superconducting electrons may be described by an effective wave function as an order parameter. The wave function is related to the superfluid density by

$$n_s = |\psi(r)|^2 \tag{2.12}$$

Furthermore it was postulated a difference of free energy between the normal and the superconducting phase of the form

$$F_s(T) - F_n(T) = \int d^3r \left(-\frac{1}{2m^*}\psi^*(r)\left|(\nabla + ie^*A)\right|^2\psi(r) + \alpha(T)|\psi(r)|^2 + \frac{1}{2}\beta(T)|\psi(r)|^4 \right), \tag{2.13}$$

where m^* and e* were the effective mass and charge that in the microscopic theory turned out to be 2m and 2e respectively. One can look for a constant wave function minimizing the free energy. We find

$$\alpha(T)\psi + \beta(T)\psi|\psi|^2 = 0 \tag{2.14}$$

Giving

$$\psi^2 = -\frac{\alpha(T)}{\beta(T)} \tag{2.15}$$

And for the free energy density

$$f_s(T) - f_n(T) = -\frac{1}{2}\frac{\alpha^2(T)}{\beta(T)} = -\frac{{H_c}^2(T)}{8\pi} \tag{2.16}$$

Where the last equality follows,

$$n_s = |\psi^2| \approx \frac{1}{{\lambda_L}^2(T)} \tag{2.17}$$

We find

$$\frac{{\lambda_L}^2(0)}{{\lambda_L}^2(T)} = \frac{|\psi(T)|^2}{|\psi(0)|^2} = \frac{1}{n}|\psi(T)|^2 = -\frac{1}{n}\frac{\alpha(T)}{\beta(T)} \tag{2.18}$$

From equations (2.16) and (2.18) we get

$$n\alpha(T) = -\frac{{H_c}^2(T)}{4\pi}\frac{{\lambda_L}^2(T)}{{\lambda_L}^2(0)} \tag{2.19}$$

And

$$n^2\beta(T) = -\frac{{H_c}^2(T)}{4\pi}\frac{{\lambda_L}^2(T)}{{\lambda_L}^2(0)} \tag{2.20}$$

The equation of motion at zero electromagnetic field is

$$-\frac{1}{2m^*}\nabla^2\psi + \alpha(T)\psi + \beta(T)|\psi|^2\psi = 0 \tag{2.21}$$

We can look at solutions close to the constant one by defining $\psi = \psi_e + f$ where

$$|\psi_e|^2 = -\frac{\alpha(T)}{\beta(T)} \tag{2.22}$$

We find, at the lowest order in f

$$\frac{1}{4m^*|\alpha(T)|}\nabla^2 f - f = 0 \tag{2.23}$$

This shows an exponential decrease which we will write as

$$f \approx e^{-\sqrt{2r/\xi(T)}} \tag{2.24}$$

Where we have introduced the Ginzburg-Landau (GL) coherence length

$$\xi(T) = \frac{1}{\sqrt{2m^*|\alpha(T)|}} \tag{2.25}$$

Using the expression (2.16) for $\alpha(T)$ we have also

$$\xi(T) = \sqrt{\frac{2\pi n}{m^* H_c{}^2(T)}} \frac{\lambda_L(0)}{\lambda_L(T)} \tag{2.26}$$

Recalling that $(t = T/T_c)$

$$H_c(T) \approx (1-t^2), \qquad \lambda_L(T) \approx \frac{1}{(1-t^4)^{1/2}}, \tag{2.27}$$

We see that also the GL coherence length goes to infinity for $T \to T_c$

$$\xi(T) = \frac{1}{H_c(T)\lambda_L(T)} \approx \frac{1}{(1-t^2)^{1/2}} \tag{2.28}$$

It is possible to show that

$$\xi(T) \approx \frac{\xi_0}{(1-t^2)^{1/2}} \tag{2.29}$$

Therefore the GL coherence length is related but not the same as the Pippard's coherence length. A useful quantity is

$$\kappa = \frac{\lambda_L(T)}{\xi(T)} \tag{2.30}$$

where κ is characteristic length. When $\kappa < \frac{1}{\sqrt{2}}$ the superconductor will be Type I, when $\kappa > \frac{1}{\sqrt{2}}$ the superconductor will be Type II [45, 69].

2.13. The BCS Theory of Superconductivity

A theoretical explanation for superconductors was given based on the occurrence of electron pairs in the crystal lattice by Bardeen, Cooper and Schrieffer in 1957 [21, 32]. According to the theory which is called the BCS theory while electrons pass through a crystal lattice, the lattice is deformed by the electrons. This interaction causes to an attractive interaction between two electrons that is greater than their repulsive Coulomb interaction. Thus superelectrons occur as electron pairs which are called Cooper pairs. Superconductivity occurs via pairing of electron. The electron-lattice-electron interaction is shown in Figure 2.11.

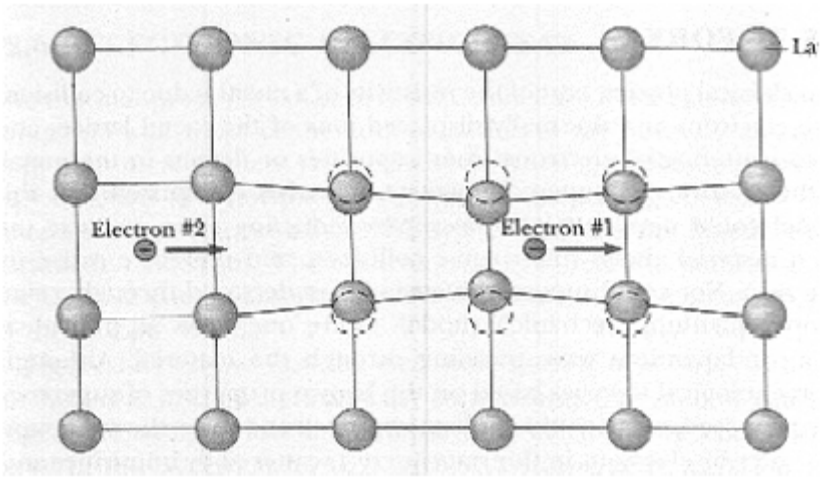

Figure 2.11 The electron-lattice-electron interaction [71].

The BCS theory contains five main ideas as follows;

1. An attractive interaction between electrons can lead to a ground state separated from excited state by an energy gap [5].

2. The electron-lattice-electron interaction leads to an energy gap of the observed magnitude [5].

3. The penetration depth and the coherence length emerge as natural consequences of the BCS theory [5].

4. The criterion for the transition temperature of an element or alloy involves the electron density of orbitals $D(\epsilon_F)$ of one spin at the Fermi level and the electron-lattice interaction U, which can be estimated from the electrical resistivity because the resistivity at room temperature is a measure of the electron-phonon interaction [5]. For $UD(\epsilon_F) \ll 1$ the BCS theory predicts

$$T_c = 1.14\theta \exp\left[\left(-1/UD(\epsilon_F)\right)\right] \tag{2.31}$$

Where θ is the Debye temperature and U is an attractive interaction.

5. Magnetic flux through a superconducting ring is quantized and the effective unit of charge is 2e rather than e [5].

2.14 Isotope Effect

Isotope effect has great significance because; it reveals the importance of the electron-phonon interaction for the Cooper pairing mechanism in superconductivity. Therefore it is evidence to support BCS theory. It has been observed that the critical temperature (T_c) of superconductors depends on the isotopic mass.

Isotope effect can be defined as,

$$\alpha = -\frac{d \ln T_c}{d \ln M} \approx -\left(\frac{M}{\Delta M}\right)\left(\frac{\Delta T_c}{T_c}\right) \tag{2.32}$$

Where α is the isotope effect coefficient, M is the atomic mass and T_c is the critical temperature. For the total isotope effect coefficient for the multiple component system is formulated as [41, 45]

$$\alpha_{total} = \sum \alpha_i = \sum \frac{-d \ln T_c}{d \ln M} \tag{2.33}$$

2.15 Josephson Tunneling

Josephson tunneling is demonstrated by Brain D. Josephson in 1962. This phenomenon is widely used in application of superconductivity. When two

superconductors separated by a thick insulating layer, we observe important effects associated with the tunneling of superconducting electron pairs from a superconductor through a layer of an insulator into another superconductor as shown in Figure 2.12.

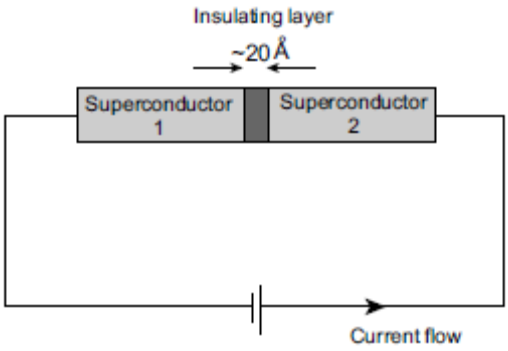

Figure 2.12 Josephson tunneling. The principle of an experiment to test Josephson's prediction about tunneling of Cooper pairs through an insulating junction between two superconductors [23].

The tunneling barrier is known as a weak link. Josephson effect can occur as three different types. The effects of pair tunneling include; DC Josephson effect, AC Josephson effect and macroscopic long-rage quantum interference. A DC current flows across the junction in the absence of any electric or magnetic field for DC Josephson effect. If a DC voltage applied across the junction causes rf current oscillations across the junction. This effect has been utilized in a precision determination of the value of ħ/e. This is known as AC Josephson effect. In third effect; A DC magnetic field applied through a superconducting circuit containing two junctions causes the maximum supercurrent to show interference effects as a function of magnetic field intensity [45].

2.16 Superconductor Systems

A lot of superconducting materials have been investigated by scientists since discovering of superconductivity. Generally, Superconducting materials divided in two groups which is known as Type I and Type II according to their behaviors in magnetic fields by A.A. Abrikosov in 1958 [11]. First group which is known as Type I superconductors includes pure metal and metalloids. The second group superconductors are mainly comprised of metallic compounds, alloys and metal-oxide ceramics and they called as oxide basis.

2.16.1 Metal and Metalloid Superconductors

The first studies about superconductivity were done with metal compounds by Heike Onnes in 1911 [1]. Two years later, tin and lead were observed to exhibit superconductivity at below 3.8 K and 7.2 K respectively [2]. Niobium loses their electrical resistance at below 9.2 K [37]. Some metals and metallic compound superconductors are given as a list in Table 2.1.

Table 2.1 Some metallic superconductors [4, 38].

SUPERCONDUCTORS	T_c (K)
MgB_2	39
Nb_3Ge	23.2
Nb_3Ga	20.3
Nb_3Al	18.9
Nb_3Sn	18.3
V_3Si	17.1
V_3Ga	15.4
Nb	9.25
Pb	7.196
La	4.88
Ta	4.47
Hg	4.15
Sn	3.72
In	3.41
Tl	2.38
Al	1.175
Ga	1.083
Mo	0.915
Ti	0.40

Also many additional elements can be passed into a superconductive state with the application of high pressure. All known elemental superconductors are showed as a periodic table in Table 2.2.

Table 2.2 Periodic table of superconducting elements [39].

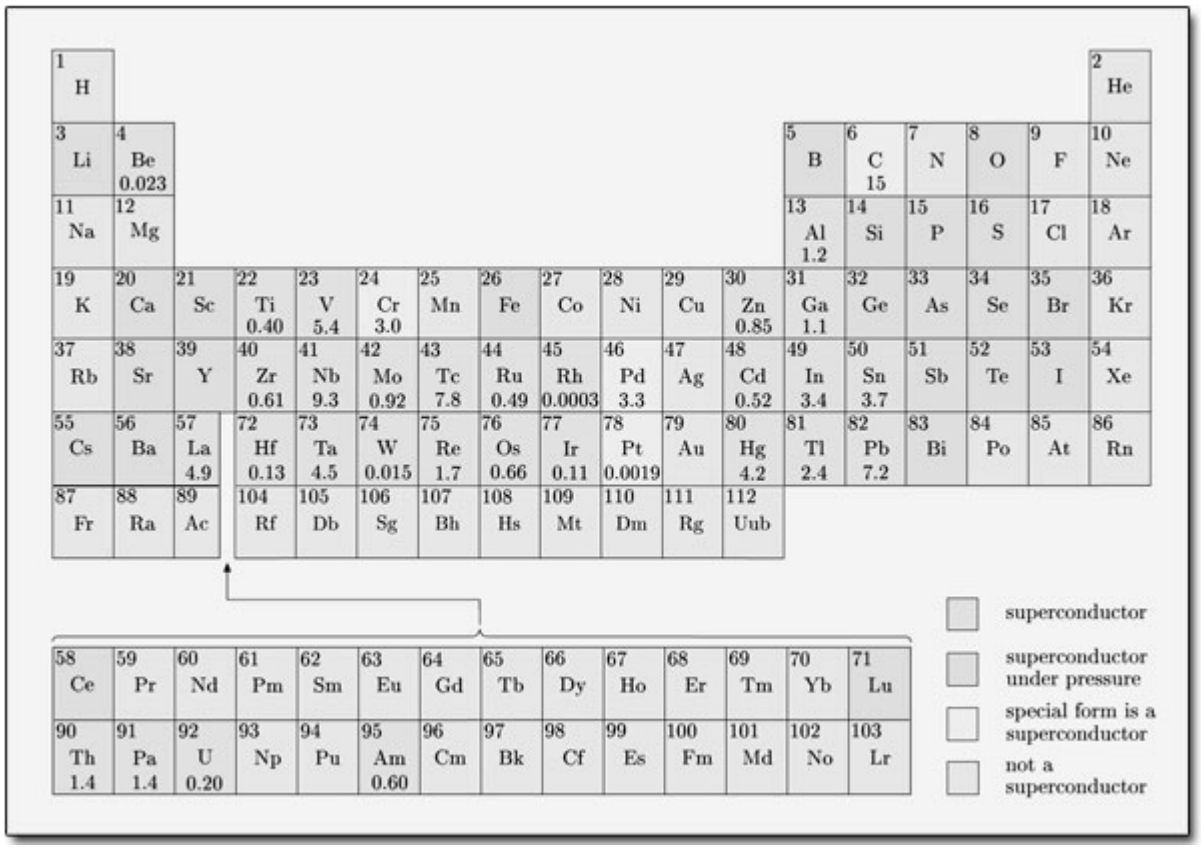

The most used low T_c superconductors are Nb-Ti and Nb_3Sn alloys. Their T_c values are 10.5 K and 18.3 K respectively [8]. In 1973, Nb_3Ge alloy observed to have superconductivity below 23.2 K [37]. Superconducting properties of MgB_2 is discovered by Akimitsu in 2001. MgB_2 superconductor has the highest T_c value (39 K) among intermetallic superconductors [16].

2.16.2 Oxide Basis and High-T_c Superconductor Systems

Type II superconductors are comprised of metallic compounds and alloys. Ceramic superconductors which are metal-oxide ceramics belong to the Type II category of superconductors. In 1986, a superconducting material LaBaCuO system

which has a transition temperature of 35 K discovered by K. A. Muller and J. G. Bednorz [22]. Then, bismuth-based which is known as BSCCO system and yttrium-based which is known as YBCO system superconductors discovered. BSCCO superconductors are comprised of bismuth, strontium, calcium, copper and oxygen and it can be synthesized in three different phases which is $Bi_2Sr_2CuO_x$ (Bi-2201), $Bi_2Sr_2CaCu_2O_x$ (Bi-2212) and $Bi_2Sr_2Ca_2Cu_3Ox$ (Bi-2223). YBCO superconductors are comprised of yttrium, barium and copper oxide. $Bi_2Sr_2Ca_2Cu_3O_x$ (Bi-2223) system has a 110 K T_c value among in the BSCCO system [8]. YBCO superconductor which is formulated as $YBa_2Cu_3O_7$ (Y123) loses electrical resistance below 93 K [13].

In 1988, Tl-Ca-Ba-Cu-O system synthesized with a T_c value of 120 K [8]. Another oxide superconductor system is the mercury based oxide superconductor. It is formulated as $HgBa_2Ca_2Cu_3O_8$ with a 133 K T_c value and discovered in 1993 [15].

Some High-T_c superconductors are given as a list in Table 2.3.

Table 2.3 Some High-T_c superconductors [8, 23, 41].

Formula	T_c (K)	Notations
$Bi_2Sr_2CuO_6$	0-20	Bi 2201
$Bi_2Sr_2CaCu_2O_8$	85	Bi 2212
$Bi_2Sr_2Ca_2Cu_3O_{10}$	110	Bi 2223
$YBa_2Cu_3O_7$	92	Y 123
$YBa_2Cu_4O_8$	80	Y 124
$Y_2Ba_4Cu_7O_{14}$	40	Y 247
$Tl_2Ba_2CuO_6$	0-80	Tl 2201
$Tl_2Ba_2CaCu_2O_8$	108	Tl 2212
$Tl_2Ba_2CaCu_3O_{10}$	125	Tl 2223
$TlBa_2CuO_5$	0-50	Tl 1201
$TlBa_2CaCu_2O_7$	80	Tl 1212
$TlBa_2Ca_2Cu_3O_9$	110	Tl 1223
$TlBa_2Ca_3Cu_4O_{11}$	122	Tl 1234
$HgBa_2CuO_{4+\&}$	94	Hg 1201
$HgBa_2CaCu_2O_{6+\&}$	127	Hg1212
$HgBa_2Ca_2Cu_3O_{8+\&}$	133	Hg 1223

CHAPTER 3

THE PROPERTIES OF MgB_2 SUPERCONDUCTORS

3.1. Introduction

Magnesium diboride (MgB_2) is a chemical compound which has been known to scientists since 1950s [24]. However, its superconducting properties discovered by Akimitsu in 2001 [16]. With announcement of superconductivity in MgB_2, a great interest on this subject began within the physics society and a lot of researches have focused to understand both the theoretical and the practical aspects of this new intermetallic superconductor.

In the past nine years, MgB_2 has been fabricated in various forms such as bulk samples, single crystals, thin films, tapes and wires [38]. A lot of research results have been published in different international journals. The main characteristic of MgB_2 is a relatively high critical temperature, simple crystal structure, high critical current density, large coherence length and transparency of grain boundaries to current flow. These properties of MgB_2 revealed that it is a promising candidate for superconductor industry.

3.2. Crystal and Electronic Structure of MgB_2

Magnesium diboride (MgB_2) intermetallic compound has a simple crystal structure. It has a hexagonal AlB_2 type crystal structure which is common among borides. Hexagonal structure possesses space group P6/mmm. It contains graphite type boron layers separated by hexagonal layers of magnesium [16, 38]. The structure of MgB_2 is shown in Figure 3.1.

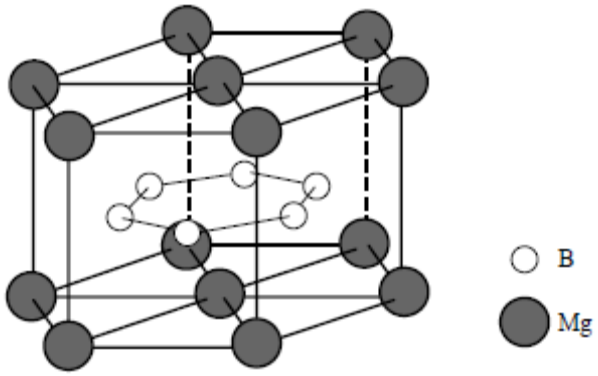

Figure 3.1 The structure of MgB_2 [26].

The lattice constants are reported as a=b= 3.0851 A° and c= 3.5201 A° [16, 38]. As seen in Figure 3.1 magnesium atoms are located at the centers of the boron hexagons. Each Mg atom donates its electron to the boron planes. Hence, MgB_2 shows a strong anisotropy in the B-B lengths. Also, the structure of MgB_2 similar to graphite and the distance between the boron planes is longer than B-B distance in the planes. The metallic B layers play an important role in the superconductivity of MgB_2 [28].

If the band structure of MgB_2 research, it gives sings of the substantial ionization of magnesium by completely transferring the electrons founding 3s orbital

to 2 dimensional boron planes [28, 38]. Therefore, covalent B-B bonds and ionic Mg-B bonds forms the hexagonal structure of MgB_2. 2p boron states have metallic character and determine the density of states at the Fermi energy [30].

3.3. Superconductivity Mechanism in MgB_2

After the discovery of superconductivity in MgB_2, scientist researched whether superconductivity of MgB_2 can be explained with BCS theory. Several experimental and theoretical studies have been done to explain superconductivity of MgB_2. It has been agreed upon that superconductivity mechanism in MgB_2 can be explained with BCS theory. According to this theory, high frequency phonons in the low atomic mass compounds produce a high T_c. Also MgB_2 seems to be a conventional BCS type superconductor according to band structure studies [31]. BCS theory assumes that the superconductivity occurs via pairing of electrons with attractive interaction between electrons sufficiently near to the Fermi surface and this interaction is mediated by phonons [32]. According to initial findings, there are some effects such as isotope effect, weak link, anisotropy and energy gap for explanation of superconducting mechanism in MgB_2.

3.3.1. Isotope Effect

The isotope effect of boron in MgB_2 superconductor is observed by Budko in 2001 [33]. Budko and his working group studied with ^{10}B and ^{11}B. They reported that the critical temperature varies from 40.2 K to 39.2 K as the average atomic mass of boron varies from 10 to 11 in MgB_2. They find the isotope effect coefficient as

α=0.28 for boron. The dependence of T_c on the isotopic mass reveals that electron-lattice interactions have a great importance on superconductivity mechanism. Hinks at al. measured the isotope effect both for Mg and B and they fond as α= 0.02 for Mg, α= 0.30 for B respectively. Also they reported that B atoms contribute more to the pairing mechanism in superconductivity of MgB_2 then Mg atoms do [34,47]. The total measured isotope effect coefficient of MgB_2 (α_t) is 0.32 and this value is smaller than 0.5 which is predicted by BCS theory. This value revealed that MgB_2 is a special material among all superconducting materials and it is a BCS type superconductor. The reducing of isotope effect coefficient explained with strong coulomb repulsion [35] and large anharmonicity of Boron vibrations [36]. The isotope effect of MgB_2 is illustrated in Figure 3.2.

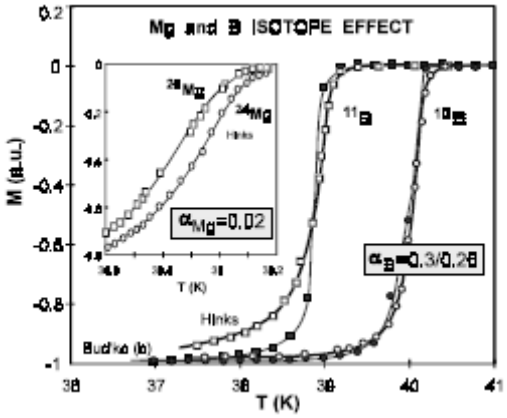

Figure 3.2 The isotope effect of MgB_2 [81].

3.3.2. Anisotropy

Because of the layered structure of some superconductors, electrons move easily in some directions and with difficultly in others. This gives rise to the property known as anisotropy [92]. Some superconducting parameters are different along

different directions within the crystal structure. Anisotropy of MgB_2 is important not only for basic understanding of this material but also practical applications, strongly affecting the pinning, thus the critical currents. The anisotropy of one material can be estimated on aligned powders, epitaxial films and single crystals [72,74]. Many groups have been measured anisotropy of MgB_2 by different methods [31,55,73]. The anisotropy factor γ can be written as

$$\gamma = \frac{\xi_{ab}}{\xi_c} = \frac{\lambda_c}{\lambda_{ab}} = \frac{H_{c2}^{\text{II}ab}}{H_{c2}^{\text{II}c}} \tag{3.1}$$

The anisotropy factor of MgB_2 powders is determined as γ=6-7 by Bud' ko et. all [38,74].

3.3.3. Absence of Weak Links

Many measurements have been done showing the absence of weak links in MgB_2 [38,77,78,81]. MgB_2 does not exhibit weak link electromagnetic behaviour at grain boundaries [77]. Dhalle [78] and Kim [81] reported that the transport measurements in high magnetic fields of dense bulk samples yields very similar J_c values as the inductive measurements. This means that the inductive current flows coherently throughout the sample, unaffected by grain boundaries. As a result the flux motion will determine J_c dependence on field and temperature [38]. The absence of weak links in MgB_2 is illustrated in Figure 3.3.

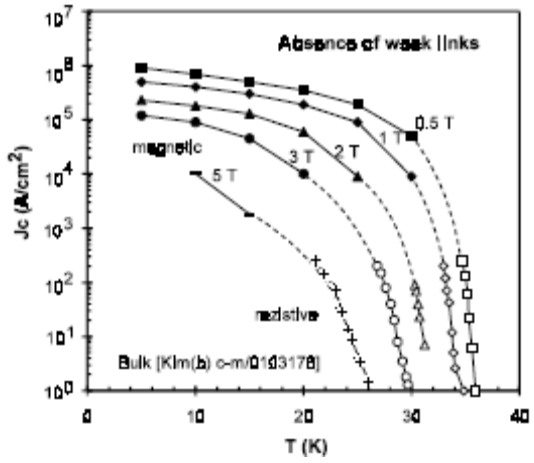

Figure 3.3 The absence of weak links in MgB_2 [81].

3.3.4. Coherence Lengths

The coherence length is one of the main parameters of superconductivity. It depends on purity of superconducting material. The size of a cooper pair in a superconductor is known as the coherence length. The coherence lengths values for MgB_2 superconductor determines along ab plane and c-axis. Different forms of MgB_2 have different coherence lengths values. The coherence lengths values along the ab-plane range between $\xi_{ab}(0)$= 3.7-12.8 nm and along c-axis between $\xi_c(0)$= 1.6-5.0 nm [38]. The coherence lengths values are showed in Table 3.1 for different form of MgB_2 superconductor.

Table 3.1 The coherence lengths values of MgB_2 superconductor [38].

Form	$\xi_{ab}(0)$ [nm]	$\xi_c(0)$ [nm]
Textured Bulk	5.5	5.0
Aligned Crystallites	6.5-7.0	4.0-4.1
Films	3.7-5.0	2.0-3.0
Single Crystals	6.1-6.5	2.5-3.7
Powders	11.4-12.8	1.6-1.7

3.3.5. Two-Gap Superconductivity of MgB_2

Energy gap values of the MgB_2 can be calculated using different methods. These methods are tunneling spectroscopy, point contact tunneling, specific heat studies, high-resolution photoemission spectroscopy (HRPS), far-infrared transmission studies (FIRT) and Raman spectroscopy [38]. Spectroscopic techniques are usually used for investigation of energy gaps in superconductors [31]. Many measurements have been done about energy gaps in MgB_2 [31,38,79]. According to measurements, there is evidence of two distinct gaps associated with the two separate segments of the Fermi surface [38,80]. The width values of these two gaps were determined to be between 1.8-3 meV for the small 3D weakly coupled gap and between 5.8-7.7 meV for the large strongly coupled gap [38].

3.4. Fabrication of MgB_2 Wire and Tape Superconductors

After the discovering of MgB_2's superconductivity, many scientists have investigated the superconducting properties of MgB_2, theoretical approaches and practical applications of MgB_2. MgB_2 material has a lot of advantages such as; high

T_c value, simple structure, light weight, absence of weak-link, high abundance of Mg and B, low anisotropy, the large coherence length and high J_c value [38,46,47]. These properties make it a good candidate for the practical applications. MgB_2 compound can fabricate in various forms that they are wires, tapes, bulk samples, single crystals and thin films [49-55]. Today, the importance of superconducting materials increases for industrial applications such as power lines, motors, generators and superconducting cables [48]. MgB_2 material must be in the form of flexible wires or tapes for the applications. Many studies have been performed to produce superconducting materials [48-55,66]. Several research groups have fabricated MgB_2 wires or tapes using powder-in-tube (PIT) methods [50-55]. There are two kinds of processes for manufacturing MgB_2 wires or tapes using PIT method, they are known as ex-situ and in-situ methods [51].

3.4.1. Powder in Tube (PIT) Method

The powder-in-tube (PIT) method is the most popular process for fabrication of good quality wires or tapes [52]. MgB_2 wires and tapes have been fabricated successfully by using the PIT method. The PIT method is very attractive for practical applications since the fabrication process has no heat treatment and low production cost [50-56]. There are two different processes for manufacturing MgB_2 wires and tapes using PIT method.

3.4.1.1. Ex-situ PIT Method

In the ex-situ method, fabrication of MgB_2 wires and tapes are made by using MgB_2 reacted powder which is available commercially [50-55]. Firstly, MgB_2 reacted powder is filled in metallic tubes. The filling must be in an inert atmosphere in order to prevent oxidation of MgB_2 powder. Than the metallic tubes are drawn or rolled into wires or tapes. Finally, heat treatment of wires or tapes is done in vacuum or inert atmosphere [55]. Generally ex situ process is more useful for obtaining highly dense and homogeneous MgB_2 wires and tapes. For this reason, the high critical current density J_c can be expected for ex situ MgB_2 conductors. But superconducting properties of ex situ MgB_2 conductors are strongly affected by the characteristic of MgB_2 powder. In ex situ PIT method, properties of MgB_2 powder are very important for fabrication of good quality MgB_2 wires and tapes. The ex situ method has some disadvantages compared to the in situ method since the filling powder is already reacted, the sinterability is poor and doping of impurities is not very effective.

In this method, high transport J_c values reported without any heat treatment [56]. The observation of high J_c without any heat treatment is very attractive because a fabrication process without any heat treatment leads to much reduction of manufacturing time and costs for wires and tapes. But a suitable heat treatment step will improve the J_c value significantly [50, 55]. The schematic representation of ex situ PIT method is observed in Figure 3.4.

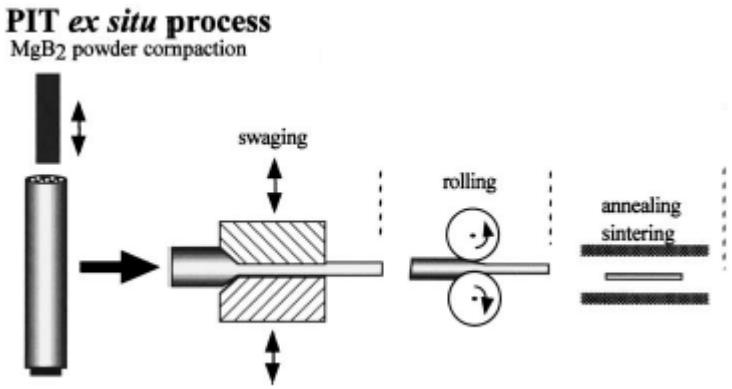

Figure 3.4 The schematic representation of ex situ PIT method [57].

3.4.1.2. In-situ PIT Method

In the in-situ method, stoichiometric compositions of Mg and B powder are filled in metallic tubes and than the metallic tubes are drawn or rolled into wires or tapes. Than performs heat treatment on wires or tapes [58]. Several research groups have prepared MgB_2 wires and tapes using in situ PIT method [50,55,58-62]. However, fabrication of MgB_2 wires or tapes which have the high critical current density J_c are difficult by using mixture of Mg and B powder. Because Mg powder can be oxidizing, many voids can occur after heat treatment. Moreover the voids after heat treatment interrupt connectivity between MgB_2 grains. Before heat treatment Mg and B powders must be mixed in vacuum or oxygen protective environment to prevent these disadvantages. Also, choosing of the metallic sheath is important because it has to play the role of a diffusion barrier for the volatile and reactive Mg. Sheath materials must be chemically compatible with the MgB_2 and should not degrade the superconductivity. The sheath metal must have adequate hardness to give mechanical support to the brittle superconducting core. Various sheath materials such as Cu, Ni, Ag, Fe, Nb, Ta, Ti, and some alloys like SS, Cu-Ni

have been tried for MgB_2 wires and tapes [61,62,76]. For most of the practical applications Fe, Ni, SS or Cu with a suitable barrier sheathed conductors are most suited [62,76]. An illustration of the in situ PIT process is given in Figure 3.5.

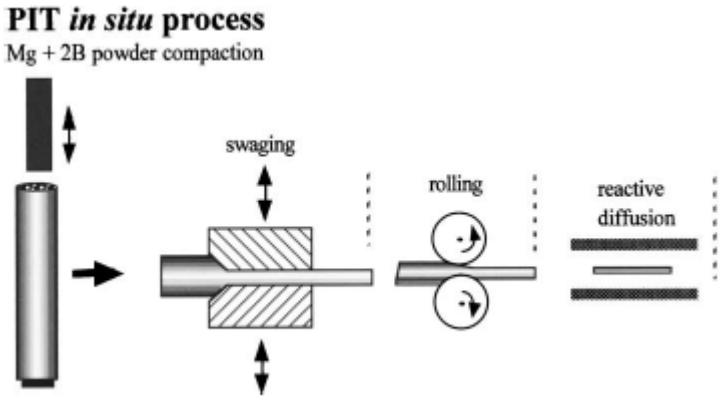

Figure 3.5 The schematic representation of in situ PIT method [57].

3.4.2. Continuous Tube Forming and Filling (CTFF) Method

Hyper Tech Research developed a modified PIT process which is called the Continuous Tube Forming and Filling (CTFF) for low cost continuous production of MgB_2 wires [64]. In the method, precursor MgB_2 powder is dispensed onto a strip of metal as it is being continuously formed into a tube. This process results in an overlap closed tube filled with powder in continuous lengths. CTFF is an alternative process for MgB_2 wires fabrication. CTFF is essentially an in situ PIT method without the long mechanical or thermo mechanical processes [65]. In this method, along the wire homogeneity is better than PIT method and there is no limit on the length of wire produced. Studies have been continuous for fabrication of superconducting wires and tapes which have high J_c values using the CTFF process. The schematic representation of the CTFF method is observed in Figure 3.6.

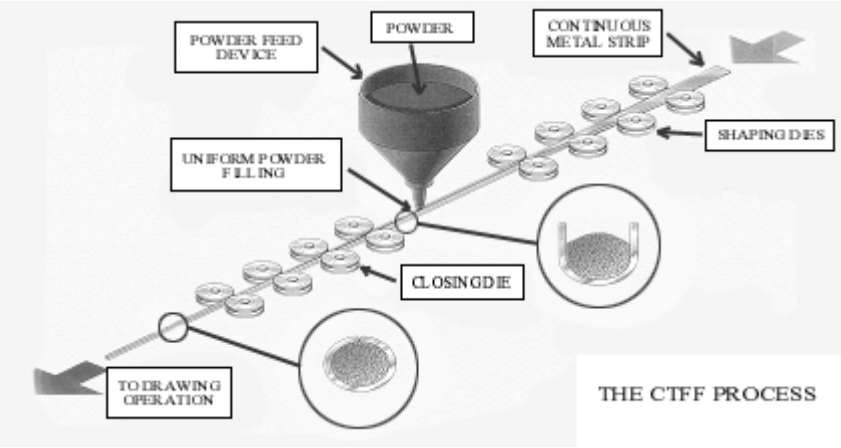

Figure 3.6 The schematic representation of the CTFF method [65].

3.4.3. Mg Diffusion Method

One of the methods to fabrication of MgB_2 wires is the diffusion method. In this method, pure Mg rods are placed at the center of a metal tube and the space between the Mg and the metal tube is filled with B powder. Than, heat treatment is applied at 800-900°C. During heat treatment Mg diffuses into boron material and converts to MgB_2 form [55,63]. Mg diffusion method is quite easy method that commercially available boron material can be converted into superconducting MgB_2 wires. The phase homogeneity of the conductors produced by diffusion is poor and the method is suitable for short samples. A schematic illustration of the internal Mg diffusion method is shown in Figure 3.7.

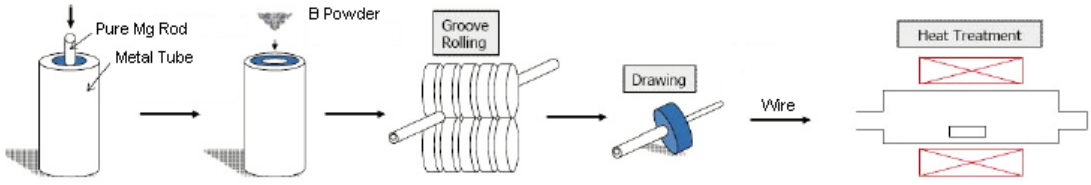

Figure 3.7 The schematic illustration of the MgB_2/Metal tube composite wire fabrication process by the internal Mg diffusion method [63].

3.5. Fabrication of Bulk MgB_2 Superconductors

After the discovery of superconductivity in MgB_2, scientists have been investigated many methods to obtain MgB_2. Fabrication of good quality MgB_2 superconductor is very important because it has wide electronics applications such as superconducting cables, motors, generators and magnetic resonance imaging (MRI). Although there are many methods to fabrication of MgB_2, all of them are mainly based on the solid state reaction of B and Mg atoms. Many groups have focused on to obtain MgB_2 as bulk, tape and thin film forms [14,75,82-88]. Fabrication of bulk MgB_2 is foremost due to its easier preparation compared with other forms of MgB_2.

MgB_2 bulks can be fabricated by two different methods which are called ex-situ and in-situ. In the first method, commercial MgB_2 powder is pressed into pellets and sintered at high temperature with normal or high pressure. In the second method, Mg and B powders are mixed together. The mixed powders are pressed into pellets and sintered under normal or high pressure.

3.6. Fabrication of Thin Film MgB_2 Superconductor

One of the fabrication methods for MgB_2 superconductor is thin film making. Many groups have attempted to prepare MgB_2 thin films. However, there are some difficulties such as high volatility of Mg, the high sensitivity of Mg to oxidation and fragility of MgB_2. MgB_2 thin films have been prepared using the different techniques such as Pulsed laser deposition (PLD), chemical vaporization, deposition of compound, Mg diffusion and magnetron plating [67].

Appropriate substrate selection is important in fabrication of MgB_2 thin film. Substrate must have good surface quality, better lattice matching and less reaction with the superconductor film. Different substrates have been used for the deposition of MgB_2 thin films. Some substrate materials have been reported as Si, SiC, SiO_2, MgO, Al_2O_3, $SrTiO_3$ and $LaAlO_3$ [68,89-91].

CHAPTER 4

EXPERIMENTAL METHOD

4.1. Fabrication of Superconducting MgB_2 Wires and Tapes

There are a number of different methods for the fabrication of superconducting MgB_2 wires and tapes, which are the powder-in-tube (PIT) method, CTFF (Continuous Tube Forming and Filling) method, and Mg diffusion method.

The PIT method is the most common fabrication technique for MgB_2 wires and tapes [50]. Superconducting monofilament and multifilament MgB_2 wires and tapes were fabricated by the PIT method and CTFF method, following the ex situ and mixture of ex situ and in situ reaction routes.

4.1.1. MgB_2/Ag Monofilament Wire Production

We have fabricated superconducting MgB_2/Ag monofilament wire by ex-situ PIT method using Ag-sheath.

One end of silver tube which is 16.8 cm in length, 6.35 mm outer diameter and a wall thickness of 1 mm was closed by groove rolling machine (Figure 4.1a and 4.1b) and this tube was heat treated at 900^{o}C under argon (Ar) gas atmosphere for 30 minutes in order to remove the work hardening and cooled down to room

temperature in the furnace. The heating and cooling rates were chosen to be $5^{o}C\ min^{-1}$.

(a) (b)

Figure 4.1 (a) One of the open ends sealed empty silver tube with an outer diameter of 6.35 mm (for the MgB_2/Ag monofilament wire production) **(b)** Groove rolling machine.

Commercially available MgB_2 superconductor powder (Cerac Co., -100 mesh, 99%) was tightly packed into a silver (Ag) (99.95%) tube which is 16.8 cm in length, 6.35 mm outer diameter and a wall thickness of 1 mm. This packing process was carried out in the air atmosphere. The remaining open end was closed by a silver plug. The tightly packed MgB_2/Ag composite tube was cold drawn into 1.96 mm diameter wire by wire drawing machine (Table 4.1). The wire drawing machine which has a length of 4 m and drawing dies are shown in Figure 4.2a and Figure 4.2b respectively.

(a)

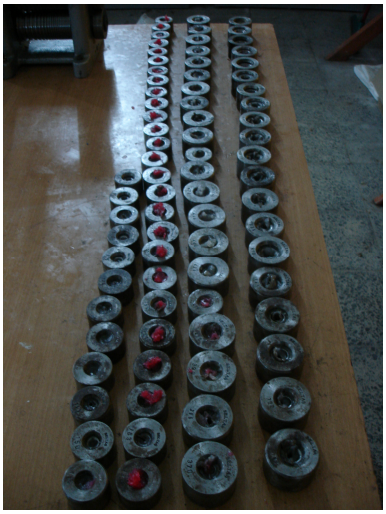

(b)

Figure 4.2 (a) Wire drawing machine. **(b)** Drawing dies.

Table 4.1 Diameters and lengths of the MgB_2/Ag monofilament wire (first fabrication).

Diameter of die (mm)	Length of wire (cm)	Diameter of wire (mm)
6.00	18.7	6.00
5.65	20.2	5.61
5.30	23.7	5.23
5.00	26.5	4.91
4.70	29.6	4.63

Table 4.1 (cont.)

4.40	33.9	4.34
4.15	36.4	4.14
3.90	42.0	3.83
3.70	45.6	3.67
3.45	52.1	3.39
3.25	58.4	3.23
3.05	65.5	3.01
2.85	76.7	2.75
2.70	30.4	2.68
2.55	33.2	2.55
2.40	37.8	2.34
2.25	41.5	2.23
2.10	47.6	2.06
2.00	52.6	1.96

Then composite wire was heat treated at 550ºC for 20 minutes in argon atmosphere. The heating rate of the temperature was chosen to be 20^{o}C min^{-1} and the cooling rate of the temperature was chosen to be 3^{o}C min^{-1}. The MgB_2/Ag monofilament wire which is 52.6 cm in length, 1.96 mm outer diameter is shown in Figure 4.3.

Figure 4.3 The MgB_2/Ag monofilament wire (first fabrication).

4.1.2. MgB_2/Ag/Fe 23 Filament Wire Production

We fabricated superconducting MgB_2/Ag monofilament wire by in-situ and ex-situ PIT method in Ag-sheath in order to fabricate MgB_2/Ag/Fe multifilament wire.

4.1.2.1. MgB_2/Ag Monofilament Wire Production

Firstly, Magnesium (Mg) powder (Alfa Aesar 99.8%), Boron (B) powder (Alfa Aesar 99%) and commercial MgB_2 powder (Cerac Co. 99%) were mixed in a stoichiometric ratio of MgB_2. This process was done by ball milling apparatus in an air atmosphere for three days. Later, one end of a silver tube 25 cm in length was closed by a silver wire and this tube was heat treated at 900^{o}C under argon (Ar) gas atmosphere for 30 minutes in order to remove the work hardening. Later, MgB_2 superconductor powder was tightly packed into this Ag-tube which is 25 cm in length, 6.35 mm outer diameter and a wall thickness of 1 mm. This packing process was carried out in an air atmosphere. The other end of silver tube was closed by silver plug and then the tightly packed MgB_2/Ag composite was cold drawn into 1.62 mm diameter wire by drawing (Table 4.2).

Table 4.2 Diameters and lengths of the MgB_2/Ag monofilament wire (second fabrication).

Diameter of die (mm)	Length of wire (cm)	Diameter of wire (mm)
6.00	31.1	5.90
5.80	34.1	5.71
5.65	35.0	5.58

Table 4.2 (cont.)

5.50	38.6	5.41
5.30	40.4	5.21
5.15	42.0	5.06
5.00	44.1	4.88
4.85	46.3	4.79
4.70	49.1	4.60
4.55	51.5	4.47
4.40	54.8	4.29
4.25	57.6	4.21
4.15	59.5	4.09
4.00	64.0	3.94
3.90	66.2	3.82
3.80	68.6	3.73
3.70	70.8	3.64
3.55	79.8	3.48
3.45	83.3	3.37
3.35	88.7	3.27
3.25	92.7	3.18
3.15	97.8	3.09
3.05	104.5	2.99
2.95	111.6	2.89
2.85	122	2.76
2.75	135	2.67
2.70	136.6	2.65
2.60	148.4	2.53
2.55	150.2	2.50
2.50	158.2	2.43
2.40	172.1	2.31

Table 4.2 (cont.)

2.30	185.8	2.24
2.25	191.2	2.21
2.15	213.2	2.09
2.10	218.4	2.03
2.00	244.9	1.91
1.90	275.2	1.82
1.85	280.1	1.77
1.80	291.6	1.73
1.70	324.6	1.62

At this stage, the wire 324.6 cm in length was cut into two pieces 166.4 cm in length and 158.2 cm in length due to length of the wire drawing machine. Then, we continued drawing procedure.

For the first wire;

Table 4.3 Diameters and lengths of the MgB_2/Ag monofilament wire (third fabrication).

Diameter of die (mm)	Length of wire (cm)	Diameter of wire (mm)
1.65	186.2	1.56
1.63	186.3	1.55
1.60	194.2	1.52
1.55	183.4	1.48
1.50	190.2	1.46
1.45	206.8	1.37
1.40	218.2	1.37
1.35	237.5	1.32
1.30	255.7	1.26

Table 4.3 (cont.)

1.25	271.6	1.21
1.20	236.8	1.15
	61.5	
1.15	244.5	1.13
	62.0	

For the second wire;

Table 4.4 Diameters and lengths of the MgB_2/Ag monofilament wire (fourth fabrication).

Diameter of die (mm)	Length of wire (cm)	Diameter of wire (mm)
1.65	160.5	1.58
1.63	160.7	1.57
1.60	170.1	1.55
1.55	181.7	1.49
1.50	191.4	1.45
1.45	205.3	1.38
1.40	215.8	1.33
1.35	236.4	1.29
1.30	252.6	1.25
1.25	265.5	1.20
1.20	300.6	1.13
1.15	309.7	1.10

At the end of wire drawing procedure, we have fabricated superconducting MgB_2/Ag monofilament wire with three pieces 1.10 mm outer diameter, 309.7 cm in length and 1.13 mm outer diameter, 244.5 cm and 62.0 cm in length. The total length of the wires reached to 616.2 cm from the initial length of 25 cm. The MgB_2/Ag monofilament wires are shown in Figure 4.4

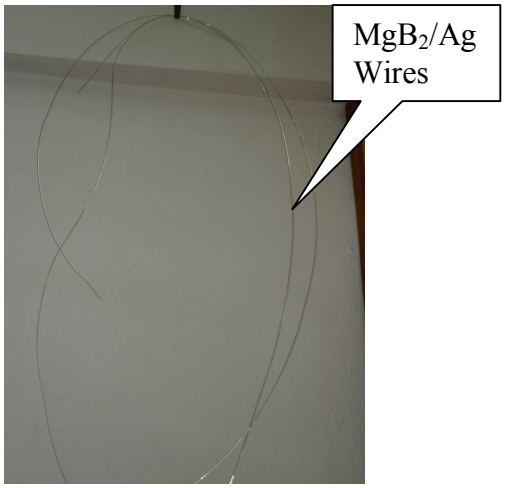

Figure 4.4 The MgB_2/Ag monofilament wires (second, third and fourth fabrications).

During the wire drawing procedures, the end of the wire broke off for some diameters. Breaking of the wire during drawing process was prevented by decreasing the speed of wire drawing machine. Then, we have fabricated superconducting MgB_2/Ag/Fe multifilament wire by PIT method using Fe-sheath.

4.1.2.2. MgB_2/Ag/Fe 23 Filament Wire Production

One end of iron tube which is 25 cm in length, 10.6 mm outer diameter and a wall thickness of 0.3 mm was closed by groove rolling machine and this tube was heat treated at 800^{o}C under argon (Ar) gas atmosphere for 2 hours in order to remove the work hardening and cooled down to room temperature in the furnace. Inert atmosphere procedure was carried out in order to prevent oxidation of the iron tube during heat treatment. The heating and cooling rates were chosen to be 5^{o}C min^{-1}. Then 23 pieces of MgB_2/Ag wires 1.10 mm outer diameters and 24 pieces of Cu wires 1.05 mm outer diameters and one piece of Cu wire 1.95 mm outer diameter

were inserted into the iron tube of outer diameter 10.6 mm and a wall thickness of 0.3 mm with a homogeneous distribution (Figure 4.5a, Figure 4.5b) in air.

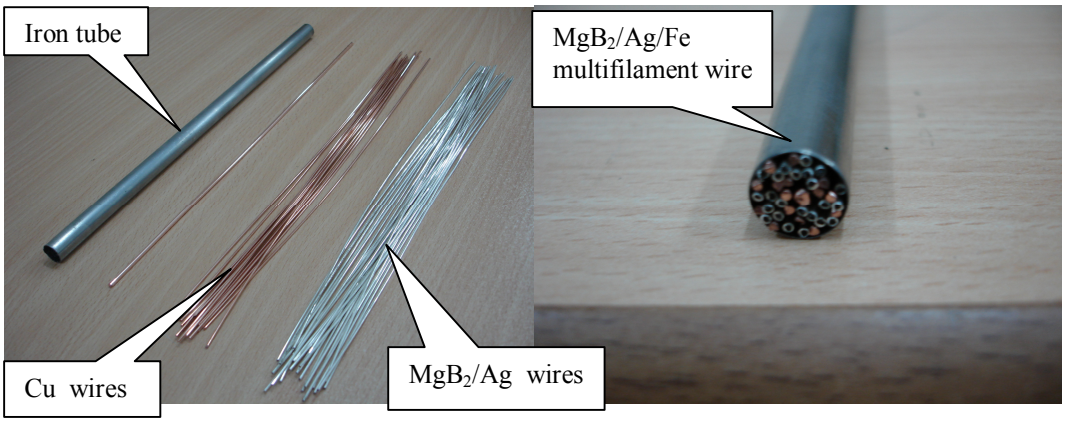

Figure 4.5 (a) MgB_2/Ag, Cu wires and Fe tube. (b) MgB_2/Ag/Fe 23 filament wire.

After insertion, the open end of iron tube was closed by groove rolling and then MgB_2/Ag/Fe composite tube was heat treated at 500ºC under argon (Ar) gas atmosphere for 2 hours in order to remove the work hardening and the cooled down to room temperature in the furnace. The heating and cooling rates were chosen to be $5^oC\ min^{-1}$. The MgB_2/Ag/Fe composite tube was cold drawn into 3.04 mm diameter wire by drawing (Table 4.5). During the wire drawing procedure the MgB_2/Ag/Fe composite tube was heat treated at 600^{o}C under argon (Ar) gas atmosphere for 3 hours for every two steps of wire drawing in order to remove the work hardening of MgB_2/Ag/Fe composite.

Table 4.5 Diameters and lengths of the MgB_2/Ag/Fe 23 filament wire.

Diameter of die (mm)	Length of wire (cm)	Diameter of wire (mm)
10.65	22.9	10.57
10.30	23.1	10.25
10.00	23.5	9.93

Table 4.5 (cont.)

9.70	24.1	9.69
9.40	24.3	9.37
9.10	24.7	9.09
8.85	24.1	8.83
8.60	25.5	8.56
8.35	25.6	8.34
8.10	24.4	8.09
7.85	25.7	7.84
7.60	26.7	7.58
7.40	28.6	7.37
7.20	28.4	7.16
7.00	29.8	6.98
6.80	31.0	6.76
6.60	32.3	6.56
6.40	33.6	6.38
6.20	35.6	6.19
6.00	39.0	5.97
5.80	40.7	5.78
5.65	42.1	5.65
5.50	44.6	5.48
5.30	47.2	5.28
5.15	51.1	5.11
5.00	53.7	4.94
4.85	55.4	4.84
4.70	60.9	4.65
4.55	63.8	4.52
4.40	69.4	4.32
4.25	72.7	4.20

Table 4.5 (cont.)

4.15	75.5	4.10
4.00	76.9	3.94
3.90	81.2	3.85
3.80	84.9	3.75
3.70	88.9	3.67
3.55	98.2	3.50
3.45	100.5	3.40
3.35	108.0	3.29
3.25	113.1	3.20
3.15	108.0	3.15
3.05	116.4	3.04

At the end of wire drawing procedure we have fabricated MgB_2/Ag/Fe 23 filament wire which is 116.4 cm in length, 3.04 mm outer diameter is shown in Figure 4.6.

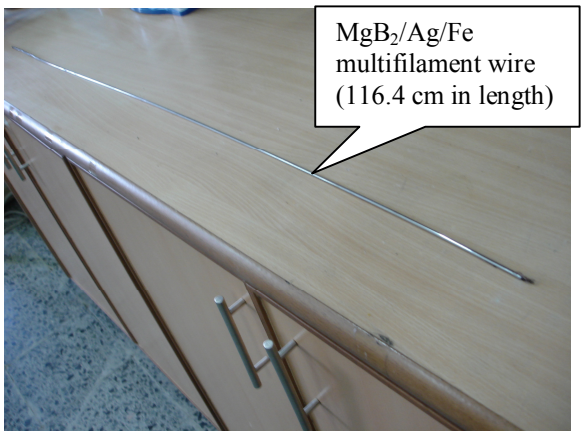

Figure 4.6 MgB_2/Ag/Fe 23 filament wire.

4.1.3. MgB_2/Ag/Fe 23 Filament Tape Production

The MgB_2/Ag/Fe multifilament wire was cut into two pieces in air. The first piece was 57.3 cm in length and the second piece was 55.5 cm in length. The second piece was rolled by the rolling machine once (Figure 4.8). We got MgB_2/Ag/Fe tape of 61.7 cm length, 0.77 mm thickness and 8.73 mm width (Figure 4.7)

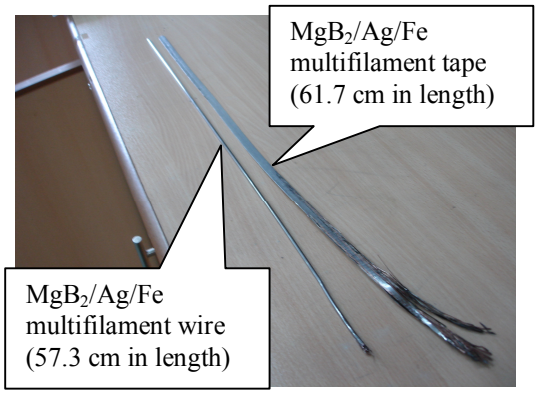

Figure 4.7 MgB_2/Ag/Fe 23 filament tape.

Figure 4.8 Rolling machine.

4.1.4. MgB_2/SS Monofilament Wire Production

With the support of National Boron Research Institute for our project called ‘‘Bor Esaslı Alaşımların Üretimi, Sentezi, Manyetik Karakterizasyonu ve Teknolojik Uygulamalar için Kalıcı Mıknatıs ve Prototip Kablo Yapımı’’ the CTFF (Continuous Tube Forming and Filling) machine has been built domestically (Figure 4.9).

In this method, wire begins with a metal tape that is formed into a tube while being filled continuously with MgB_2 powder. Initially, stainless steel tape is deformed in U shape then MgB_2 powder was filled in. Then this tape is further deformed in the form of tube. Another stainless steel tape is bent over the first tube. Meeting edges of tapes are arranged at opposite side to prevent MgB_2 powder from spilling.

At the end of CTFF process we have fabricated superconducting MgB_2/SS monofilament wire with eight pieces 3.67 mm outer diameter (Figure 4.10). The wires were cut in 50 cm long samples in air, and then both ends of the wire samples were mechanically sealed.

Figure 4.9 CTFF (Continuous Tube Forming and Filling) machine.

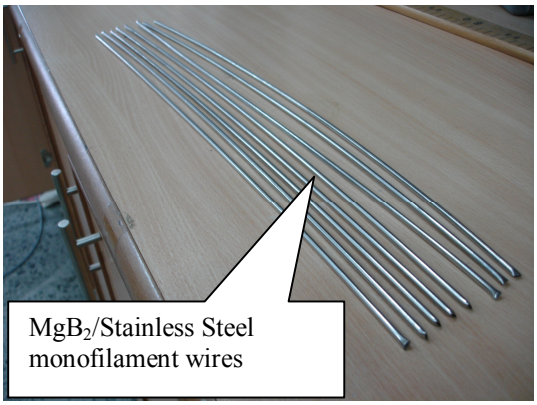

Figure 4.10 MgB_2/SS monofilament wires.

Diameters of these wires which were fabricated by CTFF method using stainless steel-sheath were reduced by the wire drawing machine. Then, we have fabricated superconducting MgB_2/Stainless Steel/Cu multifilament wire by powder-in-tube (PIT) method using copper-sheath.

4.1.5. MgB_2/SS/Cu 6 Filament Wire Production

Diameters of wires which were fabricated by CTFF method using stainless steel-sheath were reduced (Table 4.6, Table 4.7, Table 4.8) by the wire drawing machine. During the wire drawing procedure MgB_2/Stainless Steel monofilament wires of 2.55 mm outer diameters were heat treated at 630^{o}C for 1 hour one time for every all steps of wire drawing in order to remove the work hardening (MgB_2/SS) under argon (Ar) gas atmosphere and the cooled down to room temperature in the furnace. The heating and cooling rates of the temperature were chosen to be 5^{o}C min^{-1}.

For the first wire;

Table 4.6 Diameters and lengths of the MgB_2/SS monofilament wire (first fabrication).

Diameter of die (mm)	Length of wire (cm)	Diameter of wire (mm)
3.55	50.5	3.53
3.45	51.1	3.43
3.35	53.0	3.33
3.25	55.2	3.24
3.15	56.9	3.13
3.05	58.8	3.02
2.95	60.4	2.93
2.85	59.4	2.80
2.75	58.9	2.74
2.70	59.6	2.70
2.60	63.7	2.60
2.55	64.7	2.55

For the second wire;

Table 4.7 Diameters and lengths of the MgB_2/SS monofilament wire (second fabrication).

Diameter of die (mm)	Length of wire (cm)	Diameter of wire (mm)
3.55	49.7	3.54
3.45	50.6	3.43
3.35	52.3	3.32
3.25	53.4	3.23
3.15	54.8	3.14
3.05	56.3	3.04
2.95	58.8	2.95

Table 4.7 (cont.)

2.85	64.8	2.83
2.75	69.2	2.73
2.70	70.2	2.70
2.60	74.3	2.59
2.55	75.6	2.55

For the third wire;

Table 4.8 Diameters and lengths of the third wire Diameters and lengths of the MgB_2/SS monofilament wire (third fabrication).

Diameter of die (mm)	Length of wire (cm)	Diameter of wire (mm)
3.55	50.9	3.55
3.45	51.6	3.45
3.35	55.0	3.36
3.25	56.4	3.25
3.15	58.5	3.15
3.05	61.6	3.04
2.95	65.4	2.94
2.85	73.3	2.83
2.75	78.7	2.75
2.70	79.9	2.70
2.60	85.7	2.60
2.55	86.9	2.55

Then, copper tube 25 cm in length, 10 mm outer diameter and a wall thickness of 1 mm was heat treated at 800^0C for 1 hour in order to remove the work hardening. The annealing was performed under argon (Ar) gas atmosphere. The

heating and cooling rates of the temperature were chosen to be 5°C min^{-1}. Then 6 pieces of MgB_2/SS monofilament wires 2.55 mm outer diameters, 20 cm in length and one piece of Cu wire 2.70 mm in diameter, 20 cm in length were inserted into the copper tube 25 cm in length, 10 mm outer diameter and a wall thickness of 1 mm (Figure 4.11) in an air atmosphere.

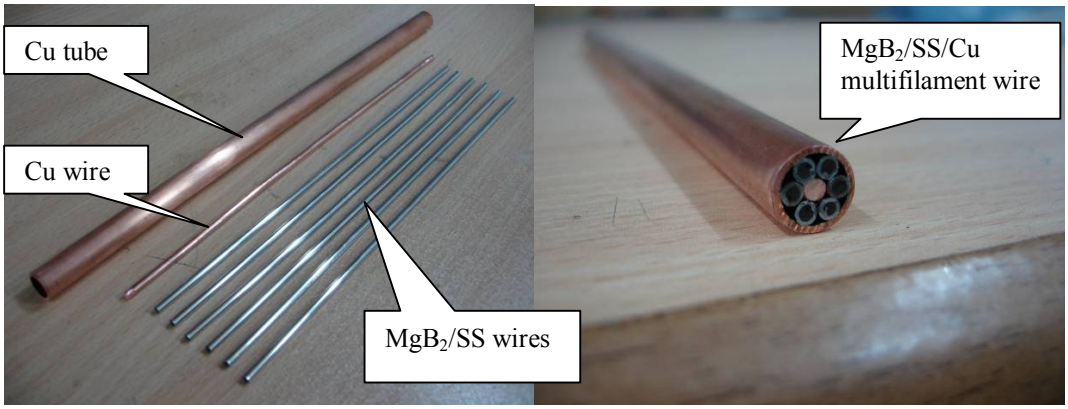

(a) (b)

Figure 4.11 (a) MgB_2/SS, Cu wires and Cu tube. (b) MgB_2/SS/Cu 6 filament wire.

Then ends of copper tube were closed by groove rolling machine and then MgB_2/SS/Cu composite tube was cold drawn into 1.43 mm diameter wire by wire drawing machine (Table 4.9). During the wire drawing procedure the MgB_2/SS/Cu composite tube was heat treated at 850°C for 30 minutes for every five steps of wire drawing in order to remove the work hardening on the composite tube under argon (Ar) gas atmosphere.

Table 4.9 Diameters and lengths of the MgB_2/SS/Cu 6 filament wire.

Diameter of die (mm)	Length of wire (cm)	Diameter of wire (mm)
10.00	25.6	9.85
9.70	25.8	9.67
9.40	26.2	9.33
9.10	27.2	9.07
8.85	27.6	8.81
8.60	27.9	8.53
8.35	28.4	8.30
8.10	29.0	8.05
7.85	30.0	7.80
7.60	31.1	7.53
7.40	33.2	7.35
7.20	32.6	7.09
7.00	34.0	6.94
6.80	35.5	6.72
6.60	37.8	6.55
6.40	39.4	6.37
6.20	41.4	6.17
6.00	43.8	5.94
5.80	46.0	5.74
5.65	47.6	5.62
5.50	50.6	5.44
5.30	53.6	5.26
5.15	18.7	5.10
	23.6	
5.00	19.7	4.92
	24.7	

Table 4.9 (cont.)

4.85	20.2 25.4	4.81
4.70	22.6 21.4	4.66
4.55	23.6 22.2	4.52
4.40	25.3 23.7	4.34
4.25	26.3 24.7	4.22
4.15	28.2 26.0	4.11
4.00	30.1 27.6	3.95
3.90	31.3 28.8	3.87
3.80	32.7 30.0	3.78
3.70	33.8 31.1	3.68
3.55	38.1 35.0	3.50
3.45	39.8 36.5	3.43
3.35	43.7 40.3	3.32
3.25	45.5 42.0	3.23

Table 4.9 (cont.)

3.15	47.8 43.9	3.15
3.05	51.9 47.9	3.05
2.95	55.0 49.4	2.92
2.85	59.6 53.6	2.78
2.75	62.8 56.7	2.71
2.70	63.0 57.7	2.66
2.60	69.9 63.5	2.56
2.55	71.0 64.6	2.54
2.50	74.4 67.7	2.47
2.40	83.3 74.2	2.36
2.30	88.6 79.0	2.26
2.25	91.6 82.1	2.22
2.15	89.9 89.1	2.11
2.10	94.5 93.0	2.06

Table 4.9 (cont.)

2.00	104.5 102.7	1.96
1.90	116.5 111.6	1.88
1.85	125.0 117.6	1.83
1.80	129.5 122.3	1.77
1.70	146.0 136.0	1.68
1.65	155.5 146.0	1.60
1.60	161.0 151.2	1.57
1.55	160.0 158.5	1.52
1.50	163.3 160.9	1.50
1.45	180.3	1.43

At the end of wire drawing procedure we have fabricated MgB_2/SS/Cu 6 filament wire which is 180.3 cm in length, 1.43 mm outer diameter. During the wire drawing procedure, the wire 53.6 cm in length broke off into two pieces. Then, we continued wire drawing procedure.

4.1.6. MgB_2/Ag/Fe 7 Filament Wire Production

We have fabricated superconducting MgB_2/Ag monofilament wire by ex-situ PIT method using Ag-sheath in order to fabricate MgB_2/Ag/Fe 7 filament wire.

4.1.6.1. MgB_2/Ag Monofilament Wire Production

One end of silver tube which is 25.6 cm in length, 6.35 mm outer diameter and a wall thickness of 1.0 mm was closed by groove rolling and this tube was heat treated at 850^{o}C under high purity argon (Ar) gas atmosphere for 1 hour in order to remove the work hardening and cooled down to room temperature in the furnace. The heating and cooling rates of the temperature were chosen to be 5^{o}C min^{-1}.

Commercially available MgB_2 powder (Alfa Aesar, -325 mesh, <44 micron) was filled into 25.6 cm long pure Ag tube with an outside diameter of 6.35 mm and wall thickness of 1.0 mm and tightly packed. This packing process was carried out in a high purity argon gas atmosphere inside of the glove box (Figure 4.12).

Figure 4.12 Glove Box.

After the remaining end was closed by silver plug, the tightly packed MgB_2/Ag composite tube was cold drawn into 3.04 mm diameter by drawing machine (Table 4.10). During the wire drawing procedure the MgB_2/Ag composite tube was heat treated at 500^oC under high purity argon (Ar) gas atmosphere for 30 minutes for 13th step of wire drawing in order to remove the work hardening on the MgB_2/Ag composite tube.

Table 4.10 Diameters and lengths of the MgB_2/Ag monofilament wire (fifth fabrication).

Diameter of die (mm)	Length of wire (cm)	Diameter of wire (mm)
6.20	27.5	6.18
6.00	28.9	5.95
5.80	29.8	5.76
5.65	30.9	5.64
5.50	33.4	5.48
5.30	35.9	5.26
5.15	37.6	5.11
5.00	40.1	4.94
4.85	41.1	4.84
4.70	45.0	4.65
4.55	47.6	4.53
4.40	51.0	4.35
4.25	52.7	4.23
4.15	55.8	4.14
4.00	61.1	3.99
3.90	63.5	3.86
3.80	67.0	3.76
3.70	69.2	3.68

Table 4.10 (cont.)

3.55	75.3	3.50
3.45	79.1	3.40
3.35	84.5	3.29
3.25	88.6	3.22
3.15	94.6	3.12
3.05	99.1	3.04

At the end of wire drawing process, diameter of MgB_2/Ag composite wire reduced to 6.35 mm from 3.04 mm and we have fabricated MgB_2/Ag composite wire which is 99.1 cm in length, 3.04 mm outer diameter.

4.1.6.2. MgB_2/Ag/Fe 7 Filament Wire Production

One end of iron tube which is 20 cm in length, 10.6 mm outer diameter and a wall thickness of 0.3 mm was closed by groove rolling machine (Figure 4.13) and this tube was heat treated at 950^oC under high purity argon (Ar) gas atmosphere for 3 hours in order to remove the work hardening and cooled down to room temperature in the furnace. Inert atmosphere was used in order to prevent oxidation of the iron tube during the heat treatment. The heating and cooling rates of the temperature were chosen to be 5^oC min^{-1}. Then, MgB_2/Ag composite wire which is 99.1 cm in length, 3.04 mm outer diameter was cut into 7 pieces in the glove box under high purity argon (Ar) gas atmosphere. Then 7 pieces of MgB_2/Ag wires 3.04 mm outer diameters, 13.0 cm in length were inserted into the iron tube of outer diameter 10.6 mm and a wall thickness of 0.3 mm in the glove box under high purity argon gas atmosphere. The open end of MgB_2/Ag/Fe composite tube was closed by silver plug.

Figure 4.13 One of the open ends sealed empty iron tube with an outer diameter of 10.6 mm (for the MgB_2/Ag/Fe 7 filament wire production).

The MgB_2/Ag/Fe composite tube was cold drawn into 1.53 mm diameter wire by drawing machine (Table 4.11). During the wire drawing procedure the MgB_2/Ag/Fe composite tube was heat treated at 850^{o}C under high purity argon (Ar) gas atmosphere for 1 hour for every seven steps of wire drawing in order to remove the work hardening of the composite.

Table 4.11 Diameters and lengths of the MgB_2/Ag/Fe 7 filament wire.

Diameter of die (mm)	Length of wire (cm)	Diameter of wire (mm)
10.30	22.1	10.27
10.00	22.4	9.92
9.70	22.6	9.70
9.40	23.0	9.34
9.10	23.3	9.06
8.85	23.8	8.79
8.60	19.8	8.54
8.35	20.2	8.32
8.10	20.9	8.09
7.85	21.8	7.81
7.60	23.1	7.58
7.40	23.2	7.35

Table 4.11 (cont.)

7.20	24.8	7.12
7.00	25.4	6.98
6.80	22.6	6.75
6.60	23.3	6.55
6.40	24.1	6.38
6.20	25.6	6.18
6.00	26.9	5.95
5.80	29.1	5.76
5.65	29.9	5.62
5.50	31.3	5.46
5.30	32.8	5.27
5.15	34.5	5.11
5.00	36.3	4.95
4.85	37.4	4.84
4.70	41.1	4.66
4.55	43.1	4.50
4.40	45.8	4.32
4.25	47.8	4.22
4.15	49.7	4.13
4.00	55.3	3.97
3.90	57.7	3.87
3.80	60.2	3.78
3.70	62.2	3.69
3.55	69.6	3.52
3.45	72.8	3.41
3.35	77.3	3.32
3.25	82.3	3.22
3.15	86.5	3.12

Table 4.11 (cont.)

3.05	91.4	3.02
2.95	91.0	2.94
2.85	100.1	2.82
2.75	105.9	2.72
2.70	107.3	2.70
2.60	117.3	2.57
2.55	119.9	2.54
2.50	125.5	2.47
2.40	137.8	2.36
2.30	149.7	2.27
2.25	154.6	2.23
2.15	142.0	2.13
2.10	145.6	2.07
2.00	158.5	1.97
1.90	171.0	1.87
1.85	182.5	1.82
1.80	189.2	1.77
1.70	212.4	1.68
1.65	229.7	1.63
1.60	238.9	1.58
1.55	239.1	1.53

Through this wire drawing steps we have fabricated MgB_2/Ag/Fe 7 filament wire 239.1 cm in length with 1.53 mm outer diameter. Figure 4.14 shows this wire.

Figure 4.14 MgB_2/Ag/Fe 7 filament wires.

4.1.7. MgB_2/Ag/Fe 7 Filament Tape Production

The MgB_2/Ag/Fe 7 filament damaged part 78.5 cm in length was cut from the MgB_2/Ag/Fe 7 filament wire 239.1 cm in length. Another MgB_2/Ag/Fe 7 filament wire 160.6 cm in length was rolled by rolling machine six times. We got MgB_2/Ag/Fe tape of 186.3 cm length, 0.37 mm thickness and 4.41 mm width.

4.1.8. MgB_2/Fe Monofilament Wire Production

We have fabricated superconducting MgB_2/Fe monofilament wire by ex-situ PIT method using Fe-sheath.

One end of iron tube which is 25 cm in length, 10.6 mm outer diameter and a wall thickness of 0.3 mm was closed by groove rolling machine (Figure 4.15) and this tube was heat treated at 1000^{o}C under high purity argon (Ar) gas for 3 hours in order to remove the work hardening and cooled down to room temperature in the

furnace. The heating and cooling rates of the temperature were chosen to be $5^{o}C\ min^{-1}$.

Figure 4.15 One of the open ends sealed empty iron tube with an outer diameter of 10.6 mm (for the MgB_2/Fe monofilament wire production).

In order to prevent the wire breaking during drawing process, diameter of iron tube was reduced from 10.6 mm to 4.95 mm by the wire drawing machine (Figure 4.16).

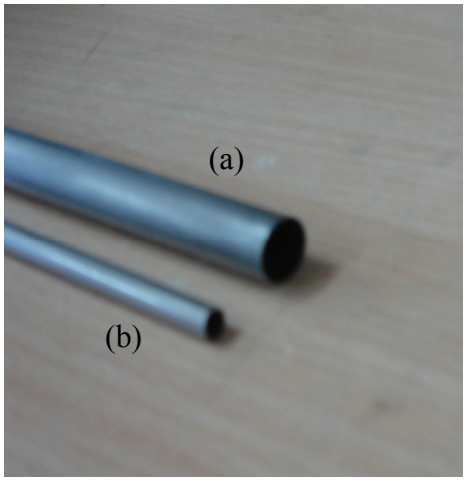

Figure 4.16 Empty iron tubes (a) 10.6 mm outer diameter (b) 4.95 mm outer diameter.

Later, one end of the Fe tube 4.95 mm outer diameter was sharpened in order to draw easily and this tube was heat treated at 1000^{o}C under high purity argon (Ar) gas atmosphere for 3 hours in order to remove the work hardening and cooled down to room temperature in the furnace (Figure 4.17). The heating and cooling rates of the temperature were chosen to be 5^{o}C min^{-1}.

Figure 4.17 One of the open ends sealed empty iron tube with an outer diameter of 4.95 mm (for the MgB_2/Fe monofilament wire production).

Commercially available MgB_2 powder (Alfa Aesar, -325 mesh, <44 micron) was filled into an 17 cm long pure Fe tube with an outside diameter of 4.95 mm and wall thickness of 0.3 mm and tightly packed. This packing process was carried out in high purity argon gas atmosphere inside the glove box. After the remaining end was closed by silver plug, the filled Fe tube was cold drawn in a number of steps with about 5% of cross-section reduction to a round Fe-clad MgB_2 wire with an outer diameter of 1.52 mm without any intermediate annealing.(Table 4.12)

Table 4.12 Diameters and lengths of the MgB_2/Fe wire (first fabrication).

Diameter of die (mm)	Length of wire (cm)	Diameter of wire (mm)
5.00	18.1	4.92
4.85	18.3	4.82
4.70	18.6	4.64

Table 4.12 (cont.)

4.55	19.0	4.52
4.40	19.5	4.32
4.25	20.0	4.21
4.15	20.4	4.11
4.00	21.4	3.95
3.90	22.3	3.84
3.80	23.0	3.75
3.70	23.5	3.67
3.55	25.1	3.50
3.45	26.1	3.39
3.35	27.8	3.29
3.25	30.8	3.21
3.15	32.2	3.11
3.05	33.6	3.01
2.95	35.8	2.91
2.85	38.2	2.77
2.75	40.5	2.69
2.70	42.5	2.67
2.60	45.7	2.56
2.55	46.8	2.53
2.50	48.3	2.47
2.40	53.2	2.34
2.30	56.6	2.26
2.25	58.1	2.22
2.15	42.7	2.11
2.10	43.5	2.07
2.00	47.4	1.95
1.90	52.2	1.87

Table 4.12 (cont.)

1.85	55.5	1.81
1.80	57.3	1.77
1.70	66.1	1.67
1.65	70.7	1.61
1.60	73.2	1.58
1.55	37.4	1.52

At the end of wire drawing procedure we have fabricated MgB_2/Fe monofilament wire which is 37.4 cm in length, 1.52 mm outer diameter.

Commercially available MgB_2 powder (Alfa Aesar, -325 mesh, <44 micron) was filled into a 22 cm long another pure Fe tube with an outside diameter of 4.95 mm and wall thickness of 0.3 mm and tightly packed. This packing process was carried out in high purity argon gas atmosphere inside of the glove box. After the remaining end was closed by silver wire, the filled Fe tube was cold drawn in a number of steps with about 5% of cross-section reduction to a round Fe-clad MgB_2 wire with an outer diameter of 1.51 mm without any intermediate annealing.(Table 4.13)

Table 4.13 Diameters and lengths of the MgB_2/Fe wire (second fabrication).

Diameter of die (mm)	Length of wire (cm)	Diameter of wire (mm)
5.00	23.4	4.94
4.85	23.6	4.84
4.70	24.1	4.67
4.55	24.2	4.53
4.40	25.5	4.36
4.25	26.3	4.24

Table 4.13 (cont.)

4.15	26.8	4.15
4.00	28.4	3.98
3.90	29.2	3.88
3.80	30.4	3.79
3.70	31.0	3.70
3.55	33.4	3.53
3.45	34.8	3.43
3.35	37.1	3.32
3.25	39.7	3.24
3.15	41.6	3.15
3.05	43.6	3.05
2.95	48.3	2.94
2.85	51.7	2.81
2.75	54.4	2.72
2.70	55.0	2.69
2.60	61.5	2.56
2.55	62.0	2.54
2.50	65.1	2.46
2.40	71.6	2.34
2.30	77.0	2.27
2.25	79.1	2.22
2.15	89.6	2.11
2.10	91.6	2.07
2.00	102.3	1.96
1.90	63.6 29.0 19.6	1.88
1.85	67.6	1.82

Table 4.13 (cont.)

1.80	71.2	1.78
1.70	79.2	1.68
1.65	85.0	1.61
1.60	88.4	1.56
1.55	32.7	1.51
	47.8	1.56

At the end of wire drawing procedure we have fabricated MgB_2/Fe monofilament wires which are 32.7 cm in length, 1.51 mm outer diameter and 47.8 cm in length, 1.56 mm outer diameter (Figure 4.18).

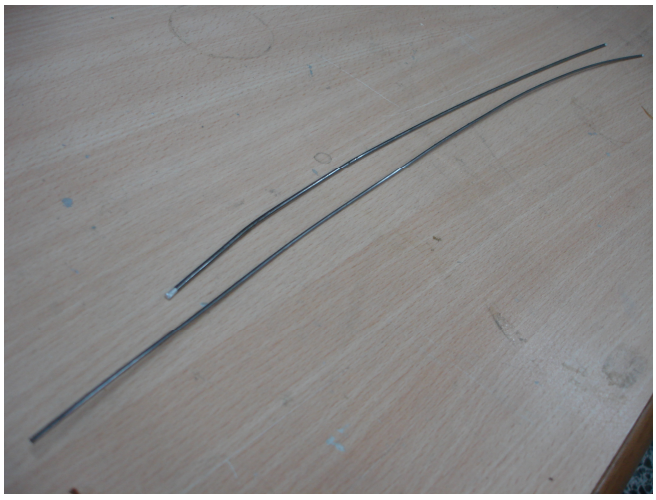

Figure 4.18 MgB_2/Fe monofilament wires.

4.1.9. MgB_2/Fe Monofilament Tape Production

The MgB_2/Fe wires which are 37.4 cm in length, 1.52 mm outer diameter, 32.7 cm in length, 1.51 mm outer diameter and 47.8 cm in length, 1.56 mm outer diameter were

rolled into tapes by rolling machine at one pass. The final size of the tape was about 2.60 mm in width and about 0.80 mm in thickness.

4.1.10. MgB_2/Fe/Cu 6 Filament Wire Production

We have fabricated superconducting MgB_2/Fe monofilament wire by ex-situ PIT method using Fe-sheath in order to fabricate MgB_2//Fe/Cu 6 filament wire.

4.1.10.1. MgB_2/Fe Monofilament Wire Production

We have fabricated superconducting MgB_2/Fe monofilament wire by ex-situ PIT method using Fe-sheath.

One end of iron tube which is 25 cm in length, 10.6 mm outer diameter and a wall thickness of 0.3 mm was closed by groove rolling machine and this tube was heat treated at 1000^{o}C under high purity argon (Ar) gas for 3 hours in order to remove the work hardening and cooled down to room temperature in the furnace. The heating and cooling rates of the temperature were chosen to be 5^{o}C min^{-1}.

In order to prevent the breaking off of the wire during the wire drawing process diameter of iron tube was reduced from 10.6 mm to 4.95 mm by the wire drawing machine.

One end of the Fe tube 4.95 mm outer diameter was sharpened in order to draw easily and this tube was heat treated at 1000^{o}C under high purity argon (Ar) gas atmosphere for 3 hours in order to remove the work hardening and cooled down to room temperature in the furnace. The heating and cooling rates of the temperature were chosen to be 5^{o}C min^{-1}.

Commercially available MgB_2 powder (Alfa Aesar, -325 mesh, <44 micron) was filled into an 16 cm long pure Fe tube with an outside diameter of 4.95 mm and wall thickness of 0.3 mm and tightly packed. This packing process was carried out in a high purity argon gas atmosphere inside of the glove box. After the remaining end was closed by silver plug, the filled Fe tube was cold drawn in a number of steps with about 5% of cross-section reduction to a round Fe-clad MgB_2 wire with an outer diameter of 1.58 mm without any intermediate annealing.(Table 4.14)

Table 4.14 Diameters and lengths of the MgB_2/Fe wire (third fabrication).

Diameter of die (mm)	Length of wire (cm)	Diameter of wire (mm)
4.85	16.3	4.83
4.70	17.3	4.65
4.55	17.8	4.51
4.40	18.5	4.34
4.25	19.1	4.23
4.15	19.5	4.14
4.00	21.0	3.97
3.90	21.6	3.86
3.80	22.5	3.77
3.70	24.6	3.69
3.55	26.3	3.52
3.45	27.2	3.41
3.35	29.0	3.31
3.25	30.0	3.23
3.15	31.4	3.13
3.05	33.5	3.04
2.95	35.8	2.93

Table 4.14 (cont.)

2.85	38.2	2.80
2.75	41.0	2.71
2.70	41.3	2.70
2.60	44.7	2.57
2.55	45.1	2.54
2.50	47.6	2.48
2.40	43.0	2.35
2.30	45.8	2.27
2.25	47.0	2.24
2.15	54.0	2.12
2.10	55.0	2.08
2.00	60.9	1.97
1.90	66.1	1.88
1.85	70.2	1.82
1.80	72.4	1.78
1.70	82.0	1.69
1.65	89.2	1.61
1.60	92.8	1.58

At the end of wire drawing procedure we have fabricated MgB_2/Fe monofilament wire which is 92.8 cm in length, 1.58 mm outer diameter.

Commercially available MgB_2 powder (Alfa Aesar, -325 mesh, <44 micron) was filled into an 21 cm long another pure Fe tube with an outside diameter of 4.95 mm and wall thickness of 0.3 mm and tightly packed. This packing process was carried out in a high purity argon gas atmosphere inside of the glove box. After the remaining end was closed by silver plug, the filled Fe tube was cold drawn in a number of steps with about 5% of cross-section reduction to a round Fe-clad MgB_2

wire with an outer diameter of 1.87 mm without any intermediate annealing.(Table 4.15)

Table 4.15 Diameters and lengths of the MgB_2/Fe wire (fourth fabrication).

Diameter of die (mm)	Length of wire (cm)	Diameter of wire (mm)
4.85	21.3	4.83
4.70	21.9	4.66
4.55	22.3	4.52
4.40	23.5	4.33
4.25	24.2	4.22
4.15	25.1	4.12
4.00	27.0	3.95
3.90	28.1	3.86
3.80	29.2	3.76
3.70	31.0	3.68
3.55	33.5	3.50
3.45	35.3	3.40
3.35	37.6	3.30
3.25	39.0	3.21
3.15	40.9	3.13
3.05	42.6	3.02
2.95	46.1	2.91
2.85	49.6	2.78
2.75	52.5	2.69
2.70	53.0	2.67
2.60	57.5	2.56
2.55	58.0	2.53
2.50	60.9	2.48
2.40	65.9	2.36

Table 4.15 (cont.)

2.30	71.2	2.28
2.25	73.1	2.23
2.15	81.4	2.12
2.10	84.6	2.08
2.00	93.5	1.97
1.90	57.2	1.87
	27.5	1.97

At the end of wire drawing procedure we have fabricated MgB_2/Fe monofilament wires which are 57.2 cm in length with 1.87 mm outer diameter and 27.5 cm in length with 1.97 mm outer diameter.

4.1.10.2. MgB_2/Fe/Cu 6 Filament Wire Production

We have fabricated superconducting MgB_2/Fe/Cu 6 filament wire by powder-in-tube (PIT) method using Cu-sheath.

One end of copper tube which is 25 cm in length, 10 mm outer diameter and a wall thickness of 1 mm was closed by groove rolling machine (Figure 4.19) and this tube was heat treated at 900^{o}C under high purity argon (Ar) gas for 3 hours in order to remove the work hardening and cooled down to room temperature in the furnace. The heating and cooling rates were both 5^{o}C min^{-1}.

Figure 4.19 One of the open ends sealed empty copper tube with an outer diameter of 10 mm (for the MgB_2/Fe/Cu 6 filament wire production).

In order to prevent the breaking off of the wire during the wire drawing process diameter of copper tube was reduced from 10 mm to 6.40 mm by the wire drawing machine (Figure 4.20).

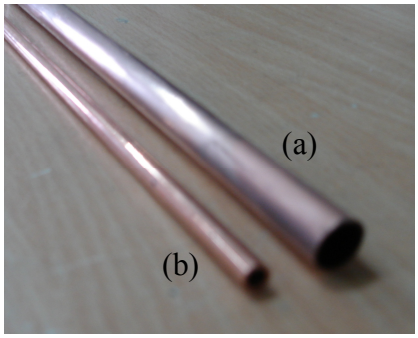

Figure 4.20 Empty copper tubes (a) 10 mm outer diameter (b) 6.40 mm outer diameter (for the MgB_2/Fe/Cu 6 filament wire production).

One end of the Cu tube 6.40 mm outer diameter was sharpened in order to draw easily and this tube was heat treated at 900^{o}C under high purity argon (Ar) gas atmosphere for 3 hours in order to remove the work hardening and cooled down to room temperature in the furnace (Figure 4.21). The heating and cooling rates of the temperature were chosen to be 5^{o}C min^{-1}.

Figure 4.21 One of the open ends sealed empty copper tube with an outer diameter of 6.40 mm (for the MgB_2/Fe/Cu 6 filament wire production).

Later, 6 pieces of MgB_2/Fe monofilament wires 1.58 mm outer diameters, 15 cm in length and one piece of Cu wire 1.58 mm in diameter, 15 cm in length were inserted into the copper tube 25.4 cm in length, 6.40 mm outer diameter in a high purity argon gas atmosphere inside of the glove box. After the remaining end was closed by silver plug, the MgB_2/Fe/Cu composite tube was cold drawn in a number of steps with about 5% of cross-section reduction to a round Cu-clad MgB_2/Fe/Cu 6 filament composite wire with an outer diameter of 2.46 mm without any intermediate annealing.(Table 4.16)

Table 4.16 Diameters and lengths of the MgB_2/Fe/Cu 6 filament wire.

Diameter of die (mm)	Length of wire (cm)	Diameter of wire (mm)
6.40	25.7	6.35
6.20	26.1	6.17
6.00	26.9	5.97
5.80	27.5	5.77
5.65	27.9	5.64
5.50	29.1	5.47
5.30	27.0	5.28
5.15	28.2	5.11

Table 4.16 (cont.)

5.00	29.5	4.94
4.85	30.1	4.84
4.70	32.6	4.66
4.55	34.0	4.52
4.40	36.0	4.34
4.25	31.1	4.21
4.15	32.5	4.11
4.00	35.6	3.96
3.90	37.0	3.84
3.80	38.3	3.76
3.70	40.7	3.68
3.55	43.8	3.49
3.45	45.6	3.39
3.35	27.9	3.29
	21.7	
3.25	29.0	3.21
3.15	19.7	3.12
	11.1	
3.05	20.1	3.01
2.95	16.8	2.91
	5.7	3.02
2.85	17.7	2.78
2.75	18.5	2.69
2.70	18.7	2.66
2.60	21.0	2.55
2.55	21.1	2.52
2.50	18.5	2.46

At the end of wire drawing procedure we have fabricated MgB_2/Fe/Cu 6 filament wires which are 19 cm in length, 3.32 mm outer diameter, 11 cm in length, 3.15 mm outer diameter, 6 cm in length, 3.0 mm outer diameter and 18.5 cm in length, 2.46 mm outer diameter. During the wire drawing procedure, MgB_2/Fe/Cu 6 filament composite wire was broken at several different diameters due to absence of intermediate heat treatment.

4.1.11. MgB_2/Fe/Cu 6 Filament Tape Production

MgB_2/Fe/Cu 6 filament wire was rolled by rolling machine with only one pass. We got MgB_2/Ag/Fe 6 filament tape of 0.91 mm thickness and 5.10 mm width.

4.1.12. MgB_2/Fe/Cu 7 Filament Wire Production

We have fabricated superconducting MgB_2/Fe monofilament wire by ex-situ PIT method using Fe-sheath in order to fabricate MgB_2//Fe/Cu 7 filament wire.

4.1.12.1. MgB_2/Fe Monofilament Wire Production

We have fabricated superconducting MgB_2/Fe monofilament wire by ex-situ powder-in-tube (PIT) method using Fe-sheath.

One end of iron tube which is 25 cm in length, 10.6 mm outer diameter and a wall thickness of 0.3 mm was closed by groove rolling machine and this tube was heat treated at 1000^{o}C under high purity argon (Ar) gas for 3 hours in order to

remove the work hardening and cooled down to room temperature in the furnace. The heating and cooling rates of the temperature were chosen to be $5^{o}C\ min^{-1}$.

In order to prevent the breaking off of the wire during the wire drawing process diameter of iron tube was reduced from 10.6 mm to 4.95 mm by the wire drawing machine.

One end of the Fe tube 4.95 mm outer diameter was sharpened in order to draw easily and this tube was heat treated at $1000^{o}C$ under high purity argon (Ar) gas atmosphere for 3 hours in order to remove the work hardening and cooled down to room temperature in the furnace. The heating and cooling rates of the temperature were chosen to be $5^{o}C\ min^{-1}$.

Commercially available MgB_2 powder (Alfa Aesar, -325 mesh, <44 micron) was filled into an 19 cm long pure Fe tube with an outside diameter of 4.95 mm and wall thickness of 0.3 mm and tightly packed. This packing process was carried out in a high purity argon gas atmosphere inside of the glove box. After the remaining end was closed by silver plug, the filled Fe tube was cold drawn in a number of steps with about 5% of cross-section reduction to a round Fe-clad MgB_2 wire with an outer diameter of 1.58 mm without any intermediate annealing.(Table 4.17)

Table 4.17 Diameters and lengths of the MgB_2/Fe wire (fifth fabrication).

Diameter of die (mm)	Length of wire (cm)	Diameter of wire (mm)
4.85	19.1	4.84
4.70	19.7	4.66
4.55	20.2	4.53
4.40	21.1	4.35

Table 4.17 (cont.)

4.25	21.8	4.24
4.15	22.3	4.14
4.00	24.0	3.98
3.90	24.8	3.87
3.80	25.0	3.78
3.70	25.5	3.70
3.55	27.2	3.52
3.45	28.5	3.42
3.35	30.5	3.32
3.25	31.6	3.24
3.15	33.2	3.14
3.05	34.7	3.04
2.95	37.2	2.93
2.85	40.0	2.80
2.75	43.1	2.70
2.70	43.5	2.69
2.60	47.2	2.56
2.55	47.7	2.52
2.50	50.1	2.46
2.40	54.1	2.35
2.30	58.6	2.27
2.25	60.2	2.22
2.15	68.6	2.11
2.10	70.2	2.07
2.00	77.4	1.96
1.90	84.1	1.87
1.85	90.4	1.81
1.80	93.6	1.77

Table 4.17 (cont.)

1.70	106.3	1.68
1.65	114.5	1.61
1.60	118.5	1.58

At the end of wire drawing procedure we have fabricated MgB_2/Fe monofilament wire which is 118.5 cm in length, 1.58 mm outer diameter.

Commercially available MgB_2 powder (Alfa Aesar, -325 mesh, <44 micron) was filled into an 20 cm long another pure Fe tube with an outside diameter of 4.95 mm and wall thickness of 0.3 mm and tightly packed. This packing process was carried out in a high purity argon gas atmosphere inside of the glove box. After the remaining end was closed by silver plug, the filled Fe tube was cold drawn in a number of steps with about 5% of cross-section reduction to a round Fe-clad MgB_2 wire with an outer diameter of 1.58 mm without any intermediate annealing.(Table 4.18)

Table 4.18 Diameters and lengths of the MgB_2/Fe wire (sixth fabrication).

Diameter of die (mm)	Length of wire (cm)	Diameter of wire (mm)
4.85	20.5	4.83
4.70	20.9	4.64
4.55	21.2	4.50
4.40	22.0	4.35
4.25	22.5	4.23
4.15	23.0	4.13
4.00	24.2	3.97
3.90	25.4	3.87
3.80	26.1	3.78

Table 4.18 (cont.)

3.70	27.4	3.67
3.55	29.3	3.49
3.45	30.7	3.39
3.35	32.6	3.29
3.25	33.4	3.24
3.15	36.1	3.11
3.05	37.8	3.01
2.95	40.8	2.91
2.85	43.7	2.77
2.75	48.0	2.69
2.70	48.4	2.67
2.60	52.1	2.56
2.55	53.2	2.53
2.50	55.7	2.49
2.40	60.0	2.34
2.30	64.5	2.27
2.25	66.5	2.21
2.15	75.2	2.10
2.10	77.0	2.07
2.00	86.6	1.95
1.90	52.0	1.89
1.85	55.0	1.83
1.80	56.7	1.78
1.70	64.4	1.69
1.65	69.0	1.62
1.60	71.4	1.58

At the end of wire drawing procedure we have fabricated MgB_2/Fe monofilament wire which is 71.4 cm in length, 1.58 mm outer diameter.

4.1.12.2. MgB_2/Fe/Cu 7 Filament Wire Production

We have fabricated superconducting MgB_2/Fe/Cu 7 filament wire by powder-in-tube (PIT) method using Cu-sheath.

One end of copper tube which is 25 cm in length, 10 mm outer diameter and a wall thickness of 1 mm was closed by groove rolling machine (Figure 4.22) and this tube was heat treated at 900^{o}C under high purity argon (Ar) gas for 3 hours in order to remove the work hardening and cooled down to room temperature in the furnace. The heating and cooling rates of the temperature were chosen to be 5^{o}C min^{-1}.

Figure 4.22 One of the open ends sealed empty copper tube with an outer diameter of 10 mm (for the MgB_2/Fe/Cu 7 filament wire production).

In order to prevent the breaking off of the wire during the wire drawing process diameter of copper tube was reduced from 10 mm to 6.40 mm by the wire drawing machine (Figure 4.23).

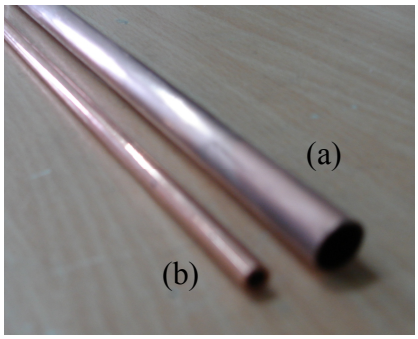

Figure 4.23 Empty copper tubes (a) 10 mm outer diameter (b) 6.40 mm outer diameter (for the MgB_2/Fe/Cu 7 filament wire production).

One end of the Cu tube 6.40 mm outer diameter was sharpened in order to draw easily and this tube was heat treated at 900^{o}C under high purity argon (Ar) gas atmosphere for 3 hours in order to remove the work hardening and cooled down to room temperature in the furnace (Figure 4.24). The heating and cooling rates of the temperature were chosen to be 5^{o}C min^{-1}.

Figure 4.24 One of the open ends sealed empty copper tube with an outer diameter of 6.40 mm (for the MgB_2/Fe/Cu 7 filament wire production).

7 pieces of MgB_2/Fe monofilament wires 1.58 mm outer diameters, 15 cm in length were inserted into the copper tube 25.7 cm in length, 6.40 mm outer diameter in a high purity argon gas atmosphere inside of the glove box. After the remaining end was closed by silver plug, the MgB_2/Fe/Cu composite tube was cold drawn in a number of steps with about 5% of cross-section reduction to a round Cu-clad

MgB_2/Fe/Cu 7 filament composite wire with an outer diameter of 3.02 mm without any intermediate annealing.(Table 4.19)

Table 4.19 Diameters and lengths of the MgB_2/Fe/Cu 7 filament wire.

Diameter of die (mm)	Length of wire (cm)	Diameter of wire (mm)
6.40	26.0	6.35
6.20	26.4	6.17
6.00	27.2	5.97
5.80	27.8	5.79
5.65	28.3	5.65
5.50	29.5	5.47
5.30	30.5	5.28
5.15	31.7	5.11
5.00	33.4	4.94
4.85	34.0	4.83
4.70	36.2	4.65
4.55	29.8	4.51
4.40	32.6	4.33
4.25	33.9	4.23
4.15	35.3	4.11
4.00	39.3	3.95
3.90	23.0	3.84
3.80	23.8	3.77
3.70	24.7	3.66
3.55	26.8	3.50
3.45	27.7	3.40
3.35	23.6	3.29
3.25	13.4	3.21
3.15	11.4	3.09

Table 4.19 (cont.)

3.05	11.7	3.02

At the end of wire drawing procedure we have fabricated MgB_2/Fe/Cu 7 filament wires which are 10.5 cm in length, 3.32 mm outer diameter, 7 cm in length, 3.44 mm outer diameter and 11.7 cm in length, 3.02 mm outer diameter. During the wire drawing procedure, MgB_2/Fe/Cu 7 filament composite wire was broken at several different diameters due to absence of intermediate heat treatment.

4.1.13. MgB_2/Fe/Cu 7 Filament Tape Production

MgB_2/Fe/Cu 7 filament wire was rolled by rolling machine one time. We got MgB_2/Ag/Fe 7 filament tape of 1.07 mm thickness and 6.60 mm width

4.2. Heat Treatments

All heat treatments of the samples were done using a (2416) Eurotherm Controller/ Programmable Carbolite tube furnace (Figure 4.25). The different pieces of the samples were placed in a stainless steel tube which is 2 m long having, 25 mm outer diameter and a wall thickness of 2 mm and sealed. The sealed stainless steel tube was then inserted in a Carbolite tube furnace. Then, the samples were heat treated at different temperatures for different periods first by obtaining vacuum and than supplying high purity argon (Ar) gas atmosphere into the stainless steel tube. All heat treatments of the samples were done under high purity argon (Ar) gas

atmosphere and all samples were cooled down to room temperature in the furnace. The heating and cooling rates of the temperature were chosen to be $5^{o}C\ min^{-1}$.

Figure 4.25 (2416) Eurotherm controller/Programmable Carbolite Tube Furnace.

4.3. R-T and I-V Measurements

The superconducting transition temperature (T_c) measurements were carried out by standard four-probe resistivity method using Keithley nanovoltmeter (Model 2182A) and Current Source (Model 238) and a constant DC bias current of 100 mA between 4-50 K temperatures in a closed cycled He cryostat which provided from CRY Industries. Standard Pb-Sn (40/60) solder was used for forming the current and voltage contacts. Both of voltage contacts were directly soldered with standard Pb-Sn (40/60) solder to the sheath materials of the samples. Both of ends of the samples were painted with silver and then both of painted ends of the samples were soldered with standard Pb-Sn (40/60) solder for current contacts. Magnetoresistivity measurements were performed by using standard four-probe method with DC current of 100 mA between 4-50 K temperatures under constant magnetic field 0.250 T,

0.500 T, 0.750 T, 1 T, 1.5 T and 2 T by superconducting solenoid type magnet respectively. The magnetic field was applied perpendicular to the current direction. DC electrical resistivity and magnetoresistivity measurement systems are shown in Figure 4.26. The current was applied to the two outer electrical contacts and the voltage drop across the two inner electrical contacts was measured against temperature. The superconducting transition temperature (T_c) was defined as resistance equal to zero. In order to convert voltage to resistivity the calculation is made as following:

$$R = \frac{\rho.L}{A} \tag{4.1}$$

$$V = I.R \tag{4.2}$$

$$\rho = \frac{R.A}{L} = \frac{V.A}{I.L} \tag{4.3}$$

where ρ is the resistivity, L is the distance between the inner contacts and A is the cross sectional area of the MgB_2 core.

Figure 4.26 DC electrical resistivity and magnetoresistivity measurement systems.

The current-voltage (I-V) characteristics of the samples were measured at various temperatures with the standard four-probe method under self-field. The critical currents (I_c) were evaluated from I-V curves taking the electric field criterion of 1 μV/cm. The transport critical current densities (J_c) were defined as I_c divided by the cross-section area of the MgB_2 core which was measured with a help of a scanning electron microscope (SEM). A Philip Harris current source, Lake Shore 331 temperature controller, Hewlett Packard 34401A multimeter and Leybold cryostat system were used for I-V measurements.

4.4. SEM and EDS Analysis

The MgB_2 wires and tapes were compressed with copper bakelite powder. The vertical cross section of MgB_2 wires and tapes were polished. Then, the surface morphologies of the MgB_2 wires and tapes were studied by using a JEOL JSM-6390 LV scanning electron microscope (SEM). JEOL JSM-6390 LV SEM system is shown in Figure 4.27.

SEM examinations give information about grain alignment, grain size and porosity of the samples. We investigated microstructures of the samples, connection and size of the grains and the presence of microvoid, microcrack.

Figure 4.27 JEOL JSM-6390 LV Scanning Electron Microscope.

SEM in a combination with an energy dispersive X-ray spectrometer (EDS) analysis was used for studying the microstructure of the samples. The chemical composition of the MgB_2 wires and tapes were analyzed using an EDS (JEOL JSM-6390 LV).

4.5. XRD Analysis

The phase composition and crystal structure investigation of the MgB_2 wires and tapes were characterized by X-ray diffraction (XRD) method using a Rigaku MultiFlex 2kW X-Ray-Diffractometer with Cu Kα radiation (λ=1.5418 Å) in the range $2\theta=3^{o}$-80^{o} with a scan speed of 5°/min and a step increment of 0.02° at room temperature. Rigaku MultiFlex 2kW X-Ray-Diffractometer system is shown in Figure 4.28.

Phase purity and the lattice parameters were determined from these XRD results. The accuracy in determining the lattice parameters a and c was ± 0.001 Å.

Figure 4.28 Rigaku MultiFlex 2kW X-Ray-Diffractometer.

4.6. Metallographic Studies

Surface structures of the MgB_2 samples were investigated by OLYMPLUS GX41 optical microscope (Figure 4.29).

The vertical cross sections of the wires and tapes were mounted in bakelite (Figure 4.30). Then, tape surfaces were polished and the surface structures of these samples were investigated by OLYMPLUS GX41 optical microscope. The polishing procedure was applied after the mounting process. SiC grinding papers of 120, 320, 1200, 2400 and 4000 mesh were used followed by polishing with 1 μm and 1/4 μm diamond paste.

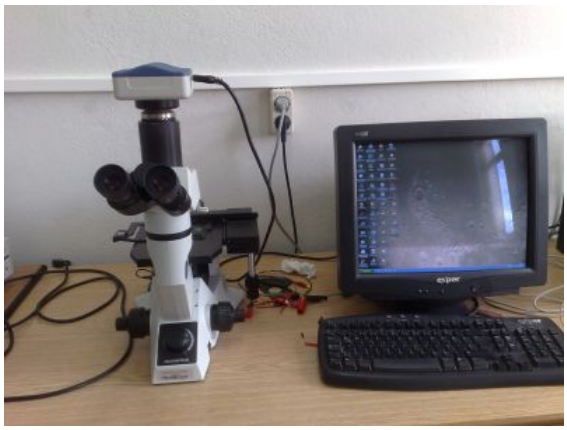

Figure 4.29 OLYMPLUS GX41 optical microscope.

Figure 4.30 MgB_2 wires and tapes which were compressed with copper bakelite powder.

The mounting machine is shown in Figure 4.31, the polishing machine is shown in Figure 4.32.

Figure 4.31 Mounting Machine.

Figure 4.32 Polishing Machine.

4.7. M-H, M-T Measurements

Magnetization properties (M-H loops and M-T graphs) were measured using a Quantum Design Physical Property Measurement System (PPMS) and Vibrating Sample Magnetometer (VSM) System. Quantum Design Physical Property Measurement System (PPMS) and Vibrating Sample Magnetometer (VSM) System are shown in Figure 4.33. The M(H) properties of MgB2 samples were measured up

to 3 T for the constant temperatures with 4.2 K, 10 K, 20 K and 30 K while the M(T) properties were measured at 0.1 T for between 10 K to 50 K temperatures under the zero field-cooling regime (ZFC). The measurements were carried out by the sweep rate of 5 mT s^{-1}.

Figure 4.33 Quantum Design Physical Property Measurement System (PPMS) and Vibrating Sample Magnetometer (VSM) System.

We estimated J_c of our samples by using Bean's critical state model. According to the Bean critical state model, the inductive critical current density J_c is associated with ΔM, the difference in the hysteresis magnetization between the increasing and decreasing magnetic fields. The inductive current density is obviously suppressed by the increasing applied field and temperature. Our sample studied for magnetization was in a cylindrical form; hence we used the formula $J_c = 30 \times \Delta M/d$, where $\Delta M = |M+|-|M-|$ comes from the measured M(H) loops and d is the diameter of the cylindrical sample.

CHAPTER 5

RESULTS AND DISCUSSIONS

5.1. Introduction

The discovery of superconductivity at 39 K in MgB_2 compound has a lot of advantages such as; high T_c value, simple structure, light weigh, absence of weak-link, high abundance of Mg and B, low anisotropy, the large coherence length and high critical current density value. The MgB_2 superconductor has the highest transition temperature in intermetallic compounds. These properties make it a good candidate for the theoretical studies and practical application [16,38,55]. The MgB_2 superconductor has been fabricated successfully in wires, tapes, bulk samples, thin films and single crystal forms using various methods by many research groups [46-64,76-126]. The magnesium diboride wires and tapes are generally fabricated by a PIT method [97-103]. There are two processes for fabricating MgB_2 wires and tapes using the PIT method which are known as ex-situ and in-situ methods. In the ex-situ method, fabrication of MgB_2 wires and tapes are made by using MgB_2 reacted powder [97,100] while, in the in-situ method, fabrication of MgB_2 wires and tapes are made by using a mixture Mg and B powder with stoichiometric composition [59,101-103]. Some metals and alloys have been used for sheath materials such as Fe [104], Cu [105], Ti [106], Ag [107], Ni [108], Ta [61], stainless steel [109], Fe/stainless steel [110], Cu-Ni [111,112] and CuSn [76] in the PIT process. The

sheath materials should be ductile for mechanical deformation and should not react with MgB_2 core and therefore degrade the superconducting properties. Iron is the most suitable sheath material due to its chemical compatibility with the MgB_2 core. Fe and Fe alloy clad MgB_2 wires and tapes have high transport critical current densities [113-117].

In this thesis, we have fabricated monofilament (MgB_2/Fe, MgB_2/Ag and MgB_2/SS) and multifilament (6 and 7 filament MgB_2/Fe/Cu, 7 and 23 filament MgB_2/Ag/Fe and 6 filament MgB_2/SS/Cu) superconducting MgB_2 wires and tapes by using powder-in-tube (PIT) method and continuous tube forming and filling (CTFF) method following the ex situ and mixture of ex situ and in situ reaction routes. We have investigated the superconducting properties of monofilament and multifilament MgB_2 superconducting samples employing X-ray diffraction (XRD), scanning electron microscope (SEM), energy dispersive X-ray spectrometer (EDS), optical microscope, critical transition temperature, critical current density, magnetoresistivity and magnetization measurements. Moreover, we have investigated the effect of extreme rolling on the superconducting properties of commercial MgB_2 tapes.

5.2. Monofilament Wires and Tapes

5.2.1. MgB_2/Fe Monofilament Wires and Tapes

The MgB_2/Fe monofilament wires and tapes were fabricated by ex-situ PIT method using commercially available MgB_2 powder (Alfa Aesar, -325 mesh, <44 micron) without any intermediate annealing as described in Experimental Method.

We have investigated the effect of annealing temperatures and times on the formation of MgB_2 phase, transition temperature (T_c), lattice parameters (*a* and *c*), full width at half maximum (FWHM), crystallinity, resistivity (ρ), residual resistivity ratio (RRR), active cross-sectional area fraction (A_F) and critical current densities (J_c) of MgB_2/Fe monofilament tapes. To obtain the optimum annealing temperature, MgB_2/Fe monofilament tapes were annealed at 650°C, 750°C, 850°C, 950°C and 1050°C for 60 minutes. Then, to obtain the optimum annealing time, the samples were annealed at 950°C for 15, 30, 60, 120, 180 and 240 minutes. The samples were characterized using X-ray diffraction (XRD), scanning electron microscope (SEM), energy dispersive X-ray spectrometer (EDS), optical microscope, critical transition temperature (T_c) and critical current density (J_c) measurements.

5.2.1.1. Optimization of the annealing temperature of the MgB_2/Fe Monofilament Tape

Several short samples 2 cm in length were cut from the MgB_2/Fe monofilament tape in order to determine optimum annealing temperature. These pieces were then heat treated at 650°C, 750°C, 850°C, 950°C and 1050°C for 60 minutes in a tube furnace. All heat treatments of the samples were done under 3 bars high purity argon (Ar) gas atmosphere and all samples were cooled down to room temperature in the furnace. The heating and cooling rates of the temperatures were chosen to be 5°C min^{-1}.

To find the optimum annealing temperature of MgB_2/Fe sample, the phase composition and microstructure properties were investigated by XRD measurements. Figure 5.1 shows intensities as a function of 2θ for non-annealed and annealed at

650°C-1050°C for 60 minutes MgB_2/Fe monofilament tapes. Miller indices are indicated in the figure. The lattice parameters *a* and *c* determined from the (*h*00) and (00*l*) peaks of the XRD data are given in Table 5.1. The crystallographic symmetry of the material was found to be hexagonal and the unit cell parameters (*a* and *c*) of the non-annealed sample were calculated as 3.0892 and 3.5246 Å, respectively. An appreciable change in the lattice parameters of the samples was found within the experimental limit. The lattice parameter *a* increases slightly from 3.0892 to 3.0967 Å and the lattice parameter *c* increases slightly from 3.5246 to 3.5386 Å with increasing the annealing temperature up to 950°C. The lattice parameter *c* for the sample annealed at 950°C for 60 min. was found to be 3.5386 Å. On the other hand, it decreases to 3.5348 Å for the sample annealed at 1050°C for 60 min. The lattice parameter *a* for the sample annealed at 950°C for 60 min. was found to be 3.0967 Å. However, it decreases to 3.0938 Å for the sample annealed at 1050°C for 60 min. These lattice parameters are reasonable consistent with other works [16,14,119].

The values of grain sizes were estimated from XRD measurements by using Scherrer-Warren formula [118].

$$D=(0.94\lambda/B\cos\theta) \qquad (5.1)$$

Where D is the crystallite size in nm, λ (15.418 nm) is the wavelength of X-ray in nm, θ is the angle of intensity peak and B is the full width at half maximum (FWHM) of the same intensity peak. The FWHM values decrease with increasing the annealing temperature from 650 to 1050°C. This behaviour of the MgB_2 samples as a function of annealing temperature can be explained by the improvement of

crystallinity with increasing the annealing temperature, resulting in increasing grain size. The grain sizes calculated from XRD patterns are about 50-60 nm for annealed at 650°C-950°C for 60 min. samples. Improvement of crystallinity is related to better grain connectivity of the MgB_2 grains.

Table 5.1 The lattice parameters *a* and *c* of the MgB_2/Fe samples annealed at 650°C-950°C for 60 minutes.

Samples	*a* (Å)	*c* (Å)
no heat treatment	3.0892	3.5246
650°C 60 min.	3.0901	3.5310
750°C 60 min.	3.0910	3.5322
850°C 60 min.	3.0923	3.5335
950°C 60 min.	3.0967	3.5386
1050°C 60 min.	3.0938	3.5348

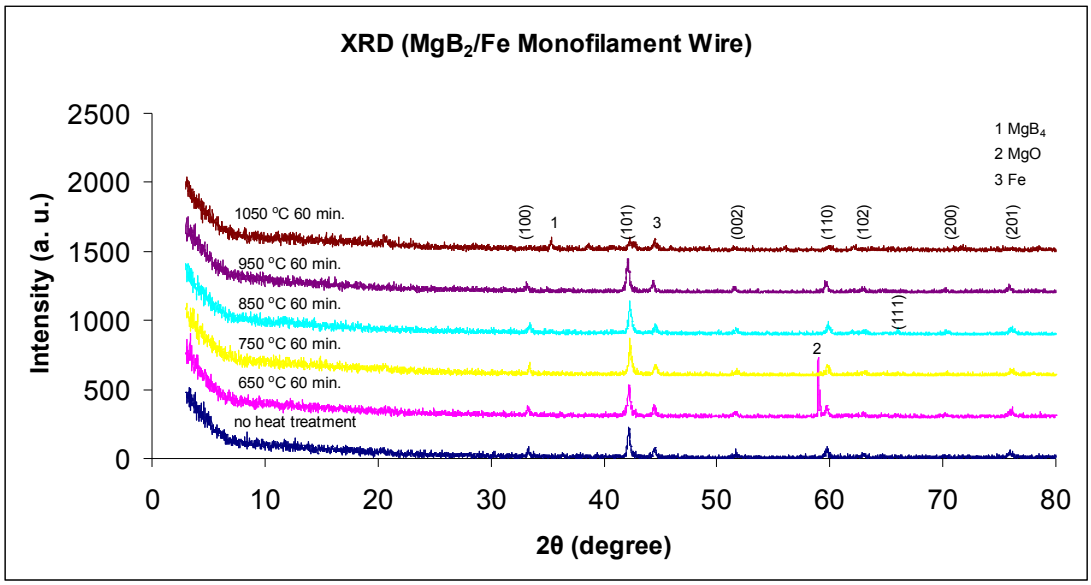

Figure 5.1 X-ray diffraction patterns of the MgB_2/Fe monofilament tapes annealed at 650°C-1050°C for 60 minutes.

MgB_2 phase formation was observed for both non-annealed and annealed (650°C-1050°C for 60 minutes) MgB_2/Fe monofilament tapes. However, some impurity phase such as MgO was observed for the sample annealed at 650°C for

60 min. while MgB_4 phase was observed for the sample annealed at 1050°C for 60 minutes. The peak (101) shifts to low angle with increasing annealing temperature. Therefore, lattice parameters *a* and *c* increases with increasing annealing temperature.

The temperature dependence of the resistivity of the samples is shown in Figure 5.2. T_c^{onset}, T_c^{offset} and ΔT_c values were tabulated in Table 5.2.

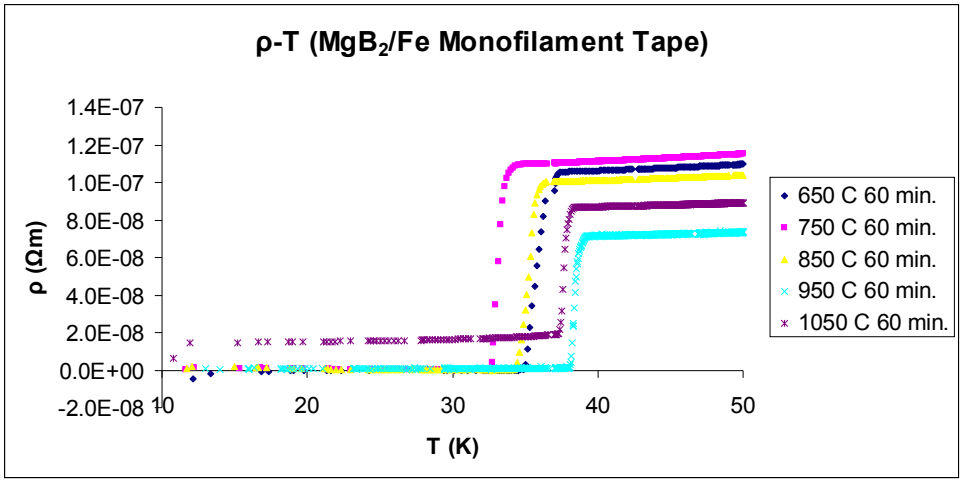

Figure 5.2 ρ-T graphs of the MgB_2/Fe monofilament tapes annealed at 650°C-1050°C for 60 minutes.

A different method was used for preparing current and voltage contacts of the MgB_2/Fe monofilament tape. Standard Pb-Sn (40/60) solder was used for forming the current and voltage contacts. Both of voltage contacts were directly soldered with standard Pb-Sn (40/60) solder to the sheath materials of the samples. Both of ends of the samples were painted with silver and then both of painted ends of the samples were soldered with standard Pb-Sn (40/60) solder for current contacts as shown in Figure 5.3. All MgB_2/Fe monofilament tapes were prepared with this method.

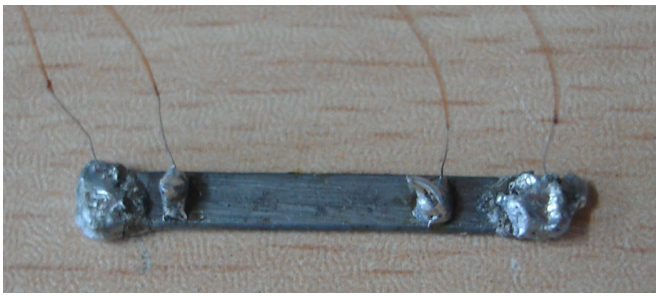

Figure 5.3 Current and voltage contacts of MgB_2/Fe monofilament tape.

As tabulated in Table 5.2 the sample annealed at 950°C for 60 minutes has the highest T_c^{onset} (39.3 ± 0.2 K) and T_c^{offset} (38.1 ± 0.2 K) values.

The active cross-sectional area fraction (A_F) values were estimated from resistivity measurements by using Rowell's connectivity analysis [120].

$$A_F = \rho_{ideal} / [\rho_{300K} - \rho_{40K}] \tag{5.2}$$

Where ρ_{ideal}=7.3 μΩcm [124,125]. In addition, the residual resistivity ratio (RRR) defined by ρ_{300K} / ρ_{40K} was also estimated [126].

Table 5.3 illustrates ρ_{40K}, ρ_{300K}, $\Delta\rho$, RRR and A_F values for MgB_2/Fe tapes with different annealing temperatures. In order to explain the connectivity between grains, A_F values are estimated for the samples annealed at 650°C-1050°C for 60 min. The estimated A_F values were 0.27, 0.28, 0.29, 0.59 and 0.23 for the samples annealed at 650°C-1050°C for 60 min., respectively. According to Rowell's connectivity analysis [120], the higher A_F value is related to the better connectivity between grains. The highest A_F value obtained for the sample annealed at 950°C for 60 min. indicates the better intergranular connection in MgB_2 grains. On the other hand, the lowest A_F value obtained for the sample annealed at 1050°C for 60 min.

shows the degradation of the grain connectivity [94,121-123]. We observed that ρ_{300K} values decreased with increasing annealing temperature up to 950°C. As the annealing temperature increases from 650°C to 950°C, the room temperature resistivity value decreases from 36.85 μΩcm to 19.51 μΩcm. This is related to the better crystallinity of MgB_2 phase due to grain growth. The room temperature resistivity value of the sample annealed at 950°C for 60 min. was found to be 19.51 μΩcm. On the other hand, it increases to 40.44 μΩcm for the sample annealed at 1050°C for 60 min. In the normal state, all the samples show metallic behaviour.

Table 5.2 T_c values of the MgB_2/Fe monofilament tapes annealed at 650°C-1050°C for 60 minutes.

Tapes	T_c^{onset} (K)	T_c^{offset} (K)	ΔT_c (K)
650°C 60 min.	37.4	34.9	2.5
750°C 60 min.	34.5	32.6	1.9
850°C 60 min.	36.4	34.2	2.2
950°C 60 min.	39.3	38.1	1.2
1050°C 60 min.	38.4	37.3	1.1

Table 5.3 ρ_{40K}, ρ_{300K}, $\Delta\rho$, RRR and A_F values for MgB_2/Fe tapes with different annealing temperatures.

Samples	$\rho_{40\,K}$ (μΩcm)	$\rho_{300\,K}$ (μΩcm)	$\Delta\rho(\rho_{300\,K}-\rho_{40\,K})$ (μΩcm)	RRR	A_F (%)
650°C 60 min.	10.63	36.85	26.22	3.46	0.27
750°C 60 min.	11.12	36.69	25.57	3.30	0.28
850°C 60 min.	10.10	35.26	25.16	3.49	0.29
950°C 60 min.	7.17	19.51	12.34	2.72	0.59
1050°C 60 min.	8.70	40.44	31.74	4.65	0.23

The current-voltage (I-V) characteristics of the samples were measured at 20 K, 25 K and 30 K with the standard four-probe method under self-field. Figures 5.4, 5.5 and 5.6 shows I-V graphs of the samples measured at 20 K, 25 K and 30 K respectively. The I_c values of all samples at 20 K, 25 K and 30 K are tabulated in Table 5.4. The highest critical current values were obtained for the sample annealed at 950°C for 60 minutes. As the temperature increased, I_c values of the samples decrease.

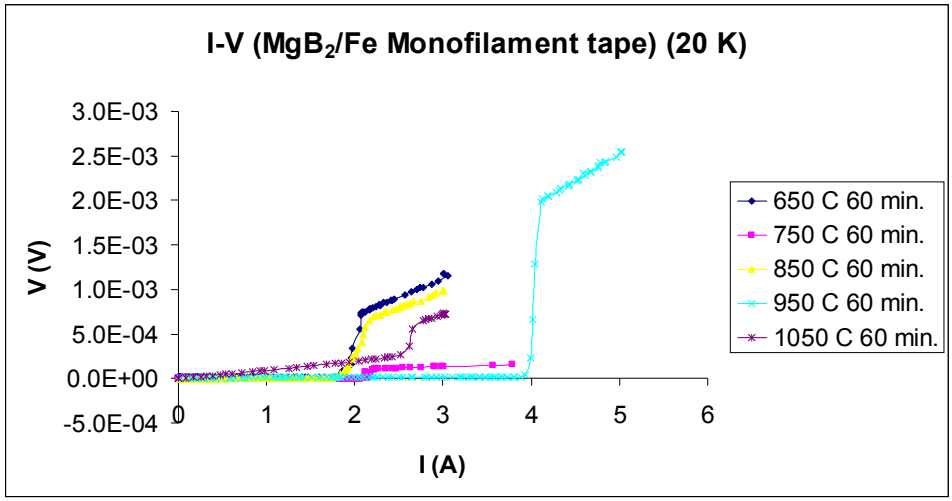

Figure 5.4 I-V graphs of the MgB_2/Fe monofilament tapes (20 K).

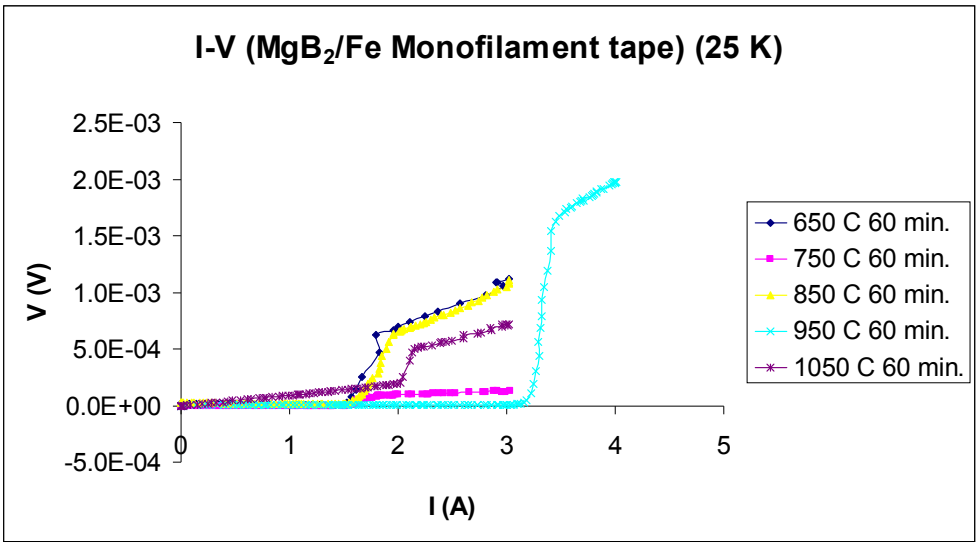

Figure 5.5 I-V graphs of the MgB_2/Fe monofilament tapes (25 K).

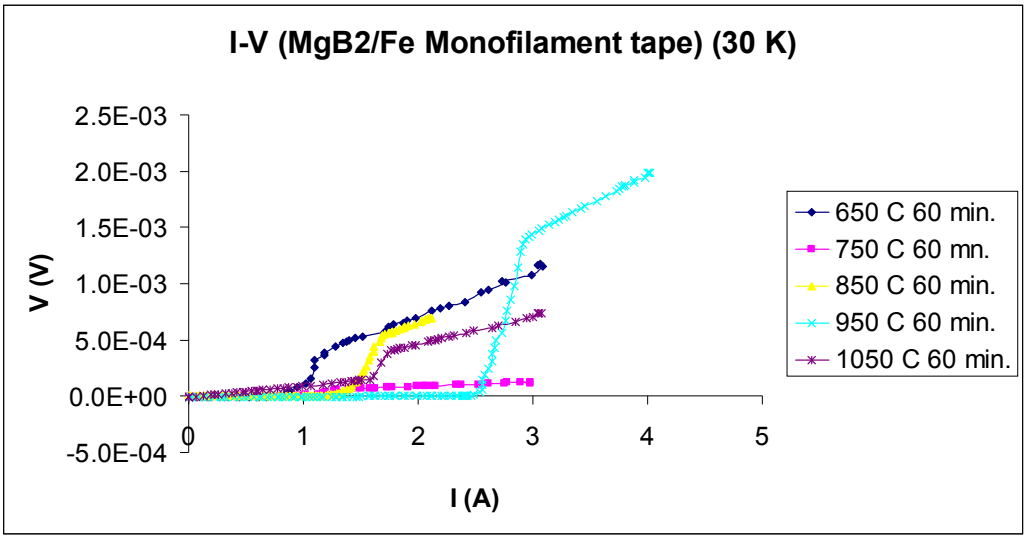

Figure 5.6 I-V graphs of the MgB_2/Fe monofilament tapes (30 K).

Table 5.4 I_c values of the MgB_2/Fe monofilament tapes annealed at 650°C-1050°C for 60 minutes.

Tapes	20 K	25 K	30 K
	I_c (A)	I_c (A)	I_c (A)
650°C 60 min.	1.82	1.52	0.75
750°C 60 min.	2.10	1.58	0.95
850°C 60 min.	1.70	1.50	1.20
950°C 60 min.	3.92	3.18	2.54
1050°C 60 min.	2.61	2.04	1.61

Figures 5.7, 5.8 and 5.9 shows the electric field as a function of critical current density for the samples measured at 20 K, 25 K and 30 K respectively. From I-V measurements, the critical current density values of the samples were calculated and are tabulated in Table 5.5. The critical current density is found to increase in the 650 to 950 °C annealing temperature range while it decreases above 950°C. The highest

critical current density values were obtained for the sample annealed at 950°C for 60 minutes.

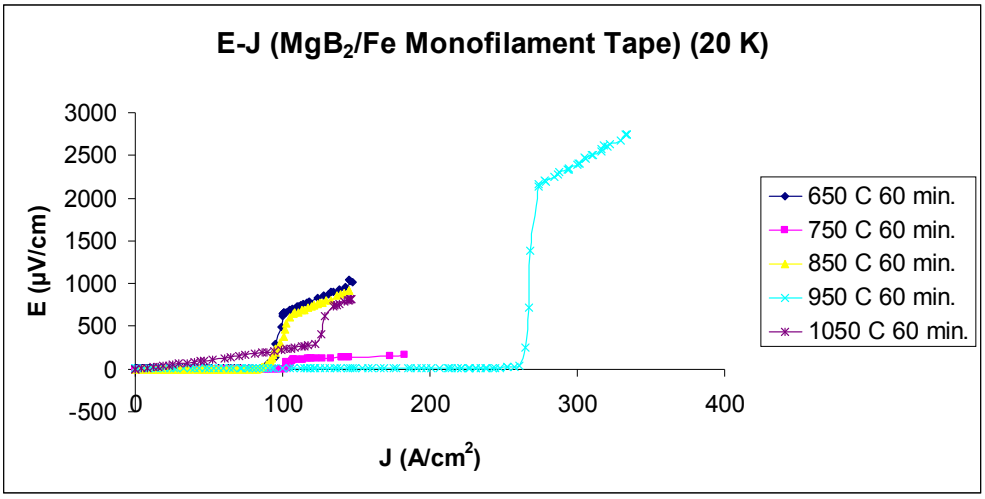

Figure 5.7 E-J graphs of the MgB_2/Fe monofilament tapes (20 K).

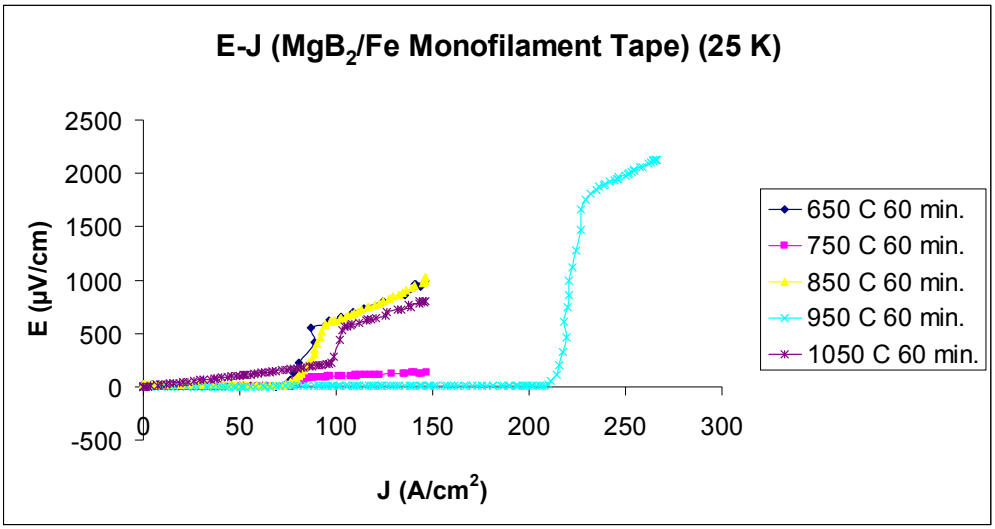

Figure 5.8 E-J graphs of the MgB_2/Fe monofilament tapes (25 K).

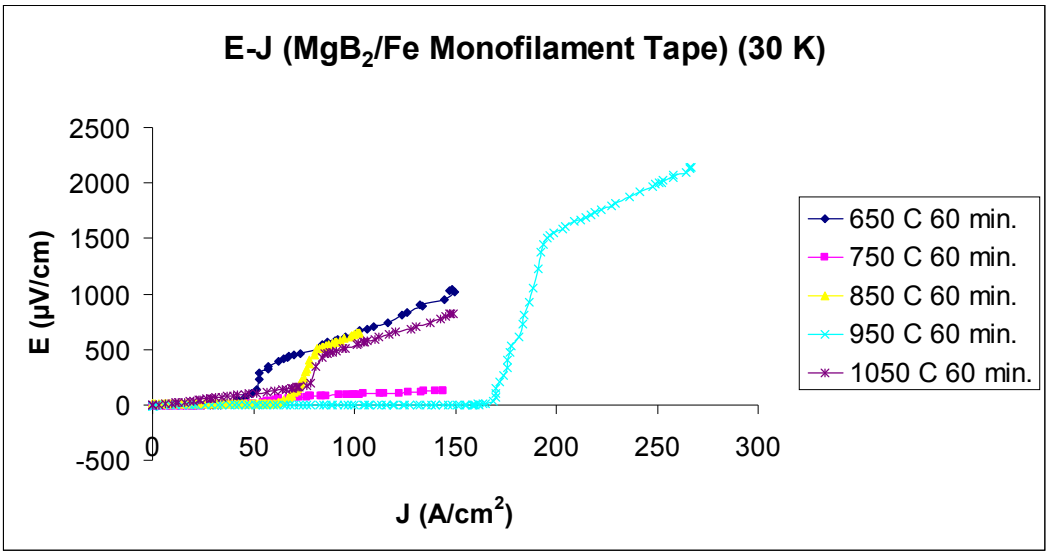

Figure 5.9 E-J graphs of the MgB_2/Fe monofilament tapes (30 K).

Table 5.5 J_c values of the MgB_2/Fe monofilament tapes.

Tapes	20 K	25 K	30 K
	J_c (A/cm^2)	J_c (A/cm^2)	J_c (A/cm^2)
650^{o}C 60 min.	88.05	73.54	36.29
750^{o}C 60 min.	101.60	76.44	45.96
850^{o}C 60 min.	82.25	72.57	58.06
950^{o}C 60 min.	260.43	211.26	168.75
1050^{o}C 60 min.	126.28	98.70	77.89

The surface morphology of the Fe-sheathed MgB_2 tapes annealed at 650^{o}C-1050^{o}C for 60 minutes are studied by SEM and the surface micrographs are displayed in Figure 5.10.

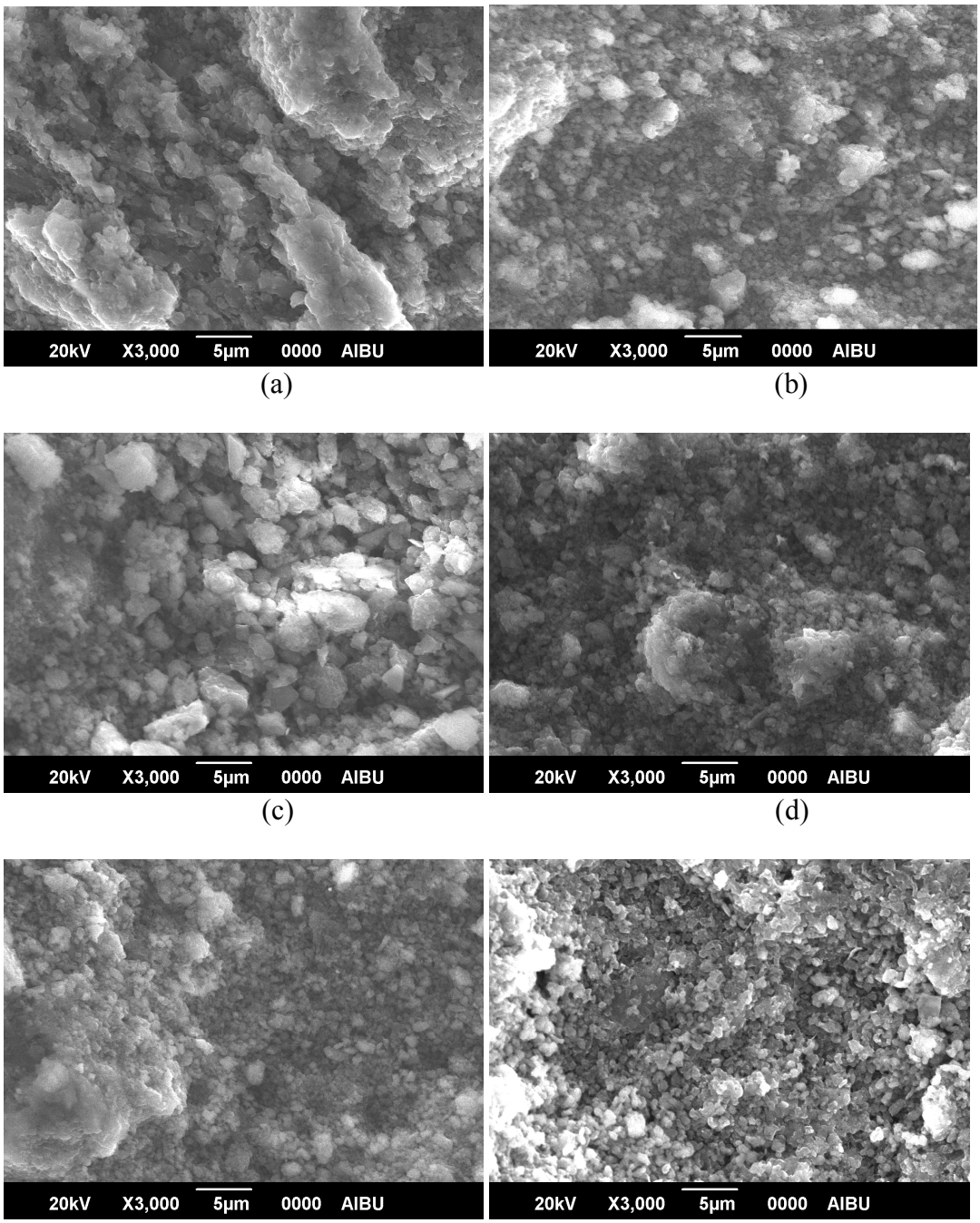

Figure 5.10 SEM pictures of Fe-sheathed MgB_2 tapes (a) non-annealed, annealed at (b) 650°C, (c) 750°C, (d) 850°C, (e) 950°C and (f) 1050°C for 60 min.

As the annealing temperature increases, the grain sizes decrease and surface of the sample becomes denser and smoother. The sample annealed at 1050°C for 60 min. shows more signs of partial melting due to higher annealing temperature.

From these over all observation, the optimum annealing temperature is found to be 950°C.

5.2.1.2. Optimization of the annealing time of the MgB_2/Fe Monofilament Tape

Several short samples 2 cm in length were cut from the MgB_2/Fe monofilament tape in order to determine optimum annealing time. These pieces were then heat treated at 950°C for 15, 30, 60, 120, 180 and 240 minutes in a tube furnace. The rest of the procedure is the same as in optimization of the annealing temperature process.

To determine the optimum annealing time of MgB_2/Fe sample, the phase composition and microstructure properties were also investigated by XRD measurements. Figure 5.11 shows intensities as a function of 2θ for no-annealed and annealed 950°C for 30-240 minutes MgB_2/Fe monofilament tapes. Miller indices are indicated in the Figure 5.11 and the lattice parameters *a* and *c* determined from the (*h*00) and (00*l*) peaks of the XRD data are given in Table 5.6. The lattice parameters *a* and *c* increase from 3.0892 to 3.0967 Å and from 3.5246 to 3.5386 Å with increasing the annealing time up to 60 minutes, respectively. The lattice parameter *c* for the sample annealed at 950°C for 60 min. was found to be 3.5386 Å. On the other hand, it decreases to 3.5163 Å for the sample annealed at 950°C for 240 min. The lattice parameter *a* for the sample annealed at 950°C for 60 min. was found to be 3.0967 Å. However, it decreases to 3.0715 Å for the sample annealed at 950°C for 240 min. The grain sizes calculated from XRD patterns are about 50 nm for annealed at 950°C for 30-240 min. samples.

Table 5.6 The lattice parameters *a* and *c* of the annealed at 950°C for 30-240 min. samples.

Samples	*a* (Å)	*c* (Å)
no heat treatment	3.0892	3.5246
950°C 30 min.	3.0957	3.5316
950°C 60 min.	3.0967	3.5386
950°C 120 min.	3.0826	3.5208
950°C 240 min.	3.0715	3.5163

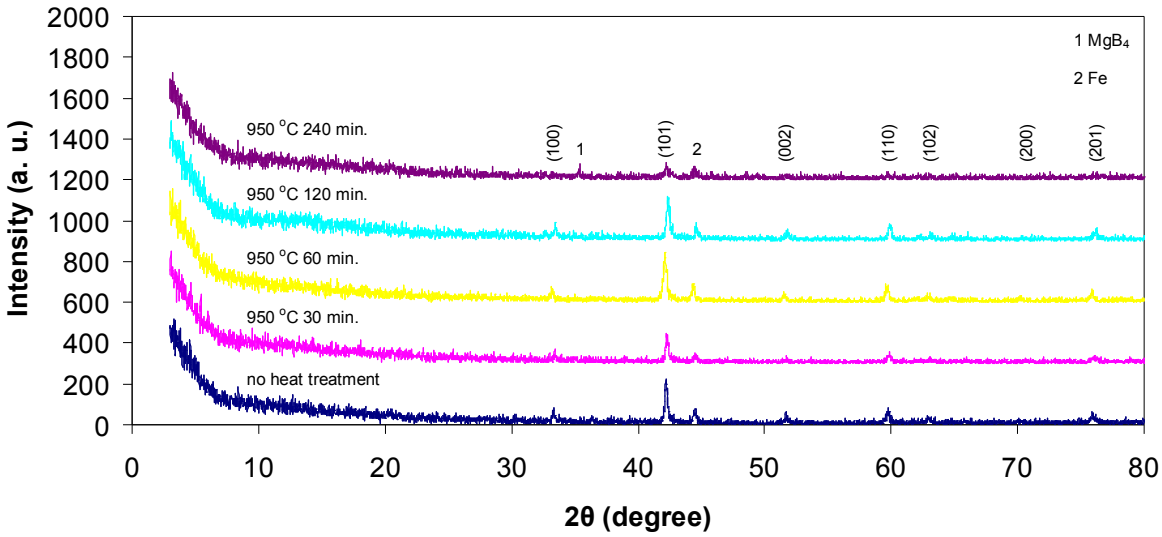

Figure 5.11 X-ray diffraction patterns of the samples (950°C for 30-240 minutes).

MgB_2 phase formation was observed for the non-annealed and annealed 950°C for 30-240 minutes MgB_2/Fe monofilament tapes. However, some impurity phase such as MgB_4 was observed for the sample annealed at 950°C for 240 minutes. The peak (101) shifts to low angle with increasing annealing time. Therefore, lattice parameters *a* and *c* increase with increasing annealing time up to 60 min., then they decrease.

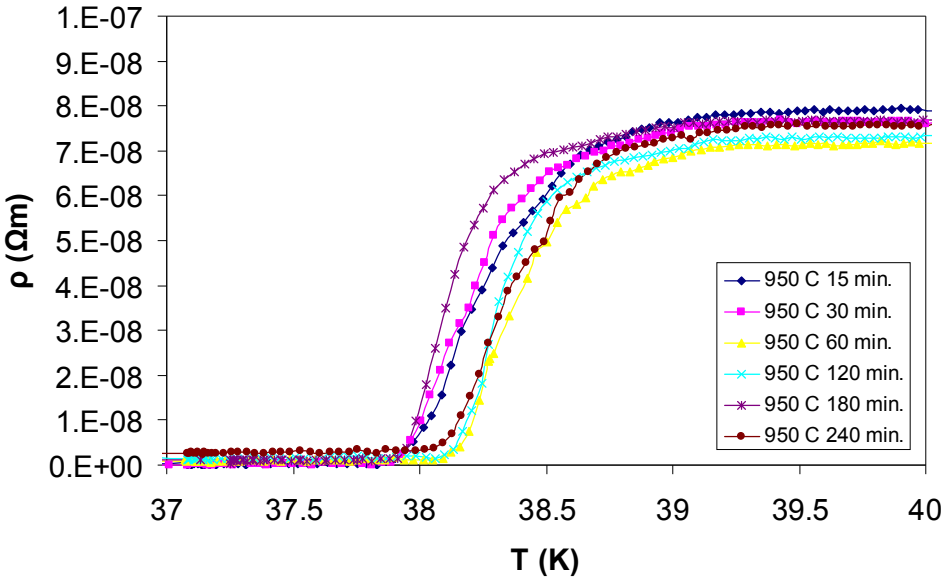

Figure 5.12 ρ-T graph of the MgB_2/Fe monofilament tape.

Figure 5.12 exhibits the resistivity versus temperature measurements for the MgB_2/Fe monofilament tape annealed at 950°C for 15-240 minutes. The results of the measurements were tabulated in Table 5.7. Table 5.8 shows ρ_{40K}, ρ_{300K}, $\Delta\rho$, RRR and A_F values for MgB_2/Fe tapes with different annealing times. In order to clarify the connectivity between grains, A_F values are estimated for the samples annealed at 950°C for 30-240 minutes. The estimated A_F values were 0.39, 0.59, 0.42 and 0.37 for the samples annealed at 950°C for 30-240 minutes respectively. The highest A_F value obtained for the sample annealed at 950°C for 60 min. indicates the better intergranular connection in MgB_2 grains. According to Rowell's connectivity analysis, it was concluded that the higher A_F value is related to the better connectivity between grains. We obtained lower A_F values for the other samples. As the annealing time increases from 30 min. to 60 min., the room temperature resistivity value decreases from 25.89 μΩcm to 19.51 μΩcm while the annealing time increases from 60 min. to 240 min. the room temperature resistivity value

increases from 19.51 μΩcm to 27.29 μΩcm. The lower room temperature resistivity value may be related to higher density and better intergranular connection between grains.

Table 5.7 T_c values of the MgB_2/Fe monofilament wires.

Şeritler	T_c^{onset} (K)	T_c^{offset} (K)	ΔT_c (K)
950°C 15 min.	39.1	37.8	1.3
950°C 30 min.	39.1	37.9	1.2
950°C 60 min.	39.3	38.1	1.2
950°C 120 min.	39.2	38.1	1.1
950°C 180 min.	39.0	37.9	1.1
950°C 240 min.	39.0	38.0	1.0

As seen in Table 5.7 the highest T_c^{onset} (39.3 ± 0.2 K) and T_c^{offset} (38.1 ± 0.2 K) values were obtained for the sample annealed at 950°C for 60 minutes.

Table 5.8 ρ_{40K}, ρ_{300K}, $\Delta\rho$, RRR and A_F values for MgB_2/Fe wires with different annealing times.

Samples	$\rho_{40\,K}$ (μΩcm)	$\rho_{300\,K}$ (μΩcm)	$\Delta\rho(\rho_{300\,K}-\rho_{40\,K})$ (μΩcm)	RRR	A_F (%)
950°C 30 min.	7.61	25.89	18.28	3.40	0.39
950°C 60 min.	7.17	19.51	12.34	2.72	0.59
950°C 120 min.	7.35	24.64	17.29	3.35	0.42
950°C 240 min.	7.68	27.29	19.61	3.55	0.37

The current-voltage characteristics of the samples were measured at 20 K, 25 K and 30 K with the standard four-probe method under self-field. Figures 5.13, 5.14 and 5.15 shows I-V graphs of the samples measured at 20 K, 25 K and 30 K

respectively. The I_c values of all samples at 20 K, 25 K and 30 K are tabulated in Table 5.9. The highest critical current values were obtained for the sample annealed at 950°C for 60 minutes. As the temperature increased, I_c values of the samples decrease.

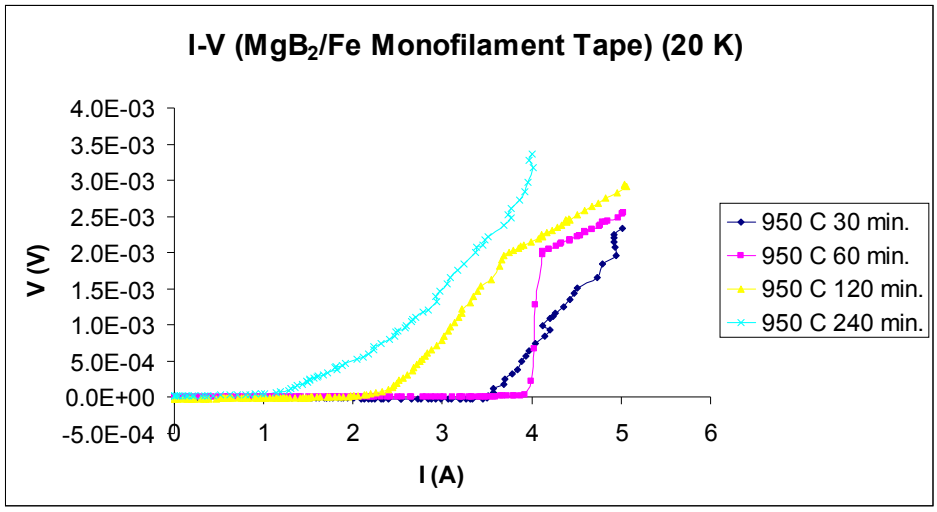

Figure 5.13 I-V graphs of the MgB_2/Fe monofilament tapes (20 K).

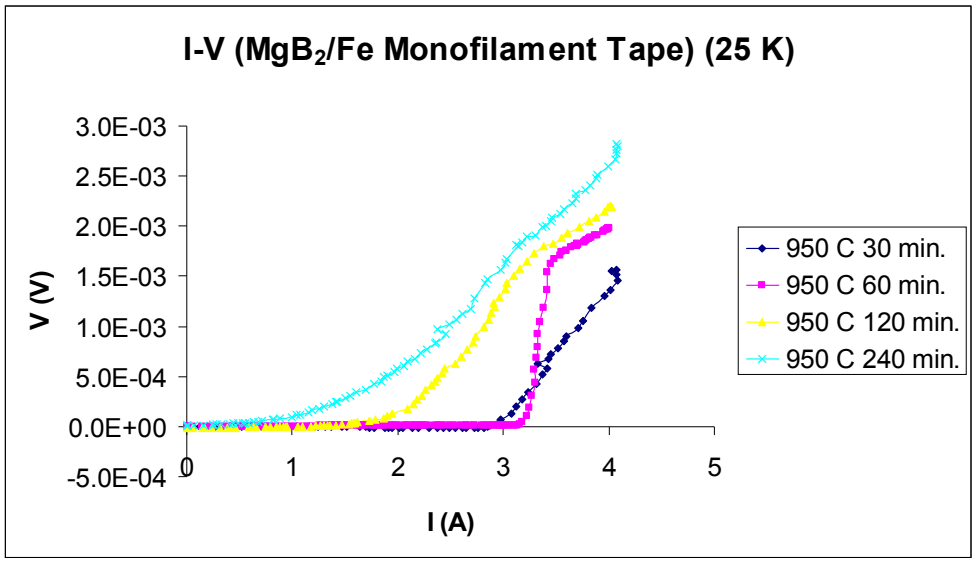

Figure 5.14 I-V graphs of the MgB_2/Fe monofilament tapes (25 K).

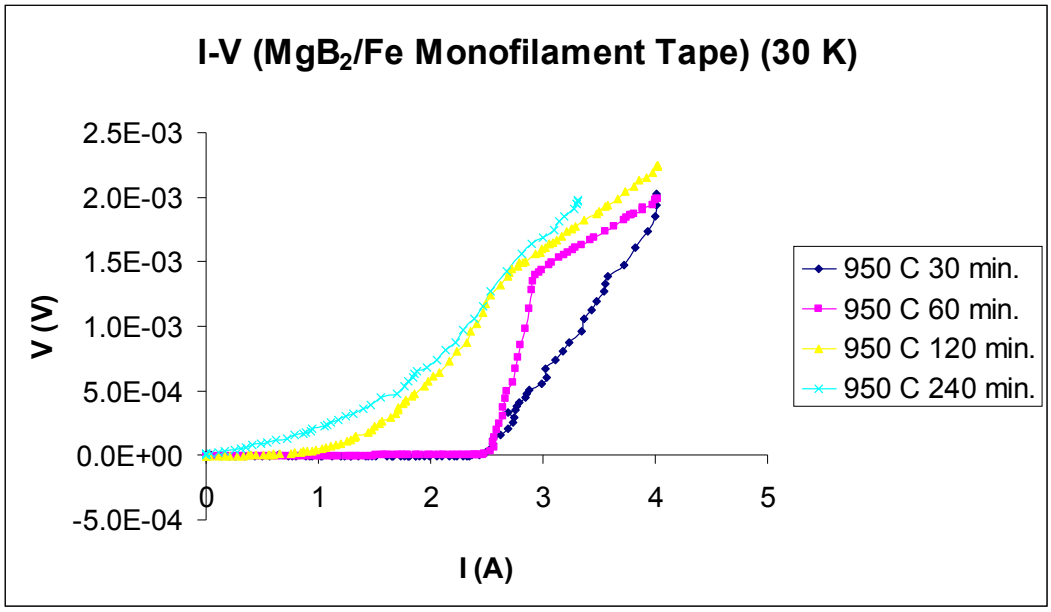

Figure 5.15 I-V graphs of the MgB_2/Fe monofilament tapes (30 K).

Table 5.9 I_c values of the MgB_2/Fe monofilament tapes annealed at 950°C for 15-240 minutes.

Tapes	20 K	25 K	30 K
	I_c (A)	I_c (A)	I_c (A)
950°C 30 min.	3.50	2.87	2.43
950°C 60 min.	3.92	3.18	2.54
950°C 120 min.	2.12	1.73	1.03
950°C 240 min.	1.28	0.99	0.72

Figures 5.16, 5.17 and 5.18 shows the electric field as a function of critical current density for the samples measured at 20 K, 25 K and 30 K respectively. From I-V measurements, the critical current density values of the MgB_2/Fe monofilament tapes annealed at 950°C for 30, 60, 120 and 240 minutes were calculated and are listed in Table 5.10. The critical current density is found to increase in the 30 to 60 minutes annealing time range while it decreases above 60 minutes. The highest critical

current density values were obtained for the sample annealed at 950°C for 60 minutes.

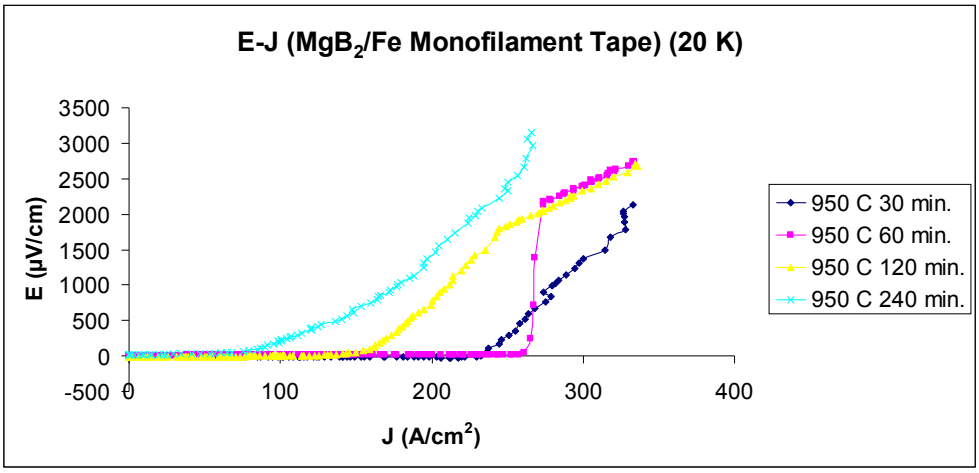

Figure 5.16 E-J graphs of the MgB_2/Fe monofilament tapes (20 K).

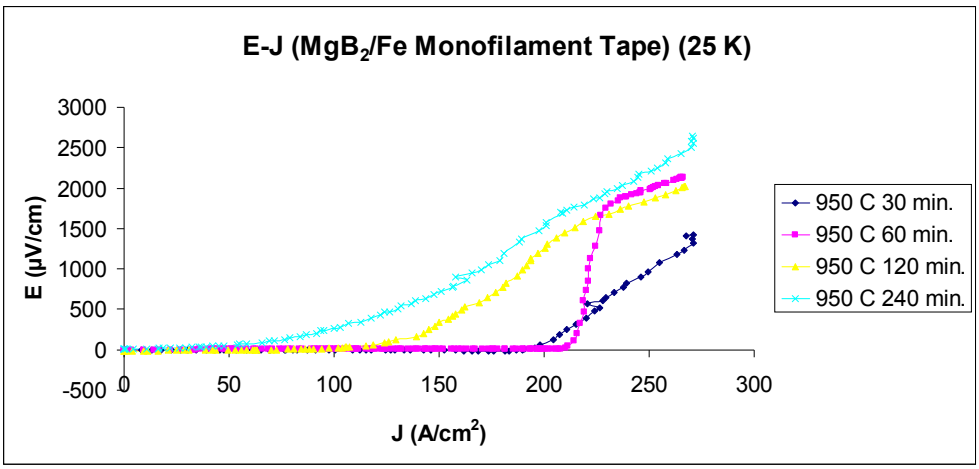

Figure 5.17 E-J graphs of the MgB_2/Fe monofilament tapes (25 K).

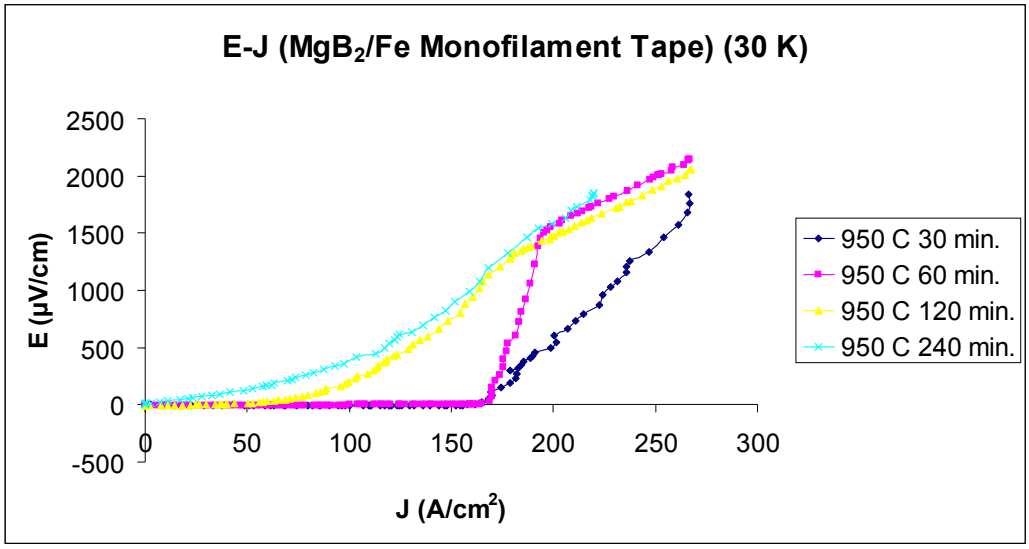

Figure 5.18 E-J graphs of the MgB_2/Fe monofilament tapes (30 K).

Table 5.10 J_c values of the MgB_2/Fe monofilament tapes annealed at 950°C for 15-240 minutes.

Tapes	20 K	25 K	30 K
	J_c (A/cm^2)	J_c (A/cm^2)	J_c (A/cm^2)
950°C 30 min.	232.53	190.67	161.44
950°C 60 min.	260.43	211.26	168.75
950°C 120 min.	140.84	114.93	68.43
950°C 240 min.	85.03	65.77	47.83

The surface morphology of the Fe-sheathed MgB_2 tapes annealed at annealed at 950°C for 30-240 minutes are studied by SEM and the surface micrographs are showed in Figure 5.19.

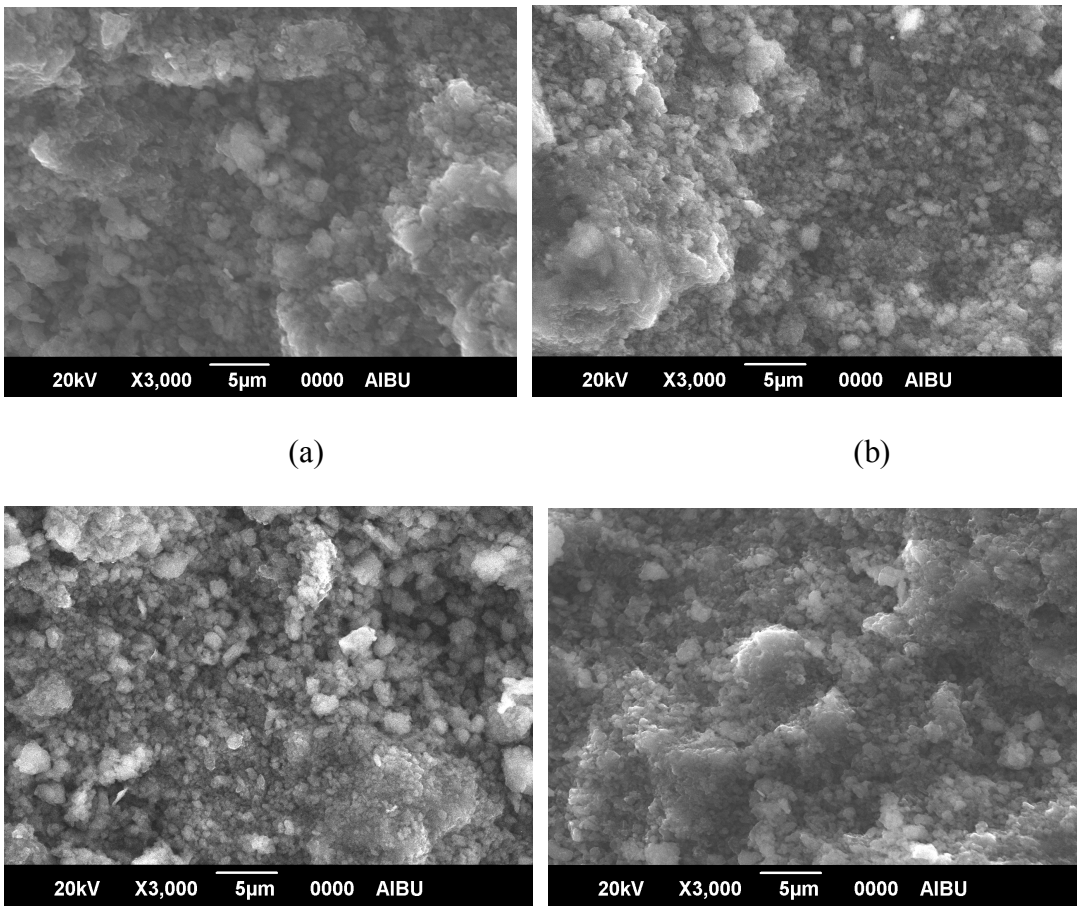

Figure 19 SEM pictures of Fe-sheathed MgB_2 tapes annealed at 950°C for (a) 30 min., (b) 60 min., (c) 120 min., (d) 240 min.

The sample annealed at 950°C for 60 min. has good grain connectivity, better surface and low porosity. Moreover, it is denser than the other samples.

From these observations, the optimum annealing temperature and time found to be 950°C and 60 min., respectively.

5.2.1.3. SEM Investigations of the MgB_2/Fe Monofilament Wires and Tapes

Microstructural investigations and surface morphologies of the MgB_2/Fe monofilament wires and tapes were studied by SEM in order to determine connection and size of the grains and the presence of microvoid and microcrack.

Figure 5.20 (a) shows SEM picture of transverse cross section of a 1.58 mm in diameter of Fe-sheathed MgB_2 wire without heat treatment. The diameter of the superconducting core was measured about 1.28 mm from SEM picture. The MgB_2/Fe monofilament wire has a regular round shape. The cross section shows uniform deformation of the composite wire without any problems such as breakage and sausaging of the components. Figure 5.20 (b) shows that the thickness of the Fe sheath is about 150 μm. Figures 5.20 (c)-(d) show a dense microstructure of MgB_2 with a grain size of about 5 μm. A sharp interface between Fe sheath and MgB_2 is a sign for no reaction.

Table 5.11 summarizes the main characteristics of the MgB_2/Fe monofilament wire.

Table 5.11 MgB_2/Fe Monofilament wire Characteristics.

Number of MgB_2 filaments	1
Preparation technique	Ex-situ PIT
Sheath material	Iron
(MgB_2/Fe) cross section	1.95967 mm^2
MgB_2 cross section	1.28614 mm^2
Iron cross section	0.67353 mm^2

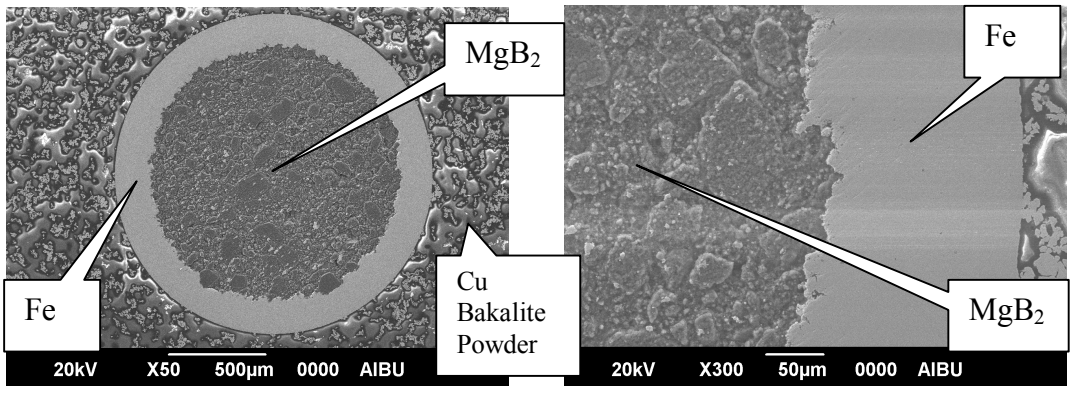

(a) (b)

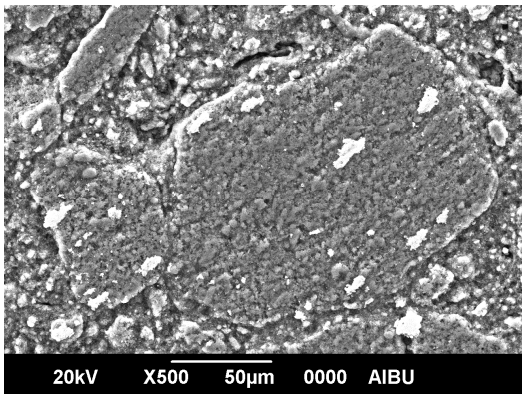

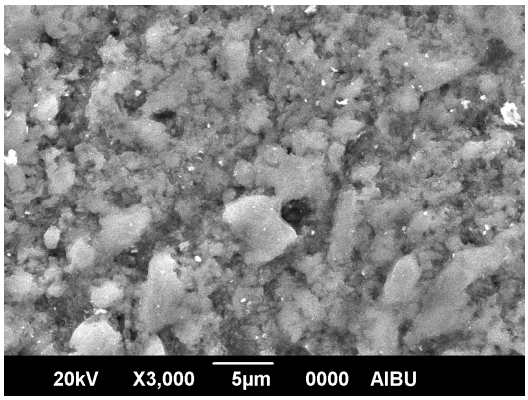

(c) (d)

Figure 5.20 (a-d) SEM pictures of transverse cross section of the MgB_2/Fe monofilament wire.

Figure 5.21(a) shows SEM picture of transverse cross section of Fe-sheathed MgB_2 tape without heat treatment. The MgB_2/Fe monofilament tape has a regular shape. Figure 5.21 (b) shows that the thickness of the Fe sheath is about 100 µm. Figure 5.21 (c)-(d) shows a dense microstructure of MgB_2 with a grain size of about 5 µm. No sign of any reaction between Fe sheathing and MgB_2 core is observed.

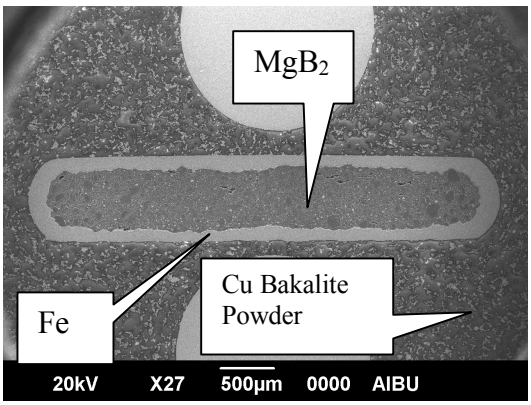

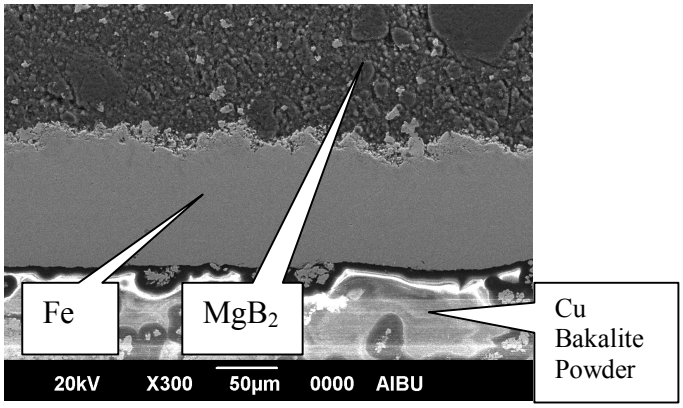

(a) (b)

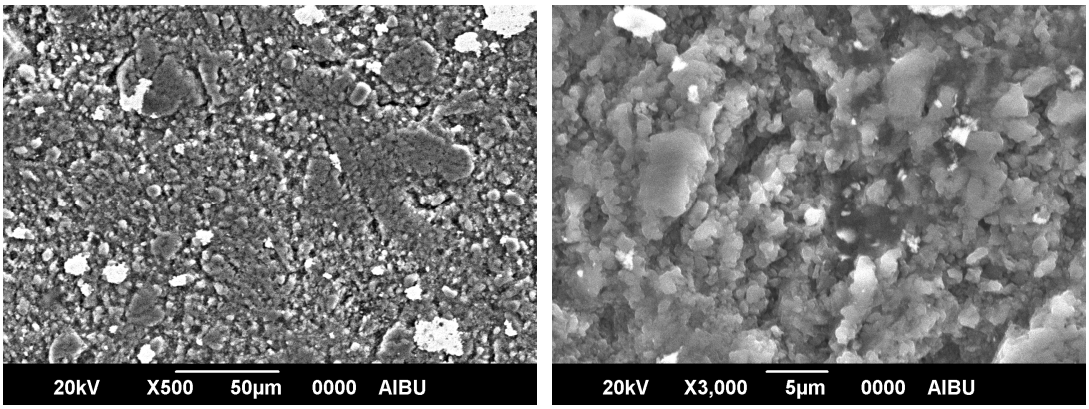

(c) (d)

Figure 5.21 (a-d) SEM pictures of transverse cross section of the MgB_2/Fe monofilament tape.

5.2.1.4. EDS Investigations of the MgB_2/Fe Monofilament Wires and Tapes

Microstructure and chemical composition investigations of the MgB_2/Fe monofilament wires and tapes that are not annealed were investigated by scanning electron microscope with an energy dispersive X-ray spectrometer (EDS) analysis.

Figures 5.22 and 5.23 show the element distribution maps of Mg, B, Fe and O in the cross section of the MgB_2/Fe monofilament wire and tape without heat treatment, respectively.

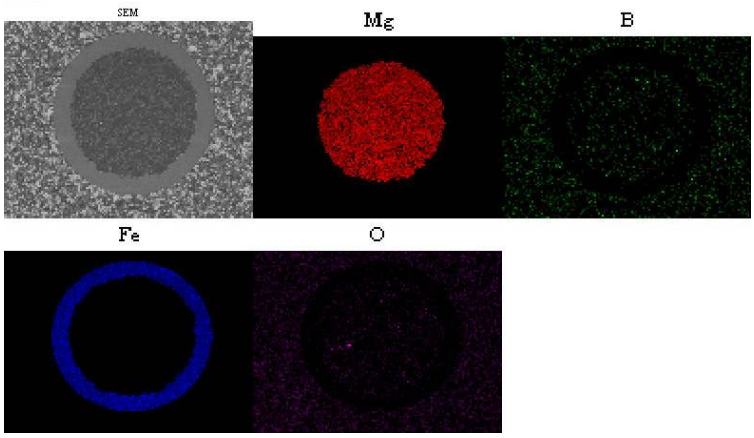

Figure 5.22 EDS picture of transverse cross section of the MgB_2/Fe monofilament wire.

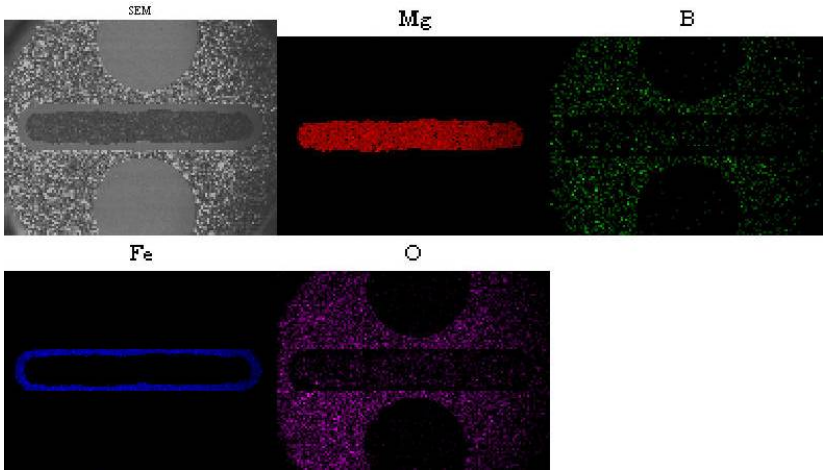

Figure 5.23 EDS picture of transverse cross section of the MgB_2/Fe monofilament tape.

5.2.1.5. Optical Microscopy Investigations of the MgB_2/Fe Monofilament Wires and Tapes

Surface structures of the monofilament and multifilament MgB_2 wires and tapes were investigated by optical microscope.

Figure 5.24 (a-d) and Figure 5.25 (a-b) show optical microscopy images of transverse cross section of the MgB_2/Fe monofilament wire and tape without heat treatment, respectively.

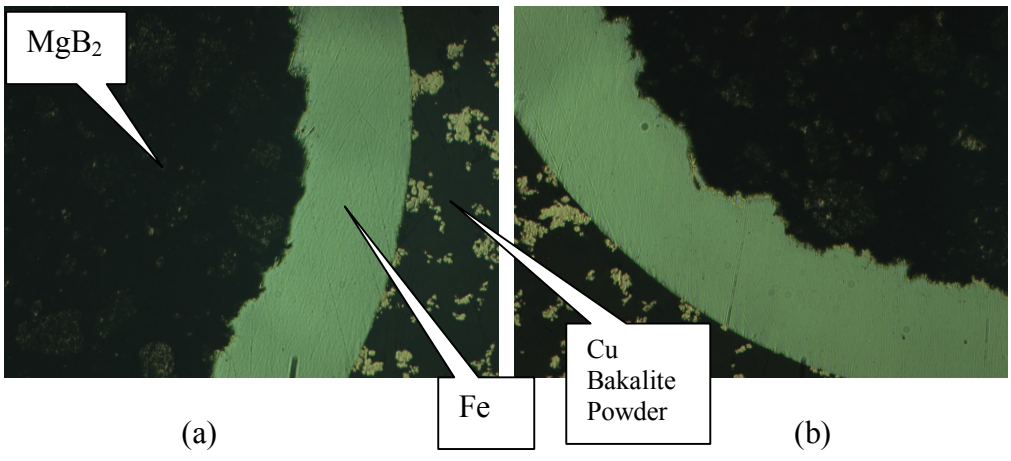

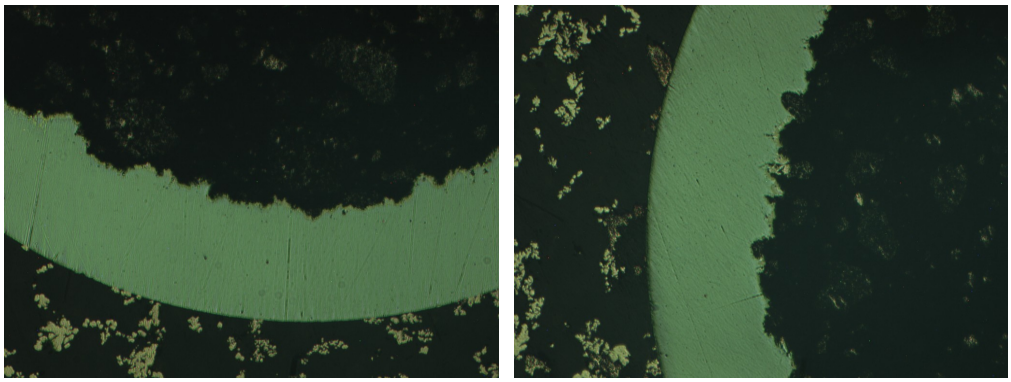

(c) (d)

Figure 5.24 (a-d) Optical microscopy images of the MgB_2/Fe monofilament wire.

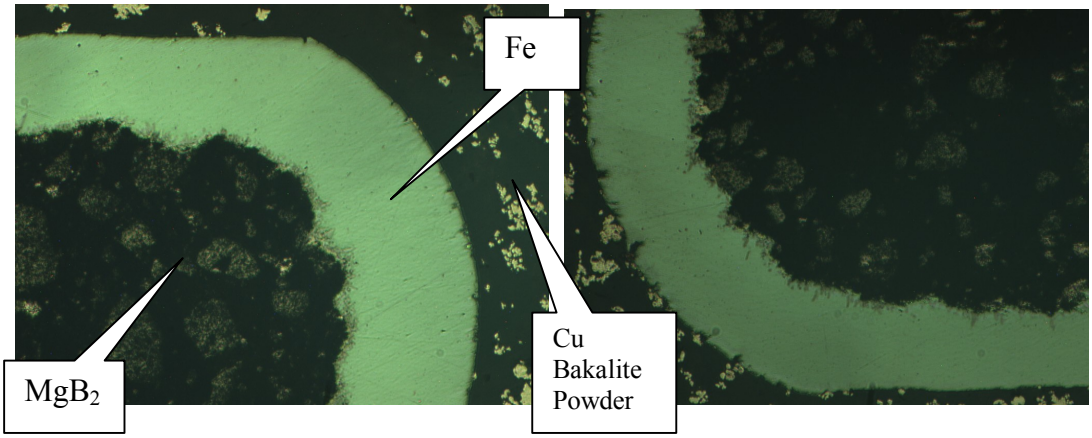

(a) (b)

Figure 5.25 (a-b) Optical microscopy images of the MgB_2/Fe monofilament tape.

5.2.1.6. Magnetoresistivity Measurements of the MgB_2/Fe Monofilament Tapes

Magnetoresistivity measurements were performed by using standard four-probe method with DC current of 100 mA between 4-50 K temperatures under constant magnetic field 0.250 T, 0.500 T, 0750 T, 1 T, 1.5 T and 2 T, respectively. The magnetic field was applied perpendicular to the current direction and parallel to the tape surface.

Several short samples 2 cm in length were cut from the MgB_2/Fe monofilament tape. These pieces were then heat treated at 650°C, 750°C, 850°C, 950°C and 1050°C for 60 minutes and 950°C for 30, 60, 120 and 240 minutes in a tube furnace. All heat treatments of the samples were done under 3 bars high purity argon (Ar) gas atmosphere and all samples were cooled down to room temperature in the furnace. The heating and cooling rates of the temperatures were chosen to be 5°C min^{-1}.

All the MgB_2/Fe monofilament tapes show similar resistive transition curves. For all the MgB_2/Fe monofilament tapes, an increase in the magnetic field caused a shift toward lower temperatures in both the onset and zero resistivity points of the superconducting transition curves. This behaviour is similar to that of conventional metallic superconductors but different from that of high T_c oxide superconductors. The temperature dependence of irreversibility fields $H_{irr}(T)$ and upper critical fields $H_{c2}(T)$ of the MgB_2/Fe monofilament tapes have been calculated from the resistive transitions at constant magnetic field using the criteria of 10% and 90% of $R(H,T_c)$, respectively [122, 126-129]. The temperature dependence of $H_{irr}(T)$ and $H_{c2}(T)$ for the MgB_2/Fe monofilament tapes annealed at 650°C-1050°C for 60 minutes and 950°C for 30-240 minutes are shown in Figures 5.26, 27, 28 and 29, respectively. For the MgB_2/Fe monofilament tape, the slope of the H_{c2}-T curve, (dH_{c2}/dT), decreases with increasing annealing temperature from 850 to 950°C. The crystallinity of the MgB_2 improved on increasing the annealing temperature from 850 to 950°C. Therefore, the density of the electron scattering defects in the MgB_2/Fe monofilament tape decreases when the annealing temperature increases from 850 to 950°C. This decrease in density of the electron scattering defects increased the coherence length and then lowered the slope of the H_{c2}-T [127]. The H_{c2}-T curves of

the other MgB_2/Fe monofilament tapes annealed at 650°C-1050°C for 60 minutes show similar behaviours. For the MgB_2/Fe monofilament tape annealed at 950°C, the dH_{c2}/dT decreased with increasing annealing time from 30 to 60 minutes. The crystallinity of the MgB_2 improved on increasing the annealing time from 30 to 60 minutes. The H_{c2}-T curves of the other MgB_2/Fe monofilament tapes annealed at 950°C for 30-240 minutes show similar behaviours. For the MgB_2/Fe monofilament tape, the slope of the H_{irr}-T curve (dH_{irr}/dT) decreased with increasing annealing temperature from 850 to 950°C as well as with increasing annealing time from 30 to 60 minutes. The critical temperatures of the MgB_2/Fe monofilament tapes increased with increasing annealing temperature up to 950°C. This is related to the better crystallinitiy of MgB_2. However, this better crystallinity decreased the slopes of the H_{c2}-T and H_{irr}-T curves of the MgB_2/Fe monofilament tapes because of larger coherence length. The improvement of the H_{c2} and H_{irr} contributes to the critical current density improvement for the MgB_2/Fe monofilament tapes annealed at 650°C-1050°C for 60 minutes and 950°C for 30-240 minutes [126-129].

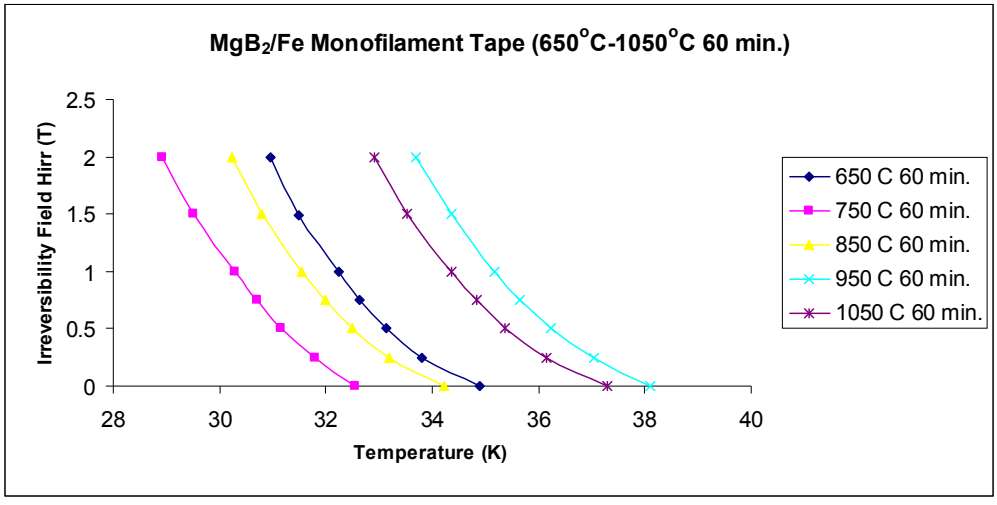

Figure 5.26 Temperature dependence of irreversibility field (H_{irr}) for the MgB_2/Fe monofilament tapes annealed at 650°C-1050°C for 60 minutes.

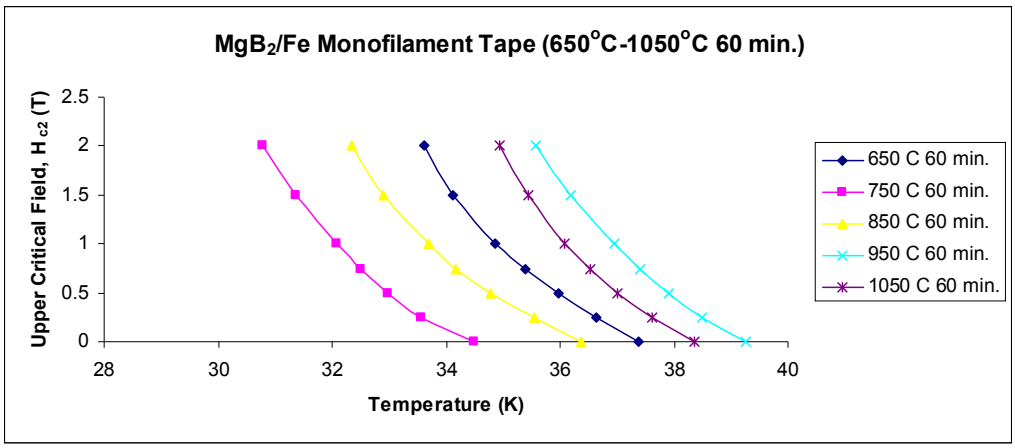

Figure 5.27 Temperature dependence of upper critical field (H_{c2}) for the MgB_2/Fe monofilament tapes annealed at 650°C-1050°C for 60 minutes.

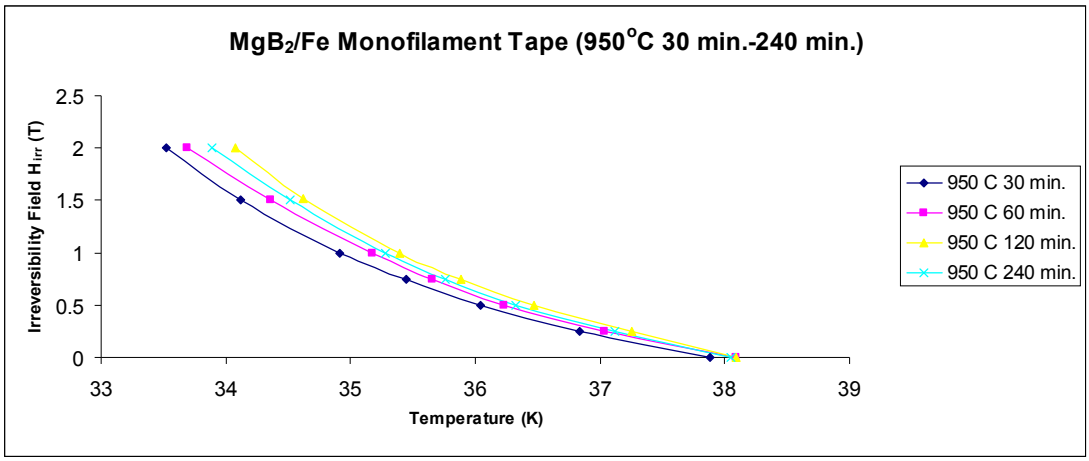

Figure 5.28 Temperature dependence of irreversibility field (H_{irr}) for the MgB_2/Fe monofilament tapes annealed at 950°C for 30-240 minutes.

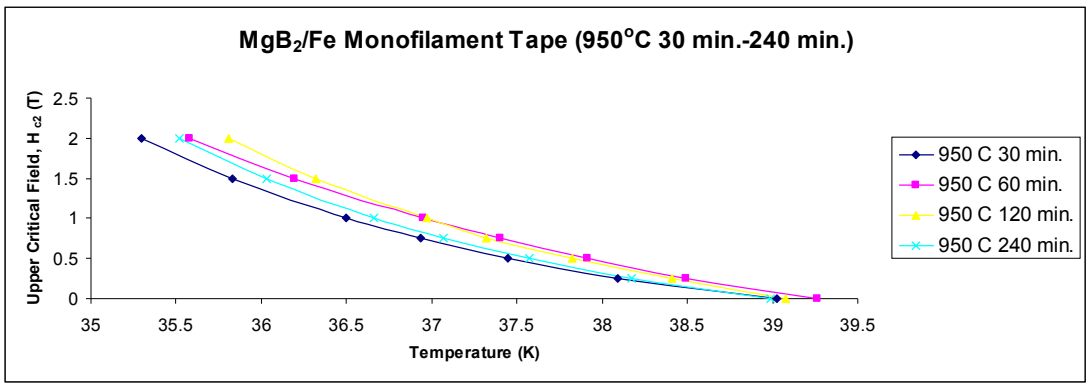

Figure 5.29 Temperature dependence of irreversibility field (H_{irr}) for the MgB_2/Fe monofilament tapes annealed at 950°C for 30-240 minutes.

Figures 5.30, 31, 32, 33 and 34 display the results of the magnetoresistivity measurements of the MgB_2/Fe monofilament tapes annealed at 650°C-1050°C for 60 minutes. Tables 5.12, 13, 14, 15 and 16 show the T_c^{onset}, T_c^{offset} and ΔT_c values of the MgB_2/Fe monofilament tapes annealed at 650°C-1050°C for 60 minutes.

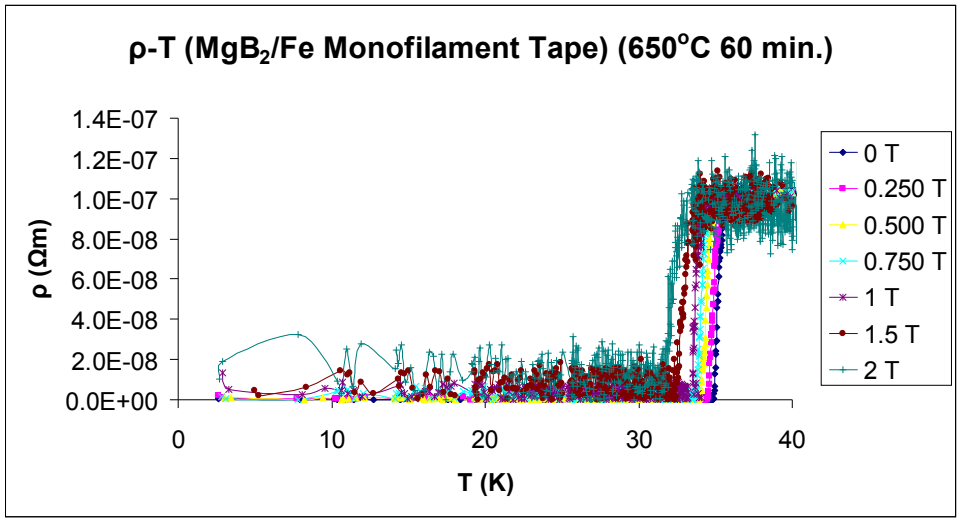

Figure 5.30 ρ-T graphs (under 0.250 T, 0.500 T, 0750 T, 1 T, 1.5 T and 2 T magnetic fields) of the MgB_2/Fe monofilament tapes annealed at 650°C for 60 minutes.

Table 5.12 T_c values of the MgB_2/Fe monofilament tapes annealed at 650°C for 60 minutes (under 0.250 T, 0.500 T, 0750 T, 1 T, 1.5 T and 2 T magnetic fields).

Magnetic Field	T_c^{onset} (K)	T_c^{offset} (K)	ΔT_c (K)
0 T	37.4	34.9	2.5
0.250 T	36.9	34.5	2.4
0.500 T	36.4	34.0	2.4
0.750 T	36.1	33.7	2.4
1 T	35.6	33.2	2.4
1.5 T	34.0	32.5	1.5
2 T	33.5	31.9	1.6

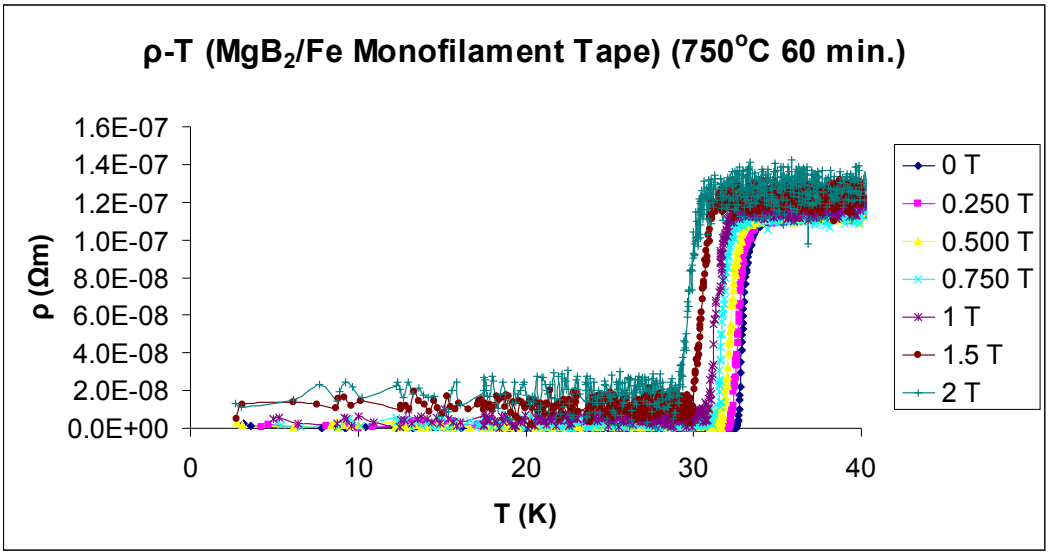

Figure 5.31 ρ-T graphs (under 0.250 T, 0.500 T, 0750 T, 1 T, 1.5 T and 2 T magnetic fields) of the MgB_2/Fe monofilament tapes annealed at 750°C for 60 minutes.

Table 5.13 T_c values of the MgB_2/Fe monofilament tapes annealed at 750°C for 60 minutes (under 0.250 T, 0.500 T, 0750 T, 1 T, 1.5 T and 2 T magnetic fields).

Magnetic Field	T_c^{onset} (K)	T_c^{offset} (K)	ΔT_c (K)
0 T	34.5	32.6	1.9
0.250 T	33.9	32.2	1.7
0.500 T	33.4	31.8	1.6
0.750 T	33.0	31.3	1.7
1 T	32.6	31.1	1.5
1.5 T	31.7	30.0	1.7
2 T	30.9	29.4	1.5

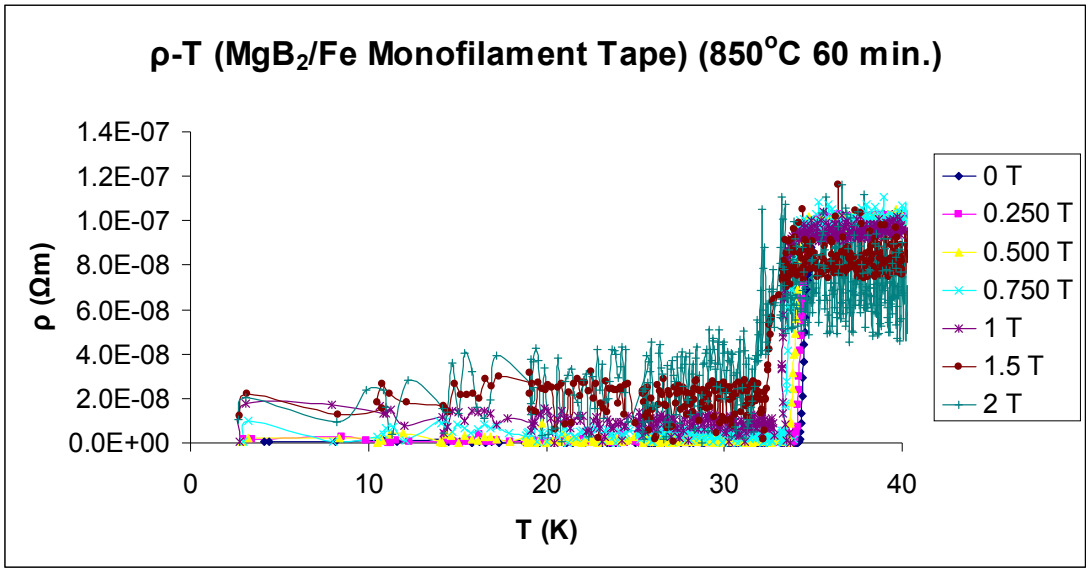

Figure 5.32 ρ-T graphs (under 0.250 T, 0.500 T, 0750 T, 1 T, 1.5 T and 2 T magnetic fields) of the MgB_2/Fe monofilament tapes annealed at 850°C for 60 minutes.

Table 5.14 T_c values of the MgB_2/Fe monofilament tapes annealed at 850°C for 60 minutes (under 0.250 T, 0.500 T, 0750 T, 1 T, 1.5 T and 2 T magnetic fields).

Magnetic Field	T_c^{onset} (K)	T_c^{offset} (K)	ΔT_c (K)
0 T	36.4	34.2	2.2
0.250 T	35.7	33.9	1.8
0.500 T	34.9	33.7	1.2
0.750 T	34.5	33.4	1.1
1 T	34.1	32.8	1.3
1.5 T	33.4	32.4	1.0
2 T	32.1	31.6	0.5

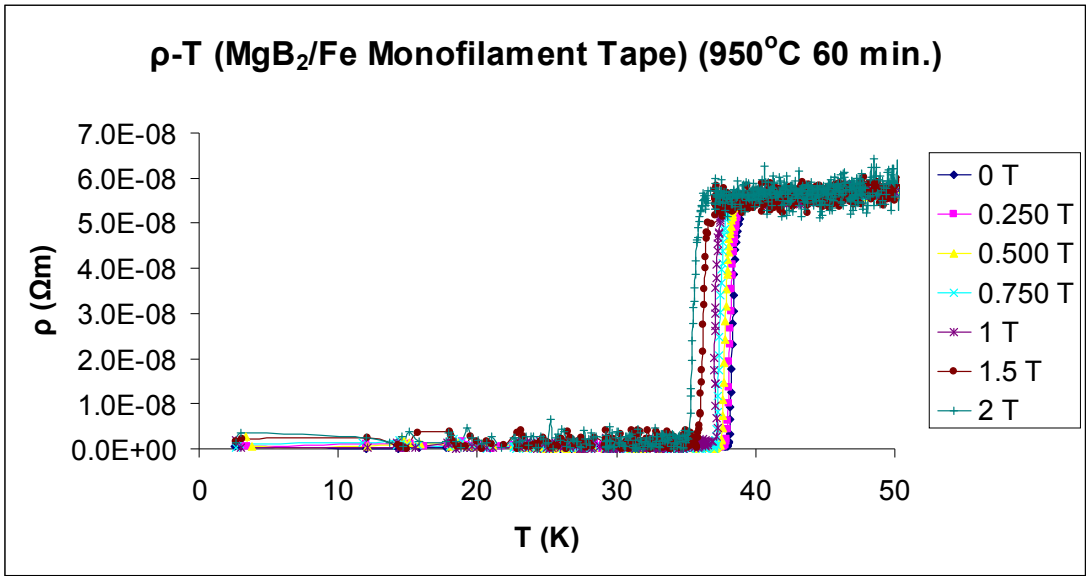

Figure 5.33 ρ-T graphs (under 0.250 T, 0.500 T, 0750 T, 1 T, 1.5 T and 2 T magnetic fields) of the MgB_2/Fe monofilament tapes annealed at 950°C for 60 minutes.

Table 5.15 T_c values of the MgB_2/Fe monofilament tapes annealed at 950°C for 60 minutes (under 0.250 T, 0.500 T, 0750 T, 1 T, 1.5 T and 2 T magnetic fields).

Magnetic Field	T_c^{onset} (K)	T_c^{offset} (K)	ΔT_c (K)
0 T	39.3	38.1	1.2
0.250 T	39.0	37.9	1.1
0.500 T	38.7	37.5	1.2
0.750 T	38.3	37.1	1.2
1 T	37.6	37.0	0.6
1.5 T	37.1	35.8	1.3
2 T	36.2	35.2	1.0

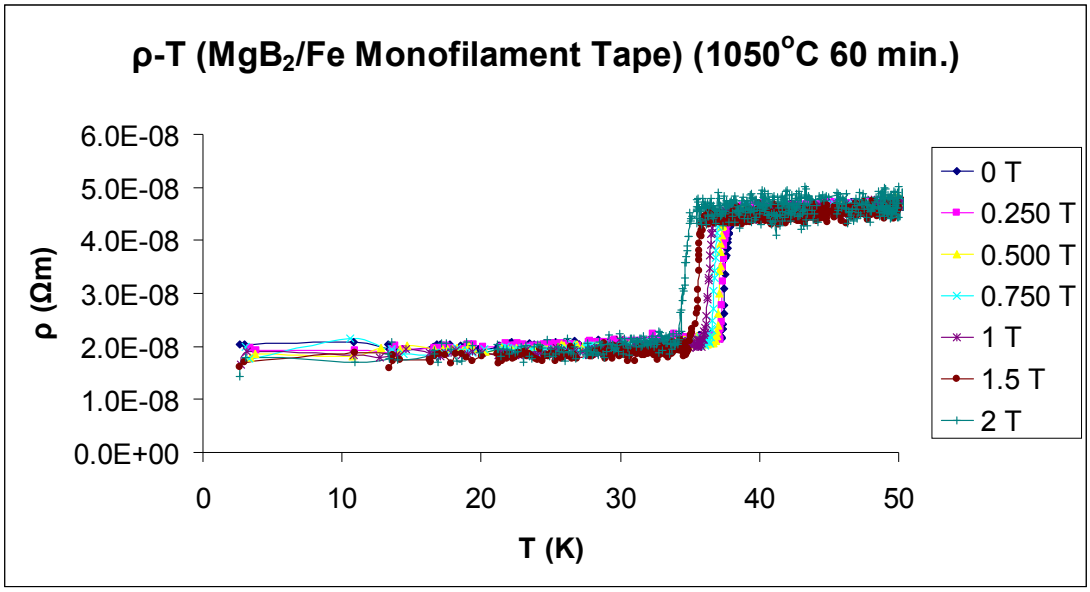

Figure 5.34 ρ-T graphs (under 0.250 T, 0.500 T, 0750 T, 1 T, 1.5 T and 2 T magnetic fields) of the MgB_2/Fe monofilament tapes annealed at 1050°C for 60 minutes.

Table 5.16 T_c values of the MgB_2/Fe monofilament tapes annealed at 1050°C for 60 minutes (under 0.250 T, 0.500 T, 0750 T, 1 T, 1.5 T and 2 T magnetic fields).

Magnetic Field	T_c^{onset} (K)	T_c^{offset} (K)	ΔT_c (K)
0 T	38.4	37.3	1.1
0.250 T	38.1	37.2	0.9
0.500 T	37.4	36.9	0.5
0.750 T	37.1	36.5	0.6
1 T	36.7	36.0	0.7
1.5 T	36.1	35.0	1.1
2 T	35.0	34.2	0.8

Figures 5.35, 36 and 37 illustrate the results of the magnetoresistivity measurements of the MgB_2/Fe monofilament tapes annealed at 950°C for 30-240 minutes. Tables 5.17, 18 and 19 display the T_c^{onset}, T_c^{offset} and ΔT_c values of the MgB_2/Fe monofilament tapes annealed at 950°C for 30-240 minutes.

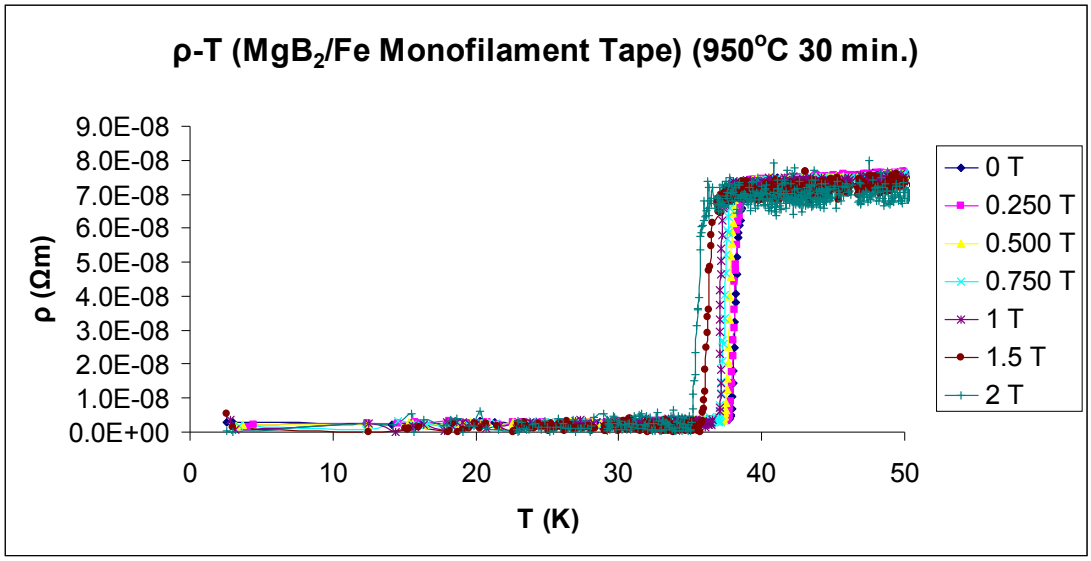

Figure 5.35 ρ-T graphs (under 0.250 T, 0.500 T, 0750 T, 1 T, 1.5 T and 2 T magnetic fields) of the MgB_2/Fe monofilament tapes annealed at 950°C for 30 minutes.

Table 5.17 T_c values of the MgB_2/Fe monofilament tapes annealed at 950°C for 30 minutes (under 0.250 T, 0.500 T, 0750 T, 1 T, 1.5 T and 2 T magnetic fields).

Magnetic Field	T_c^{onset} (K)	T_c^{offset} (K)	ΔT_c (K)
0 T	39.1	37.9	1.2
0.250 T	38.9	37.7	1.2
0.500 T	38.5	37.3	1.2
0.750 T	38.0	37.0	1.0
1 T	37.6	36.6	1.0
1.5 T	36.9	35.7	1.2
2 T	36.0	35.1	0.9

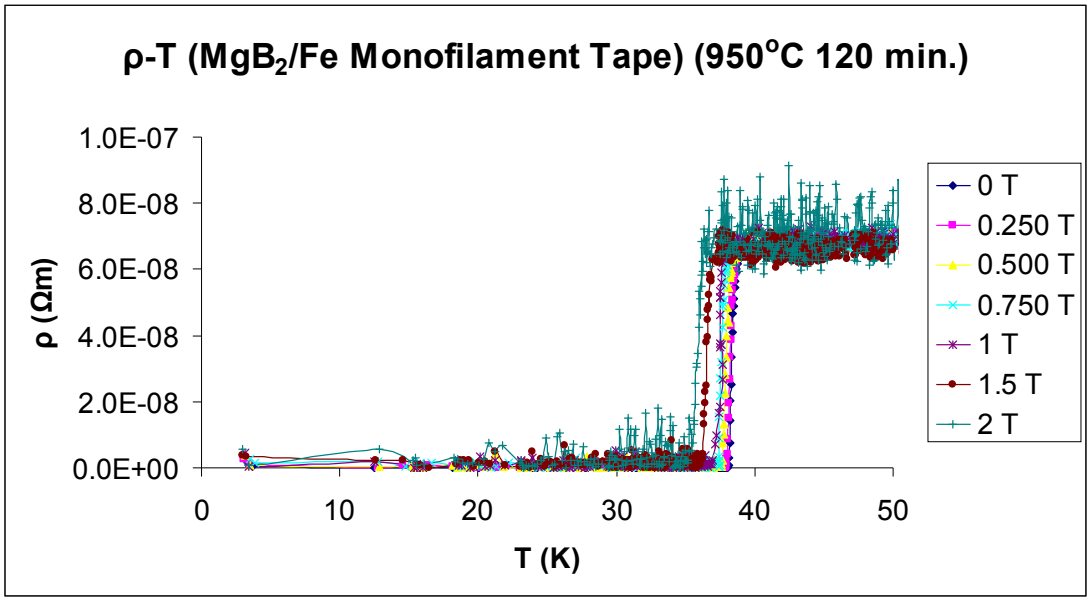

Figure 5.36 ρ-T graphs (under 0.250 T, 0.500 T, 0750 T, 1 T, 1.5 T and 2 T magnetic fields) of the MgB_2/Fe monofilament tapes annealed at 950°C for 120 minutes.

Table 5.18 T_c values of the MgB_2/Fe monofilament tapes annealed at 950°C for 120 minutes (under 0.250 T, 0.500 T, 0750 T, 1 T, 1.5 T and 2 T magnetic fields).

Magnetic Field	T_c^{onset} (K)	T_c^{offset} (K)	ΔT_c (K)
0 T	39.2	38.1	1.1
0.250 T	38.9	37.9	1.0
0.500 T	38.6	37.6	1.0
0.750 T	38.3	37.4	0.9
1 T	37.7	36.9	0.8
1.5 T	36.9	36.2	0.7
2 T	36.2	35.5	0.7

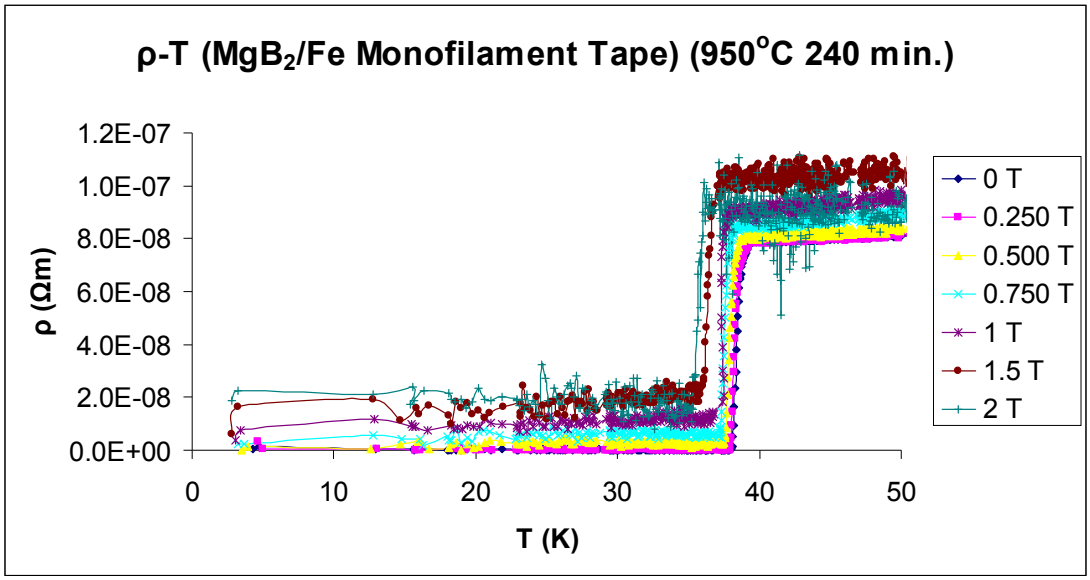

Figure 5.37 ρ-T graphs (under 0.250 T, 0.500 T, 0750 T, 1 T, 1.5 T and 2 T magnetic fields) of the MgB_2/Fe monofilament tapes annealed at 950°C for 240 minutes.

Table 5.19 T_c values of the MgB_2/Fe monofilament tapes annealed at 950°C for 240 minutes (under 0.250 T, 0.500 T, 0750 T, 1 T, 1.5 T and 2 T magnetic fields).

Magnetic Field	T_c^{onset} (K)	T_c^{offset} (K)	ΔT_c (K)
0 T	39.0	38.1	0.9
0.250 T	38.8	37.9	0.9
0.500 T	38.6	37.5	1.1
0.750 T	38.1	37.2	0.9
1 T	37.7	36.8	0.9
1.5 T	37.1	36.0	1.1
2 T	36.0	35.5	0.5

5.2.1.7. Activation Energy Calculations of the MgB_2/Fe Monofilament Tapes

We calculated the activation energy of the MgB_2/Fe monofilament tapes using the Arrhenius activation energy law

$$\rho = \rho_0 \exp\left[-\frac{U(B,T)}{k_B T}\right]. \tag{5.3}$$

Where U(B,T) is the activation energy that depends on temperature and magnetic field, but in this particular case, the activation energy can be taken as temperature independent due to the narrow temperature region of the low resistivity part. The U(B) value can be calculated from the slope of the ln(ρ) versus 1/T plots and it must give a straight line in the low resistivity part [130].

Figures 5.38, 39, 40, 41 and 42 show the plots of ln(ρ) versus 1/T of the MgB_2/Fe monofilament tapes annealed at 650°C-1050°C for 60 minutes. The calculated U(B) values of the MgB_2/Fe monofilament tapes annealed at 650°C-1050°C for 60 minutes are presented in Table 5.20. We found that activation energy U(B) decreased with increasing magnetic field. In general, a decrease in the activation energy may cause a decrease in the critical current density of the samples by increasing the magnetic field. The critical current density, one of the most important parameters in considering superconductor wires and tapes for practical applications, can be determined by the pinning properties and the flux motion of the superconductors. The flux motion is related to the activation energy that plays role as a potential energy barrier to keep the magnetic flux in pinning centre. Because of the motion of the vortices over pinning centres in the superconductors which is defined

as flux creep decreases the critical current density [131,132]. We observed that the activation energies of the MgB_2/Fe monofilament tapes annealed at 650°C-1050°C for 60 min. increased with increasing annealing temperature up to 950°C. The highest activation energy obtained for the sample annealed at 950°C for 60 min. As the annealing temperature increases from 950°C to 1050°C, the activation energy of the MgB_2/Fe monofilament tape decreases from 3.588 eV to 1.795 eV. This decrease suggests reducing of the pinning centres in the sample [130].

Figures 5.43, 44 and 45 display the plots of ln(ρ) versus 1/T of the MgB_2/Fe monofilament tapes annealed at 950°C for 30-240 minutes. The calculated U(B) values of the MgB_2/Fe monofilament tapes annealed at 650°C-1050°C for 60 minutes are presented in Table 5.21. We observed that the activation energies of the MgB_2/Fe monofilament tapes annealed at 950°C for 30-240 min. increased with increasing annealing time up to 60 min. As the annealing time increases from 60 min. to 240 min., the activation energy of the MgB_2/Fe monofilament tape decreases from 3.588 eV to 2.063 eV.

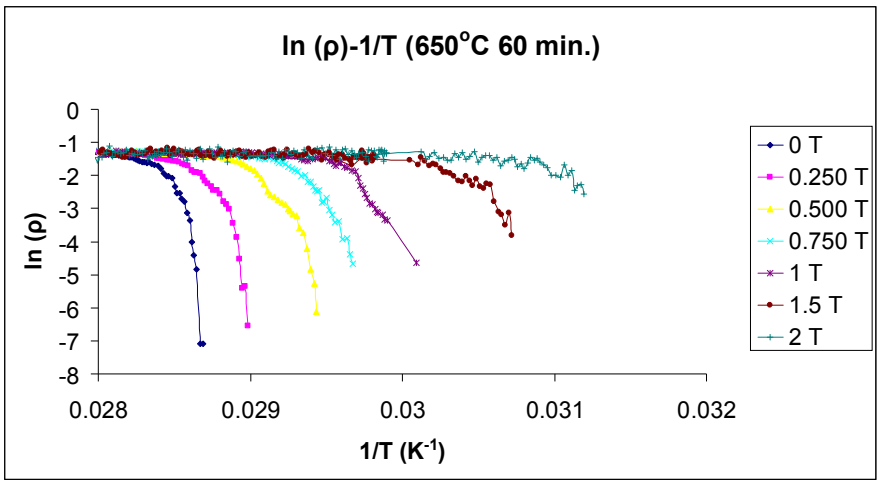

Figure 5.38 Arrhenius plot of the MgB_2/Fe monofilament tape annealed at 650°C for 60 minutes.

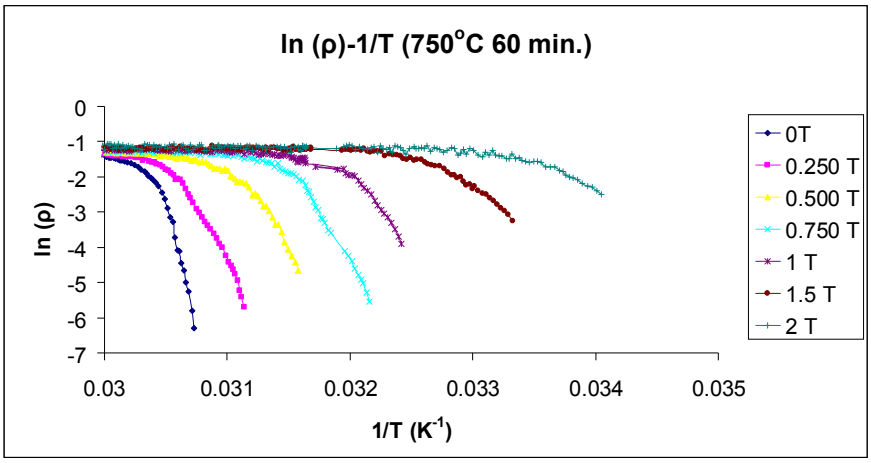

Figure 5.39 Arrhenius plot of the MgB_2/Fe monofilament tape annealed at 750°C for 60 minutes.

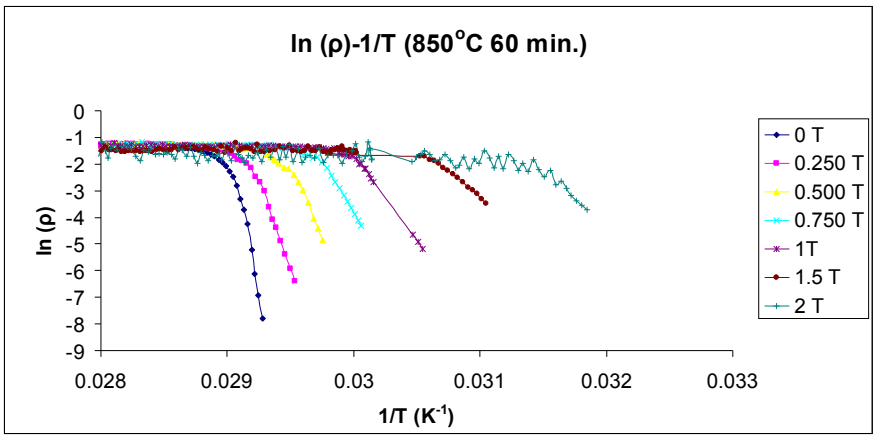

Figure 5.40 Arrhenius plot of the MgB_2/Fe monofilament tape annealed at 850°C for 60 minutes.

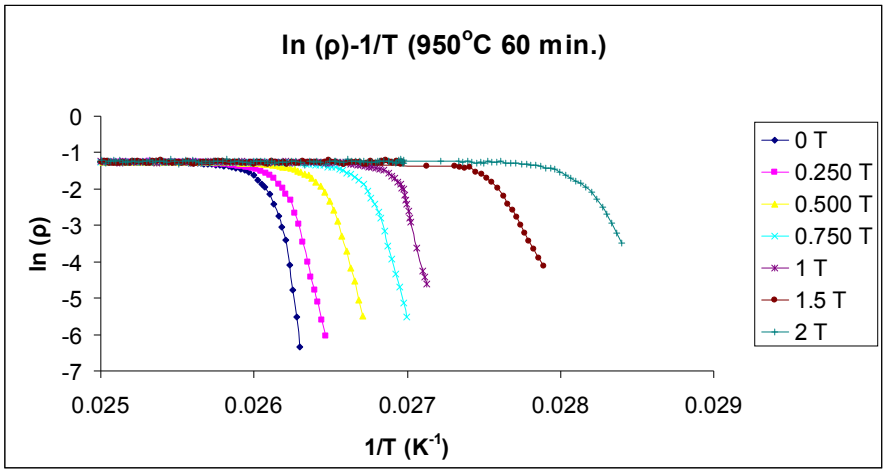

Figure 5.41 Arrhenius plot of the MgB_2/Fe monofilament tape annealed at 950°C for 60 minutes.

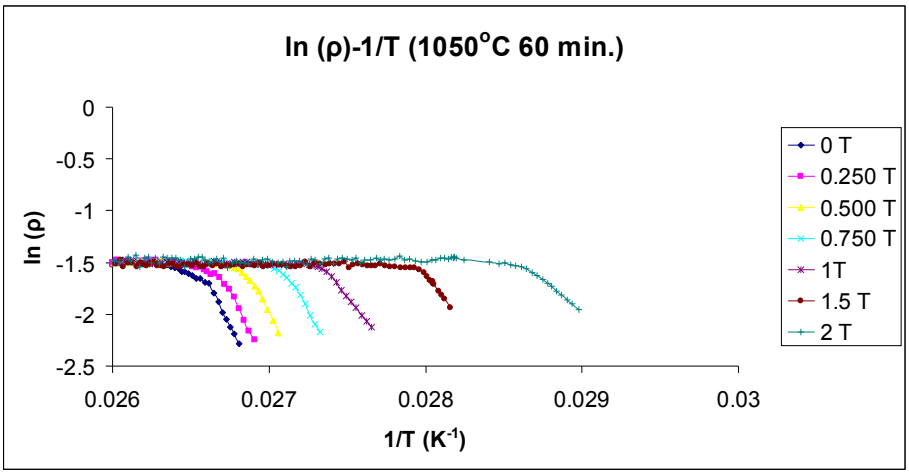

Figure 5.42 Arrhenius plot of the MgB_2/Fe monofilament tape annealed at 1050°C for 60 minutes.

Table 5.20 Calculated activation energies U(B) K, of the MgB_2/Fe monofilament tapes (650°C-1050°C for 60 minutes) at different magnetic fields.

Magnetic Field	Activation Energies (eV)				
	650°C 1 h	750°C 1 h	850°C 1 h	950°C 1 h	1050°C 1 h
0 T	1.490	1.997	2.532	3.588	1.795
0.250 T	1.313	1.768	2.350	3.200	1.572
0.500 T	1.027	1.334	1.792	2.742	1.078
0.750 T	0.815	1.052	1.524	2.256	0.867
1 T	0.533	0.748	1.071	1.739	0.674
1.5 T	0.231	0.359	0.847	1.330	0.314
2 T	0.060	0.174	0.405	0.928	0.092

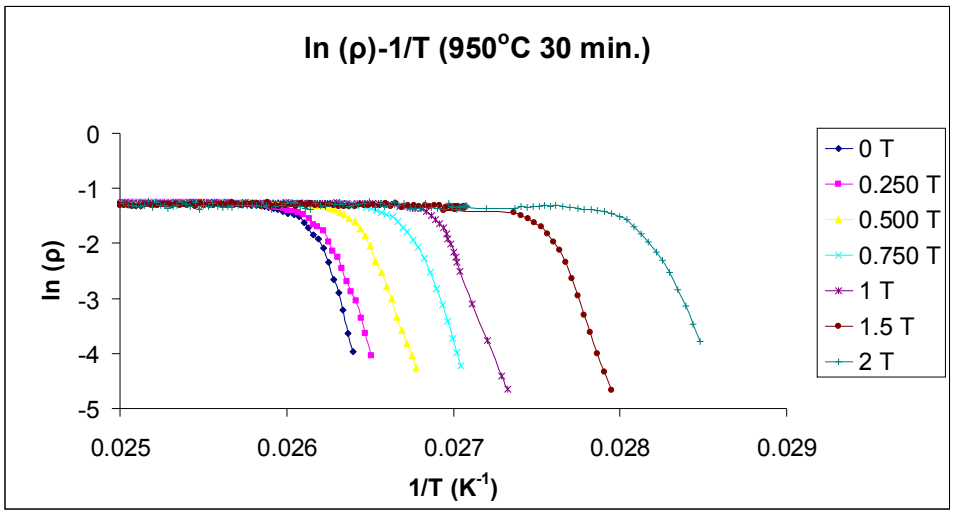

Figure 5.43 Arrhenius plot of the MgB_2/Fe monofilament tape annealed at 950°C for 30 minutes.

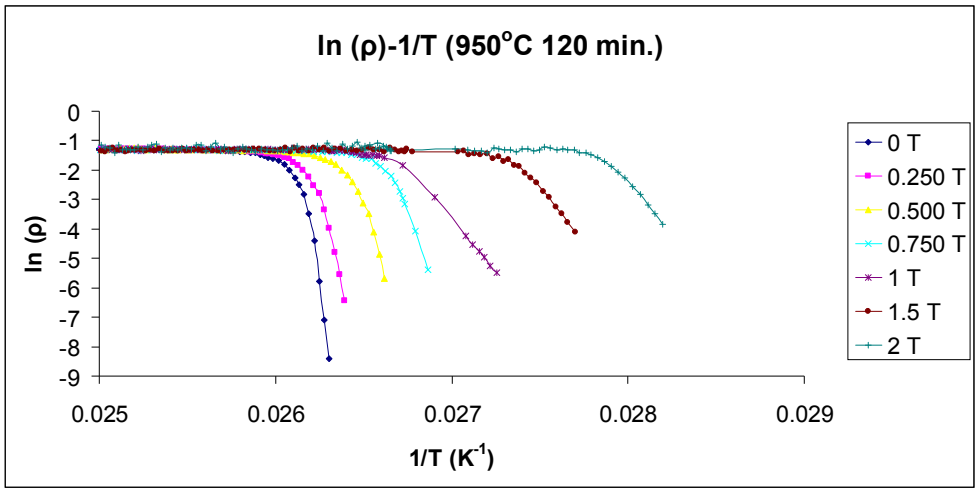

Figure 5.44 Arrhenius plot of the MgB_2/Fe monofilament tape annealed at 950°C for 120 minutes.

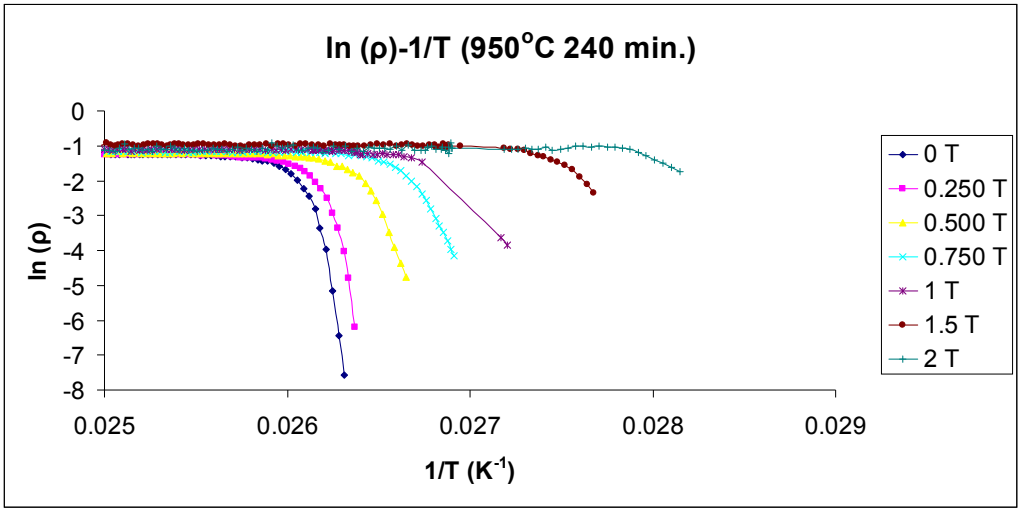

Figure 5.45 Arrhenius plot of the MgB_2/Fe monofilament tape annealed at 950°C for 240 minutes.

Table 5.21 Calculated activation energies U(B) K, of the MgB_2/Fe monofilament tapes (950°C for 30-240 minutes) at different magnetic fields.

Magnetic Field	Activation Energies (eV)			
	950°C 30 min.	950°C 60 min.	950°C 120 min.	950°C 240 min.
0 T	3.319	3.588	2.408	2.063
0.250 T	2.875	3.200	1.980	1.815
0.500 T	2.496	2.742	1.621	1.382
0.750 T	2.170	2.256	1.304	1.048
1 T	1.643	1.739	1.001	0.776
1.5 T	1.135	1.330	0.668	0.445
2 T	0.745	0.928	0.390	0.270

5.2.1.8. Magnetization Measurements of the MgB_2/Fe Monofilament Wires

The M-H graph (0.1 T magnetic field was applied at 10 K) of MgB_2/Fe monofilament wire annealed at 950°C for 60 minutes is shown in Figure 5.46. The M-H graph of the MgB_2/Fe monofilament wire annealed at 950°C for 60 minutes has a ferromagnetic property. The Fe sheath of the MgB_2 core screened the contribution of the MgB_2 core. Therefore, the contribution of the MgB_2 core could not be observed. The M-T graph (0.1 T magnetic field was applied between 10K and 50K) of MgB_2/Fe monofilament wire annealed at 950°C for 60 minutes is shown in Figure 5.47. The offset superconducting transition temperature of the MgB_2/Fe monofilament wire annealed at 950°C for 60 minutes was also determined as 37.3 K by measuring the magnetization as a function of temperature which is in consistent with the resistivity measurements in the present work.

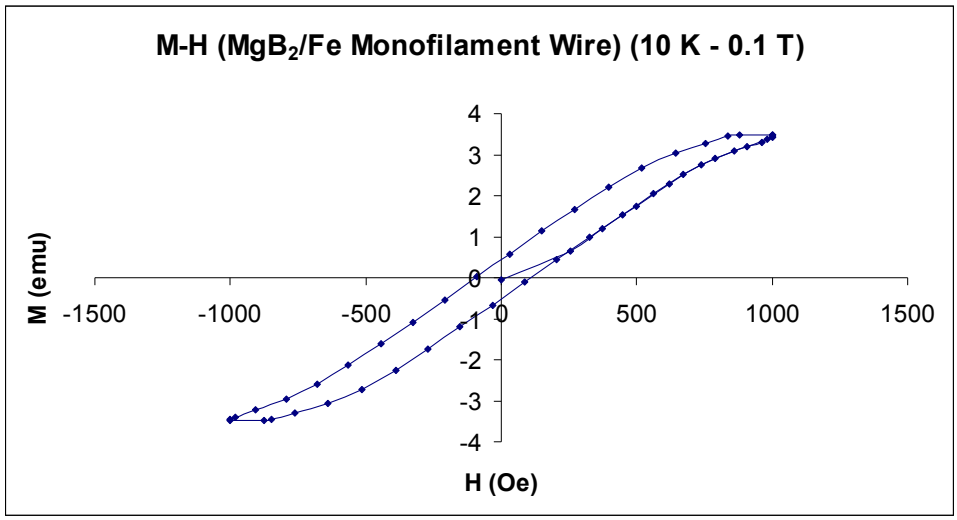

Figure 5.46 M-H graph of MgB_2/Fe monofilament wire.

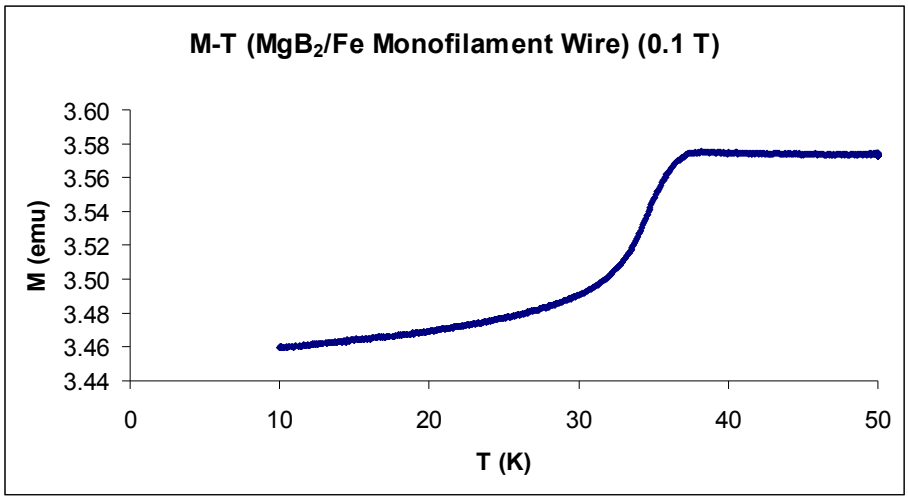

Figure 5.47 M-T graph of MgB_2/Fe monofilament wire.

5.2.2. MgB_2/Ag Monofilament Wires and Tapes

We have fabricated superconducting MgB_2/Ag monofilament wires and tapes by ex-situ PIT method using commercially available MgB_2 powder (Cerac Co., -100 mesh, 99%) as described in Experimental Method.

The MgB_2/Ag monofilament wire was characterized using scanning electron microscope, energy dispersive X-ray spectrometer, optical microscope, inductive critical current density and a vibrating sample magnetometer.

5.2.2.1. SEM Investigation of the MgB_2/Ag Monofilament Wire

Surface morphologies of the MgB_2/Ag monofilament wires were studied by SEM in order to determine average grain size, connection of the grains and the presence of microvoid and microcrack.

Figure 5.48 shows SEM picture of polished transverse cross section of a 1.10 mm in diameter of Ag-sheathed MgB_2 monofilament wire. The diameter of the

superconducting core was measured about 800 μm from SEM picture. Table 5.22 summarizes the main characteristics of the MgB_2/Ag monofilament wire.

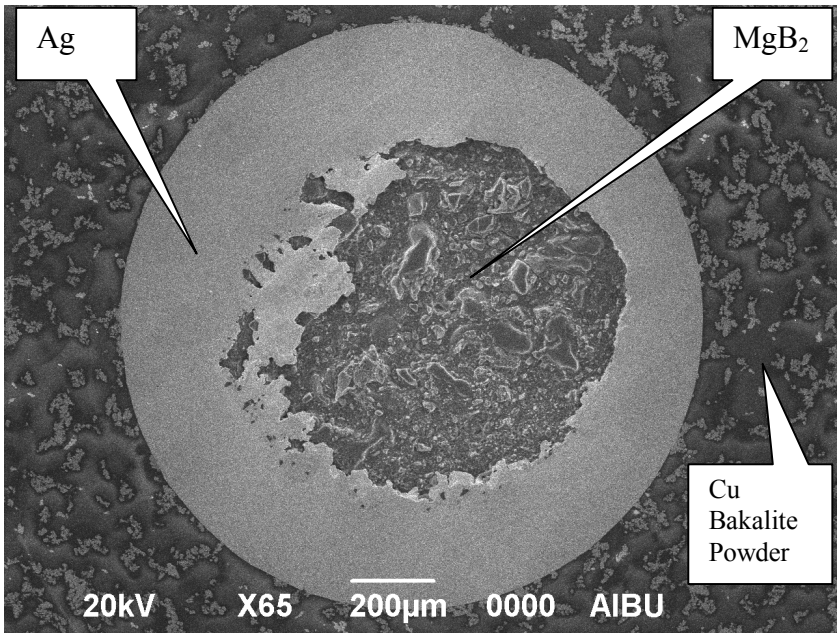

Figure 5.48 SEM picture of transverse cross section of the MgB_2/Ag monofilament wire.

Table 5.22 MgB_2/Ag Monofilament wire Characteristics.

Number of MgB_2 filaments	1
Preparation technique	Ex-situ PIT
Sheath material	Silver
(MgB_2/Ag) cross section	1.40631 mm^2
MgB_2 cross section	0.54178 mm^2
Silver cross section	0.86453 mm^2

Figure 5.49 shows scanning electron microscope image of a superconducting core from the MgB_2/Ag wire after sintering. Highly packed grains with an average grain size of about 30 μm can be seen.

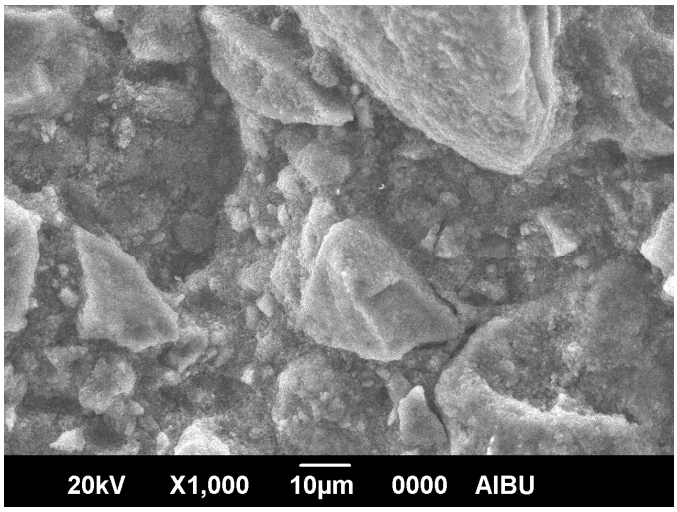

Figure 5.49 High magnification scanning electron micrograph of superconducting core of the MgB_2/Ag wire.

5.2.2.2. EDS Investigation of the MgB_2/Ag Monofilament Wire

Figure 5.50 shows the element distribution maps of Mg, B, O and Ag in the cross section of the MgB_2/Ag monofilament wire. The electron dispersive spectroscopy surface analysis indicates that there is no interface layer between the MgB_2 core and Ag sheath material, no reaction between core and sheath metals at this resolution.

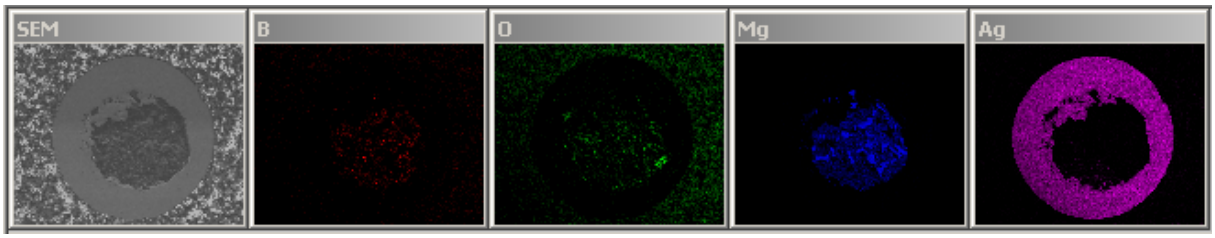

Figure 5.50 EDS picture of transverse cross section of the MgB_2/Ag monofilament wire.

5.2.2.3. Optical Microscopy Investigation of the MgB_2/Ag Monofilament Wire

Figure 5.51 (a-b) shows optical microscopy images of transverse cross section of the MgB_2/Ag monofilament wire.

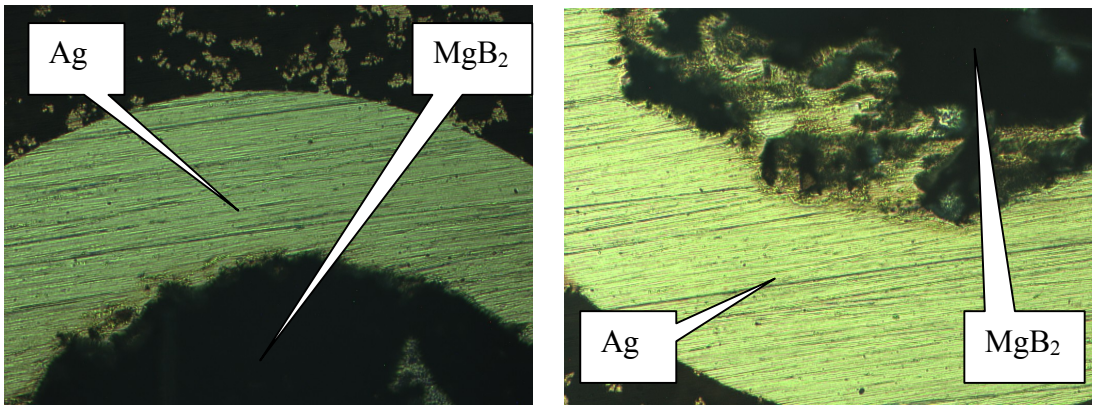

(a) (b)

Figure 5.51 (a-b) Optical microscopy images of the MgB_2/Ag monofilament wire.

In some places of the MgB_2/Ag monofilament wire, Ag layers were observed near the MgB_2 layer.

5.2.2.4. Magnetization Measurements of the MgB_2/Ag Monofilament Wire

The magnetic measurements were carried out on 12 mm long samples using a vibrating sample magnetometer. The magnetic field was applied perpendicular to the axis of the MgB_2/Ag monofilament wire which has a non-magnetic sheath.

In Figure 5.52, we show the magnetic hysteresis M(H) loops for the 550°C annealed MgB_2/Ag monofilament wire at 4.2K, 10K, 20K and 30 K with applied different fields (H). 1T and 3T magnetic fields were applied at 4.2 K and 3T

magnetic field was applied at 10K, 20K and 30K. The measured M-H loops are completely due to MgB_2 superconducting material because silver sheath does not have magnetic property. As seen in Figure 5.52 magnetic hysteresis loops depend on the temperature. The hysteresis loop measurement shows that the area of the hysteresis loops decreases with the increasing temperature. However, critical current density decreases with increasing the magnetic field. In Figure 5.52 we observed that MgB_2/Ag monofilament wire behaves as a superconductor.

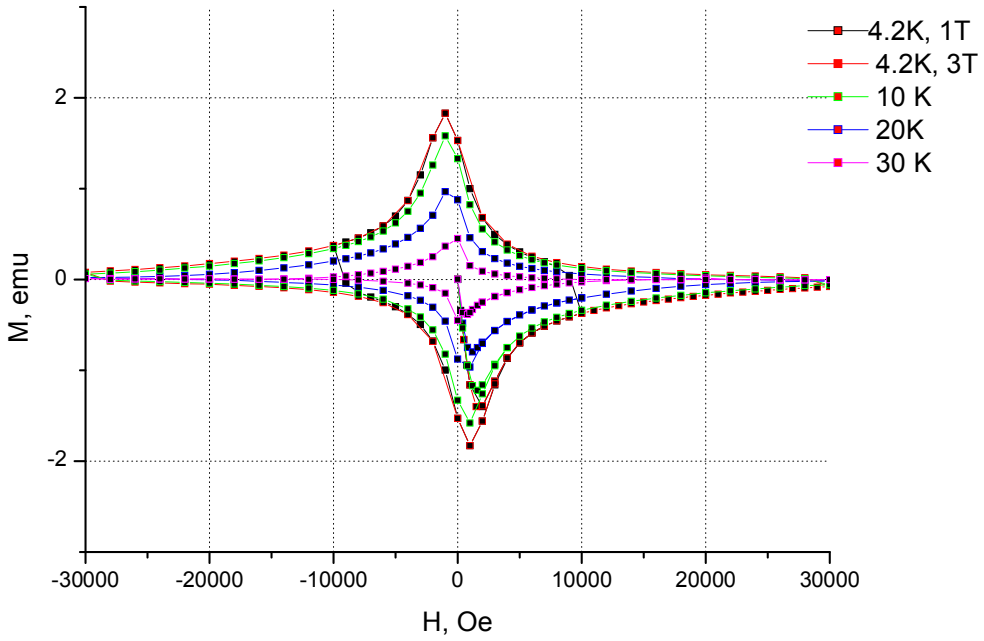

Figure 5.52 M-H graph for MgB_2/Ag monofilament wire.

We estimated the J_c of our sample by using Bean's critical state model. According to the Bean critical state model, the inductive critical current density J_c is associated with ΔM, the difference in the hysteresis magnetization between the increasing and decreasing magnetic fields. The inductive current density is obviously suppressed by the increasing applied field and temperature. Our sample studied for magnetization was in a cylindrical form; hence we used the formula,

$$J_c = 30 \times \Delta M/d \qquad (5.4)$$

where $\Delta M = |M+|-|M-|$ comes from the measured M(H) loops and d is the diameter of the cylindrical sample. The plots of J_c as a function of H at 4.2K are shown in Figure 5.53.

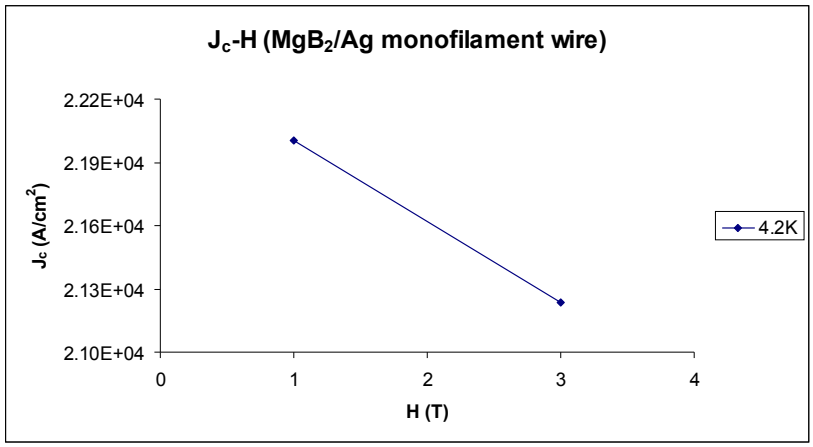

Figure 5.53 J_c-H graph for MgB_2/Ag monofilament wire.

Figure 5.53 shows that the critical current density decreases with the increasing magnetic field. The plots of J_c as a function of T (temperature) at 3T are shown in Figure 5.54.

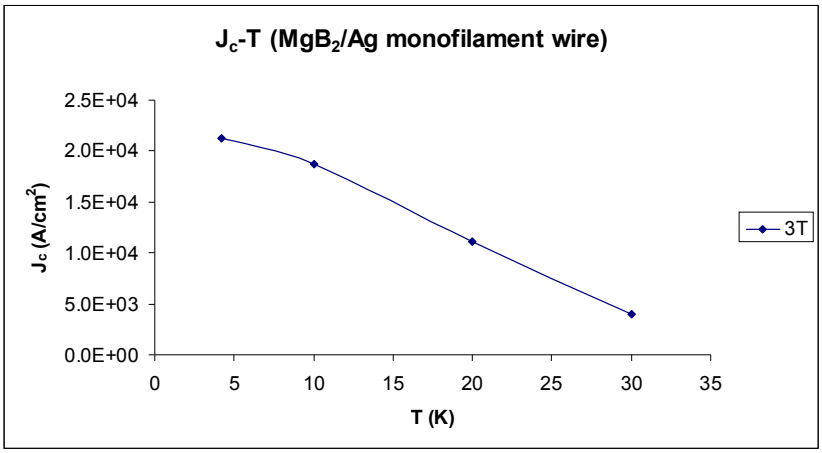

Figure 5.54 J_c-T graph for MgB_2/Ag monofilament wire.

Figure 5.54 shows that the inductive critical current density decreases with the increasing temperature. The inductive critical current density (J_c) values of MgB_2/Ag monofilament wire at different values of temperature and magnetic field were tabulated in Table 5.23. As seen from Table 5.23, the inductive critical current density values of the MgB_2/Ag monofilament wire decrease with increasing magnetic field and temperature. As the magnetic field increases from 1 T to 3 T at 4.2 K, the inductive critical current density decreases from $2.20x10^4$ A/cm^2 to $2.12x10^4$ A/cm^2. As the temperature increases from 4.2 K to 30 K at 3 T, the inductive critical current density decreases from $2.12x10^4$ A/cm^2 to $0.40x10^4$ A/cm^2.

Table 5.23 J_c values of the MgB_2/Ag monofilament wires at different temperatures and magnetic fields.

Temperature (K)	Magnetic Field (T)	Critical Current Density (A/cm^2)
4.2	1	$2.20x10^4$
4.2	3	$2.12x10^4$
10	3	$1.87x10^4$
20	3	$1.10x10^4$
30	3	$0.40x10^4$

5.2.3. MgB_2/SS Monofilament Wires

We have fabricated superconducting MgB_2/SS monofilament wires by CTFF method using commercially available MgB_2 powder (Cerac Co., -100 mesh, 99%) as described in Experimental Method.

The MgB_2/SS monofilament wire was characterized using X-ray diffraction, scanning electron microscope, energy dispersive X-ray spectrometer, optical microscope and transport measurements.

5.2.3.1. XRD Characterizations of the MgB_2/SS Monofilament Wires

The phase composition and crystal structure of the MgB_2/SS monofilament wire which was fabricated by CTFF method using stainless steel-sheath were characterized by XRD method. For study of the sample, the stainless steel sheath was mechanically removed to expose the core. Figure 5.55 shows intensities as a function of 2θ for non-annealed and annealed at 950^oC for 30 minutes MgB_2/SS monofilament wires. Miller indices are indicated in the figure. The lattice parameters *a* and *c* determined from the (*h*00) and (00*l*) peaks of the XRD data are given in Table 5.24. MgB_2 phase formation was observed for both non-annealed and annealed MgB_2/SS monofilament wire. However, some peaks of impurities such as MgO_2, MgO and MgB_4 were observed for the sample annealed at 950^oC for 30 min. while MgO and MgB_4 phase were observed for the non-annealed sample. The lattice parameter *a* for the non-annealed sample was found to be $3.0836\,\mathring{A}$. However, it increases to $3.0937\,\mathring{A}$ for the sample annealed at 950^oC for 30 minutes. The lattice parameter *c* for the non-annealed sample was found to be $3.5171\,\mathring{A}$. On the other hand, it increases to $3.5336\,\mathring{A}$ for the sample annealed at 950^oC for 30 min. The grain size estimated from XRD measurement by Scherrer-Warren formula are about 60 nm for annealed at 950^oC for 30 minutes sample.

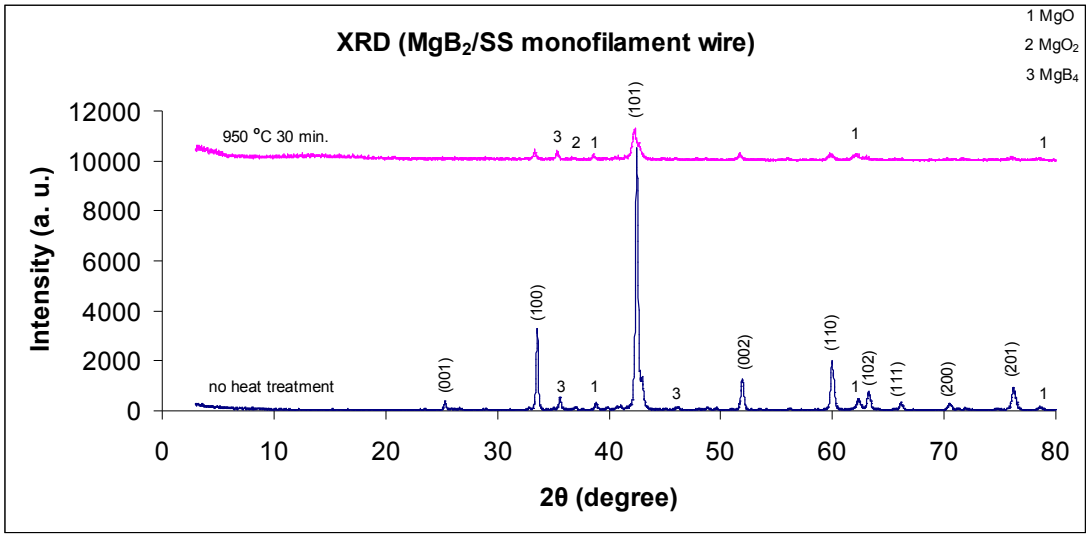

Figure 5.55 X-ray diffraction patterns of the MgB_2/SS wire non-annealed and annealed at 950°C for 30 minutes.

Table 5.24 The lattice parameters *a* and *c* of the MgB_2/SS samples non-annealed and annealed at 950°C for 30 minutes.

Samples	*a* (Å)	*c* (Å)
no heat treatment	3.0836	3.5171
950°C 30 min.	3.0937	3.5336

5.2.3.2. SEM Investigation of the MgB_2/SS Monofilament Wire

Microstructural investigations of the MgB_2/SS monofilament wire were studied by scanning electron microscope. Figure 5.56 shows SEM picture of polished transverse cross section of a 2.55 mm in diameter of stainless steel-sheathed MgB_2 monofilament wire. The diameter of the superconducting core was measured about 1.9 mm from SEM picture. The thickness of the stainless steel sheath is about 400 μm. The MgB_2/SS monofilament wire has a regular round shape.

Table 5.25 summarizes the main characteristics of the MgB_2/SS monofilament wire.

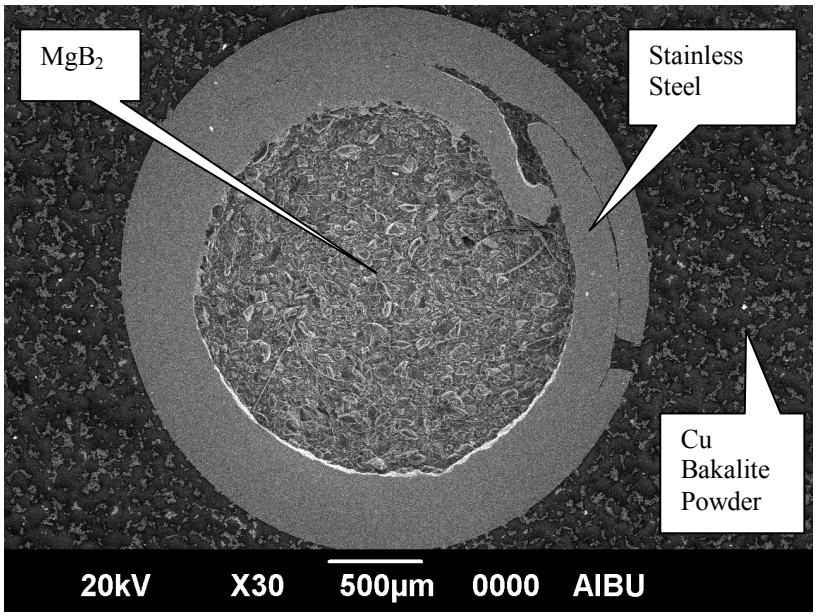

Figure 5.56 SEM picture of transverse cross section of the MgB_2/SS monofilament wire.

Table 5.25 MgB_2/SS Monofilament wire Characteristics.

Number of MgB_2 filaments	1
Preparation technique	CTFF
Sheath material	SS
(MgB_2/SS) cross section	6.18826 mm^2
MgB_2 cross section	2.90310 mm^2
SS cross section	3.28516 mm^2

5.2.3.3. EDS Investigation of the MgB_2/SS Monofilament Wire

Figure 5.57 shows the element distribution maps of Mg, B, O, Fe, Ni and Co in the cross section of the MgB_2/Stainless Steel monofilament wire.

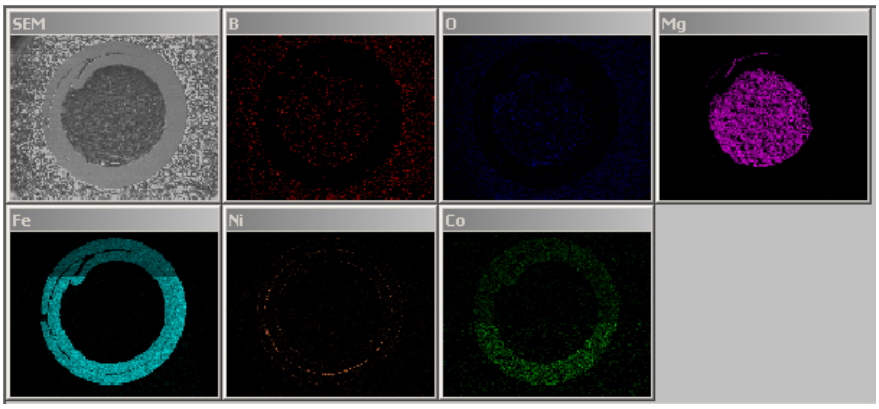

Figure 5.57 EDS picture of transverse cross section of the MgB_2/Stainless Steel monofilament wire.

5.2.3.4. Optical Microscopy Investigation of the MgB_2/SS Monofilament Wire

Figure 5.58 (a-d) shows optical microscopy images of transverse cross section of the MgB_2/Stainless Steel monofilament wire.

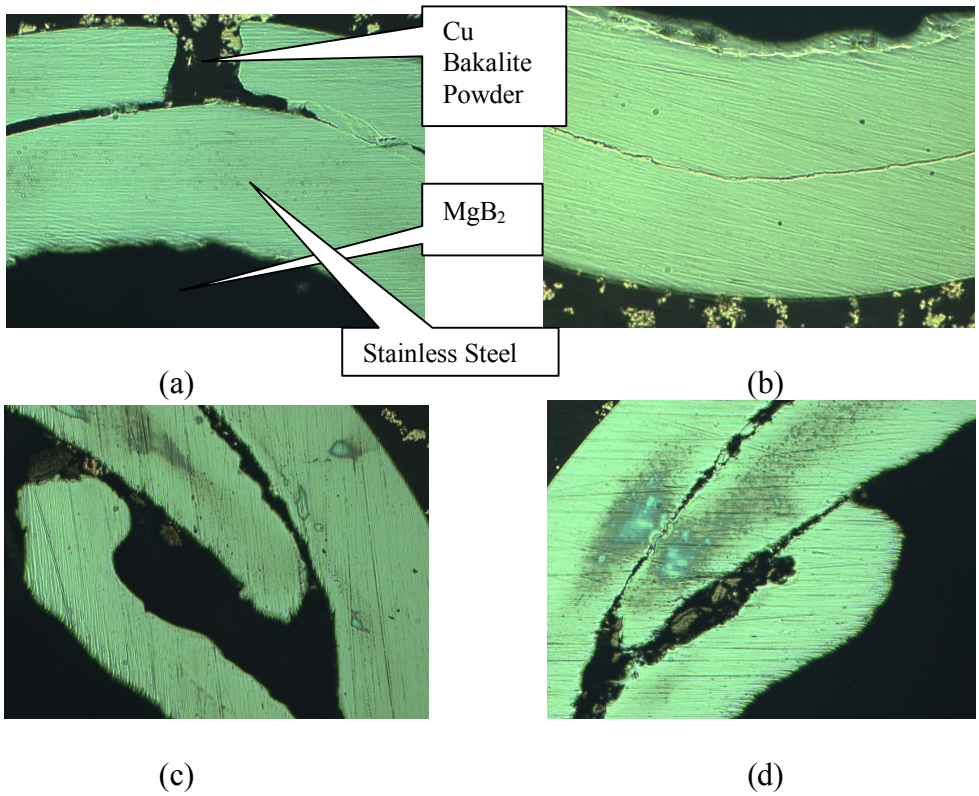

Figure 5.58 (a-d) Optical microscopy images of the MgB_2/Stainless Steel monofilament wire.

Optical microscopy images of MgB_2/Stainless Steel monofilament wire indicate that there is a small gap at the upper sheath material. Also, there are small gaps between the upper sheath material and the bottom sheath material.

5.2.3.5. Resistivity Measurements of the MgB_2/SS Monofilament Wires

The temperature dependence of the resistivity MgB_2/Stainless Steel monofilament wire which is annealed at 950^0C for 10 and 30 minutes is shown in Figure 5.59.

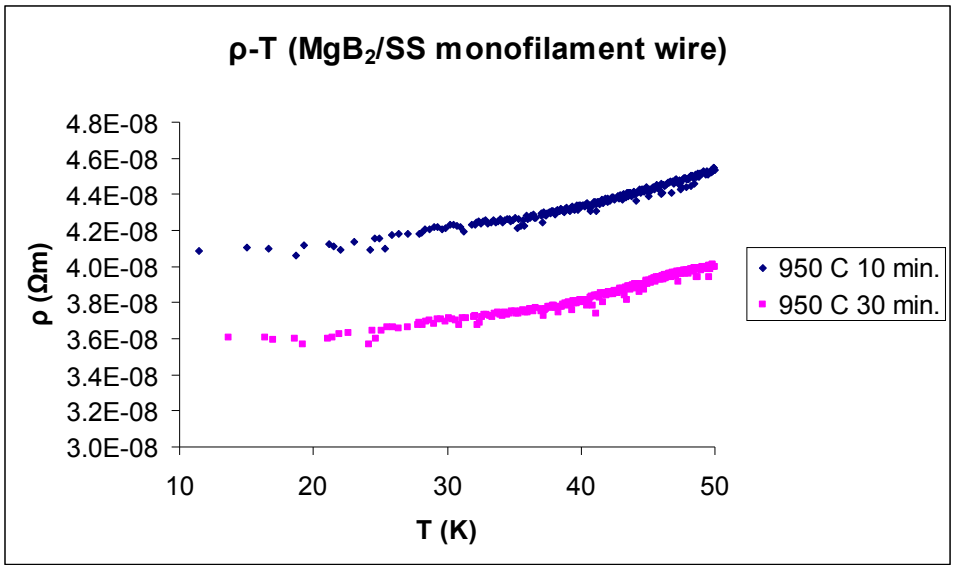

Figure 5.59 ρ-T graphs of the MgB_2/Stainless Steel monofilament wires.

In this graphs, superconductivity was not observed for the samples. The reasons of this; a) Starting powder may be of poor quality. b) Lack of a perfect inert atmosphere during the heat treatments. c) Temperature and period of the heat treatments may have been insufficient. d) Due to impurity phases in the sample.

5.3. Multifilament Wires and Tapes

5.3.1. MgB_2/Fe/Cu 6 and 7 Filament Wires and Tapes

The MgB_2/Fe/Cu 6 and 7 filament wires and tapes were fabricated by ex-situ PIT method using commercially available MgB_2 powder (Alfa Aesar, -325 mesh, <44 micron) without any intermediate annealing as described in Experimental Method.

The MgB_2/Fe/Cu 6 and 7 filament wires and tapes were characterized using X-ray diffraction, scanning electron microscope, energy dispersive X-ray spectrometer, optical microscope, quantum design physical property measurement system, vibrating sample magnetometer system, critical transition temperature and critical current density measurements.

5.3.1.1. XRD Characterizations of the MgB_2/Fe/Cu 6 and 7 Filament Wires

The crystal structure and phase composition of the MgB_2/Fe/Cu 6 and 7 filament wires which were fabricated by PIT method using copper-sheath were characterized by XRD method. The samples of MgB_2 multifilamentary tapes will be hereafter denoted as M6A (MgB_2/Fe/Cu 6 filament wire non-annealed), M6B (MgB_2/Fe/Cu 6 filament wire annealed at 900^{o}C for 2 h.), M7A (MgB_2/Fe/Cu 7 filament wire non-annealed), and M7B (MgB_2/Fe/Cu 7 filament wire annealed at 900^{o}C for 2 h.). Figure 5.60 shows intensities as a function of 2θ for the M6A, M6B, M7A and M7B samples. Miller indices are indicated in the figure. The lattice parameters *a* and *c* determined from the (*h*00) and (00*l*) peaks of the XRD data are given in Table 5.26. MgB_2 phase formation was observed for the M6A, M6B, M7A

and M7B samples. However, some peaks of impurities such as CuO, MgO and MgB_4 were observed for the samples M7A and M7B while MgO and MgB_4 phase were observed for the samples M6A and M6B. The lattice parameter *a* for the sample M6A was found to be 3.0891 Å. However, it increases to 3.0986 Å for the sample M6B. The lattice parameter *c* for the sample M6A was found to be 3.5271 Å. On the other hand, it increases to 3.5392 Å for the sample M6B.

The lattice parameter *a* for the sample M7A was found to be 3.0890 Å. However, it decreases to 3.0863 Å for the sample M7B. The lattice parameter *c* for the sample M7A was found to be 3.5265 Å. On the other hand, it decreases to 3.5247 Å for the sample M7B. The grain sizes estimated from XRD measurements by Scherrer-Warren formula are approximately 50-60 nm for the all samples.

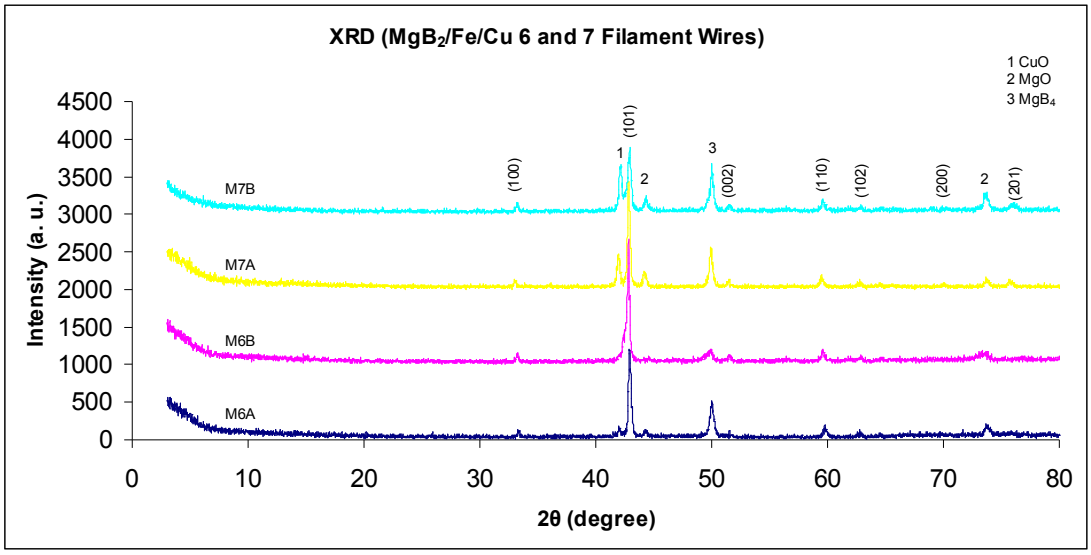

Figure 5.60 X-ray diffraction patterns of the M6A, M6B, M7A and M7B samples.

Table 5.26 The lattice parameters *a* and *c* of the M6A, M6B, M7A and M7B samples.

Samples	*a* (Å)	*c* (Å)
M6A	3.0891	3.5271
M6B	3.0986	3.5392
M7A	3.0890	3.5265
M7B	3.0863	3.5247

5.3.1.2. SEM Investigations of the MgB_2/Fe/Cu 6 and 7 Filament Wires and Tapes

Figure 5.61(a) shows SEM picture of polished transverse cross section of a 2.46 mm in diameter of the composite (MgB_2/Fe/Cu) without heat treatment. The matrix metal of the conductor is copper. A copper stabilizer is located in the conductor. Between MgB_2 and copper, an iron barrier is placed in order to prevent diffusion of copper to MgB_2 during heat treatment. The composite (MgB_2/Fe/Cu) has a regular round shape. The cross section shows uniform deformation of the composite wire without any problems such as breakage and sausaging of the components. Figure 5.61(b) shows that the thickness of the Fe sheath is about 100 μm. Figure 5.61 (c) shows a dense microstructure with a grain size of about 5 μm.

Table 5.27 summarizes the main characteristics of the composite (MgB_2/Fe/Cu)

Table 5.27 MgB_2/Fe/Cu 6 Filament wire Characteristics.

Number of MgB_2 filaments	6
Preparation technique	Ex-situ PIT
Sheath material	Copper
Diffusion barrier material	Iron
Composite (MgB_2/Fe/Cu) cross section	9.18167 mm^2
MgB_2 cross section	2.30790 mm^2
Iron cross section	0.70650 mm^2
Copper cross section	6.16727 mm^2

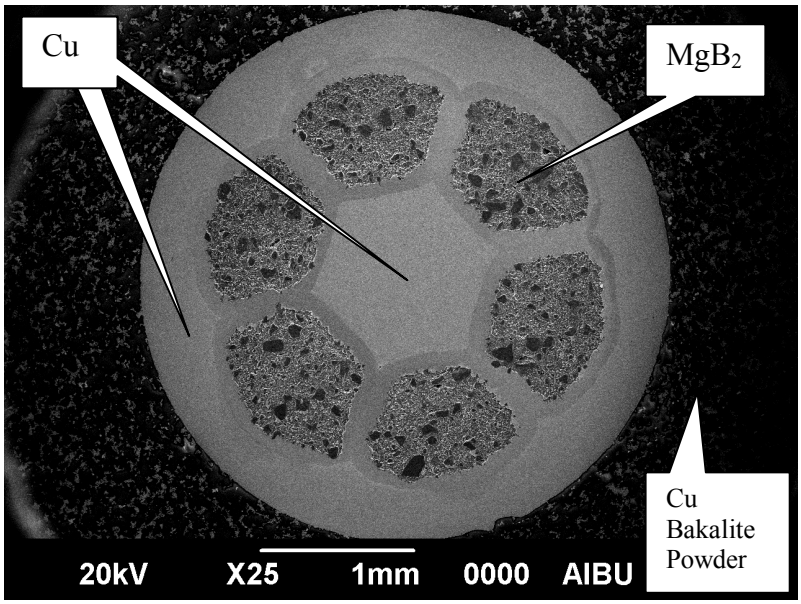

(a)

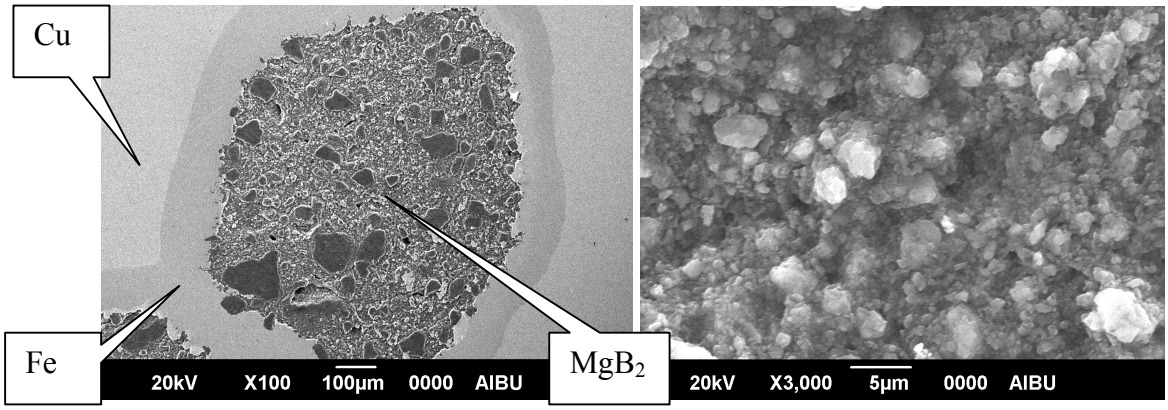

(b) (c)

Figure 5.61 (a-c) SEM pictures of transverse cross section of the MgB_2/Fe/Cu 6 filament wire.

Figure 5.62 shows SEM picture of polished transverse cross section of the MgB_2/Fe/Cu 6 filament tape without heat treatment. The composite (MgB_2/Fe/Cu) tape has a regular shape. Cu stabilizer in the centre is helpful for obtaining evenly distributed filaments in tape making via rolling. Iron sheathing as barrier is also beneficial for the same purpose.

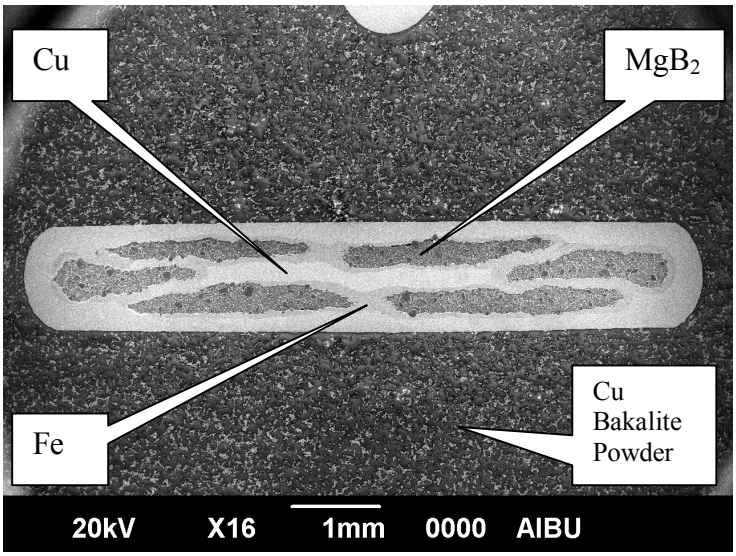

(a)

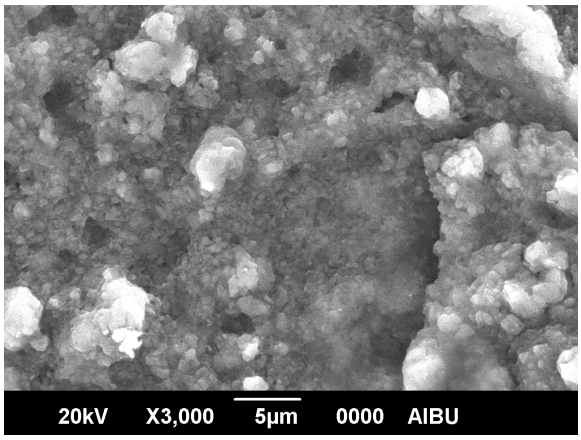

(b)

Figure 5.62 (a-b) SEM pictures of transverse cross section of the MgB_2/Fe/Cu 6 filament tape.

Figure 5.63 shows SEM picture of polished transverse cross section of a 3.02 mm in diameter of the MgB_2/Fe/Cu 7 filament wire without heat treatment. The matrix metal of the conductor is copper. Between MgB_2 and copper, an iron barrier is placed in order to prevent diffusion of copper to MgB_2 during heat treatment. The composite (MgB_2/Fe/Cu) has a regular round shape. The cross section shows uniform deformation of the composite wire with no breakage and sausaging of the components.

Table 5.28 summarizes the main characteristics of the MgB_2/Fe/Cu 7 filament wire

Table 5.28 MgB_2/Fe/Cu 7 Filament wire Characteristics.

Number of MgB_2 filaments	7
Preparation technique	Ex-situ PIT
Sheath material	Copper
Diffusion barrier material	Iron
Composite (MgB_2/Fe/Cu) cross section	16.6106 mm^2
MgB_2 cross section	5.49500 mm^2
Iron cross section	3.22886 mm^2
Copper cross section	7.88674 mm^2

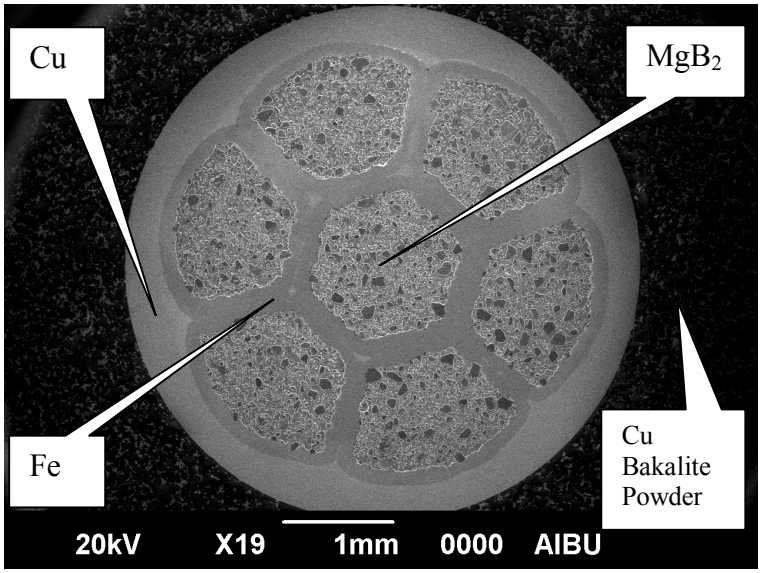

(a)

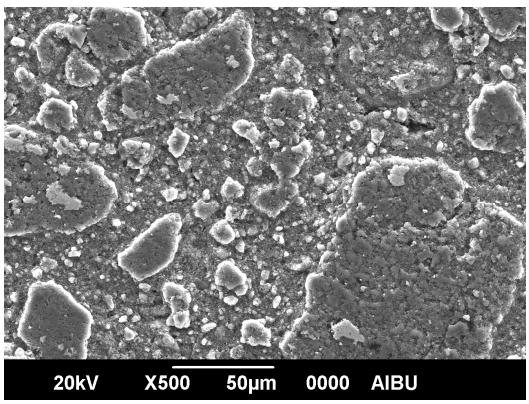

(b)

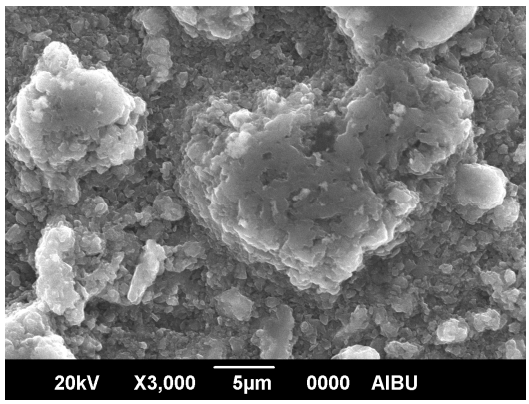

(c)

Figure 5.63 (a-c) SEM pictures of transverse cross section of the MgB_2/Fe/Cu 7 filament wire.

Figure 5.64 shows SEM picture of polished transverse cross section of the MgB_2/Fe/Cu 7 filament tape without heat treatment. The composite (MgB_2/Fe/Cu) tape has a regular shape.

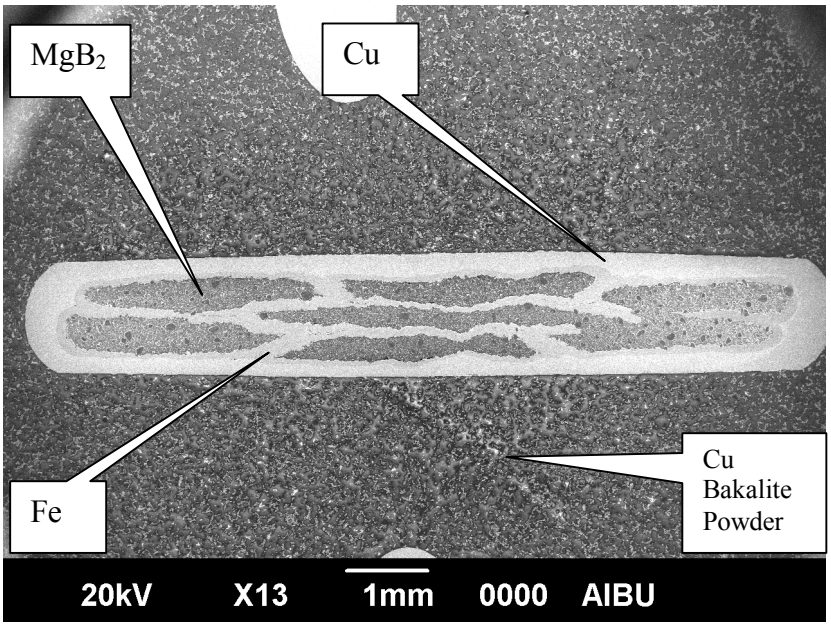

(a)

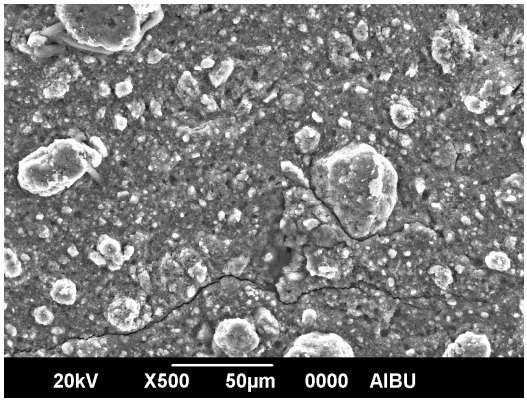

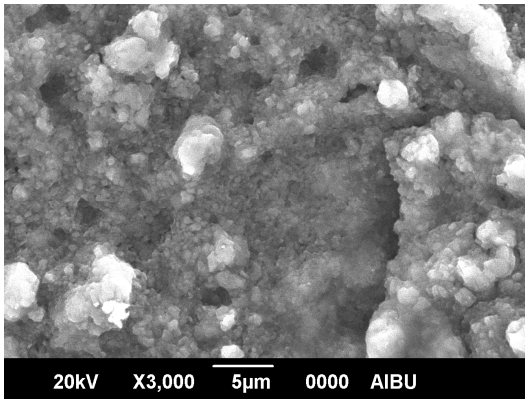

(b) (c)

Figure 5.64 (a-c) SEM pictures of transverse cross section of the MgB_2/Fe/Cu 7 filament tape.

5.3.1.3. EDS Investigations of the MgB_2/Fe/Cu 6 and 7 Filament Wires and Tapes

We have performed EDS measurements for elemental analysis. Figures 5.65, 66, 67 and 68 show the element distribution maps of Mg, B, Fe, O and Cu in the polished cross section of the MgB_2/Fe/Cu 6 and 7 filament wires and tapes without heat treatment, respectively. The MgB_2/Fe/Cu 6 and 7 filament wires have a regular round shape. In general, all the wires and tapes display good filament uniformity with approximate filament areas of 0.3847 mm^2 and 0.7850 mm^2 for the MgB_2/Fe/Cu 6 and 7 filament wires, respectively.

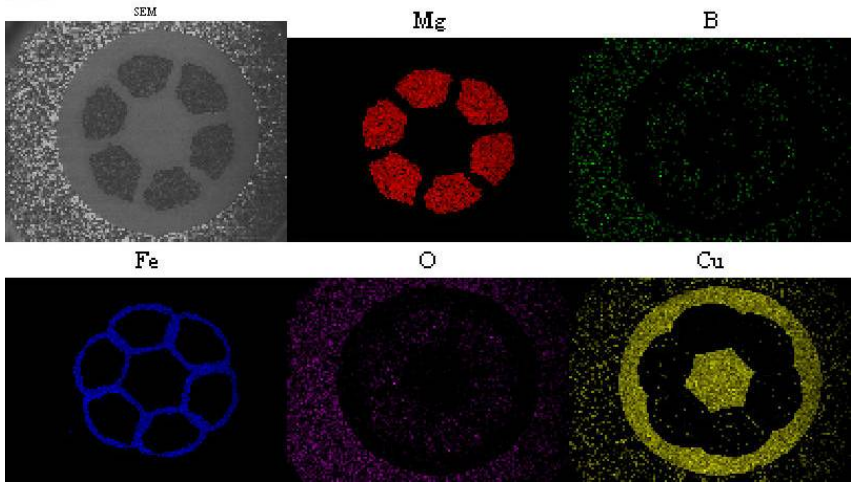

Figure 5.65 EDS picture of transverse cross section of the MgB_2/Fe/Cu 6 filament wire.

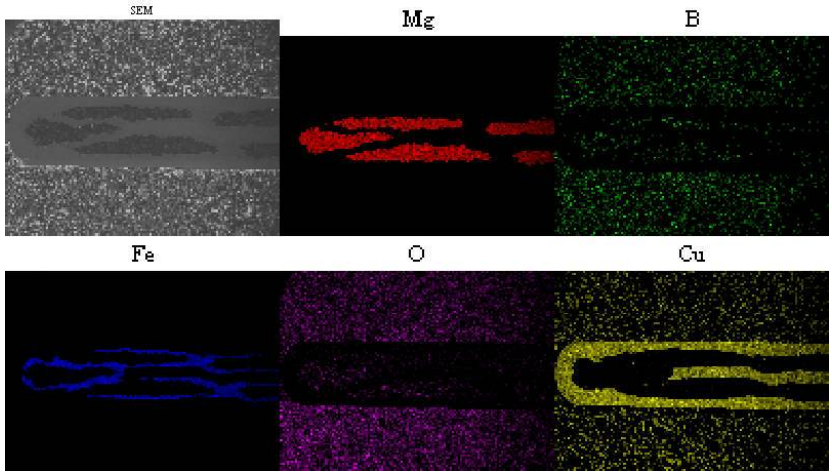

Figure 5.66 EDS picture of transverse cross section of the MgB_2/Fe/Cu 6 filament tape.

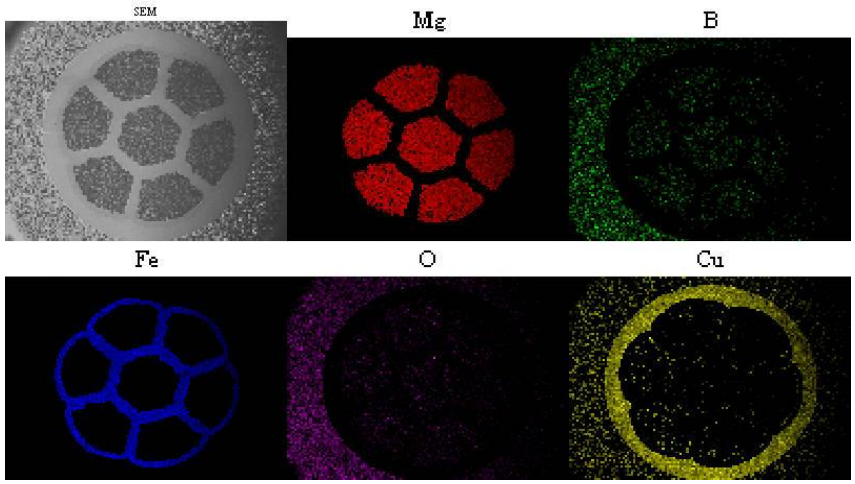

Figure 5.67 EDS picture of transverse cross section of the MgB_2/Fe/Cu 7 filament wire.

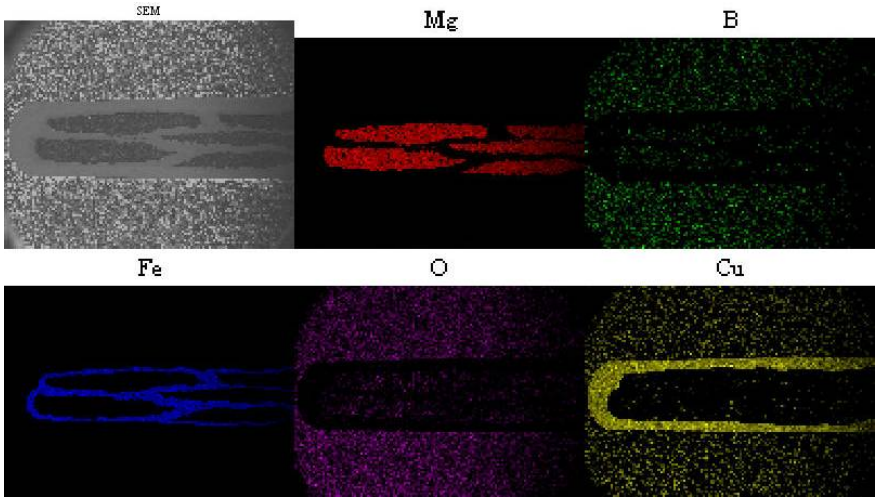

Figure 5.68 EDS picture of transverse cross section of the MgB_2/Fe/Cu 7 filament tape.

5.3.1.4. Optical Microscopy Investigations of the MgB_2/Fe/Cu 6 Filament Wires and Tapes

Surface structures of the MgB_2/Fe/Cu 6 and 7 filament wires and tapes were investigated by optical microscope.

Figures 5.69, 70, 71 and 72 show optical microscopy images of polished transverse cross section of the 6 and 7 filament wires and tapes without heat treatment, respectively.

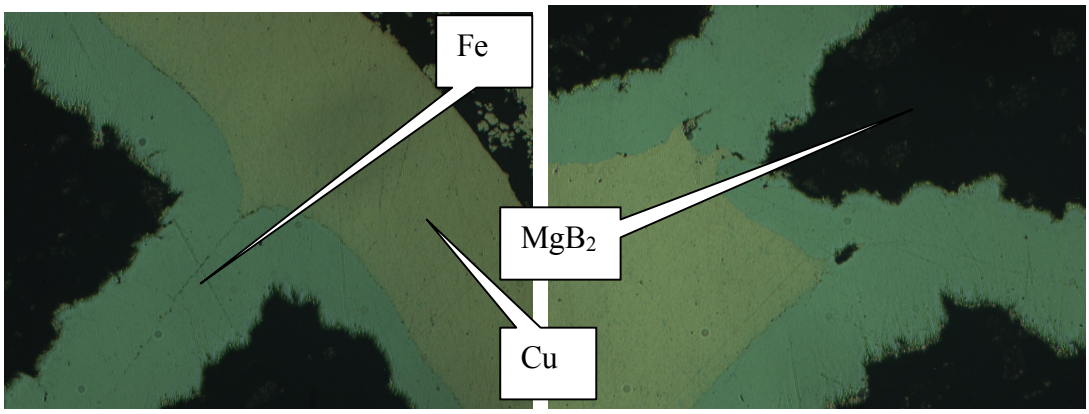

(a) (b)

Figure 5.69 (a-b) Optical microscopy images of the MgB_2/Fe/Cu 6 filament wire.

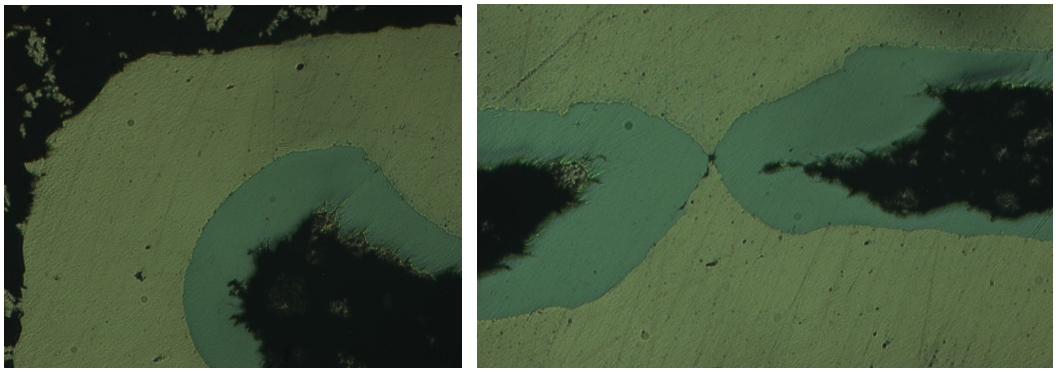

(a) (b)

Figure 5.70 (a-b) Optical microscopy images of the MgB_2/Fe/Cu 6 filament tape.

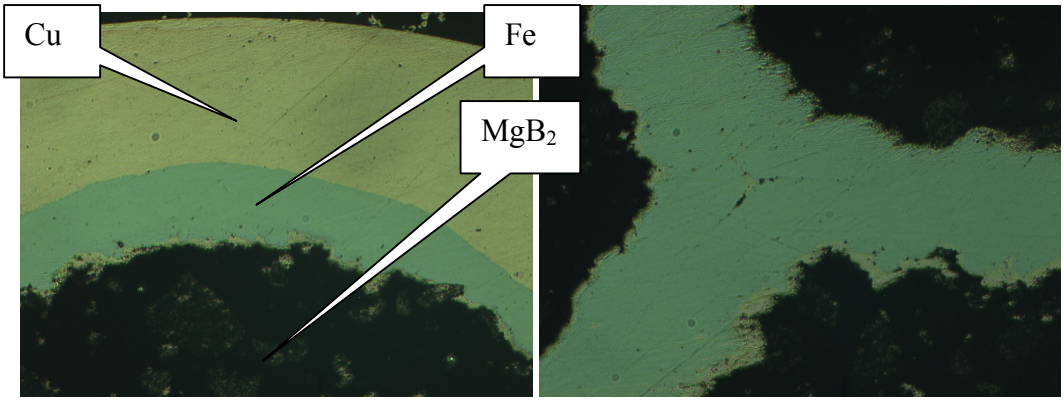

(a) (b)

Figure 5.71 (a-b) Optical microscopy images of the MgB_2/Fe/Cu 7 filament wire.

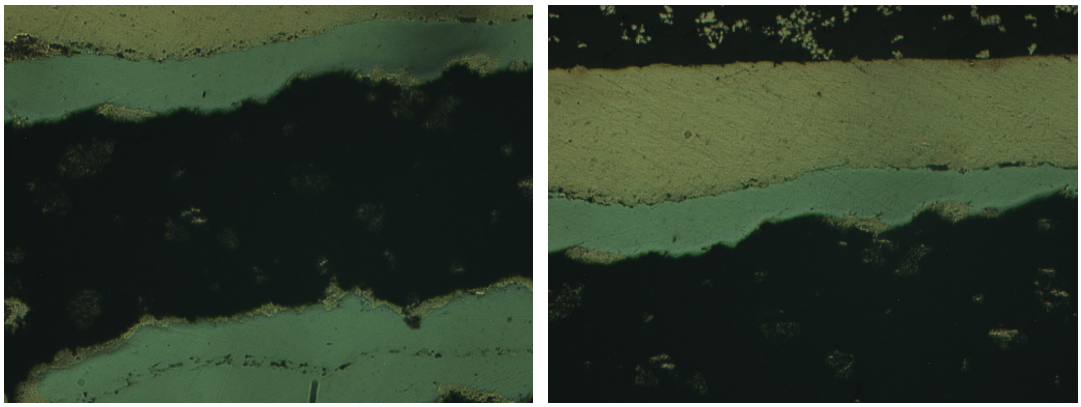

(a) (b)

Figure 5.72 (a-b) Optical microscopy images of the MgB_2/Fe/Cu 7 filament tape.

5.3.1.5. Resistivity Measurement of the MgB_2/Fe/Cu 6 and 7 Filament Tapes

Several short samples 2 cm in length were cut from the 6 and 7 filament MgB_2/Fe/Cu tapes. MgB_2/Fe/Cu 6 and 7 filament tapes were annealed at 900^{o}C for 120 minutes in high purity argon (Ar) gas atmosphere. A different method was used for preparing current and voltage contacts of the MgB_2/Fe/Cu 6 and 7 filament tapes. Standard Pb-Sn (40/60) solder was used for forming the current and voltage contacts. Both of voltage contacts were directly soldered with standard Pb-Sn (40/60) solder to

the sheath materials of the samples. Both of ends of the samples were painted with silver and then both of painted ends of the samples were soldered with standard Pb-Sn (40/60) solder for current contacts as shown in Figure 5.73.

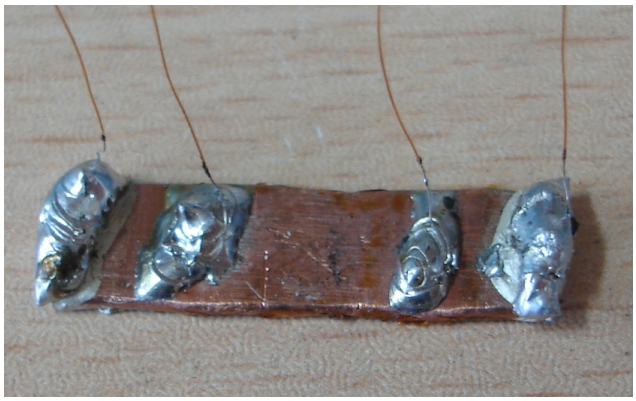

Figure 5.73 Current and voltage contacts of MgB_2/Fe/Cu multifilament tape.

The temperature dependence of the resistivity of the MgB_2/Fe/Cu 6 and 7 filament tapes is shown in Figure 5.74. T_c^{onset}, T_c^{offset} and ΔT_c values were tabulated in Table 5.29. The T_c^{offset} (K) values of the M6B and M7B samples were obtained as 36.7 K and 36.3 K, respectively.

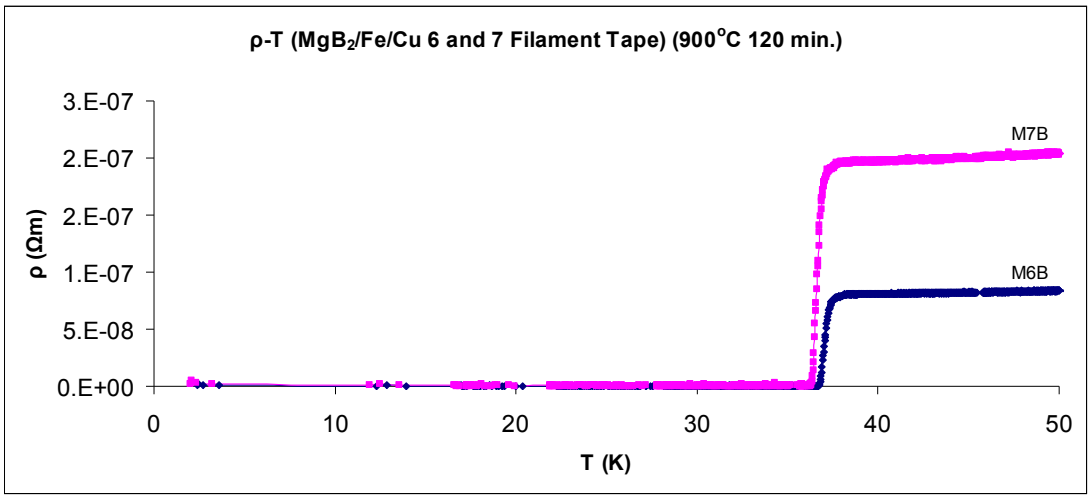

Figure 5.74 ρ-T graphs of the M6B and M7B samples.

Table 5.29 T_c values of the M6B and M7B samples.

Tapes	T_c^{onset} (K)	T_c^{offset} (K)	ΔT_c (K)
M6B	37.6	36.7	0.9
M7B	37.2	36.3	0.9

The active cross-sectional area fraction (A_F) values were estimated from resistivity measurements by using Rowell's connectivity analysis $A_F = \rho_{ideal}/[\rho_{300K} - \rho_{40K}]$ where ρ_{ideal}=7.3μΩcm. In addition, the residual resistivity ratio (RRR) defined by ρ_{300K}/ρ_{40K} was also estimated. Table 5.30 illustrates ρ_{40K}, ρ_{300K}, $\Delta\rho$, RRR and A_F values for M6B and M7B samples. In order to explain the connectivity between grains, A_F values are estimated for the M6B and M7B samples. The estimated A_F values were 4.62 and 0.23 for the M6B and M7B samples, respectively. According to Rowell's connectivity analysis, the higher A_F value is related to the better connectivity between grains. The estimated A_F value of the M6B sample was obtained higher than M7B sample. This result indicates the better intergranular connection in MgB_2 grains for the M6B sample. The room temperature resistivity value of the M6B sample was obtained lower than M7B sample. This is related to the better crystallinity of MgB_2 phase due to grain growth for the M6B sample.

Table 5.30 ρ_{40K}, ρ_{300K}, $\Delta\rho$, RRR and A_F values for M6B and M7B samples.

Samples	$\rho_{40\,K}$ (μΩcm)	$\rho_{300\,K}$ (μΩcm)	$\Delta\rho(\rho_{300\,K}-\rho_{40\,K})$ (μΩcm)	RRR	A_F (%)
M6B	0.81	2.39	1.58	2.95	4.62
M7B	1.97	5.98	3.92	3.03	1.86

5.3.1.6. Critical Current Measurement of the MgB_2/Fe/Cu 6 and 7 Filament Tapes

Short samples 2 cm in length were cut from the MgB_2/Fe/Cu 6 and 7 filament tapes. These pieces were then heat treated at 900^oC for 120 minutes in a tube furnace. Heat treatment of the sample was done under 3 bars high purity argon (Ar) gas atmosphere and the sample was cooled down to room temperature in the furnace. The heating and cooling rates of the temperature were chosen to be 5^oC min^{-1}. The current-voltage (I-V) characteristic of the samples were measured at 20 K with the standard four-probe method under self-field. Figures 5.75 and 5.77 shows I-V graphs of the MgB_2/Fe/Cu 6 and 7 filament tapes measured at 20 K. The critical current values of the MgB_2/Fe/Cu 6 and 7 filament tapes were obtained as 5.01 A and 4.45 A, respectively. Figures 5.76 and 5.78 show the electric field as a function of critical current density for the samples measured at 20 K. The critical current density values of the MgB_2/Fe/Cu 6 and 7 filament tapes were calculated from I-V measurements as 447.74 A/cm^2 and 188.18 A/cm^2, respectively. The critical current and critical current density values of the MgB_2/Fe/Cu 6 filament tape was obtained higher than MgB_2/Fe/Cu 7 filament tape at 20 K.

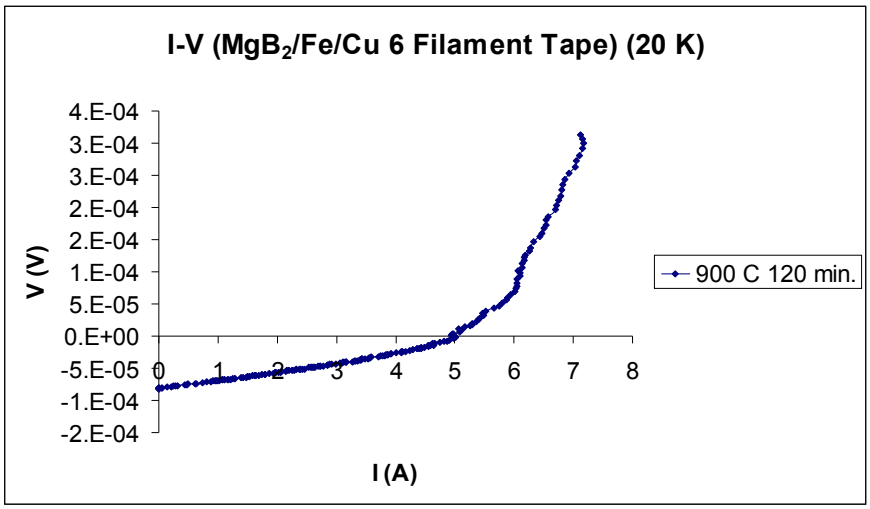

Figure 5.75 I-V graph of the MgB_2/Fe/Cu 6 filament tape.

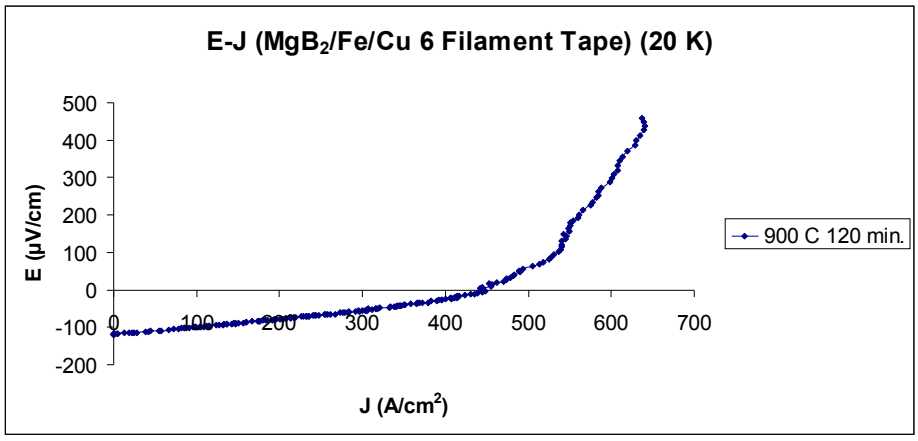

Figure 5.76 E-J graph of the MgB_2/Fe/Cu 6 filament tape.

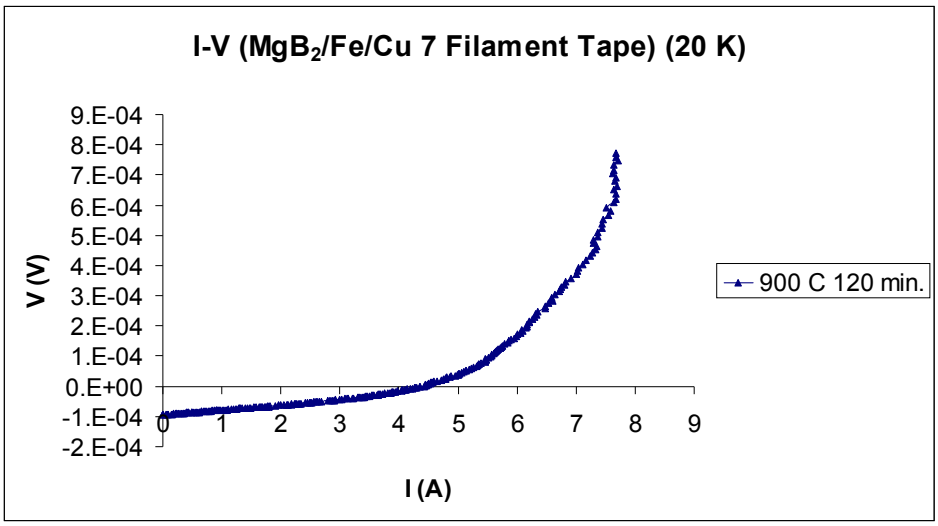

Figure 5.77 I-V graph of the MgB_2/Fe/Cu 7 filament tape.

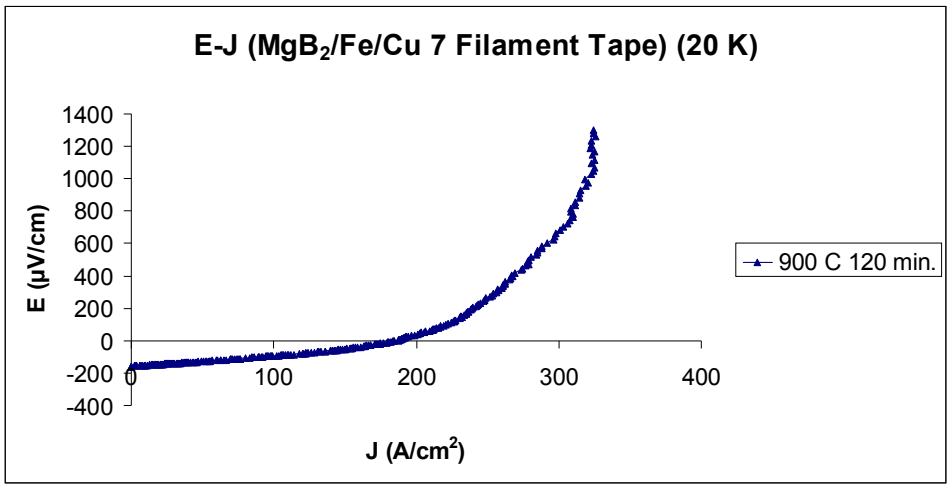

Figure 5.78 E-J graph of the MgB_2/Fe/Cu 7 filament tape.

5.3.1.7. Magnetization Measurements of the MgB_2/Fe/Cu 6 and 7 Filament Wires

The M-H graphs (3T magnetic field was applied at 10K) of the MgB_2/Fe/Cu 6 and 7 filament wires annealed at 900°C for 120 minutes are shown in Figure 5.79 and Figure 5.81. The M-H graphs (3T magnetic field was applied at 10K) of the MgB_2/Fe/Cu 6 and 7 filament wires annealed at 900°C for 120 minutes have a ferromagnetic property. The Fe sheath of the MgB_2 core screened the contribution of the MgB_2 core. Therefore, the contribution of the MgB_2 core could not be observed.

The M-T graphs (0.1T magnetic field was applied between at 10K and 50K) of the MgB_2/Fe/Cu 6 and 7 filament wires annealed at 900°C for 120 minutes are shown in Figure 5.80 and 5.82. The offset superconducting transition temperature values of the MgB_2/Fe/Cu 6 and 7 filament wires were determined as approximately 36.8 K and 36.6 K from the M-T graphs. These inductive superconducting transition temperature values are consistent with the superconducting transition temperatures

which were obtained from transport measurements of the MgB_2/Fe/Cu 6 and 7 filament wires.

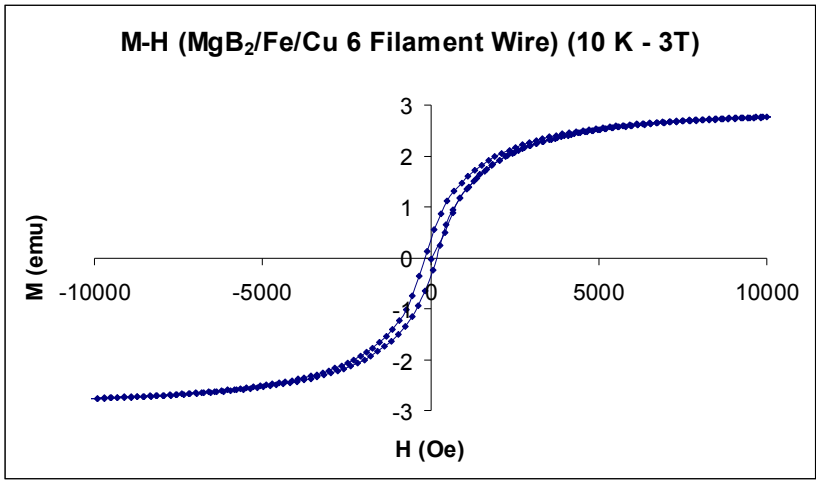

Figure 5.79 M-H graph of MgB_2/Fe/Cu 6 filament wire.

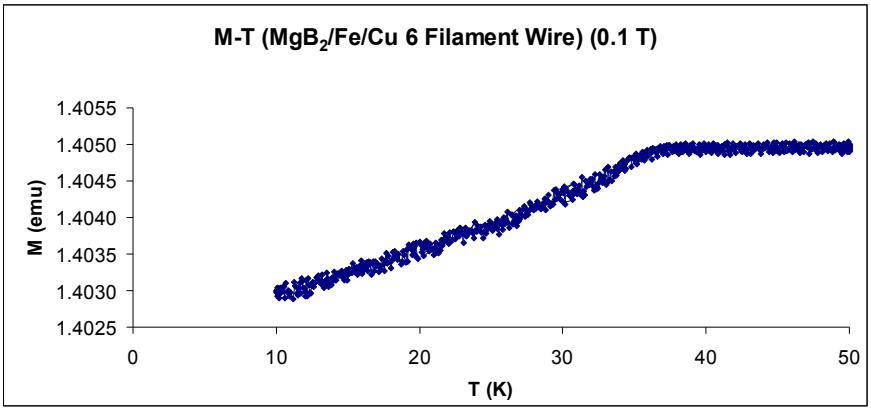

Figure 5.80 M-T graph of MgB_2/Fe/Cu 6 filament wire.

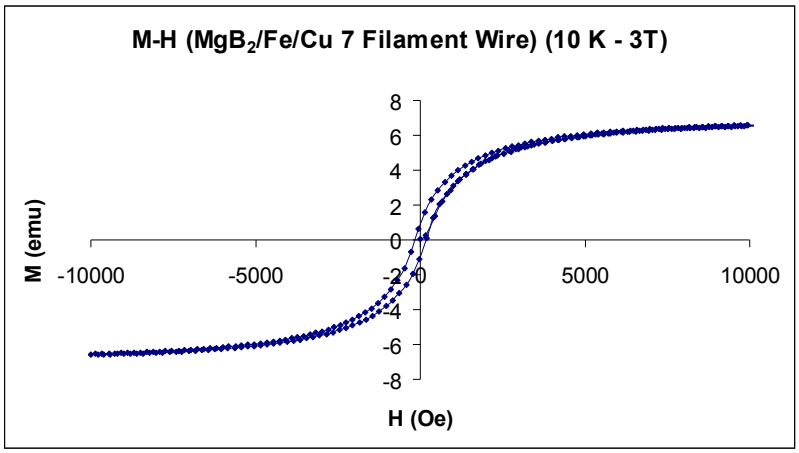

Figure 5.81 M-H graph of MgB_2/Fe/Cu 7 filament wire.

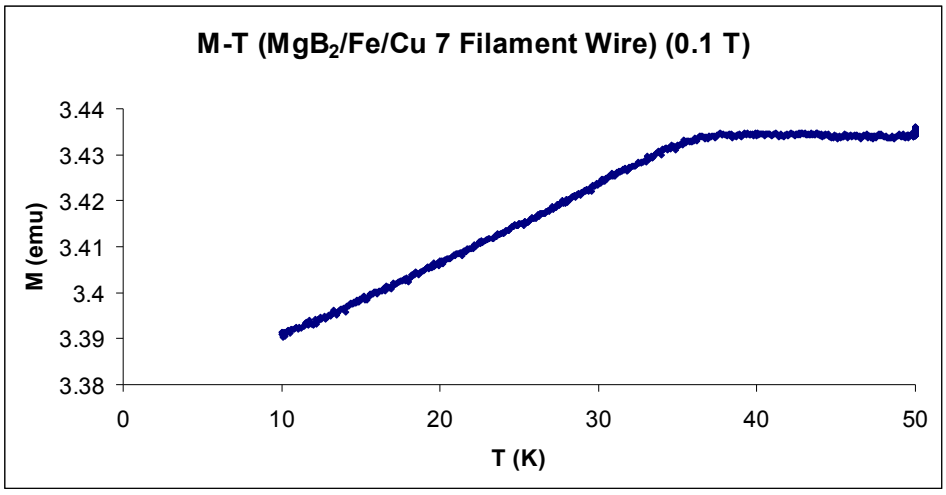

Figure 5.82 M-T graph of MgB_2/Fe/Cu 7 filament wire.

5.3.2. MgB_2/Ag/Fe 7 and 23 Filament Wires and Tapes

5.3.2.1. SEM Investigations of the MgB_2/Ag/Fe 7 and 23 Filament Wires and Tapes

Microstructure and surface morphology investigations of the MgB_2/Ag/Fe 7 and 23 filament wires and tapes were studied by SEM.

Figure 5.83 shows SEM picture of transverse cross section of a 1.53 mm in diameter of the MgB_2/Ag/Fe 7 filament wire. The matrix metal of the conductor is iron. The composite (MgB_2/Ag/Fe) wire has a regular round shape.

Table 5.31 summarizes the main characteristics of the MgB_2/Ag/Fe 7 filament wire

Table 5.31 MgB_2/Ag/Fe 7 Filament wire Characteristics.

Number of MgB_2 filaments	7
Preparation technique	Ex-situ PIT
Sheath material	Iron
Diffusion barrier material	Silver
Composite (MgB_2/SS/Cu) cross section	2.1186 mm^2
MgB_2 cross section	0.44633 mm^2
Silver cross section	1.4022 mm^2
Iron cross section	0.2700 mm^2

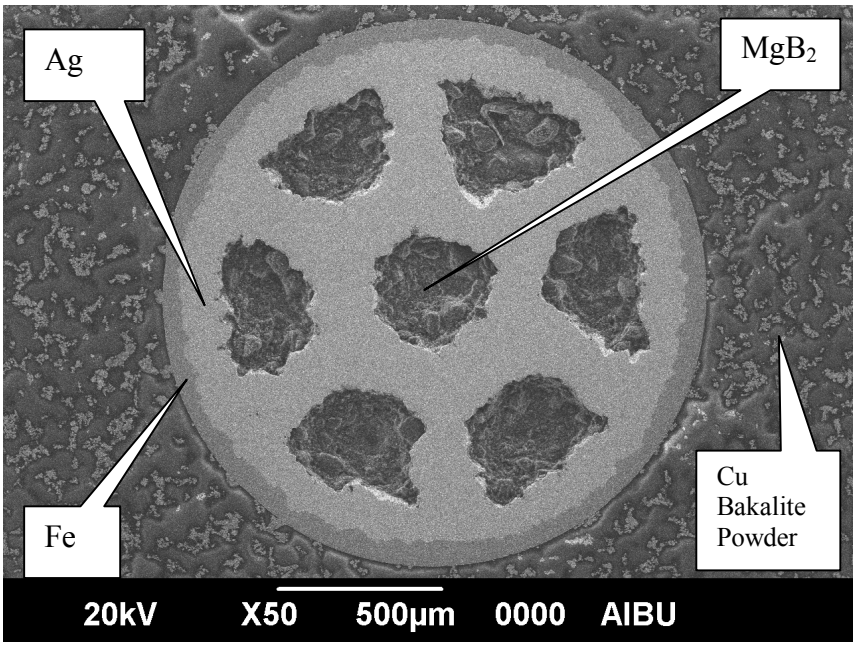

Figure 5.83 SEM picture of transverse cross section of the MgB_2/Ag/Fe 7 filament wire.

Figure 5.84 shows SEM picture of transverse cross section of the MgB_2/Ag/Fe 7 filament tape. The composite (MgB_2/Ag/Fe) tape has a regular shape. The filament right in the middle elongated far more than other filaments. Softness of Ag permitted uneven deformation of MgB_2 filaments.

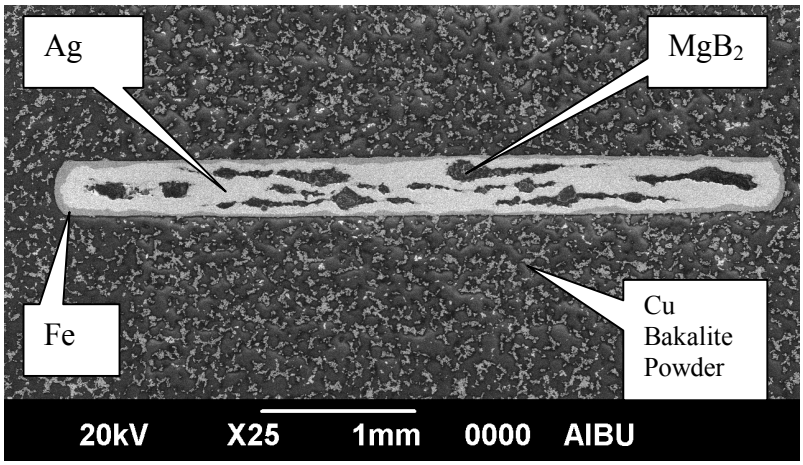

Figure 5.84 SEM picture of transverse cross section of the MgB_2/Ag/Fe 7 filament tape.

Figure 5.85 shows SEM picture of transverse cross section of a 3.04 mm in diameter of the MgB_2/Ag/Fe 23 filament wire. The matrix metal of the conductor is iron. A copper stabilizer is located in the conductor. Between MgB_2 and copper, a silver barrier is placed in order to prevent diffusion of copper to MgB_2 during heat treatment. The MgB_2/Ag/Fe 23 filament wire has a regular round shape but MgB_2 cores did not scatter orderly in the wire. The cross section shows uniform deformation of the composite.

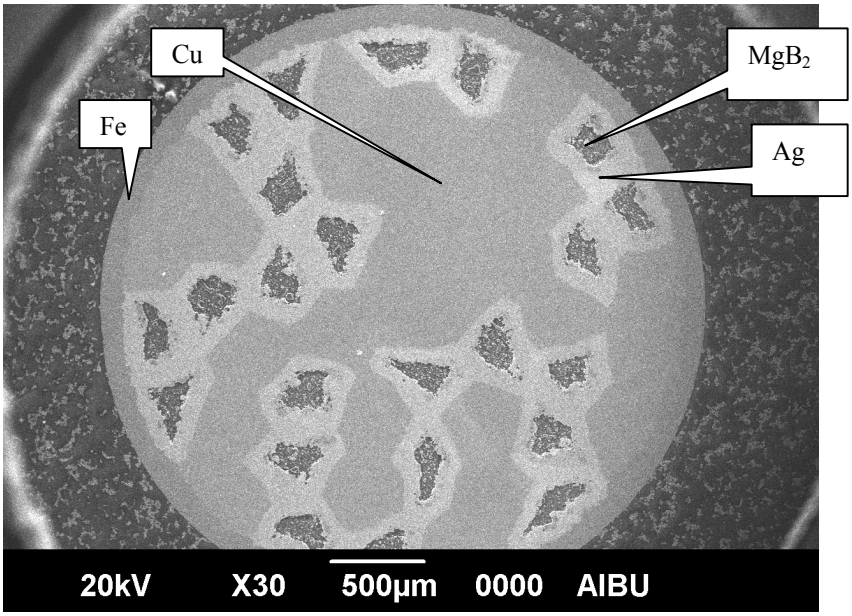

Figure 5.85 SEM picture of transverse cross section of the MgB_2/Ag/Fe 23 filament wire.

Figures 5.86a and 5.86b show SEM picture of transverse cross section of the MgB_2/Ag/Fe 23 filament tape. The MgB_2/Ag/Fe 23 filament tape has a regular shape but MgB_2 cores did not scatter orderly in the tape. The cross section shows regular deformation of the composite tape without any problem such as breakage.

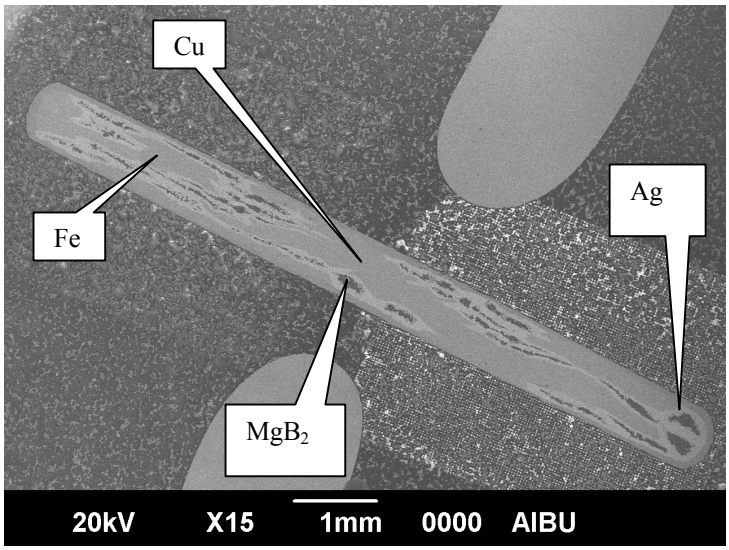

(a)

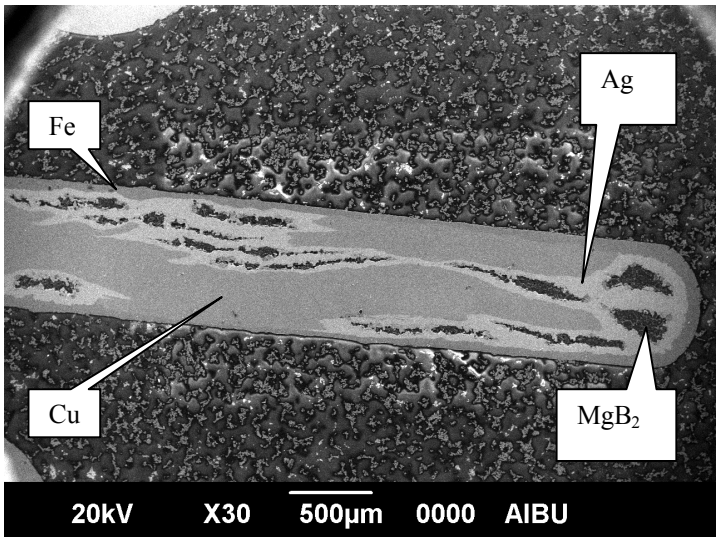

(b)

Figure 5.86 (a-b) SEM pictures of transverse cross section of the MgB_2/Ag/Fe 23 filament tape.

5.3.2.2. EDS Investigations of the MgB_2/Ag/Fe 7 and 23 Filament Wires and Tapes

Microstructure and chemical composition investigations of the MgB_2/Ag/Fe 7 and 23 filament wires and tapes that are not annealed were investigated by scanning electron microscope with an energy dispersive X-ray spectrometer (EDS) analysis.

Figures 5.87, 88, 89 and 90 show the element distribution maps of Mg, B, Fe and Ag in the cross section of the MgB_2/Ag/Fe 7 and 23 filament wires and tapes, respectively. Figure 5.89 shows EDS surface analyses and SEM micrographs results indicate there are no visible reaction between the MgB_2 cores and the Cu thermal stabilization material.

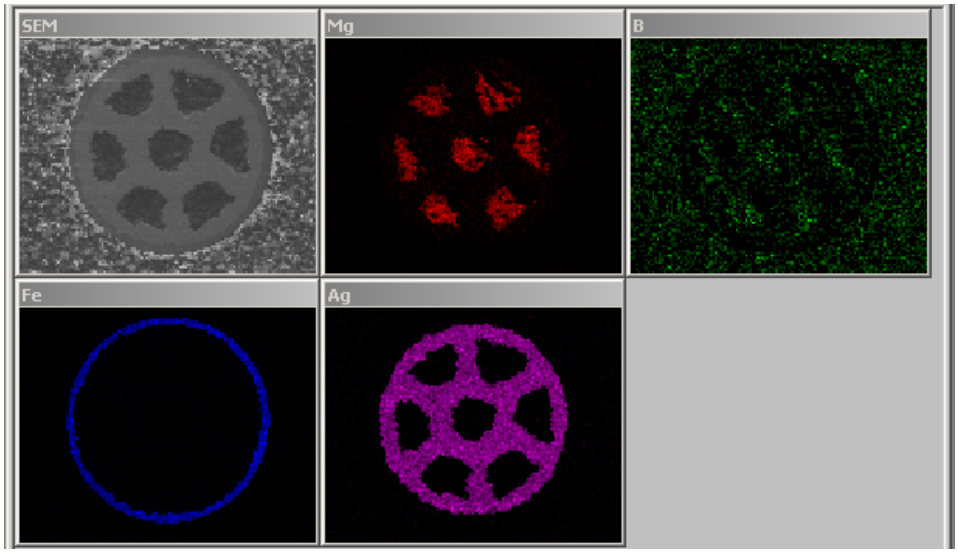

Figure 5.87 EDS picture of transverse cross section of the MgB_2/Ag/Fe 7 filament wire.

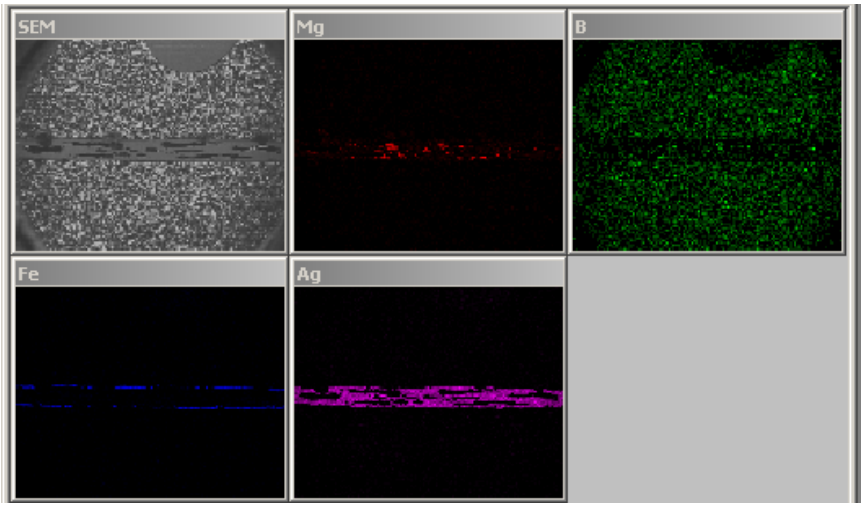

Figure 5.88 EDS picture of transverse cross section of the MgB_2/Ag/Fe 7 filament tape.

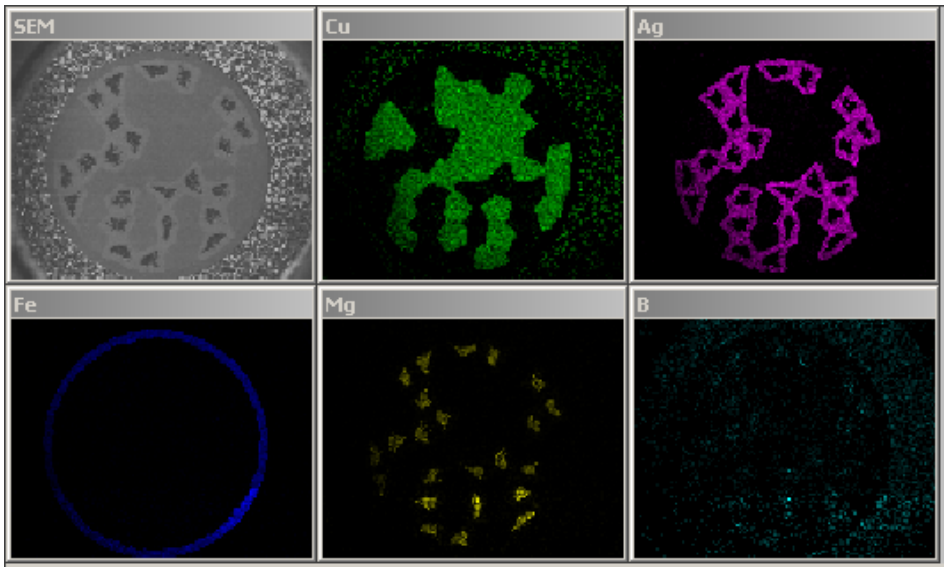

Figure 5.89 EDS picture of transverse cross section of the MgB_2/Ag/Fe 23 filament wire.

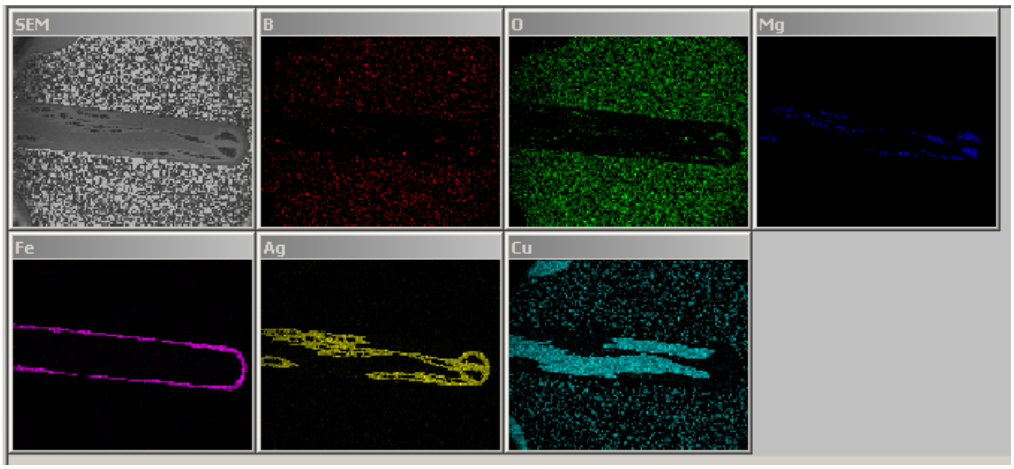

Figure 5.90 EDS picture of transverse cross section of the MgB_2/Ag/Fe 23 filament tape.

5.3.2.3. Optical Microscopy Investigations of the MgB_2/Ag/Fe 7 and 23 Filament Wires and Tapes

Figure 5.91 and 5.92 show optical microscopy images of transverse cross section of the MgB_2/Ag/Fe 7 filament wire and tape. Figure 5.93 shows optical microscopy images of transverse cross section of the MgB_2/Ag/Fe 23 filament wire.

Optical microscopy image of MgB_2/Ag/Fe 23 filament wire indicate there are no visible reaction between the MgB_2 cores and the Cu thermal stabilization material.

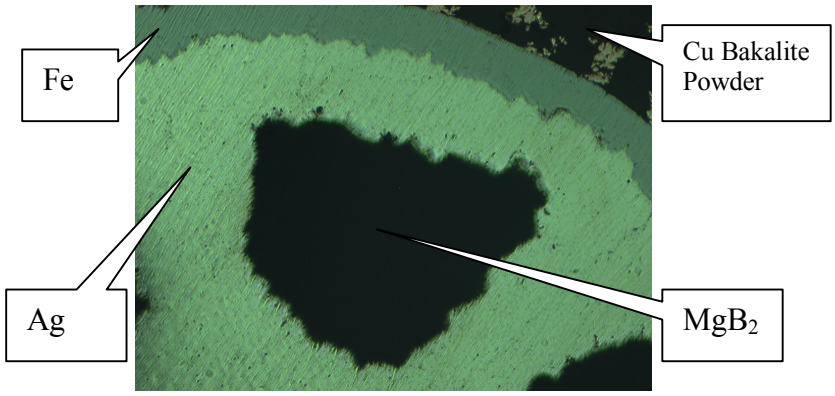

Figure 5.91 Optical microscopy image of the MgB_2/Ag/Fe 7 filament wire.

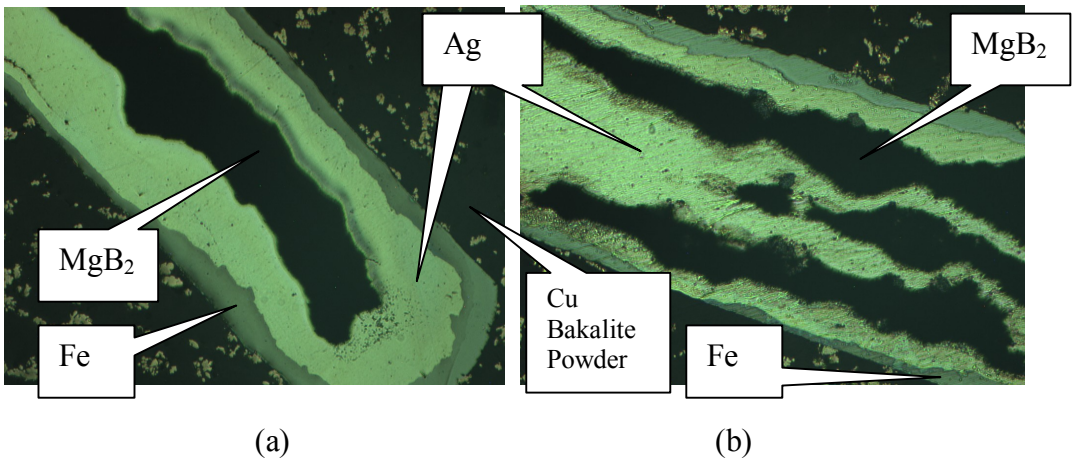

Figure 5.92 (a-b) Optical microscopy images of the MgB_2/Ag/Fe 7 filament tapes.

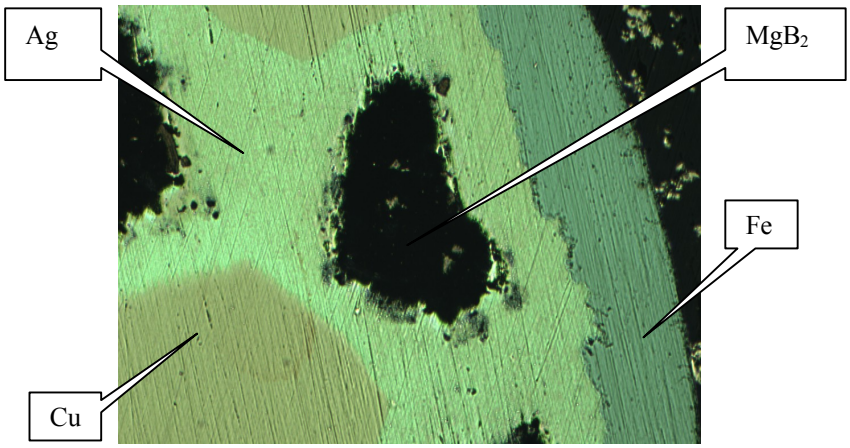

Figure 5.93 Optical microscopy image of the MgB_2/Ag/Fe 23 filament wire.

5.3.2.4. Resistivity Measurement of the MgB_2/Ag/Fe 7 and 23 Filament Tapes

The temperature dependence of the resistivity measurement of the MgB_2/Ag/Fe 7 filament tape annealed at 950°C for 60 minutes is shown in Figure 5.94. According to resistivity measurement of the MgB_2/Ag/Fe 7 filament tape annealed at 950°C for 60 minutes was observed superconductor characteristics. T_c^{onset}, T_c^{offset} and ΔT_c values of the MgB_2/Ag/Fe 7 filament tape were determined as 39.7 K, 37.0 K and 2.7 K, respectively.

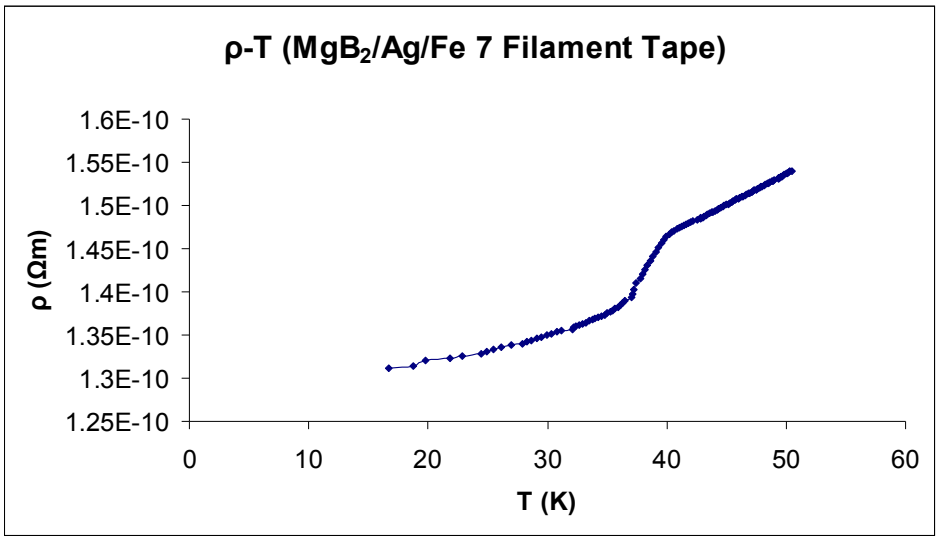

Figure 5.94 ρ-T graph of the MgB_2/Ag/Fe 7 filament tape.

Figures 5.95 and 5.96 show the temperature dependence of the resistivity measurements of the MgB_2/Ag/Fe 23 filament wires annealed at 750°C for 30 and 120 minutes and MgB_2/Ag/Fe 23 filament tape annealed at 750°C for 120 minutes, respectively but in these graphs superconductivity characteristics were not observed for the MgB_2/Ag/Fe 23 filament wires and tape. The reasons of this a) Starting powder may be of poor quality. b) Starting powder may have oxidized during the preparation of starting powder. c) Lack of a perfect inert atmosphere during the heat

treatments. d) Temperature and period of the heat treatments may have been insufficient. e) Due to impurity phases in the sample.

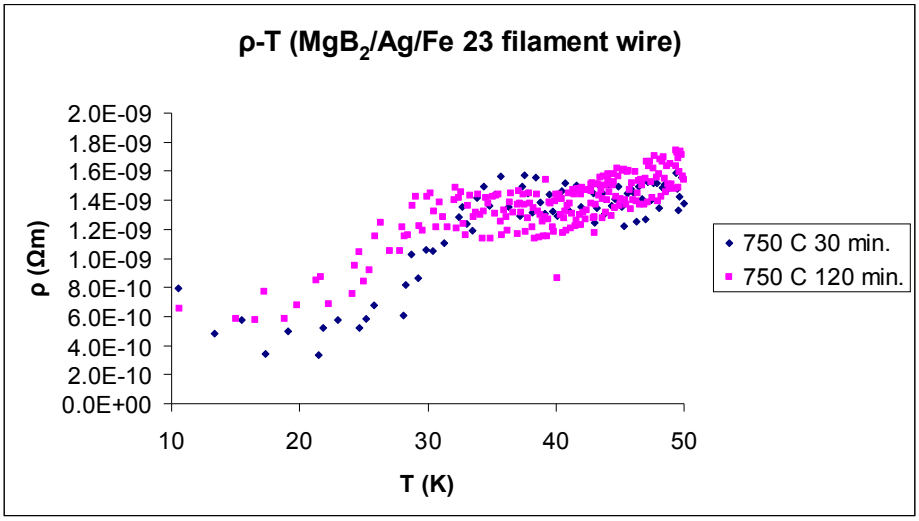

Figure 5.95 ρ-T graphs of the MgB_2/Ag/Fe23 filament wires.

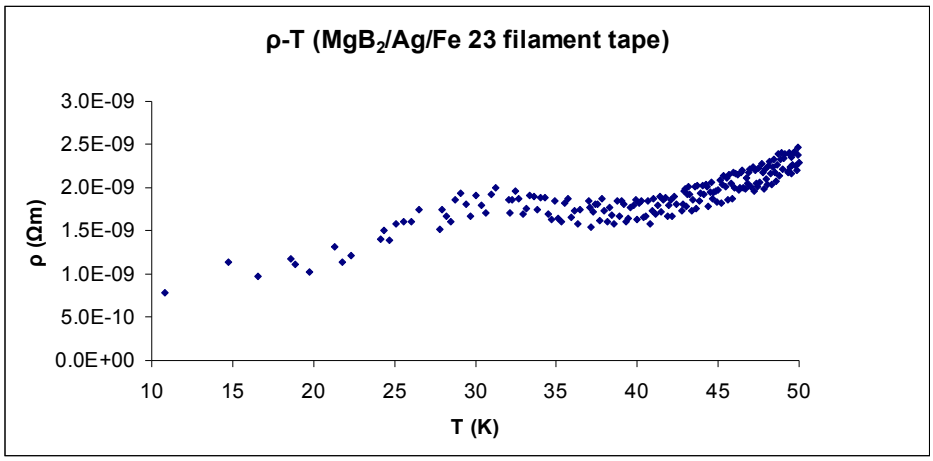

Figure 5.96 ρ-T graph of the MgB_2/Ag/Fe23 filament tape.

5.3.3. MgB_2/SS/Cu 6 Filament Wires and Tapes

5.3.3.1. SEM Investigation of the MgB_2/SS/Cu 6 Filament Wire

Figure 5.97 shows SEM picture of transverse cross section of a 1.43 mm in diameter of the MgB_2/SS/Cu 6 filament wire. The matrix metal of the conductor is

copper. A copper stabilizer is located in the conductor. Between MgB_2 and copper, a stainless steel barrier is placed in order to prevent diffusion of copper to MgB_2 during heat treatment. The composite (MgB_2/SS/Cu) has a regular round shape. The cross section shows uniform deformation.

Table 5.32 summarizes the main characteristics of the MgB_2/SS/Cu 6 filament wire

Table 5.32 MgB_2/SS/Cu 6 Filament wire Characteristics.

Number of MgB_2 filaments	6
Preparation technique	Ex-situ PIT
Sheath material	Copper
Diffusion barrier material	Stainless Steel
Composite (MgB_2/SS/Cu) cross section	1.60 mm^2
MgB_2 cross section	0.49 mm^2
Stainless Steel cross section	0.43 mm^2
Copper cross section	0.68 mm^2

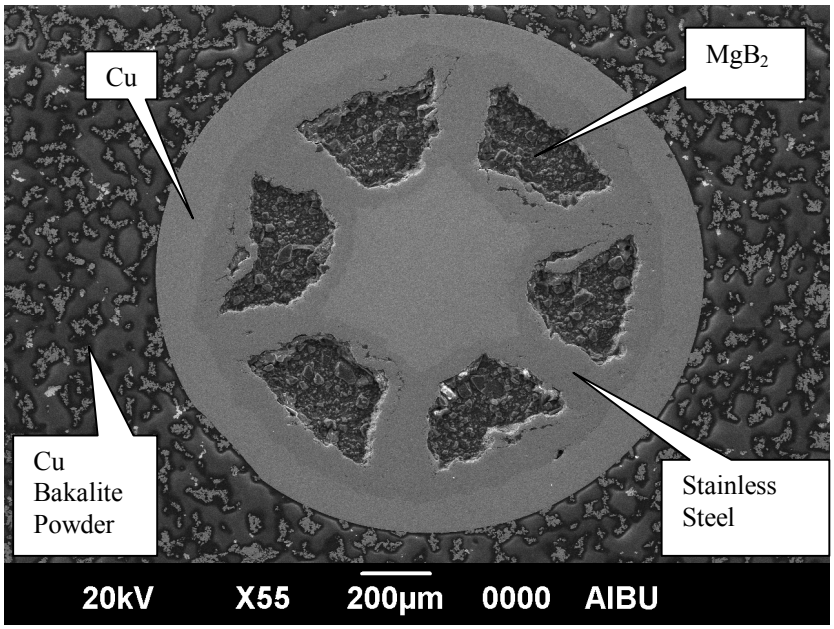

Figure 5.97 SEM picture of transverse cross section of the MgB_2/SS/Cu 6 filament wire.

5.3.3.2. EDS and Optical Microscopy Investigations of the MgB_2/SS/Cu 6 Filament Wire

Figure 5.98 shows the element distribution maps of Mg, B, O, Co, Ni and Fe in the cross section of the MgB_2/SS/Cu 6 filament wire. Figure 5.99 shows optical microscopy images of transverse cross section of the MgB_2/SS/Cu 6 filament wire. EDS surface analyses, SEM micrographs results and optical microscopy image of the MgB_2/SS/Cu 6 filament wire indicate there are no visible reaction between the MgB_2 cores and the Cu thermal stabilization material.

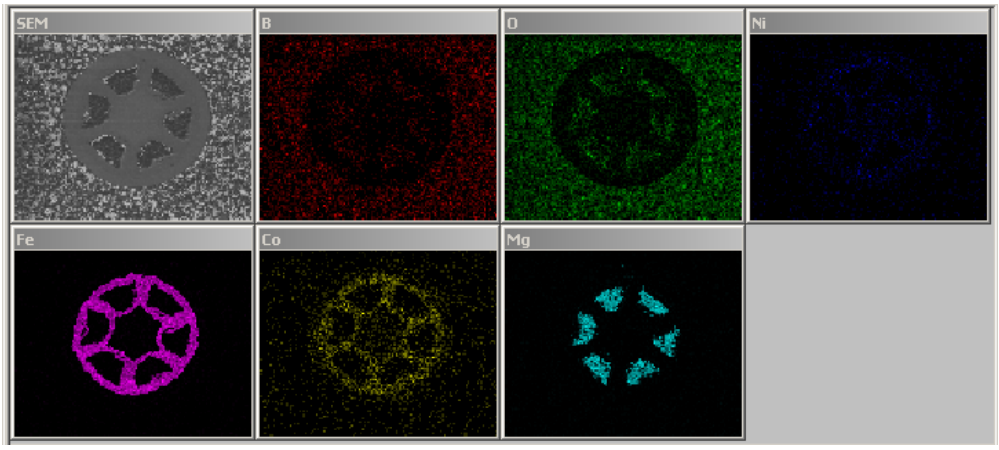

Figure 5.98 EDS picture of transverse cross section of the MgB_2/SS/Cu 6 filament wire.

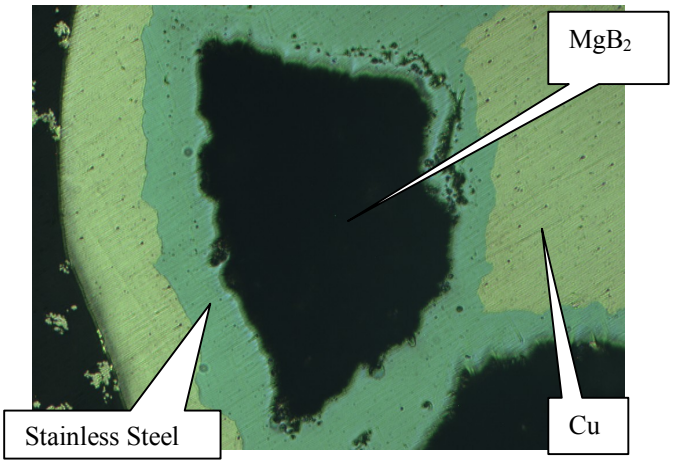

Figure 5.99 Optical microscopy image of the MgB_2/SS/Cu 6 filament wire.

5.3.4. Effect of extreme rolling on the superconducting properties of commercial MgB_2 tapes

In this study we have investigated the effect of extreme rolling on the properties of commercial MgB_2 tapes. The MgB_2 tapes were kindly provided by Columbus Superconductors. The MgB_2/Ni/Fe/Cu superconducting tapes were 0.65 mm thick and 3.60 mm wide. A transverse cross section of the MgB_2/Ni/Fe/Cu superconducting tape is shown in Figure 5.100.

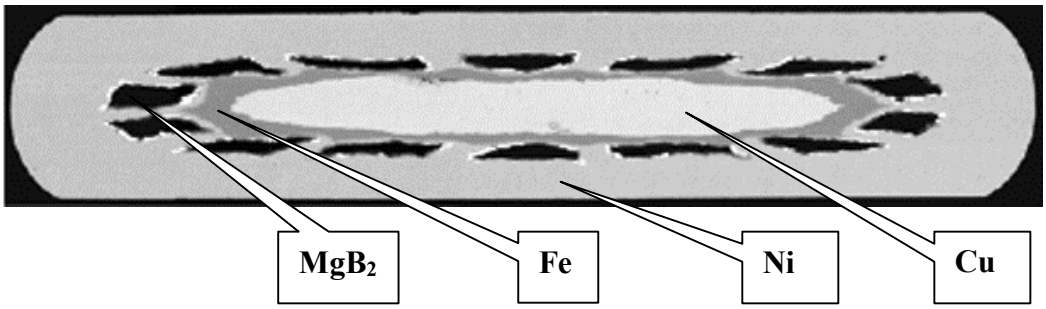

Figure 5.100 Transverse cross section of the MgB_2/Ni/Fe/Cu superconducting tape manufactured by Columbus Superconductors.

Table 5.33 summarizes the main characteristics of the MgB_2/Ni/Fe/Cu superconducting tape manufactured by Columbus Superconductors

Table 5.33 MgB_2/Ni/Fe/Cu Tape Characteristics.

Number of MgB_2 filaments	14
Preparation technique	Ex-situ PIT
Sheath material	Nickel
Diffusion barrier material	Iron
Typical tape dimensions	0.65 x 3.6 mm^2
MgB_2 cross section	0.21 mm^2
Nickel cross section	1.54 mm^2
Iron cross section	0.19 mm^2
Copper cross section	0.35 mm^2

In order to investigate the effect of extreme rolling and heat treatment on the superconducting properties of MgB_2 tapes, we prepared 6 different samples 5 cm in length. Three of the samples were cut from the tape which was rolled four times and the remaining three samples were cut from the unrolled tape.

After four times rolling, the final length of the tape became 105 cm from the initial value of 81.6 cm. Similarly, the thickness and the width of the tape increased from the initial values of 0.65 mm to 0.24 mm and 3.60 mm to 6.08 mm respectively.

To investigate the effect of heat treatment on the superconducting properties of the tapes, we heat treated rolled and unrolled samples at 550^{o}C and 630^{o}C for 20 minutes. All the heat treatments were done in argon atmosphere. The results of the measurements on the heat treated samples were compared to those which were not heat treated. The heat treatment procedure and the naming of the samples are shown in Table 5.34.

Table 5.34 Heat treatments of the commercial MgB_2 tapes.

Temperature	Period (minute)	Rolled 4 times	Unrolled
630^{o}C	20	T4	T1
550^{o}C	20	T5	T2
no heat treatment	_	T6	T3

Figure 5.101 shows the ρ-T characteristics of the samples measured with dc current of 50mA through them in a cryostat.

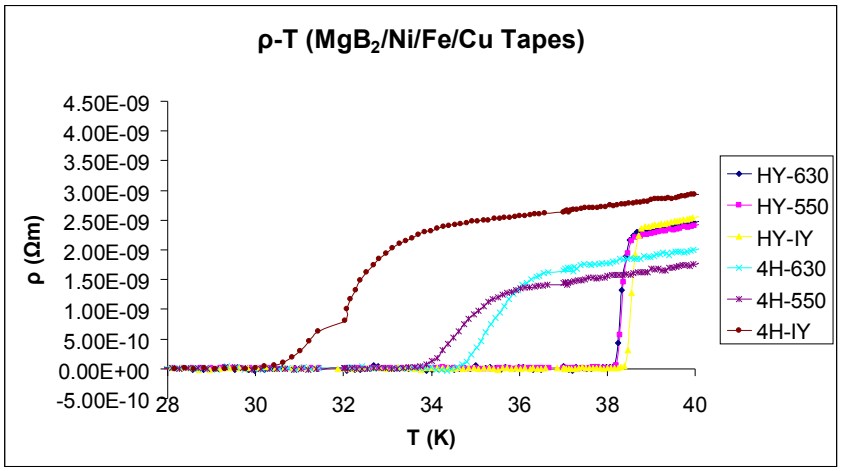

Figure 5.101 Temperature dependence of the resistivity for all of the commercial MgB_2 samples.

Table 5.35 shows the legends of the Figure 5.101.

Table 5.35 The legends of the Figure 5.101

Tapes	Specification
T1 (HY-630)	unrolled tape was heat treated at 630°C for 20 minutes
T2 (HY-550)	unrolled tape was heat treated at 550°C for 20 minutes
T3 (HY-IY)	unrolled tape was not heat treated
T4 (4H-630)	rolled (4 times) tape was heat treated at 630°C for 20 minutes
T5 (4H-550)	rolled (4 times) tape was heat treated at 550°C for 20 minutes
T6 (4H-IY)	rolled (4 times) tape was not heat treated

The critical temperature (T_c) values of the tapes are shown in Figure 5.102.

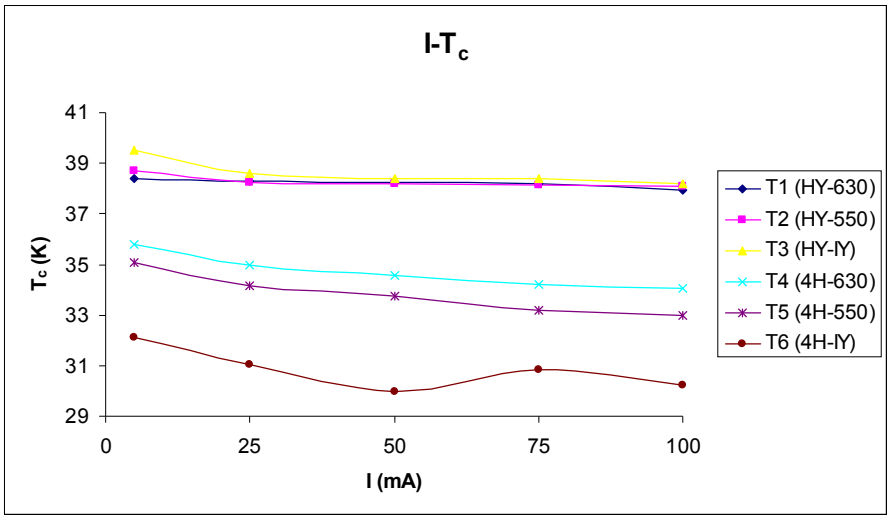

Figure 5.102 Critical temperature (T_c) values for all of the samples.

The transport critical current (I_c) was measured by the standard four-probe method between 10K-35K, in self field with a voltage criterion of 1μV/cm. Figure 5.103 shows the E-J characteristics of the samples measured at10K.

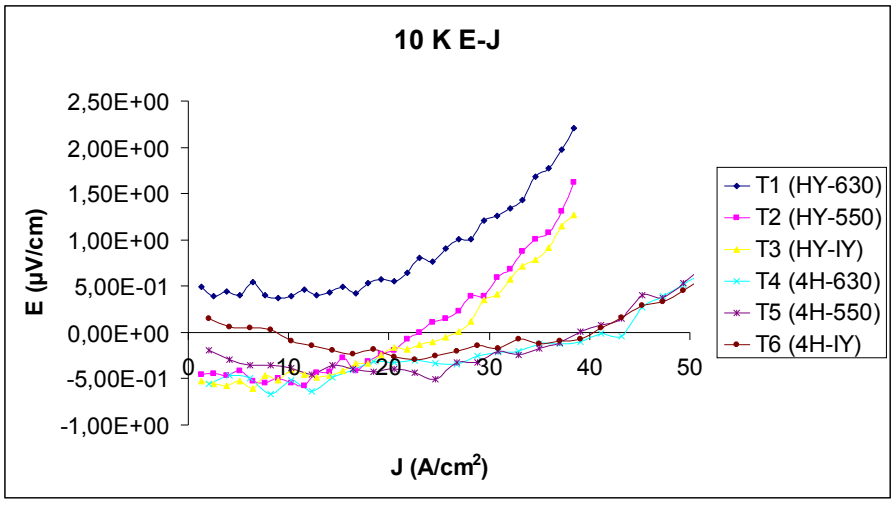

Figure 5.103 The typical E-J curves of the samples at 10 K.

The engineering critical current density J_e is defined as the critical current per cross-sectional area of the entire tape. The engineering critical current density (J_e) values of the tapes are shown in Figure 5.104.

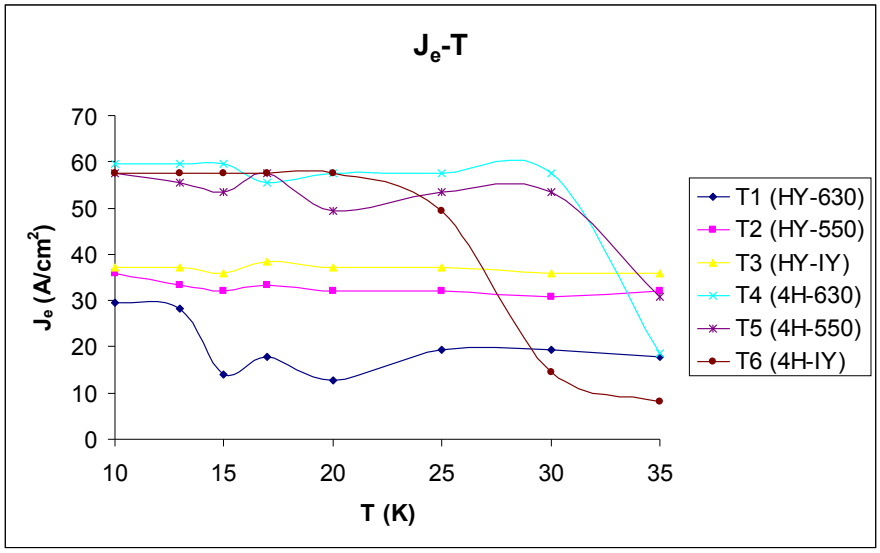

Figure 5.104 Engineering critical current density (J_e) values for all of the samples.

The vertical cross sections of the tapes were mounted in bakelite. Then, tape surfaces were polished and the surface structures of these tapes were investigated by OLYMPLUS GX41 optical microscope.

Figure 5.105 show optical micrographs of vertical cross section for unrolled MgB_2/Ni/Fe/Cu multifilament tape and four times rolled MgB_2/Ni/Fe/Cu multifilament tape.

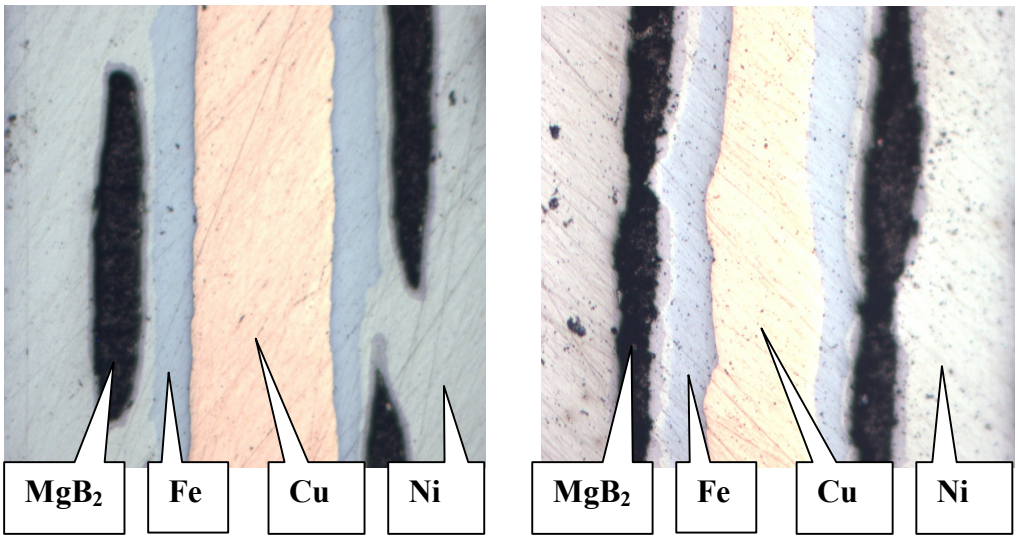

(a) (b)

Figure 5.105 (a) MgB_2/Ni/Fe/Cu multifilament tapes unrolled and **(b)** four times rolled.

Optical microscopy images of the MgB_2/Ni/Fe/Cu multifilament tapes indicate uniform deformation of the composite tapes and there are no visible reaction between the MgB_2 cores and the Cu thermal stabilization material for MgB_2/Ni/Fe/Cu multifilament tape which was rolled four times.

Rolling clearly reduced the critical temperature (T_c) values of the tapes. Application of heat treatment after rolling reduces the decrease in T_c. For rolled tapes critical temperature (T_c) values increased with increase of heat treatment temperature. Heat treatment at 900^{o}C after rolling is expected to produce better results for T_c. The transition width (ΔT) significantly increases due to rolling. The increase in ΔT is reduced when annealing is applied. Rolling increased the engineering critical current density (J_e) values of the tapes.

CHAPTER 6

CONCLUSIONS

In this thesis, we have fabricated monofilament (MgB_2/Fe, MgB_2/Ag and MgB_2/SS) and multifilament (6 and 7 filament MgB_2/Fe/Cu, 7 and 23 filament MgB_2/Ag/Fe and 6 filament MgB_2/SS/Cu) superconducting MgB_2 wires and tapes by using powder-in-tube (PIT) and continuous tube forming and filling (CTFF) method following the ex-situ and mixture of ex-situ and in-situ reaction routes.

The monofilament and multifilament MgB_2 wires and tapes have been characterized by using XRD, SEM, EDS, optical microscope, critical current density, transport, magnetoresistivity and magnetization measurements to investigate the superconducting and microstructure properties. Moreover, we have investigated the effect of extreme rolling on the superconducting properties of commercial MgB_2 tapes.

We have obtained the following results for the superconducting samples;

1. The MgB_2/Fe monofilament superconducting materials were fabricated by ex-situ PIT method using commercially available MgB_2 powder (Alfa Aesar, -325 mesh, <44 micron) without any intermediate annealing. We have investigated the effect of annealing temperature and time on the phase formation, lattice parameters, FWHM, crystallinity, ρ, RRR, A_F and critical current densities of MgB_2/Fe monofilament tapes. The MgB_2/Fe superconducting materials have been characterized by using of XRD, SEM, EDS, optical microscope, and transport

measurements to obtain the optimum annealing temperature and time. From these characterizations, the optimum annealing temperature and time were found to be 950°C and 60 minutes for the MgB_2/Fe monofilament tape, respectively. The lattice parameters and A_F values increase while the FWHM, ρ_{40K}, ρ_{300K} and RRR values decrease with increasing the annealing temperature from 650 to 950°C. The highest J_c and T_c^{offset} values were determined as 260.43 A/cm^2 at 20 K and 38.1 K for the MgB_2/Fe monofilament tape, respectively. The T_c and J_c values of the MgB_2/Fe monofilament tape samples increased with increasing the annealing temperature up to 950°C. Moreover, the transport and microstructure properties are remarkably enhanced with increasing annealing temperature. The highest value of critical current density is obtained after annealing at 950°C. This result is attributed to microcrack eliminations and good grain connectivity. We observed that the activation energies of the MgB_2/Fe monofilament tapes annealed at 650°C-1050°C for 60 min. increased with increasing annealing temperature up to 950°C. The highest activation energy obtained for the sample annealed at 950°C for 60 min. As the annealing temperature increases from 950°C to 1050°C, the activation energy of the MgB_2/Fe monofilament tape decreases from 3.588 eV to 1.795 eV. This decrease suggests reducing of the pinning centres in the sample. We observed that the activation energies of the MgB_2/Fe monofilament tapes annealed at 950°C for 30-240 min. increased with increasing annealing time up to 60 min. As the annealing time increases from 60 min. to 240 min., the activation energy of the MgB_2/Fe monofilament tape decreases from 3.588 eV to 2.063 eV. The activation energy U(B) values also decreased with increasing magnetic fields. For the MgB_2/Fe monofilament tape, dH_{c2}/dT and dH_{irr}/dT decrease with increasing annealing temperature from 850 to 950°C as well as with increasing annealing time from 30 to 60 minutes. The crystallinity of the

MgB_2 improved on increasing the annealing temperature from 850 to 950°C and the annealing time from 30 to 60 minutes. However, this better crystallinity decreased the slopes of the H_{c2}-T and H_{irr}-T curves of the MgB_2/Fe monofilament tapes due to larger coherence length. The improvement of the H_{c2} and H_{irr} contributes to the critical current density improvement for the MgB_2/Fe monofilament tapes annealed at 650°C-1050°C for 60 minutes and 950°C for 30-240 minutes.

2. The MgB_2/Ag monofilament superconducting materials were fabricated by ex-situ PIT method using commercially available MgB_2 powder (Cerac Co., -100 mesh, 99%). The MgB_2/Ag monofilament wire was also characterized using SEM, EDS, optical microscope, inductive critical current density and a vibrating sample magnetometer. The highest inductive critical current density value of the MgB_2/Ag monofilament wire was found to be 2.20×10^4 A/cm^2 at 4.2 K and 1 T. The inductive critical current density values of the MgB_2/Ag monofilament wire decrease with the increasing magnetic field and temperature.

3. The MgB_2/Fe/Cu 6 and 7 filament wires and tapes were fabricated by ex-situ PIT method using commercially available MgB_2 powder (Alfa Aesar, -325 mesh, <44 micron) without any intermediate annealing. The MgB_2/Fe/Cu 6 and 7 filament wires and tapes were characterized using XRD, SEM, EDS, optical microscope, quantum design physical property measurement system, vibrating sample magnetometer system, critical transition temperature and critical current density measurements. In order to explain the connectivity between grains, A_F values are estimated for the MgB_2/Fe/Cu 6 and 7 filament tapes. The estimated A_F value of the MgB_2/Fe/Cu 6 filament tape was obtained higher than that of MgB_2/Fe/Cu 7 filament tape. This result indicates the better intergranular connection in MgB_2 grains for the MgB_2/Fe/Cu 6 filament tape. The room temperature resistivity value of the

MgB_2/Fe/Cu 6 filament tape was obtained lower than that of MgB_2/Fe/Cu 7 filament tape. This is related to the better crystallinity of MgB_2 phase due to grain growth for the MgB_2/Fe/Cu 6 filament tape. The J_c values of the MgB_2/Fe/Cu 6 and 7 filament tapes were obtained as 447.74 A/cm^2 and 188.18 A/cm^2, respectively. The J_c value of the MgB_2/Fe/Cu 6 filament tape was obtained higher than that of MgB_2/Fe/Cu 7 filament tape at 20 K. The offset superconducting transition temperature values of the MgB_2/Fe/Cu 6 and 7 filament wires were extracted as 36.8 K and 36.6 K from the M-T graphs. These inductive superconducting transition temperature values are consistent with the superconducting transition temperatures which were obtained from transport measurements of the MgB_2/Fe/Cu 6 and 7 filament wires.

4. We have investigated the effect of extreme rolling on the superconducting properties of commercial MgB_2/Ni/Fe/Cu tapes. Rolling clearly reduced the T_c values of the tapes. Application of heat treatment after rolling reduces the decrease in T_c. For rolled tapes, T_c values increased with increase of heat treatment temperature. Heat treatment at 900^{o}C after rolling is expected to increase T_c. The transition width (ΔT) significantly increases due to rolling. The increase in ΔT is reduced with annealing. Rolling increased the engineering critical current density (J_e) values of the tapes.

REFERENCES

[1] Kamerlingh Onnes, H., The Superconductivity of Mercury. Comm. Phys. Lab. Univ. Leiden, 1911. 122 and 124: p. 1226.

[2] Kamerlingh Onnes, H., The sudden disappearance of the ordinary resistance of tin and the superconductive state of lead. Comm. Phys. Lab. Leiden, 1913. 133d: p. 51.

[3] Mourachkine A., 2004. *Room-Temperature Superconductivity*, p. 3, Cambridge International Science Publishing, U.K.

[4] Ford P.J., Saunders G.A., 2005. *The Rise of the Superconductors*, p. 22, CRC Press, United States of America.

[5] Kittel C., 1996. *Introduction to Solid State Physics*, pp. 354-355, Seventh Edition, John Wiley, New York.

[6] Kamimura H, Ushio H, Matsuno S, Hamada T, 2005. *Theory of Copper Oxide Superconductors*, p. 2, Springer, Germany.

[7] John R H, 2003, Applications of high-temperature superconductors in power technology, *Rep. Prog. Phys.*, 66, 1865-1886.

[8] http://superconductors.org/

[9] Belenli, I., 1993, Investigation Of Processing Routes For The Production Of Wires And Tapes From Bismuth-Based High Temperature Superconducting (HTS) Ceramic Oxides, PhD Thesis, Pembroke College, Oxford.

[10] Ginzburg, V.L. and L.D. Landau, On the theory of superconductivity. Hurnal Eksperimental noi I Teorticheskoi Fiziki, 1950. 20: p. 1064-1082.

[11] Abrikosov A.A., Soviet Physics JETP, 1957, p. 1174-1182.

[12] Josephson, B.D., Possible new effects in superconductive tunnelling. Phys. Lett., 1962. 1: p. 251-253.

[13] Wu, M.K., J.R. Ashburn, C.J. Torng, P.H. Hor, R.L. Meng, L. Gao, Z.J. Huang, Y.Q. Wang and C.W. Chu, Superconductivity at 93 K in a new mixed-phase Yb-Ba-Cu-O compound system at ambient pressure. Physical Review Letters, 1987. 58 (9): p. 908-910.

[14] Terzioglu, C., Varilci, A., Belenli, I., 2009. Investigation of effect of annealing temperature on mechanical properties of MgB_2. *Journal of Alloys and Compounds.* 478:836–841.

[15] Contani, M., A. Schilling, H.V. Nissen and H. R. Ott, Characterisation of superconducting Hg-Ba-Ca-Cu-oxides. Structural and Physical aspects. Physica C-Superconductivity and Its Applications, 1993. 215 (1-2): p. 11-18.

[16] Nagamatsu, J., N. Nakagawa, T. Muranaka, Y. Zenitani and J. Akimitsu, Superconductivity at 39 K in magnesium diboride. Nature, 2001. 410 (6824) : p. 63-64.

[17] J. Kortus, I.I. Mazin, K.D. Belashchenko, V.P. Antropov and L.L. Boyer, Phys. Rev. B 86, 4656 (2001).

[18] J.M. An and W.E. Pickett, Phys. Rev. Lett. 86, 4366 (2001).

[19] S.L. Bud'ko, G. Lapertot, C. Petrovic, C.E. Cunningham, N. Anderson and P.C. Canfield, Phys. Rev. Lett. 86, 1877 (2001).

[20] A. Sharoni, I. Felner, O. Millo, Phys. Rev. B 63, 2205081 (2001).

[21] Bardeen, J., Cooper, L.N., Schieffer, J.R. 1957. 'Microscopic Theory of Superconductivity', Physical Review. Vol. 106. p. 162.

[22] Bednorz, G. and K.A. Müller, Possible high T_c superconductivity in the Ba-La-Cu system. Z. Phys. B, 1986. 64: p. 189-197.

[23] Ford P.J., Saunders G.A., 2005. *The Rise of the Superconductors*, CRC Press, United States of America. p. 227.

[24] Jones, M. And R. Marsh, The preparation and structure of magnesium boride, MgB_2. Journal of American Society, 1954. 76: p. 1434.

[25] Mourachkine A., 2004. *Room-Temperature Superconductivity*, p. 27, Cambridge International Science Publishing, U.K.

[26] Fossheim K., Sudbø A. 2004 *Superconductivity Physics and Applications* p. 53, John Wiley & Sons Ltd, England.

[27] Ford P.J., Saunders G.A., 2005. *The Rise of the Superconductors*, p. 122, CRC Press, United States of America.

[28] Korkus, J. Mazin, I.I., Belashchenko, K.D., Antrapov, P.V. and Boyer, L.L. 2001, Superconductivity of metallic boron in MgB_2, Phys. Rev. Lett. 86 4656.

[29] Mourachkine A., 2004. *Room-Temperature Superconductivity*, pp. 33-34 Cambridge International Science Publishing, U.K.

[30] J.M., An, W.E., Pickett, 2001. Phys. Rev. Lett. 86:4366.

[31] Xi, X.X., 2008. Two-band superconductor magnesium diboride. *Rep. Prog. Phys.* 71:116501.

[32] Bardeen, J., Cooper, L.N., Schieffer, J.R. 1957. Theory of Superconductivity, Physical Review. Vol. 108:5.

[33] Budko, S.L., Lapertot, G., Petroviç, C., Cuningham, C.E., Anderson, N., and Canfield, P.C. 2001. 'Boron Isotope Effect in Superconducting MgB_2', Physical Review Letters Vol. 86, p. 1877.

[34] Hinks, D.G., Claus, H., and Jorgensen, J.D. 2001. 'The Reduced Total Isotope Effect and its Implications on the Nature of Superconductivity in MgB_2', Nature Vol. 411, p. 457.

[35] Lorenz, B., Meng, R.L., Chu, C.W. 2001. 'High-Pressure Study on MgB_2', Physical Review B. Vol. 64, p. 012507.

[36] Bordet, P., Mezovar, M., Nunez-Regueiro, M., Monteverde, M., D., Rogado, N., Regan K.A., Hayward, M.A., He, T., Loureiro, S.M. and Cava, R.T. 2001. 'Absence of a Structural Transition up to 40 GPa in MgB_2 and The Relevance of Magnesium Nonstoichometry', Physical Review B. Vol. 64, p. 172502.

[37] Fossheim K., Sudbø A. 2004 *Superconductivity Physics and Applications*, John Wiley & Sons Ltd, England. p. 427.

[38] Buzea, C., Yamashita, T., 2001. Review of superconducting properties of MgB_2. *Supercond. Sci. Technol.* 14 (2001) R115–R146.

[39] http://openlearn.open.ac.uk/mod/resource/view.php?id=192974

[40] Rose-Innes, A.C., Rhoerick E.H., 1978. Introduction to Superconductivity, Pergamon Press Ltd., U.K. p. 237.

[41] Mourachkine A., 2004. *Room-Temperature Superconductivity*, Cambridge International Science Publishing, U.K. p. 310.

[42] Vidali G., 1993. Superconductivity: The Next Revolution, Cambridge University Press, U.K. p. 165.

[43] Ruvalds, J., 1996. Theoretical prospects for high-temperature superconductors. *Supercond. Sci. Technol.* 9:905–926.

[44] Nattermann, T., Scheidl, S., 2000. Vortex-glass phases in type-II superconductors Advances in Physics, 49:607-704

[45] Kittel C., 1996. *Introduction to Solid State Physics*, Seventh Edition, John Wiley, New York. p. 673.

[46] Akimitsu, J., Muranaka, T., 2003. Superconductivity in MgB_2. *Physica C*. 388–389:98–102.

[47] Canfield, P.C., Budko, S.L., Finnemore, D.K., 2003. An overview of the basic physical properties of MgB_2. *Physica C* 385:1–7.

[48] Zhou, S., Pan, A.V., Liu, H., Dou S., 2002. Single and multi-filamentary Fe-sheathed MgB_2 wires. *Physica C*. 382:349–354.

[49] Holubek, T., Schlachter T.I., Goldacker, W., 2009. Fabrication and transport properties of superconducting MgB_2 cables. *Supercond. Sci. Technol.* 22:055011.

[50] Kumakura, H., Matsumoto, A., Nakane, T., Kitaguchi H., 2007. Fabrication and properties of powder-in-tube-processed MgB_2 tape conductors. *Physica C*. 456:196–202.

[51] Glowacki, B.A., Majoros, M., Vickers, M., Evetts, J.E., Shi, Y., McDougall, I., 2001. Superconductivity of powder-in-tube MgB_2 wires. *Supercond. Sci. Technol*. 14:193–199.

[52] Braccini, V., Nardelli, D., Penco, R., Grasso, G., 2007. Development of ex situ processed MgB_2 wires and their applications to magnets. *Physica C*. 456:209–217.

[53] Malagoli, A., Braccini, V., Scati, N., Roncallo, S., Siri, A.S., Grasso G., 2002. Fabrication and superconducting properties of powder-in-tube processed MgB_2 tapes. *Physica C*. 372–376:1245–1247.

[54] Nakane, T., Kitaguchi, H., Kumakura, H., 2006. Ex situ fabrication of MgB_2/Al tapes with high critical current density. *Supercond. Sci. Technol*. 19:528–533.

[55] Vinod, K., Kumar, R.G.A., Syamaprasad, U., 2007. Prospects for MgB_2 superconductors for magnet application. *Spercond. Sci. Technol.* 20:R1-R13.

[56] Tanaka, K., Okada, M., Kumakura, H., Kitaguchi, H., Togano, K., 2002. Fabrication and transport properties of MgB_2 wire and coil. *Physica C*. 382:203–206.

[57] Glowacki, B.A., Majoros, M., 2002. MgB_2 conductors for dc and ac applications. *Physica C*. 372–376:1235–1240.

[58] Fu, B.Q., Feng, Y., Yan, G. Liu, C.F., Zhou, L. Cao, L.Z., Ruan, K.Q., Li, X.G., 2003. High transport critical current in MgB_2/Fe wire by in situ powder-in-tube process, *Physica C.* 392–396:1035–1038.

[59] Machi, T., Shimura, S., Koshizuka, N., Murakami, M., 2003. Fabrication of MgB_2 superconducting wire by in situ PIT method. *Physica C*. 392–396:1039–1042.

[60] Gencer, A., Kılıç, A., Okur, S., Güçlü, N., Özyüzer, L., Belenli I., 2005. Low-Field Behavior of Ti-Added MgB_2/Cu Superconducting Wires. *IEEE Transactions On Applied Superconductivity*, 15:2.

[61] Feng, Y.,Yan, G., Zhao, Y., Liu, C.F., Fu, B.Q., Zhou, L., Cao, L.Z., Ruan, K.Q., Li, X.G., Shi, L., Zhang, Y.H., 2003. Superconducting properties of MgB_2 wires and tapes with different metal sheaths. *Physica C*. 386:598–602.

[62] Flükiger, R., Suo, H.L., Musolino, N., Beneduce, C., Toulemonde, P., Lezza, P., 2003. Superconducting properties of MgB_2 tapes and wires. *Physica C*. 385:286–305.

[63] Hur, J.M., Togano, K., Matsumoto, A., Kumakura, H., Wada, H., and Kimura, K, 2008, Fabrication of high-performance MgB_2 wires by an internal Mg diffusion process, *Supercond. Sci. Technol*. 21: 032001.

[64] Tomsic, M., Rindfleisch, M., Yue, J., McFadden, K., Doll, D., Phillips, J., Sumption, M.D., Bhatia, M., Bohnenstiehl, S., Collings, E.W., 2007. Development of magnesium diboride (MgB_2) wires and magnets using in situ strand fabrication method. *Physica C*. 456:203–208.

[65] http://www.hypertechresearch.com/page4.html

[66] Kılıc, A., Okur, S., Guclu, N., Kolemen, U., Uzun, O., Ozyuzer, L., Gencer A., 2004. Structural and low-field magnetic characterization of superconducting MgB_2 wires. *Physica C*. 415:51–56.

[67] Xi, X.X., 2009. MgB_2 thin films. *Supercond. Sci. Technol.* 22:043001.

[68] X.X. Xi, A.V. Pogrebnyakov, S.Y. Xu, K. Chen, Y. Cui, E.C. Maertz, C.G. Zhuang, Qi Li, D.R. Lamborn, J.M. Redwing, Z.K. Liu, A. Soukiassian, D.G. Schlom, X.J. Weng, E.C. Dickey, Y.B. Chen, W. Tian, X.Q. Pan, S.A. Cybart, R.C. Dynes, 2007. MgB_2 thin films by hybrid physical–chemical vapor deposition. Physica C. 456:22–37.

[69] Casalbuoni, R., 2003. Lecture Notes on Superconductivity: Condensed Matter and QCD, Lectures at the University of Barcelona, Spain, p. 120.

[70] Shimura, S., Machi, T., Murakami, M., Koshizuka, N., Mochizuki, K., Ishikawa, I., Shibata, N., 2004. Copper sheath MgB_2 wires fabricated by an in situ PIT method *Physica C*. 412–414:1179–1183.

[71] http://www.physics.carleton.ca/courses/75.364/mp-2html/node16.html

[72] Collings, E.W., Sumption, M.D., Bhatia, M, Susner, M.A., Bohnenstiehl, S.D., 2008. Prospects for improving the intrinsic and extrinsic properties of magnesium diboride superconducting strands, *Supercond. Sci. Technol.* 21:103001.

[73] Kortus, J., 2007. Current progress in the theoretical understanding of MgB_2 *Physica C.* 456:54–62.

[74] Bud'ko, S.L., Canfield, P.C., Kogan, V.G., 2002. Magnesium diboride: basic physical properties and high upper critical field anisotropy. *Physica C.* 382:85–92.

[75] Gencer, A., 1993, Time Dependent Magnetisation and Flux Dynamics of High Temperature Superconductors. Ph.D. Thesis. University of Birmingham, England.

[76] Schlachter, S.I., Frank, A., Ringsdorf, B., Orschulko, H., Obst, B., Liu, B., Goldacker, W., 2006. Suitability of sheath materials for MgB_2 powder-in-tube superconductors. *Physica C*. 445–448:777–783.

[77] Larbalestier, D.C., Cooley, L.D., Rikel, M,O., Polyanskii, A.A., Jiang, J., Patnaik, S., Cai, X.Y., Feldman, D.M., Gurevich, A., Squitieri, A.A., Naus, M.T., Eom, C.B., Hellstrom, E.E., Cava, R.J., Regan, K.A., Rogado, N., Hayward, M.A., He, T., Slusky, J.S., Khalifah, P., Inumaru, K., Haas, M., 2001. Strongly linked current flow in polycrystalline forms of the superconductor MgB_2, *Nature*. 410:186.

[78] Dhalle, M., Toulemonde, P., Beneduce, C., Musolino, N., Decroux, M., Flukiger, R., 2001. Preprint, Transport and inductive critical current densities in superconducting MgB_2.*condmat*. 0104395.

[79] Örd, T., Kristoffel, N., 2002. Modeling MgB_2 two-gap superconductivity. *Physica C*. 370:17–20.

[80] Choi, H.J., Cohen, M.L., Louie, S.G., 2003. Anisotropic Eliashberg theory of MgB_2: Tc, isotope effects, superconducting energy gaps, quasiparticles, and specific heat. *Physica C*. 385:66–74.

[81] Kim, K.H.P, Kang, W.N., Kim, M.S., Jung, C.U., Kim, H.J., Choi, E.M., Park, M.S., Lee, S.I., 2001. Preprint, Origin of the high DC transport critical current density for the MgB_2 superconductor, *cond-mat*. 0103176.

[82] Ozogul, O., Guclu, N., Gencer, A., 2004. Ac magnetic response of MgB_2 bulk superconductor based on the Anderson–Kim model. *Physica C*. 402:209–215.

[83] Perner, O., Habler, W., Eckert, J., Fischer, C., Mickel, C., Fuchs, G., Holzapfel, B., Schultz, L., 2005. Effects of oxide particle addition on superconductivity in nanocrystalline MgB_2 bulk samples. *Physica C*. 432:15–24.

[84] Yamamoto, A., Shimoyama, J., Ueda, S., Katsura, Y., Iwayama, I., Horii, S., Kishio, K., 2005. Effects of sintering conditions on critical current properties and microstructures of MgB_2 bulks. *Physica C*. 426–431:1220–1224.

[85] Mikheenko, P., Martinez, E., Bevan, A., Abell, J.S., MacManus-Driscoll, J.L., 2007. Grain boundaries and pinning in bulk MgB_2. *Supercond. Sci. Technol.* 20:S264–S270.

[86] Wu, Y.F., Lu, Y.F., Li, J.S., Chen, S.K., Yan, G., Pu, M.H., Li, C.S., Zhang, P.X., 2007. The microstructures and superconducting properties of MgB_2 bulks prepared by a high-energy milling method. *Physica C*. 467:38–42.

[87] Gencer, A., 2002. Harmonic susceptibilities of a bulk superconductor MgB_2 at low magnetic fields. *Supercond. Sci. Technol.* 15:247–253.

[88] Zhou, S, Zhang, Y., Pan, A.V., Dou, S.X., Chung, K.C., Kim, Y.K., Yoo, J.M., 2009. Effects of sintering atmosphere on the superconductivity of MgB_2. *Supercond. Sci. Technol.* 22:045018.

[89] Chenggang Zhuang, Teng Tan, YazhouWang, Shanshan Bai, Xiaobai Ma, Huan Yang, Guohua Zhang, Yusheng He, HaihuWen, X X Xi, 2009. Qingrong Feng and Zizhao Gan Supercond. Clean MgB_2 thin films on different types of single-crystal substrate fabricated by hybrid physical–chemical vapor deposition. *Sci. Technol.* 22:025002.

[90] Yue Zhao, Mihail Ionescu, Josip Horvat and Shi Xue Dou, 2004. Comparative study of in situ and ex situ MgB_2 films prepared by pulsed laser deposition *Supercond. Sci. Technol.* 17:S482–S485.

[91] Seung-HyunMoon, Hyun-Mi Kim, Sung-Soo Yim, Ki-Bum Kim, Young-Woon Kim, Sang-Im Yoo and Ho-Nyun Lee, 2004. Superconducting properties and microstructures of MgB_2 thin films prepared by the ex situ annealing process *Supercond. Sci. Technol.* 17:S15–S19.

[92] Sheahen Thomas P., 2002. Introduction to High-Temperature Superconductivity, p. 149, Kluwer Academic Publishers, United States of America.

[93] Birajdara B. and Eibl O., 2009. Microstructure critical current density model for MgB_2 wires and tapes. *Journal of Applied Physics* 105:033903.

[94] Zhao Q., Liu Y. , Han Y., Ma Z., Shi Q., Gao V., 2009. Effect of heating rates on microstructure and superconducting properties of pure MgB_2. *Physica C* 469:857-861.

[95] Sakurai H., Kuramochi T., Furuya Y., Oike H., Kato T., Hoshi K., 2008. Synthesis of MgB_2 film by electrochemical process. *Physica C* 468:1097-1099.

[96] Rogacki K., Oganisian K., Sulkowski C., Zhigadlo N., Katrych S., Karpinski J., 2008. Transport properties of MgB_2 single crystals doped with electrons and holes. *Journal of Physics and Chemistry of Solids* 69:3202-3204.

[97] Lee C. M., Park J. H., Hwang S. M., Lim J. H., Joo J., Kang V, Kim C. J., 2009. Fabrication of ex situ processed MgB_2 wires using nano carbon doped powder. *Physica C* 469:527-1530.

[98] Braccini V., Malagoli A., Tumino A., Vignolo M., Bernini C., Fanciulli C., Romano G., Tropeano M., Siri A. S., and Grasso G., 2007. Improvement of Magnetic Field Behavior of Ex-Situ Processed Magnesium Diboride Tapes. *IEEE Transactions on Applied Superconductivity* 17:2.

[99] Malagoli A., Braccini V., Tropeano M., Vignolo M., Bernini C., Fanciulli C., Romano G., Putti M., Ferdeghini C., Mossang E., Polyanskii A., and Larbalestier D. C., 2008. Effect of grain refinement on enhancing critical current density and upper critical field in undoped MgB_2 ex situ tapes. *Journal of Applied Phyics* 104:103908.

[100] Vignolo M., Romano G., Malagoli A., Braccini V., Bernini C., Tropeano M., Martinelli A., Cubeda V., Tumino A., Putti M., Ferdeghini C., and Siri A. S., 2008. Development of MgB_2 Powders and Study of the Properties and Architecture of Ex-Situ PIT Wires. *IEEE Transactions on Applied Superconductivity*18:2.

[101] Shimura S., Machi T., Nakao K., Koshizuka N., Tanaka S., Mochizuki K., Shibata N., Ushio K., 2005. Copper sheath MgB_2 wires fabricated by an in situ PIT method. *Physica C* 426-431:1254-1260.

[102] Asthana A., Matsumoto A., Kitaguchi H., Matsui Y., Hara T., Watanabe K., Yamada H., Uchiyama N. and Kumakura H., 2008. Structural microstructural characteristics and its correlations with the superconducting properties of in situ PIT processed MgB_2 tapes with ethyltoluene and SiC powder added. *Supercond. Sci. Technol.* 21:115013.

[103] Hata S., Yoshidome T., Sosiati H., Tomokiyo Y., Kuwano N., Matsumoto A., Kitaguchi H. and Kumakura H., 2006. Microstructures of MgB_2/Fe tapes fabricated by an in situ powder in tube method using MgH_2 as a precursor powder. *Supercond. Sci. Technol.* 19:161–168.

[104] Hur J., Togano K., Matsumoto A., Kumakura H., Wada H., and Kimura K., 2009. High Critical Current Density MgB_2/Fe Multicore Wires Fabricated by an Internal Mg Diffusion Process. *IEEE Transactions on Applied Superconductivity*19:3.

[105] Nakane T., Takahashi K., Kitaguchi H., Kumakura H., 2009. Fabrication of Cu-sheathed MgB_2 wire with high J_c–B performance using a mixture of in situ and ex situ PIT techniques. *Physica C* 469:1531–1535.

[106] Fang H., Alessandrini M., Hoyt C., Liang G., Lv B., and Salama K., 2009. In-Field J_c Enhancement on Ti-Sheathed MgB_2 Wires Doped With TiC Nanoparticles. *IEEE Transactions on Applied Superconductivity* 19:3.

[107] Soltanian S., Wang X. L., Horvat J., Li A. H., Liu H. K., Dou S. X., 2002. Improvement of critical current density in the Cu/MgB_2 and Ag/MgB_2 superconducting wires using the fast formation method. *Physica C* 382:187-193.

[108] Tachikawa K., Yamada Y., Enomoto M., Aodai M., Kumakura H., 2003. Structure and critical current of Ni-sheathed PIT MgB_2 tapes with In metal powder addition. *Physica C* 392-396:1030-1034.

[109] Song K. J., Kim S. W., Park C., Joo J. H., Choi S. J., Ko R. K., Ha H. S., Ha D.W., Oh S. S., 2004. The effect of geometry of composite MgB_2/stainless-steel (SS) wires fabricated by PIT process on the superconducting properties. *Physica C* 407:17-22.

[110] Soltaniana S., Wanga X. L., Lia A. H., Collingsb E. W., Sumptionb M. D., Leeb E., Liua H. K., Dou S. X., 2002. Fabrication and critical current density in 16-filament stainless steel/Fe/MgB_2 square wire. *Solid State Communications* 124:59–62.

[111] Fu M., Chen J., Jiao Z., Kumakura H., Togano K., Ding L., Zhang Y., Chen Z., Han H., Chen J., 2004. Mechanical properties and bending strain effect on Cu–Ni sheathed MgB_2 superconducting tape. *Physica C* 406:53-57.

[112] Togano K., Hur J. M., Matsumoto A . and Kumakura H., 2009. Fabrication of seven-core multi-filamentary MgB_2 wires with high critical current density by an internal Mg diffusion process. *Supercond. Sci. Technol.* 22 :015003.

[113] Ruan K. Q., Li H. L., Yu Y., Wang C. Y., Cao L. Z., Liu C. F., Du S. J., Yan G., Feng Y., Wu X., Wang J. R., Liu X. H., Zhang V, Wu X. Z., Zhou L., 2003. Transport critical current density of Fe sheath MgB_2 tapes sintered at different temperatures. *Physica C* 386:578–580.

[114] Wang X. L., Soltanian S., Horvat J., Liu A. H., Qin M. J., Liu H. K., Dou S. X., 2001. Very fast formation of superconducting MgB_2/Fe wires with high J_c. *Physica C* 361:149-155.

[115] Balamurugan S., Nakamura T., Osamura K., Muta I., Hoshino T., 2004. Structural and superconducting properties of PIT processed sintered MgB_2/Fe wires. *Physica C* 412–414:1184–1188.

[116] Wang D., Ma Y., Yu Z., Gao Z., Zhang X., Watanabe K. and Mossang E., 2007. Strong influence of precursor powder on the critical current density of Fe-sheathed MgB_2 tapes. *Supercond. Sci. Technol.* 20:574–578.

[117] Yamamoto K., Osamura K., Balamurugan S., Nakamura T., Hoshino T. and Muta I., 2003. Mechanical and superconducting properties of PIT-processed MgB_2 wire after heat treatment. *Supercond. Sci. Technol.* 16:1052–1058.

[118] Cullity B. D., 1978. Element of X-ray Diffraction, Addition-Wesley, Reading, MA.

[119] Fischer C., Haßler W. , Rodig C., Perner O., Behr G., Schubert M., Nenkov K., Eckert J., Holzapfel B., Schultz L., 2004. Critical current densities of superconducting MgB_2 tapes prepared on the base of mechanically alloyed precursors. *Physica C* 406:121–130.

[120] Rowell John M., 2003. The widely variable resistivity of MgB_2 samples. *Supercond. Sci. Technol.* 16:R17–R27.

[121] Kim J.H, Dou S.X, Wang J.L, Shi D.Q, Xu X., Hossain M.S.A., Yeoh W.K, Choi S. and Kiyoshi T., 2007. The effects of sintering temperature on superconductivity in MgB_2/Fe wires. *Supercond. Sci. Technol.* 20:448–451.

[122] Kim J.H., Dou S.X., Shi D.Q., Rindfleisch M. and Tomsic M., 2007. Study of MgO formation and structural defects in in situ processed MgB_2/Fe wires. *Supercond. Sci. Technol.* 20:1026–1031.

[123] Malagoli A., Braccini V., Tropeano M., Vignolo M., Bernini C., Fanciulli C., Romano G., Putti M., Ferdeghini V, Mossang E., Polyanskii A., and Larbalestier D. C., 2008. Effect of grain refinement on enhancing critical current density and upper critical field in undoped MgB_2 ex situ tapes. *Journal of Applied Physics* 104:103908.

[124] Wilke R. H. T., Budko S. L., Canfield P. C., Finnemore D. K., Suplinskas Raymond J., Hannahs S. T., 2005. Synthesis and optimization of $Mg(B_{1-x}\ C_x)_2$ wire segments. *Physica C* 424:1–16.

[125] Jiang J., Senkowicz B.J., Larbalestier D.C. and Hellstrom E.E., 2006. Influence of boron powder purification on the connectivity of bulk MgB_2. *Supercond. Sci. Technol.* 19:L33–L36.

[126] Xu X., Kim J. H., Dou S. X., Choi S., Lee J. H., Park H. W., Rindfleish M., and Tomsic M., 2009. A correlation between transport current density and grain connectivity in MgB_2 /Fe wire made from ball-milled boron. *Journal of Applied Physics* 105:103913.

[127] Kumakura H., Kitaguchi H., Matsumoto A. and Yamada H., 2005. Upper critical field, irreversibility field, and critical current density of powder-in-tube-processed MgB_2/Fe tapes. *Supercond. Sci. Technol* 18:1042–1046.

[128] Kitaguchi H., Matsumoto A., Hatakeyama H. and Kumakura H., 2004. High temperature performance of MgB_2 powder-in-tube composite tapes. *Supercond. Sci. Technol*. 17:S486–S489.

[129] Ojha N., Varma G. D., Singh H. K., and Awana V. P. S., 2009. Effect of rare-earth doping on the superconducting properties of MgB_2. *Journal of Applied Physics* 105:07E315

[130] Aksan M.A., Guldeste A., Balcı Y., Yakıncı M.E., 2006. Degradation of superconducting properties in MgB_2 by Cu addition. *Solid State Communications* 137:320–325.

[131] Qin M. J., Wang X. L., Soltanian S., Li A. H., Liu H. K., and Dou S. X., 2001. Dependence of the flux-creep activation energy on current density and magnetic field for the MgB_2 superconductor. *Physical Review B* 64:060505(R).

[132] Fabbricatore P., Greco M., Musenich R., Kovac P., Husek I. and Gomory F., 2003. Influence of the sintering process on critical currents, irreversibility lines and pinning energies in multifilamentary MgB_2 wires. *Supercond. Sci. Technol.* 16:364-370.

CURRICULUM VITAE

Name : Ersin YÜCEL

Permanent Address : Sümer Mah. Ayhan Sokak No: 21/6 BOLU

Degree and date to be conferred : Ph.D., 2010

Place Date of Bird : Bursa, 1978

Collegiate instituons attended	**Degree**	**Date of degree**
Uludag Univesity	B.Sc.	2000
Uludag Univesity	M.Sc.	2003
Abant Izzet Baysal University	Ph.D.	2010

Publications:

1. E. Yucel, C. Terzioglu, A. Varilci, A. Gencer and I. Belenli, "Fabrication and superconducting properties of ex-situ processed MgB_2/Fe monofilament tapes without any intermediate annealing", Journal of Materials Science (Submitted) (2010).

2. E. Yucel, C. Terzioglu, A. Varilci, A. Gencer and I. Belenli, "Fabrication and magnetoresistance properties of ex-situ processed MgB_2/Fe monofilament tapes without any intermediate annealing", Journal of Materials Science (Submitted) (2010).

3. E. Yucel, C. Terzioglu, A. Varilci, A. Gencer and I. Belenli, "Fabrication and superconducting properties of ex-situ processed MgB_2/Fe/Cu multifilament wires without any intermediate annealing", Journal of Superconductivity and Novel Magnetism (Submitted) (2010).

4. BEKTORE Y., **YUCEL E**., ERTURK K., HACIISMAILOGLU M. C., "Investigation of electrical and optical properties of n-Type Si/Au Schottky barrier diode", Romanian Journal of Physics, 49 (1-2), 105-112 (2004).

5. K.Ertürk, Y.Bektöre, **E. Yücel**, "I-V and C-V Characteristics of Schottky Barrier Diodes", Romanian Journal of Physics, 48, 1-4 (2003).

6. Y.Bektöre, K.Ertürk, **E. Yücel**, "n-tipi Si/Ag ve p-tipi Si/Ag Schottky Diyotların Elektriksel Özellikleri", Süleyman Demirel Üniversitesi Fen Bilimleri Enstitüsü Dergisi, Cilt:8 Sayı:2, 162-166 (2004).

Conferences, Workshops and Symposiums:

1. E. YUCEL, A. GENCER and I. BELENLİ, "Fabrication and superconducting properties of ex-situ processed MgB_2/Fe/Cu multifilament wires without any intermediate annealing", INTERNATIONAL CONFERENCE ON SUPERCONDUCTIVITY AND MAGNETISM (ICSM-2010), Page 282, APRIL 25-30, 2010-ANTALYA, TURKEY (**Poster**).

2. MUSTAFA AKDOGAN, Abant Izzet Baysal University OZGUR OZTURK, Kastamonu University **ERSIN YUCEL**, ERDAL BEKIROGLU, Abant Izzet Baysal University MUSTAFA YILMAZLAR, Sakarya University CABIR TERZIOGLU, Abant Izzet Baysal University, "Influence of diffusion-annealing time on the mechanical properties of bulk $Bi_{1.8}Pb_{0.35}Sr_{1.9}Ca_3Cu_{2.1}O_y$ superconductors diffusion-

doped with Fe", AMERICAN PHYSICAL SOCIETY (APS) MARCH MEETING, Page 151, March 16-20, 2009 PITTSBURGH, AMERICA (**Poster**).

3. E. Yücel, A. Gencer and İ. Belenli, "Fabrication and inductive critical current densities of MgB_2/Ag superconducting wire", 4. Ulusal Süperiletkenler Sempozyumu (Fourth National Superconductors Symposium), Sayfa 44, 10-13 Ağustos 2009 KTÜ TRABZON (**Poster**).

4. E. YUCEL and I. BELENLİ, "The effect of extreme rolling on the properties of commercial MgB_2 tapes", INTERNATIONAL CONFERENCE ON SUPERCONDUCTIVITY AND MAGNETISM (ICSM-2008), Page 247, AUGUST 25-29, 2008-SİDE-ANTALYA, TURKEY (**Poster**).

5. Y.Bektöre, **E. Yücel**, K.Ertürk, M.C. Hacıismailoglu, "Investigation of electrical and optical properties of n-Type Si/Au Schottky barrier diode", The Fourth International Balkan Workshop on Applied Physics (4th IBWAP 2003), Page 14, September 25-27, 2003 Constanta, Romania (**Talk**).

6. Kadir Erturk, Yüksel Bektöre, **Ersin Yucel**, "I-V and C-V CHARACTERISTICS OF SCHOTTKY BARRIER DIODES", THE THIRD INTERNATIONAL BALKAN WORKSHOP ON APPLIED PHYSICS (3rd IBWAP 2002), Page 86, JUNE 26-28, 2002 TARGOVISTE, ROMANIA (**Poster**).

7. K. ERTÜRK, Y. BEKTÖRE ve **E. YÜCEL**, "n-TİPİ Si/Ti VE p-TİPİ Si/Ti SCHOTTKY DİYOTLARIN ELEKTRİKSEL ÖZELLİKLERİ", TÜRK FİZİK DERNEĞİ 21. FİZİK KONGRESİ (TFD-21), Sayfa 222, 11-14 EYLÜL 2002 SDÜ ISPARTA (**Poster**).

8. Winter School on Basic Principles, Theories and Technological Application Fields of Superconductivity**,** 24 January - 1 February 2009, ANTALYA

9. Metallography 09 Seminar**,** Applied Laboratory Systems (als), 13th May 2009, ISTANBUL

10. National Student Workshop on Superconductivity and Magnetism (NSWSM-2008)**,** Ankara University – ÖRSEM – Çolaklı – Side – ANTALYA, 28th September - 5th October, 2008, TURKEY

11. III. National Symposium of High Temperature Superconductors, Abant Izzet Baysal University, 20-22 June 2005 – BOLU

Projects:

1. 'Fabrication, Synthesis and Magnetic Characterization of Boron Based Alloys And Prototype cable And Permanent Magnet Production For Technological Applications' **National Boron Research Institute**, Project No: 2006–22-Ç21–15. **Researcher**.

2. 'Production of B(P)SCCO-2223 superconducting tapes with continuous tube forming and filling technique and their use in the construction of superconducting transformer' **TUBITAK Research Project**, Project No: 108M201. **Researcher**.